Programa de Doctorado en Arquitectura

NUEVOS MORTEROS DE CEMENTO-CAL CON MATERIALES DE CAMBIO DE FASE (PCM) PARA LA MEJORA DE LA EFICIENCIA ENERGÉTICA DE CERRAMIENTOS

Tesis Doctoral presentada por

CYNTHIA GUARDIA MARTÍN

Director:
DR. GONZALO BARLUENGA BADIOLA

Alcalá de Henares, 2020

A mi abuelo Francisco

AGRADECIMIENTOS

Este trabajo de tesis se ha llevado a cabo en el Departamento de Arquitectura de la Universidad de Alcalá al cual quiero agradecer la oportunidad que me ha brindado con la aceptación en su Programa para la elaboración de esta tesis.

Primero quiero agradecer de forma muy especial a mi tutor y director de tesis el Prof. Dr. Gonzalo Barluenga Badiola el apoyo, confianza y enseñanza depositados en mi a lo largo de toda la elaboración del trabajo. Su exigencia, tesón y paciencia han sido fundamentales en esta larga andadura tanto profesional como personal.

Gracias a mi compañera Irene Palomar por su ayuda, comprensión y apoyo en cada uno de los pasos dados durante todo este proceso. A mi compañero Javier Puentes por nuestras conversaciones durante las largas horas en el laboratorio. A Hugo Varela por su ánimo y apoyo en los últimos meses.

Agradecer también al Dr. Nelson Flores (ULPGC), a la Dra. Consuelo Cid (UAH), al Dr. Gonzalo Diarce (UPV-EHU), al Dr. -ing Antonio Caggiano y al Dr. -ing Diego Said por su colaboración. A BASF Construction Chemicals España S.L, a Omya Clariana S.L y a Cementos Portland Valderrivas por el suministro de algunos de los materiales utilizados en esta investigación.

Al Prof. Dr. Ir. Eddie Koenders y a todo su equipo por acogerme y hacerme sentir una más durante los 3 meses de estancia realizados en el Institut für Werkstoffe im Bauwesen – Technische Universität Darmstadt (Alemania).

Por último, el más profundo agradecimiento a mis padres Jesús Mª y Francisca por ser mi pilar y ejemplo, porque sin su sacrificio, esfuerzo y apoyo incondicional hoy no estaría escribiendo estas líneas. A mi hermana Naiara y sobrinos Pablo y Jaime por su comprensión y ánimo en cada paso. A mis suegros Gonzalo y Mª de los Dolores por su apoyo en todo este tiempo. A mi esposo Gonzalo, por su paciencia, empatía y tenacidad durante todos estos años sin las cuales no hubiera podido llegar hasta aquí. A mi hija Constanza.

ÍNDICE

RESUMEN

En la actualidad existe una búsqueda constante de materiales o sistemas constructivos para mejora de la eficiencia energética de los edificios existentes. Los morteros de cemento-cal con diferentes adiciones tales como fibras de celulosa o áridos ligeros que modifiquen sus prestaciones son algunos de los materiales desarrollados para tal fin. Los materiales de cambio de fase o *Phase Change Materials* (PCM) se presentan como otra posible alternativa para la mejora del comportamiento térmico de los morteros por su capacidad como acumuladores térmicos.

Este estudio plantea el diseño y caracterización de nuevos morteros en base cemento-cal que, por un lado, logre mejorar la capacidad de aislamiento térmico con la adición de fibras de celulosa, áridos ligeros o la combinación de ambas y, por otro lado, logre adquirir la capacidad de acumulación térmica con la adición del PCM.

Se proponen doce tipos de morteros. Primero, se evalúan las propiedades físicas mecánicas y térmicas de cada uno de los morteros diseñados. A partir de los resultados experimentales obtenidos se realiza una simulación numérica con métodos no lineales de elementos finitos, en colaboración con un grupo de investigación de la Universidad de Darmstadt (Alemania). También se analiza la microestructura de los diferentes morteros, así como el comportamiento térmico de las mezclas durante condiciones ambientales de calentamiento y enfriamiento con técnicas no destructivas como la transmisión de ondas de ultrasonidos y mediciones de flujo de calor. Como último paso, una vez estudiadas las propiedades, se incluyen los diferentes morteros dentro de un cerramiento multicapa. Para ello se simulan ciclos de calentamiento y enfriamiento y se evalúa su comportamiento dependiendo de la composición del mortero ensayado.

Los resultados experimentales obtenidos permiten determinar la influencia de la adición de PCM y su combinación con otros componentes en las propiedades de los morteros. Se puede relacionar la influencia del PCM en la relación de la densidad y porosidad abierta de la microestructura y el comportamiento mecánico de las dosificaciones. A partir de los resultados experimentales obtenidos de absorción capilar por succión de agua se logra realizar una simulación numérica de estos resultados. También se

consigue identificar la diferencia en el comportamiento térmico de los morteros dependiendo del estado del PCM, líquido o sólido, a través de la modificación de la conductividad térmica de los morteros.

La técnica de ultrasonidos utilizada permite analizar los cambios en la microestructura y la identificación del estado del PCM durante las diferentes condiciones ambientales simuladas. La capacidad de acumulación térmica de los morteros y de los cerramientos multicapa a través de la evaluación del flujo de calor y la entalpía de estos dependiendo de la dosificación estudiada es evaluada cualitativa y cuantitativamente.

Por último, los resultados de la investigación dentro del desarrollo de la tesis se recogen en tres artículos publicados en revistas indexadas en primer y segundo cuartil de las categorías de tecnología de construcción y edificación, ciencia de materiales, termodinámica e ingeniería civil, un artículo enviado para su publicación en una revista indexada, dos comunicaciones en congresos internacionales RILEM con publicación de capítulo de libro, una ponencia invitada en congreso internacional y un primer premio a la mejor presentación en jornadas internacionales de investigación en el área de estudio.

Palabras clave: Materiales de cambio de fase (PCM); mortero de cemento-cal; fibras de celulosa; áridos ligeros; caracterización experimental, eficiencia energética; rehabilitación; cerramientos; transporte de humedad; propiedades térmicas; simulación numérica; técnicas no destructivas; entalpía; condiciones ambientales.

ABSTRACT

Today, there is a great interest in the study of new building materials and construction systems able to improve the energy efficiency of existing buildings. Cement-lime mortars with different additions such as cellulose fibers or lightweight aggregates are among these materials. Furthermore, Phase Change Materials (PCM) are an innovative solution for this purpose because of their heat storage capacity and can be also added to mortars. The aim of this study is the development of new cement-lime mortars that, on one hand, could improve thermal insulation with the addition of cellulose fibers and lightweight aggregates and, on the other hand, supply heat storage capacity with the addition of PCM. Physical, mechanical and thermal properties of the twelve mortars under study were evaluated. A numerical simulation with non-linear finite element methods (FEM), calibrated by experimental results, was carried out. Mortars' microstructure was also analyzed. The thermal behavior of the mixtures was evaluated using non-destructive techniques (NDT) such as ultrasonic wave transmission and heat flow measurements during heating and cooling cycles. Finally, multilayered building enclosures enhanced including a layer of the mortars studied were evaluated under heating and cooling cycles. The obtained results pointed out the influence of the addition of PCM and its combination with other components on mortars' properties. The addition of PCM was related to changes on apparent density, open porosity and mechanical properties of the mortars. A numerical simulation of the experimental results obtained from capillary water absorption tests was carried out. Furthermore, PCM physical state (liquid or solid) was identified to have influence on mortars' thermal conductivity. Ultrasonic pulse velocity technique was used to analyze the mortars' microstructure and to identify PCM physical state. Through heat flux and enthalpy evaluation, mortars heat storage capacity and multilayered building enclosures enhanced with PCM mortars were analyzed.

The scientific results of this PhD thesis can be summarized as: three indexed articles in Q1 and Q2 journals (JCR-WoK) and another one submitted for publication, two oral presentations in RILEM international conferences, published as book chapters, an

invited oral presentation in an international conference and a first price award to the best oral presentation in an international youth forum.

Keywords: Phase Change Materials (pcm); cement-lime mortars; cellulose fibers; lightweight aggregates; experimental characterization; water transport; thermal properties; numerical simulation; non-destructive techniques; enthalpy; environmental conditions.

ZUSAMMENFASSUNG

Derzeit wird ständig nach Materialien oder Konstruktionssystemen gesucht, die zur Verbesserung der Energieeffizienz von Gebäuden beitragen. Zement-Kalk-Mörtel mit verschiedenen Additiven wie Cellulosefasern oder leichten Zuschlagstoffen, die ihre Leistung verändern, sind einige der für diesen Zweck entwickelten Materialien. Phase Change Materials (PCM) werden als eine mögliche Alternative zur Verbesserung des Wärmeverhaltens von Mörteln aufgrund ihrer Fähigkeit als Wärmespeicher vorgestellt. In dieser Forschungsarbeit wird ein Zement-Kalk-Mörtel vorgeschlagen, der die Wärmedämmkapazität durch Cellulosefasern und leichte Aggregate verbessert und die Akkumulationskapazität durch Zugabe von PCM erreicht. Zuerst wurden die physikalischen, mechanischen und thermischen Eigenschaften der vorgeschlagenen Mörtel bewertet. Aus den erhaltenen experimentellen Ergebnissen wurde eine numerische Simulation mit nichtlinearen Finite-Elemente-Methoden durchgeführt. Die Mikrostruktur und das thermische Verhalten der Mörtel wurden mit der *Non-Destructive Technique* (NDT) (z.B. Ultraschallwellen und Wärmestrommessung) während der Heiz- und Kühlprozesse analysiert. Schließlich, nachdem die Eigenschaften der Mörtel untersucht worden waren, wurden die verschiedenen Mörtel in eine verbesserte *multilayered enclousure* aufgenommen. Hierzu wurden Heiz- und Kühlprozesse simuliert und deren Verhalten in Abhängigkeit von der Zusammensetzung des getesteten Mörtels bewertet. Die erhaltenen experimentellen Ergebnisse konnten den Einfluss der Zugabe von PCM und seiner Kombination mit anderen Komponenten auf die Eigenschaften der Mörtel feststellen. Es war möglich, den Einfluss des PCM auf den Zusammenhang zwischen der Dichte und offenen Porosität der Mikrostruktur und das mechanische Verhalten der Mischungen in Beziehung zu setzen. Zusätzlich wurde aus den experimentellen Ergebnissen, die aus der Kapillarabsorption erhalten wurden, eine numerische Simulation dieser Ergebnisse durchgeführt. Es war auch möglich, den Unterschied im Wärmeverhalten der Mörtel in Abhängigkeit vom Zustand des PCM aufgrund der Änderung der Wärmeleitfähigkeit der Mörtel zu identifizieren. Die Ultraschalltechnik ermöglichte es, die Mikrostruktur zu analysieren. Außerdem konnte

man den Zustand des PCM unter verschiedenen Heiz- und Kühlprozessen identifizieren. Die Wärmeakkumulationskapazität der Mörtel und der durch die Bewertung des Wärmeflusses und deren Enthalpie in Abhängigkeit von dem untersuchten Mörtel verbesserten *multilayer enclousures* wurden qualitativ und quantitativ bewertet. Die Ergebnisse der Forschung während der Entwicklung dieser Arbeit haben dazu geführt: drei Artikel, die im Q1 und Q2 in Journals veröffentlicht wurden; ein Artikel, der zum Einsenden an ein indiziertes Journal vorbereitet wurde; zwei Konferenzen auf internationalen Kongressen mit der Veröffentlichung von Buchkapiteln (RILEM); eine Gastpräsentation auf einem international Kongress und ein erster Preis für die beste Präsentation auf internationalen Forschungskonferenzen im Studienbereich.

Schlüsselwörter: Phase Change Material (PCM); Zement-Kalk-Mörtel; Cellulosefasern; leichte Aggregate; experimentelle Charakterisierung; Wassertransport; thermische Eigenschaften; numerische Simulation; Non-Destructive Technique (NDT); Enthalpie; Umweltbedingungen.

NOMENCLATURA

Símbolo	Descripción	Unidad
a/cg	Relación agua conglomerante en peso	Kg/kg
AC	Coeficiente de absorción de agua por succión capilar	$Kg/m^2min^{0.5}$
AT_{PCM}	Coeficiente de atenuación de la onda de ultrasonidos según el estado del PCM	dB/mm
v	Coeficiente de Poisson	-
λ_s	Conductividad térmica (PCM estado sólido)	W/mK
λ_s	Conductividad térmica (PCM estado líquido)	W/mK
DA	Densidad aparente	g/cm^3 o kg/m^3
D_G	Densidad geométrica	kg/m^3
$D_{Húmeda}$	Densidad en húmedo	kg/m^3
D_{Seca}	Densidad en seco	kg/m^3
H	Entalpía	J/g
ø	Flujo de Calor	W/m^2
HR/RH	Humedad relativa	%
K	Módulo de compresibilidad	GPa
E	Módulo de Young	GPa
B	Parámetro Raleigh-Ritz	mm^{-1}
VD	Permeabilidad al vapor de agua	-
PA	Porosidad abierta	%
T	Temperatura	ºC

Abreviatura	Descripción
L / LWA	Áridos ligeros
DSC	Differential Scanning Calorimetry – Calorimetría diferencial de barrido
F	Fibras de Celulosa
FC	Flujo de calor
B	Ladrillo - Brick
PCM	Material de cambio de fase – Phase Change Material
Pw	Onda de ultrasonidos de compresión o longitudinal -Tipo P
Sw	Onda de ultrasonidos de cortante o transversal -Tipo S
XPS	Poliestireno extruído

LISTADO DE FIGURAS Y TABLAS

FIGURAS

CAPÍTULO 1

CAPÍTULO 3

CAPÍTULO 4

CAPÍTULO 5

TABLAS

CAPÍTULO 3

CAPÍTULO 4

CAPÍTULO 5

1. INTRODUCCIÓN

Esta tesis doctoral plantea el desarrollo de nuevos morteros en base cemento-cal con materiales de cambio de fase (PCM) y diferentes adiciones (fibras de celulosa y perlita) para la rehabilitación energética mediante la mejora del comportamiento térmico de los cerramientos de los edificios existentes.

Para dicho fin, se evaluaron las propiedades físicas, mecánicas y térmicas de los diferentes morteros a partir de una caracterización experimental; se realizó una simulación numérica de los resultados experimentales obtenidos de absorción de agua por succión capilar a partir de la propuesta de un nuevo modelo; se estudió el comportamiento térmico del nuevo material bajo diferentes condiciones ambientales con técnicas no destructivas; y se propuso un sistema constructivo multicapa dentro del cual se introdujo el nuevo mortero, simulando y evaluando su comportamiento térmico en diferentes condiciones ambientales.

1.1 ANTECEDENTES

El parque edificatorio de viviendas en España construido en la segunda mitad del siglo XX se encuentra en un estado de necesaria mejora debido al deficiente comportamiento energético de sus fachadas. En la actualidad la mayoría de las fachadas de estos edificios no cumplen con las exigencias mínimas requeridas por la normativa vigente, tanto en España (CTE-DB-HE,2019) como en Europa (Nearly- Zero- Energy- Buildings), en materia de eficiencia y ahorro energético de los edificios. En el caso de la normativa española, dentro de las nuevas exigencias del documento básico HE-1 titulado "Condiciones para el control de la demanda energética" se especifica lo siguiente: "*Los edificios dispondrán de una envolvente térmica de características tales que limite las necesidades de energía primaria para alcanzar el bienestar térmico en función de la zona climática, de su ubicación, del régimen de verano y de invierno, del uso del edificio y, en el caso de edificios existentes del alcance de la intervención.*"

Varios estudios constatan que la causa de la deficiencia energética se encuentra principalmente en los sistemas constructivos empleados en dichas fachadas (Terés-Zubiaga J. et al, 2015). Estos sistemas carecen, en ocasiones, de aislamiento térmico o de sistemas que favorezcan la mejora de la eficiencia energética de los edificios (Terés-Zubiaga J. et al, 2013). Por esta razón, estos edificios cuentan con una alta demanda energética.

En la actualidad, se están adoptando diferentes soluciones para la mejora del comportamiento energético de las fachadas existentes como, por ejemplo, la adición o incremento de aislamiento térmico por el exterior de los cerramientos (SATE- Sistema de Aislamiento Térmico por el Exterior) (S. Lucas, 2010); o la instalación de fachadas ventiladas permitiendo la circulación de aire por el exterior (Oria, A., 2011). En ambos casos, la mejora de la eficiencia energética se alcanza a través del incremento del espesor de las fachadas sin aprovechar una posible capacidad de acumulación térmica de los propios materiales que se instalan.

Otros autores están llevando a cabo investigaciones que abordan la rehabilitación de las fachadas a través de la mejora de los materiales de revestimiento de estas (Stefanidaou M., 2014, Schiavoni, S. 2016, Veiga R., 2017). Dentro de estos materiales se encuentran los morteros de cemento o cemento-cal debido a su adaptabilidad y compatibilidad con los materiales existentes en las fachadas (Elert, K, 2002, Palomar I., 2015). Cuando el cemento utilizado es el blanco, cuenta con la ventaja de poder pigmentarse según las necesidades requeridas. A estos morteros se les añaden a su vez diferentes adiciones que complementan sus características térmicas (Herrero, S., 2013, Palomar I., 2017). Algunas de las adiciones utilizadas en estas investigaciones son las fibras de celulosa (Bentchikou, M., 2012) y los áridos ligeros (Silva L.M., 2010, Sala E. et al., 2016) como la perlita. Estos trabajos demuestran que dichas adiciones mejoran las propiedades térmicas y, en ocasiones, acústicas de los morteros y, por lo

tanto, de las fachadas existentes. Sin embargo, estos materiales no abordan la mejora del comportamiento térmico desde la acumulación térmica, sino que lo hacen exclusivamente desde el aislamiento térmico.

Por otro lado, en la actualidad existen nuevos materiales que gracias a su singular característica térmica pueden ayudar a la mejora del comportamiento térmico de las fachadas a través de la acumulación térmica. Un ejemplo de estos materiales son los materiales de cambio de fase (PCM- Phase Change Materials) (Edsjø Kalnæs, 2015, Sharma v.v., 2009). Los PCM cambian de fase (estado), de sólido a líquido y viceversa, a una determinada temperatura (temperatura de fusión). Cuando este cambio ocurre, la temperatura se mantiene constante (calor latente) mientras que el material absorbe o libera energía en forma de calor (Cabeza, L.F.., 2011, Zhou D, 2012). La Figura 1 muestra un esquema del proceso de cambio de fase de un PCM (Juárez D. 2012).

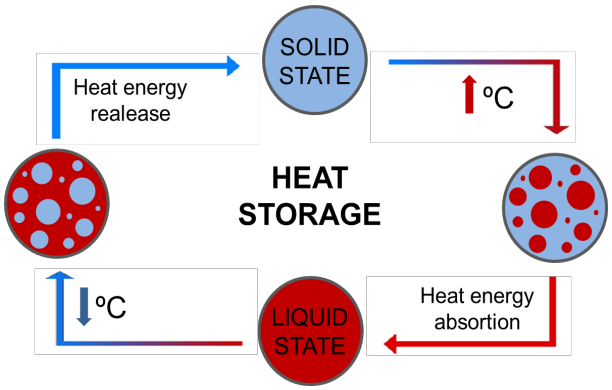

Figura 1. Proceso de cambio de fase y funcionamiento de un PCM.
(Figura adaptada de Juárez D. 2012).

Los materiales de cambio de fase líquido-sólido más comunes en el rango de temperaturas 20ºC - 80ºC (temperaturas usadas en el ámbito de la construcción) son las ceras de parafina, sales hidratadas, mezclas eutécticas y ácidos grasos. Estos materiales se clasifican en dos grupos: los inorgánicos y los orgánicos (Sharma A, 2009, Oliver A, 2009).

Dentro de los materiales inorgánicos se encuentran las mezclas eutécticas y las sales hidratadas. Una de las principales ventajas de estos materiales es su elevada conductividad térmica. Tienen una temperatura de cambio de fase claramente definida y su densidad de almacenamiento térmico es elevada. Por último, son reciclables y biodegradables y tienen un precio de mercado económico (Cabeza, L.F., 2011, Zhou D, 2012).

En contraposición se encuentra el problema de su durabilidad, ya que su uso prolongado necesita aditivos que reducen la capacidad del material de almacenamiento térmico. Además, existe la posibilidad de una segregación del material durante su uso, siendo susceptibles de subenfriamiento. Los materiales inorgánicos también son corrosivos en contacto con otros materiales (Cabeza, L.F., 2011).

Por otro lado, se encuentra el grupo de los materiales de cambio de fase orgánicos, dentro del cual se encuentran mezclas orgánicas, los ácidos grasos y las parafinas. La principal ventaja de estos materiales es su estabilidad térmica y química sin necesidad de aditivos, pudiendo cambiar de fase tantas veces como sea necesario sin que sus características se vean mermadas. Al contrario que los materiales inorgánicos, no sufren subenfriamiento y no son corrosivos. Los materiales orgánicos también son reciclables y ecológicamente inocuos. Por último, estos materiales debido a su facilidad de uso están comercialmente más desarrollados (Jayalath A, 2016, Ali Memon S., 2014).

Sin embargo, los materiales de cambio de fase orgánicos presentan bajas conductividades térmicas y bajos valores de entalpía (Cabeza, L.F., 2011). Además, experimentan grandes cambios de volumen durante el cambio de fase. Estos materiales son potencialmente combustibles y su precio en el mercado es algo más elevado.

La incorporación de los materiales de cambio de fase a otros materiales puede realizarse de diferentes formas: incorporación directa, inmersión y encapsulado. Esta última es la más utilizada para la incorporación de los PCM en materiales de construcción ya que facilita su aplicación y evita el contacto directo del PCM con el resto de los materiales.

Existen dos formas de encapsulación: la macro y la microencapsulación (Oliver A. 2009). La forma de las partículas macroencapsuladas es esférica, introduciéndose estas esferas en recipientes como tubos, esferas y paneles para su utilización en la construcción. El tamaño de estas partículas es de milímetros. Una de sus características principales es la capacidad de conseguir diferentes rangos de temperatura según la necesidad que exista. En la microencapsulación la forma de las partículas es esférica y el material que las envuelve es continuo. Las características principales de la microencapsulación son: la posibilidad de contar con diferentes rangos de temperatura según la necesidad, el reducido tamaño de las partículas (micras), la forma de estas y la estabilidad que proporciona al material a temperaturas elevadas.

En este trabajo se plantea la combinación de un mortero de cemento-cal con la adición de fibras de celulosa y perlita y dos cantidades de PCM, 10% y 20%. A través de estos componentes se busca dotar al mortero con la adición de las fibras y áridos ligeros de capacidad de aislamiento térmico y con la incorporación del PCM, de capacidad de acumulación térmica.

El material de cambio de fase elegido para este trabajo es una parafina microencapsulada denominada comercialmente MICRONAL DS 5040X suministrado por BASF Construction Chemical Company. Se trata de un PCM orgánico (BASF, 2013).

A continuación, se muestra una imagen (Figura 2) de varias microcápsulas del material de cambio de fase utilizado en este trabajo (MICRONAL DS 5040X). Como se puede observar, las microcápsulas de color blanco muestran una forma esférica y su tamaño varía entre 40µm y 235µm aproximadamente (coincidiendo con las indicaciones del fabricante 50µm -300µm).

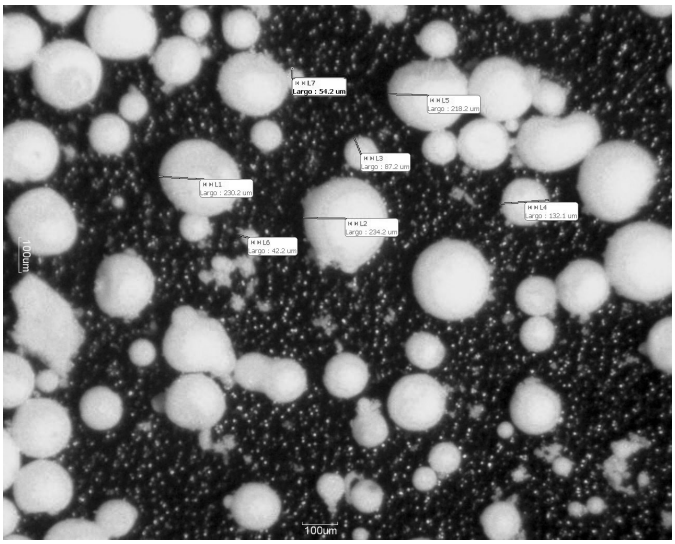

Figura 2. Imagen del PCM, parafina microencapsulada, utilizado en el trabajo - Laboratorio de Materiales de la Universidad de Alcalá. (Sección 10.1.1)

Una de las características principales de esta parafina es su temperatura de fusión, experimentando en 23ºC aproximadamente el cambio de fase de sólido a líquido y de líquido a sólido. Esta temperatura es muy próxima a la considerada como temperatura de confort en el interior de los edificios.

Por esta razón, se consideró una buena opción su utilización en este trabajo. Las microcápsulas de parafina vienen presentadas en forma de polvo, lo cual favorece a su integración y mezcla con el resto de los componentes que forman los morteros a estudiar.

Por todo lo anteriormente expuesto, este trabajo de tesis propone la evaluación de un nuevo mortero de cemento-cal con PCM y adiciones para la mejora del comportamiento térmico de los cerramientos. Para ello, se evaluó el comportamiento y propiedades del material desde el laboratorio, pasando por su comportamiento bajo diferentes condiciones ambientales y finalizando con la evaluación de su comportamiento dentro de un cerramiento multicapa. De esta forma, se pretende abarcar desde el inicio el material en si mismo hasta llegar a su aplicación.

1.2 OBJETIVOS

El objetivo principal de este estudio es el diseño, caracterización y evaluación de un nuevo material de cemento-cal con PCM para la mejora del comportamiento térmico de las fachadas existentes. Para lograr dicho objetivo, se diseñaron doce dosificaciones de morteros de cemento-cal, fibras de celulosa, sustitución del 50% de los áridos silíceos por áridos ligeros y se añadieron dos cantidades de PCM (10% y 20%). La investigación se compone de tres objetivos específicos que se detallan a continuación:

- **Diseño y caracterización de morteros de cemento-cal con PCM y adiciones para la mejora del comportamiento térmico de las fachadas existentes**. Para alcanzar este objetivo, se desarrolló un mortero que logre mejorar tanto su capacidad de aislamiento térmico como de acumulador térmico. Para la caracterización de estos morteros se definió un plan experimental que englobara los diferentes ensayos necesarios para la evaluación de propiedades físicas, mecánicas y térmicas de los morteros. Además, se desarrolló un modelo numérico a partir de los resultados experimentales obtenidos.

- **Evaluación térmica de morteros de cemento-cal con PCM durante ciclos de calentamiento y enfriamiento con técnicas no destructivas.** Para lograr este propósito, se utilizaron técnicas no destructivas para el análisis en cámara climática de los morteros bajo diferentes condiciones ambientales. Se detectó el estado del PCM durante los ciclos de calentamiento y enfriamiento con el uso de ondas de ultrasonidos. También se analizó la microestructura de cada uno de los morteros propuestos. Todo ello se evaluó a partir de los coeficientes de atenuación obtenidos con la atenuación de las ondas. El flujo de calor a través de los materiales y la entalpía se midió y evaluó para la realización de un análisis cualitativo y cuantitativo de la influencia del PCM en el comportamiento de los morteros.

- **Simulación experimental de modelos de cerramiento multicapa incluyendo morteros de cemento-cal con PCM.** Para la consecución de este objetivo, se simuló un cerramiento multicapa (revestimiento con placa de yeso al interior, mortero de cemento-cal con PCM, aislamiento térmico XPS, ladrillo de hueco doble y mortero de revestimiento al exterior) y se sometió a un ciclo de calentamiento y de enfriamiento para la evaluación de su comportamiento térmico. Para ello se registraron temperaturas en todas las capas del cerramiento, así como en la cara interior y exterior de este. Se midió el flujo de calor a ambos lados del cerramiento y se evaluó la cantidad de calor que fue capaz de pasar por todo el cerramiento y cuanto tardó en hacerlo en función de la composición de cemento-cal con PCM que estuviera incluida.

1.3 APORTES ORIGINALES

A continuación, se resumen los principales aportes de este trabajo de tesis:

- Diseño y caracterización física, mecánica y térmica de morteros en base cemento-cal con PCM y adiciones de fibras de celulosa y áridos ligeros (perlita). La adición de áridos ligeros y PCM disminuyeron la densidad y las resistencias a compresión y flexo tracción. Las conductividades térmicas no sólo variaron en función de los componentes de las dosificaciones, sino que también dependieron del estado sólido o líquido del PCM siendo más baja para el PCM en estado líquido. **(Secciones 10.1.1 y 10.1.2).**

- Evaluación e identificación de la relación entre los parámetros físicos, mecánicos y térmicos de los morteros estudiados. La influencia de la adición de PCM, fibras de celulosa, áridos ligeros y su combinación en estos parámetros también se identificó. **(Secciones 10.1.1 y 10.1.2).**

- Simulación numérica del comportamiento frente a la permeabilidad al agua a través de la absorción capilar a partir de los resultados experimentales obtenidos. Se encontró relación directa entre la adición de PCM y la capacidad del material para el transporte de agua por absorción capilar con la ayuda de los parámetros obtenidos en el modelo de Raleigh-Ritz. **(Sección 10.1.3).**

- Evaluación térmica con técnicas no destructivas de morteros de cemento-cal con PCM durante procesos de calentamiento y enfriamiento. Detección con ondas de ultrasonidos del cambio de fase del PCM (líquido-sólido) en el interior de los morteros durante los procesos de cambio de temperatura. Se analizó la capacidad de acumulación y de intercambio de energía con el entorno (entalpía)

de cada uno de los morteros estudiados. **(Sección 10.2.1, 10.2.2, 10.2.3 y 10.2.4).**

- Evaluación del comportamiento térmico de un sistema constructivo multicapa con morteros mejorados en su interior durante procesos de calentamiento y enfriamiento. Se detectó el retardo del paso del flujo de calor exterior-interior aportado por la adición de PCM y el aumento de dicho retardo con la adición de áridos ligeros. **(Sección 10.3.1).**

2. ORGANIZACIÓN DE LA TESIS

Este trabajo de tesis se presenta como un conjunto de compendio de publicaciones realizadas que incluyen 3 artículos publicados en revistas indexadas, un artículo finalizado y enviado para su publicación en una revista de investigación indexada, dos comunicaciones en congresos internacionales con publicación (capítulo de libro RILEM) y dos ponencias en congresos internacionales (uno como ponencia invitada) y un primer premio como mejor ponencia en un congreso de jóvenes investigadores nacional.

Los artículos publicados en revistas indexadas son los siguientes:

1. *Thermal enhanced cement-lime mortars with phase change materials (PCM), lightweight aggregate and cellulose fibers*, publicado en 2019 en la revista *Construction and Building Materials* que se encuentra en el primer cuartil (Q1) de la categoría de revistas de investigación de *Construction & Building Technology* y en el primer cuartil (Q1) de la categoría de *Civil Engineering*. (**Sección 10.1.2)**

2. *On the capillary wáter absorption of cement-lime mortars containing phase change materials: Experiments and simulations*, publicado en 2019 en la revista *Building Simulation* que se encuentra en el segundo cuartil (Q2) de la categoría de revistas de investigación de *Thermodynamics* y en el segundo cuartil (Q2) de la categoría de *Construction & Building Technology*. (**Sección 10.1.3)**

3. *PCM Cement-lime Mortars for Enhanced Energy Efficiency of Multilayered Building Enclosures under Different Climatic Conditions,* publicado en 2020 en la revista *Materials* que se encuentra en el segundo cuartil (Q2) de la categoría de revistas de investigación de *Materials Science.* (**Sección 10.3.1)**

Las dos comunicaciones en congresos internacionales con publicación en capítulo de libro fueron las siguientes:

1. *Phase Change Material cement-lime mortars for thermal retrofitting of façades*, presentado y publicado en el libro del 2nd International Conference on Bio-based Buildung Materials & 1st Conference on ECOlogical valorisation of GRAnular and Fibrous materials. (RILEM PRO 119). RILEM Publications SARL. Clermont-Ferrand (France), celebrado en 2017. (**Sección 10.1.1)**

2. *Thermal evaluation of cement-lime based materials with PCM.* Capítulo en libro de actas del 4th International Conference on Service Life Design for Infrastructures (RILEM PRO 125). RILEM Publications SARL., Delft (Países Bajos) celebrado en 2018. (**Sección 10.2.1)**

Una ponencia invitada en un congreso internacional y otra ponencia galardonada con el 1er premio a la mejor ponencia:

1. Ponencia invitada con el título *Evaluación De Morteros De Cemento-cal Con Materiales De Cambio De Fase (pcm) Para La Rehabilitación De Fachadas*, dentro del V Congreso Hispano-Luso de Cerámica y Vidrio / LVI Congreso Nacional de la SECV celebrado en Barcelona en 2018. (**Sección 10.2.3)**

2. Primer premio a la mejor ponencia con el título *Morteros funcionales de cemento-cal con PCM para la rehabilitación de fachadas* en las I Jornadas de Jóvenes Científicos en Materiales de Construcción co-organizado por el Instituto Eduardo Torroja,- CSIC, instituto de Cerámica y Vidrio – CSIC, la Universidad Politécnica de Madrid, la Real Sociedad Española de Química (RSEQ) y la Sociedad Española de cerámica y vidrio, celebrado en Madrid en 2018. (**Sección 10.2.4)**

El trabajo se organiza en 10 capítulos que incluyen un resumen amplio del trabajo y las publicaciones realizadas. A continuación, se describen brevemente los contenidos de cada uno de ellos:

En el primer capítulo se introduce el tema de estudio elegido y la hipótesis de trabajo. Se realiza una descripción de los antecedentes y estado de la cuestión. A partir de la identificación de la problemática y de las necesidades existentes se establecen tres objetivos específicos. Estos objetivos sirven como punto de partida para el desarrollo de los capítulos 3, 4 y 5 y de las publicaciones de investigación descritas en la sección 10.

El capítulo 2 es el actual, e incluye una descripción detallada de la organización de la tesis.

El tercer capítulo incluye el diseño y caracterización de los morteros de cemento-cal con PCM y adiciones. Se incorpora una evaluación y análisis de los resultados obtenidos de las propiedades físicas, mecánicas y térmicas de los morteros. Estos resultados se detallan en las secciones 10.1.1 y 10.1.2. Además, contiene una simulación numérica a partir de los resultados experimentales obtenidos en laboratorio que se puede ver en la sección 10.1.3.

En el cuarto capítulo se presenta la evaluación térmica con técnicas no destructivas de los morteros de cemento-cal con PCM durante procesos de calentamiento y enfriamiento. Destaca la detección del estado del PCM a lo largo de cada proceso y la evaluación de la capacidad de acumulación térmica de cada una de las mezclas. Este capítulo está basado en los resultados que se recogen en las secciones 10.2.1., 10.2.2., 10.2.3 y 10.2.4.

La simulación experimental de modelos de cerramiento multicapa mejorados con morteros de cemento-cal con PCM se incluye en el capítulo 5. Se presenta la evaluación de los parámetros térmicos obtenidos durante los procesos de calentamiento y enfriamiento. Los resultados publicados en relación con este capítulo pueden verse más detallados en la Sección 10.3.1.

En el capítulo 6 y 7 (en inglés y alemán) se resumen las principales conclusiones a partir de los resultados obtenidos en los capítulos anteriores.

En el capítulo 8 se presentan futuras líneas de investigación sobre morteros de cemento-cal con PCM a partir de las conclusiones obtenidas.

Las referencias bibliográficas más significativas encontradas en la literatura a lo largo de todo el trabajo de tesis se recogen en el capítulo 9.

En el capítulo 10 se recogen las publicaciones realizadas a partir de cada uno de los tres objetivos específicos planteados en este trabajo.

A continuación, se detallan y clasifican las publicaciones realizadas según el objetivo al que se refieren:

- **Sección 10.1. Diseño y caracterización de los morteros de cemento-cal con PCM y adiciones para la mejora del comportamiento térmico de las fachadas existentes.**
    - **10.1.1 (Capítulo de libro internacional)** Phase Change Material cement-lime mortars for thermal retrofitting of facades, 2017.

- **10.1.2 (Artículo en revista indexada)** Thermal enhanced cement-lime mortars with phase change materials (PCM), lightweight aggregate and cellulose fibers, 2019.
- **10.1.3 (Artículo en revista indexada,)** On the capillary water absorption of cement-lime mortars containing phase change materials: Experiments and simulations, 2019.

- **Sección 10.2. Evaluación térmica de los morteros de cemento-cal con PCM con técnicas no destructivas durante procesos de calentamiento y enfriamiento.**

  - **10.2.1 (Capítulo de libro internacional)** Thermal evaluation of cement-lime based materials with PCM, 2018.
  - **10.2.2 (Artículo enviado para publicación)** Novel thermal characterization with NDT of PCM cement-lime mortars with lightweight aggregate and cellulose fibres
  - **10.2.3 (Ponencia invitada en Congreso Internacional)** Thermal evaluation of cement-lime based materials with PCM, 2018
  - **10.2.4 (Primer Premio a la mejor presentación)** Morteros funcionales de cemento-cal con PCM para la rehabilitación de fachadas. (2018)

- **Sección 10.3. Simulación experimental de modelos de cerramiento multicapa incluyendo morteros de cemento-cal con PCM.**

  - **10.3.1 (Artículo en revista indexada,)** PCM Cement-lime Mortars for Enhanced Energy Efficiency of Multilayered Building Enclosures under Different Climatic Conditions, 2020.

La fase experimental de esta tesis se realizó en el Laboratorio de Materiales de Construcción de la Escuela de Arquitectura de la Universidad de Alcalá. También se realizaron ensayos y usaron equipos en las instalaciones de los Departamentos de Arquitectura y Física y Matemáticas de la Universidad de Alcalá; en el laboratorio del grupo de investigación ENEDI del Departamento de Máquinas y Motores Térmicos de la Escuela Universitaria de Ingeniería Técnica de Minas y Obras Públicas de la Universidad del País Vasco y en el laboratorio del Institut für Werkstoffe im Bauwesen de la Technische Universität Darmstadt (Alemania).

Además, durante el desarrollo de la tesis la autora realizó una estancia de 3 meses de duración en el Institut für Werkstoffe im Bauwesen de la Technishce Universität Darmstadt (Alemania), bajo la supervisión del Prof. Dr. -ir Koenders en donde se estableció una colaboración cuyo resultado forma una parte de este trabajo de tesis.

3. DISEÑO Y CARACTERIZACIÓN DE MORTEROS DE CEMENTO-CAL CON PCM Y ADICIONES PARA LA MEJORA DEL COMPORTAMIENTO TÉRMICO DE FACHADAS.

3.1 INTRODUCCIÓN

Debido a la necesidad de mejorar la eficiencia energética de los edificios existentes a través de la mejora del comportamiento térmico de sus fachadas, se están llevando a cabo numerosos estudios para el desarrollo de nuevos materiales que satisfagan las nuevas exigencias y necesidades requeridas (Pavlík, Z 2009, Palomar I, 2015, Veiga R. 2017). Entre los diferentes materiales estudiados, se encuentran los morteros de cemento - cal con diferentes adiciones para la mejora del comportamiento térmico de los mismos (Stefanidou M, 2014, Sala. E, 2016). Según estas investigaciones, algunos de los componentes que mejor han funcionado para la mejora del comportamiento térmico de los morteros son las fibras de celulosa (Bentchikou M., 2012, Palomar I. 2015) y los áridos ligeros como la perlita expandida (Silva L.M, 2010, Palomar I. 2015).

Otros materiales que aportan mejoras en el comportamiento térmico de los edificios son los materiales de cambio de fase (Phase Change Materials – PCM) (Lucas s, 2010, Ali Memon, S, 2014). Los PCM abordan la mejora del comportamiento térmico de los materiales a través del calor latente y por tanto de la acumulación térmica (Pavlík Z. 2016, Vankateswara V, 2018). Por esta razón, en este trabajo se plantea el desarrollo de un nuevo material que de forma simultánea tenga la capacidad de aislar térmicamente y de acumular energía a través del propio material. De esta forma se pretende que el nuevo material propuesto mejore el comportamiento térmico de las fachadas existentes sobre las que se aplique.

Con el fin de conocer el funcionamiento de este nuevo material se realizó una caracterización completa del comportamiento de los morteros en estado fresco y endurecido. En ella se midieron, con diferentes técnicas experimentales, las propiedades físicas, mecánicas y térmicas de los doce morteros analizados. También se realizó una caracterización microestructural de los mismos. Estos morteros incluyen

la adición a un mortero base de cemento cal de fibras de celulosa, áridos ligeros (ambos como aislantes térmicos) y PCM (como acumulador térmico) en diferentes cantidades. Además, se estudió la influencia de los diferentes componentes en el comportamiento no sólo de los morteros si no que también del propio PCM y cómo puede afectar al comportamiento de los morteros y a la formación de su microestructura.

3.2 METODOLOGÍA PARA EL DISEÑO Y LA CARACTERIZACIÓN DE MORTEROS

3.2.1 Diseño del mortero

Para el diseño de los morteros de cemento-cal con PCM y la adición de fibras de celulosa y áridos ligeros (perlita) se planteó el esquema de la Figura 3 para la definición del criterio de diseño de las dosificaciones a estudiar.

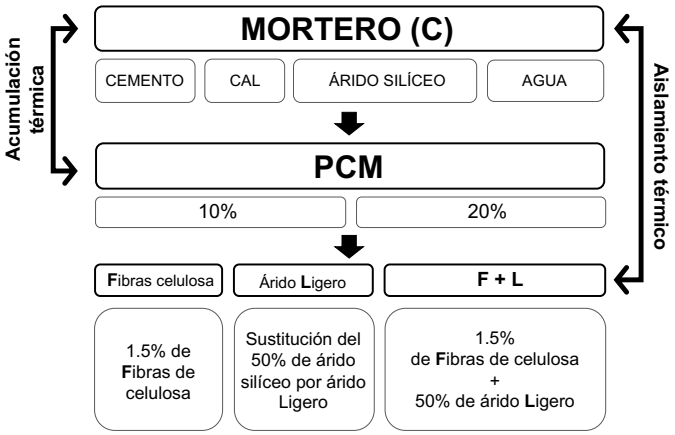

Figura 3. Esquema para la definición del criterio de diseño de las dosificaciones. (Sección 10.1.2)

El principal objetivo de este estudio fue el diseño de un mortero que aunara, por un lado, la capacidad de aislamiento térmico por parte del material, y por otro, la capacidad de acumulador térmico del mismo.

Primero, se diseñó un mortero base con cemento blanco (posibilitando la opción de pigmentación si fuera necesario) tipo BLII/B-L acorde a la UNE-EN 197-1, cal aérea (por

su versatilidad, gran adaptabilidad a los materiales existentes y por la posibilidad de incorporación de pigmentos inorgánicos que modifiquen el color de los materiales) con clasificación CL 90-S según normativa europea UNE-EN 459-1, árido silíceo (arena con un tamaño de grano de 0-4 mm) y agua.

Posteriormente, con el fin de dotar al mortero de capacidad de aislamiento térmico, se le añadieron dos tipos de adiciones. Por un lado, fibras de celulosa (con un tamaño de 1mm y ø20μm) y, por otro, áridos ligeros más concretamente, perlita expandida.

La cantidad de adición de cada uno de los componentes se estableció a partir de la bibliografía existente, donde otros autores han estudiado y trabajado las cantidades optimas para cada una de las adiciones (Cunha S, 2016, Lucas S, 2010).

De acuerdo con la literatura, se añadió, por un lado, un 1.5% (en volumen) de fibras de celulosa, y por otro, se sustituyó el 50% de los áridos silíceos por el 50% de perlita expandida. Por último, se realizó una dosificación con la combinación de ambas adiciones.

Con el fin de dotar a los morteros de capacidad acumuladora, se añadieron dos cantidades de PCM (parafina microencapsulada de 50-300μm de tamaño y con una temperatura de fusión de 23ºC aproximadamente): 10% y 20% de PCM del volumen del mortero en estado fresco.

Por lo tanto, en este trabajo se analizó un total de doce dosificaciones diferentes: tres morteros de referencia con 0%, 10% y 20% de PCM; tres morteros con la adición de fibras de celulosa y 0%, 10% y 20% de PCM; tres morteros con la sustitución del 50% de los áridos silíceos por áridos ligeros (perlita) y, por último, tres dosificaciones con la combinación de ambas adiciones (fibras de celulosa y perlita) y 0, 10 y 20% de PCM.

A continuación, la Tabla 1 muestra las cantidades utilizadas para cada uno de los morteros evaluados en este trabajo tomando como referencia el criterio de diseño mostrado en la Figura 3.

Tabla 1. Dosificaciones de los morteros de cemento-cal con PCM.

(los componentes se presentan en kg).

	C	C_{10}	C_{20}	CF	CF_{10}	CF_{20}	CL	CL_{10}	CL_{20}	CLF	CLF_{10}	CLF_{20}
Cemento BLII/B-L 32.5N	348	348	348	348	348	348	348	348	348	348	348	348
Cal aérea CL 90-S	55	55	55	55	55	55	55	55	55	55	55	55
Árido silíceo (0-4)	1403	1403	1403	1403	1403	1403	702	702	702	702	702	702
PCM	-	42.3	84.6	-	42.3	84.61	-	42.3	84.6	-	42.3	84.6
Fibras Celulosa	-	-	-	0.40	0.62	0.66	-	-	-	0.49	0.62	0.59
Perlita	-	-	-	-	-	-	94	94	94	94	94	94
Agua añadida	220	140	200	220	180	240	240	240	250	240	305	380
a/cg	0.73	0.53	0.68	0.73	0.63	0.78	0.69	0.69	0.71	0.69	0.85	0.79
D_{seca} (kg/m^3)	1400	1448	1357	1387	1260	1440	845	964	868	822	-	-
$D_{húmeda}$ (kg/m^3)	2264	1857	1937	2165	1904	1885	1711	1682	1562	1854	1433	1561

La relación utilizada de cemento, cal y áridos fue de 1: 0.5: 4.5 en volumen. Para la relación agua/conglomerante se tuvo en cuenta la humedad de los áridos silíceos cuyo valor ascendía a 5.3%. Esta relación se ajustó para conseguir una consistencia plástica similar para todos los morteros (UNE-EN 1015-3:2000).

3.2.1 Plan experimental

Para la caracterización física, mecánica y térmica de los morteros de cemento-cal con PCM y la adición de fibras de celulosa y áridos ligeros se realizaron diferentes ensayos en laboratorio. La Tabla 2 presenta los diferentes parámetros evaluados, el

procedimiento de ensayo que se llevó a cabo y el tipo de probeta que se utilizó para las medidas realizadas en laboratorio.

Tabla 2. Ensayos realizados para la caracterización de los morteros. (Tabla adaptada de Palomar. I, 2017b)

ENSAYOS EXPERIMENTALES			
Evaluación	**Medida**	**Referencia**	**Probeta (mm)**
Estado fresco			
Trabajabilidad	Consistencia Tensión de fluencia	UNE-EN 1015-3 Murata (1984)	Altura 60 Øsup 70 Øsup 100
Efecto ambiental	Retracción	Barluenga (2007)	500 x 100 x 50
Estado endurecido			
Propiedades físicas	Densidad aparente	UNE-EN 1015-10	40 x 40 x 160
	Porosidad abierta	UNE-EN 1015-10	40 x 40 x 160
	Absorción por succión capilar	UNE-EN 1015-18	40 x 40 x 160
	Permeabilidad al vapor de agua	UNE-EN 1015-19	Ø 35
Propiedades mecánicas	Resistencia a compresión	UNE-EN 1015-11	40 x 40 x 40
	Resistencia a flexotracción	UNE-EN 1015-11	40 x 40 x 160
	Constantes elásticas	Boumiz (1996)	40 x 40 x 160
Microestructura	Morfología	MEB	-
Propiedades térmicas	Conductividad térmica	UNE-EN ISO 8990	210 x 210 x 25
	Entalpía	DSC- IEA task 42-Annex 29	-

A continuación, se describen las técnicas de ensayo en relación con las propiedades térmicas y de evaluación mediante técnicas no destructivas:

Para la evaluación del comportamiento térmico de los morteros en estado endurecido se realizaron dos tipos de ensayos que permitieron medir la conductividad térmica de los morteros (λ) y la capacidad de acumulación térmica de estos en función de la temperatura durante procesos de calentamiento y enfriamiento (entalpía):

Conductividad térmica

Para obtener los valores de conductividad térmica se utilizó una cámara aislada térmicamente. Se establecieron dos escenarios: En el primero la temperatura interior media de las placas se situó por debajo de los 23ºC (temperatura de fusión de PCM). En el segundo, la temperatura interior media de las placas se situó por encima de la temperatura de fusión del PCM. Una vez se alcanzó el régimen estacionario para cada uno de los dos escenarios se calcularon λ_s y λ_l (λ_s donde T<23ºC y λ_l donde T>23ºC) de acuerdo con la formulación de la normativa de referencia (UNE-EN ISO 8990:1996).

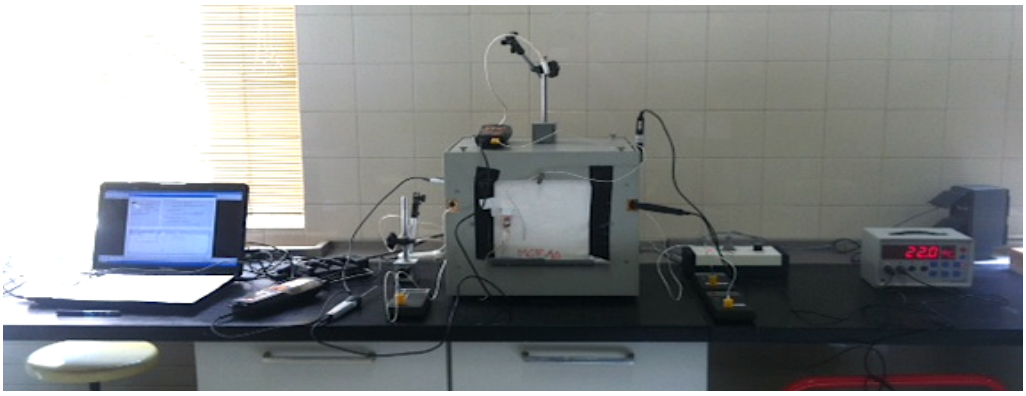

Figura 4. Ensayo de hot-box (caja caliente) para condutividad térmica – Laboratorio del Departamento de Física y Matemáticas de la UAH.

Entalpía

Para el cálculo de la entalpía en un intervalo de temperatura (entre 10ºC y 28ºC) durante ciclos de calentamiento y enfriamiento se utilizó el equipo DSC (Calorimetría diferencial de barrido) (Jin X. 2014, Drissi S, 2015).

El equipo utilizado para la evaluación de la entalpía en función de la temperatura fue un Mettler Toledo DSC1 (Figura 5). El procedimiento estandarizado usado para el cálculo de la entalpía en función de la temperatura fue el IEA Task 42 Annex 29 (Gschwander S. , 2015, Ristić A. 2016). Para ello se introdujo material de cada una de las doce dosificaciones en crisoles de aluminio de 25ml. Estos se introdujeron finalmente en equipo (el procedimiento de ensayo completo está explicado con detalle en la **Sección 10.1.2**).

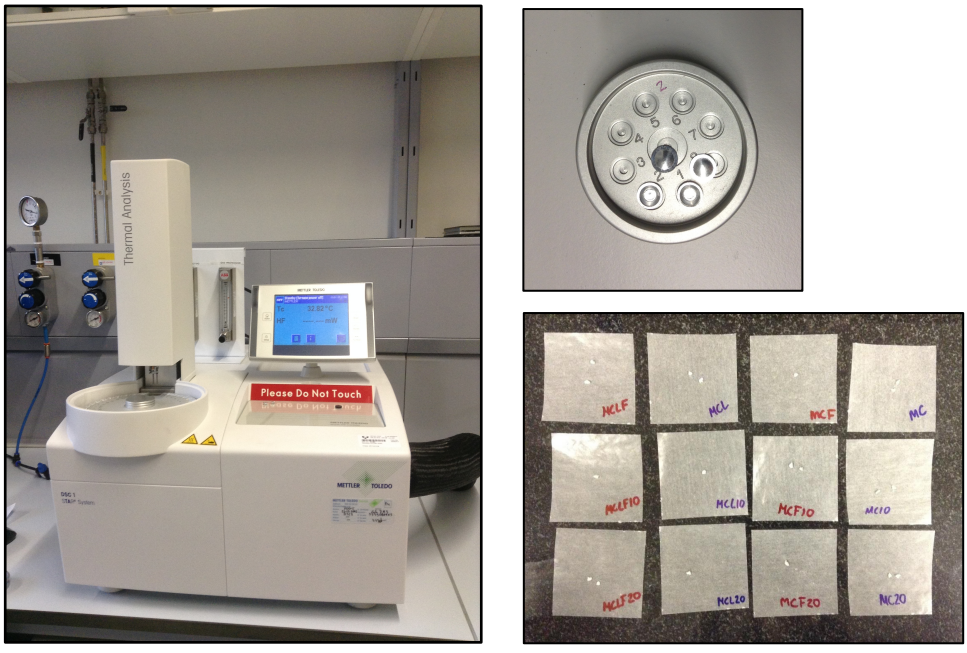

Figura 5. Ensayo para determinar la entalpía. DSC, calorimetría diferencial de barrido – Departamento de Máquinas y Motores Térmicos de la Escuela Universitaria de Ingeniería Técnica de Minas y Obras Públicas de la Universidad del País Vasco.

Técnicas no destructivas

Para la evaluación de las propiedades con técnicas no destructivas, se midió sobre las probetas de 40 x 40 x160 mm el tiempo de transmisión y la amplitud de dos ondas de ultrasonidos (ondas de compresión, Pw y cortante, Sw) usando transductores de 54 y 250 kHz respectivamente. De esta forma, se calcularon las constantes elásticas; módulo de Young (E), módulo de compresibilidad (K) y el coeficiente de Poisson (v). El montaje, procedimiento y métodos de cálculo puede encontrarse detallado en las **Secciones 10.1.1 y 10.1.2.**

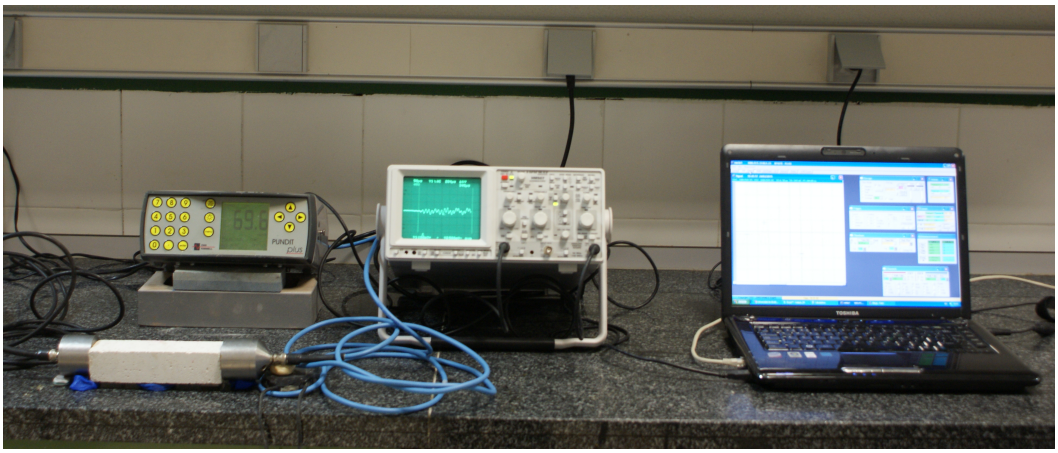

Figura 6. Ensayo para analizar el tiempo de transmisión y la amplitud de las ondas de ultrasonidos – Laboratorio de Materiales de la Universidad de Alcalá.

3.3 RESULTADOS Y DISCUSIÓN

En este apartado se presentan los resultados obtenidos en el laboratorio correspondientes a las propiedades en estado fresco y endurecido de los morteros, así como su microestructura y las relaciones entre los diferentes parámetros.

En estado fresco se midió la retracción durante 24 horas y el inicio de esta para todas las dosificaciones sin PCM y con 20% de PCM.

Por otro lado, las propiedades en estado endurecido se ensayaron pasados los 28 días de curado del material. Se midieron (con las técnicas mencionadas en el apartado anterior 3.2.1) las propiedades físicas, mecánicas y térmicas de las distintas dosificaciones objeto de este trabajo.

En cuanto a las propiedades físicas, se evaluaron la densidad aparente (DA), la porosidad abierta (PA), la absorción de agua por succión capilar (AC), así como la permeabilidad al vapor de agua en estado húmedo (VD).

También se obtuvieron los valores de resistencia a compresión y de resistencia a flexotracción de cada una de las doce dosificaciones. Junto con estos valores se estimaron las constantes elásticas como el módulo de Young (E), el módulo de compresibilidad (K) y el coeficiente de Poisson (v). Estos tres últimos parámetros se calcularon con la técnica no destructiva de ultrasonidos (Palomar I, 2017, Barluenga G, 2018).

En cuanto a las propiedades térmicas, se midió la conductividad térmica en dos situaciones diferentes dependiendo del estado (λ_s =sólido o λ_l =líquido) en el que se encontrase el PCM (Guardia C, 2017). λ_s se midió cuando la temperatura media del material se encontró estable por debajo de 23ºC, asegurando de esta forma el estado sólido del PCM. λ_l se midió una vez la temperatura del mortero estuvo estable a más de 23ºC, asegurado de esta forma el PCM en estado líquido.

Además, se realizó un análisis de la estructura del material a través de las imágenes obtenidas con el ensayo de microscopia electrónica de barrido.

Por último, a partir de los resultados obtenidos tras la evaluación de la absorción de agua por succión capilar se desarrolló una simulación numérica de la evolución de AC a lo largo del tiempo, más concretamente, a lo largo de las 24 horas que duró el ensayo.

3.3.1 Caracterización e influencia de la combinación del PCM con las diferentes adiciones en las propiedades físicas y mecánicas de los morteros.

La Tabla 3 muestra un resumen de los valores obtenidos para cada uno de los parámetros de caracterización de los morteros descritos en el apartado 3.2.1.

Los resultados de retracción libre a lo largo de las primeras 24 horas muestran que todos los morteros retrajeron entre 0.16mm/m (CLF) y 1.94mm/m (C_{20}). La retracción con la adición de PCM aumentó y el inicio de la misma se adelantó.

Tabla 3. Propiedades físicas y mecánicas de los morteros de cemento-cal con PCM.

	C	C_{10}	C_{20}	CF	CF_{10}	CF_{20}	CL	CL_{10}	CL_{20}	CLF	CLF_{10}	CLF_{20}
Estado fresco												
Consistencia mm	178	170	166	160	173	170	195	173	170	170	180	170
a/cg	0.73	0.53	0.68	0.73	0.63	0.78	0.69	0.69	0.71	0.69	0.85	0.79
Retracción libre mm/m	1.30	-	1.94	0.98	-	0.66	0.24	-	0.42	0.16	-	0.74
T.inicial h min	2h10	-	2h00	2h10	-	1h50	2h40	-	2h00	3h10	-	1h40
Prop. Físicas												
Densidad aparente kg/m^3	1900	1690	1600	1960	1720	1660	1430	1180	1270	1430	1110	1160
Porosidad abierta %	19.56	16.68	17.72	18.93	16.90	16.77	20.95	22.99	23.33	23.94	22.10	23.09
Ab.capilar $kg/m^2min^{0.5}$	1.02	0.48	0.48	1.08	0.45	0.28	0.35	0.52	0.53	0.72	0.53	0.45
VD (-)	4.13	4.02	4.29	3.85	3.57	3.47	3.54	3.63	3.62	3.80	3.12	3.26
Prop Mecánicas												
Resist. Compresión MPa	14.33	7.30	7.17	10.83	6.83	5.83	9.40	5.33	6.00	12.67	4.60	5.33
Resist. Flexión MPa	3.36	2.26	2.40	2.66	1.98	2.20	3.18	2.24	1.79	3.46	1.84	2.16
E GPa	15.67	9.44	8.31	13.59	9.55	8.25	9.13	5.02	4.48	9.57	3.96	4.29
K GPa	8.59	6.29	6.46	9.29	6.44	4.62	5.85	2.94	3.23	6.06	2.49	2.77
v	0.19	0.25	0.29	0.26	0.25	0.20	0.24	0.22	0.27	0.23	0.23	0.24

En referencia a los resultados obtenidos de las propiedades físicas, se observó cómo la adición de PCM originó en todas de las dosificaciones un descenso en la densidad aparente (DA) de aproximadamente $300kg/m^3$, variando los valores entre $1960kg/m^3$ (CF) y $1110kg/m^3$ (CLF_{10}). La porosidad abierta (PA) varió entre 16.68% (C_{10}) y 23,94% (CLF). La combinación del PCM con los áridos ligeros aumentó considerablemente la PA de los morteros (Palomar I, 2015, Silva L.M, 2010). Por el contrario, la combinación de PCM con fibras de celulosa disminuyó la porosidad abierta respecto a los valores obtenidos en la dosificación de referencia (C) (Lucas.S, 2013).

Respecto a los valores de absorción de agua por succión capilar (AC), la dosificación CF_{20} (0.28kg/$m^2$$min^{0.5}$) presentó el valor más bajo mientras que la dosificación CF el más alto (1.08kg/$m^2$$min^{0.5}$). Observando estos resultados se puede decir que el PCM en combinación con la perlita aumenta la AC del material, mientras que en combinación con la fibra o la fibra más la perlita, disminuye la AC. En cuanto a los resultados obtenidos de VD no se identificaron relaciones directas con la adición de PCM, los áridos ligeros o las fibras de celulosa.

A partir de estos resultados, se establecieron relaciones entre los diferentes parámetros para determinar el efecto de las composiciones de los morteros en la microestructura de estos y, por tanto, en la porosidad y propiedades de transporte de. La Figura 7 muestra la relación entre la absorción capilar de agua y la porosidad abierta de los morteros. En general, se observa que existe una relación lineal entre la porosidad abierta y la absorción de agua por succión capilar. Del mismo modo, se observan dos grupos de comportamientos en función de las adiciones: sin o con perlita, siendo para las dosificaciones sin perlita un 20% menor la porosidad abierta que para las mezclas con PCM. La adición de PCM en combinación con los áridos ligeros disminuye AC.

Por lo tanto, como era lo esperado (Lucas S, 2013), los áridos ligeros influyen considerablemente en la estructura porosa de los morteros mientras que las microcápsulas de PCM actúan como relleno de los huecos libres dentro de la microestructura, disminuyendo tanto la AC como la PA.

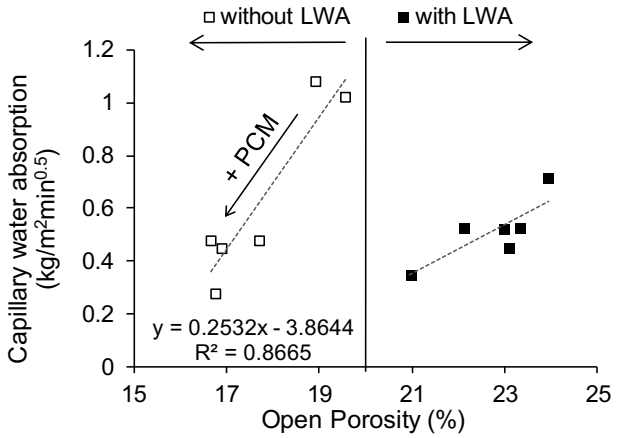

Figura 7. Efecto del PCM y áridos ligeros en la relación entre la absorción capilar y la porosidad abierta de los morteros (Sección 10.1.2)

Los resultados referentes a las propiedades mecánicas se presentan también en la Tabla 3. Las resistencias a compresión variaron entre 4.6MPa (CLF_{10}) y 14.33MPa (C) mientras que los valores de resistencia a flexotracción variaron entre 1.79MPa (CL) y 3.46MPa (CLF). La adición de PCM disminuyó en todos los casos la resistencia a compresión de los morteros (Cunha S., 2015, Haurie L., 2016) (en todos los casos, los valores de resistencia a compresión se encuentran por encima de los 3.5MPa exigidos por la norma UNE-EN 998-1 para morteros de rehabilitación de grado CS-III). Sin embargo, no se observa relación directa entre la resistencia a flexotracción y la adición de PCM u otras adiciones. Además, el módulo de Young varió entre 3.96 GPa (CLF_{10}) y 15.67 GPa (C), K entre 2.49 GPa (CLF_{10}) y 9.29 GPa (CF) y el coeficiente de Poisson entre 0.19 y 0.29. Se puede observar como E disminuyó, como era lo esperado (Silva L.M., 2010, Palomar, 2017), con la adición de PCM y de áridos ligeros. Sin embargo, no se observa ninguna relación entre la adición PCM y los valores obtenidos para K y v.

En la Figura 8 se muestra la influencia que tiene la composición de los morteros en las propiedades mecánicas de los mismos. Más concretamente se puede ver como existe una relación entre la resistencia a compresión y la porosidad abierta de los morteros. La

Figura 8 muestra que la adición de los áridos ligeros disminuyó levemente la resistencia a compresión aumentando sin embargo en mayor medida la porosidad abierta.

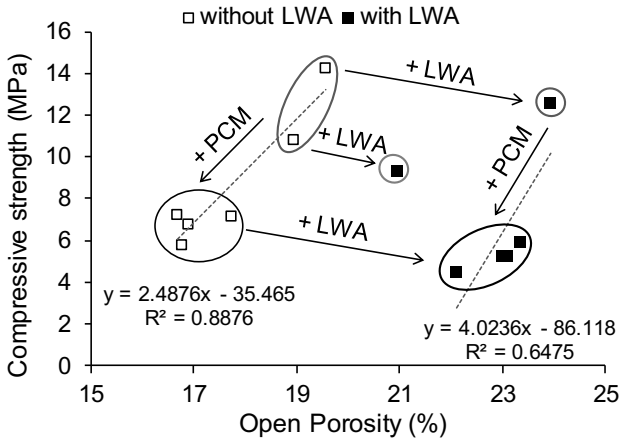

Figura 8. Efecto del PCM y áridos ligeros en la relación entre la resistencia a compresión y la porosidad abierta de los morteros). (Sección 10.1.2)

Por el contrario, la adición de PCM produjo el efecto inverso, reduciendo levemente la porosidad abierta mientras que disminuyó en mayor medida la resistencia a compresión. Esta situación puede ser consecuencia de la relación agua/conglomerante, ya que las dosificaciones con PCM, como se observa en la Tabla 3, requirieron más agua para conseguir una consistencia plástica de los morteros y esta adición de agua disminuyó lla resistencia a compresión (Figura 9a).

Junto con la relación existente entre la resistencia a compresión y la cantidad de agua añadida a la mezcla, la Figura 9b muestra la relación entre la resistencia compresión y el módulo de Young (E). Se puede ver que la adición de los áridos ligeros supuso una disminución leve de ambos parámetros (resistencia a compresión y E). La adición de PCM originó este mismo efecto, pero mucho más pronunciado. Es decir, en este caso la adición de PCM influyó más en las propiedades mecánicas que las otras adiciones.

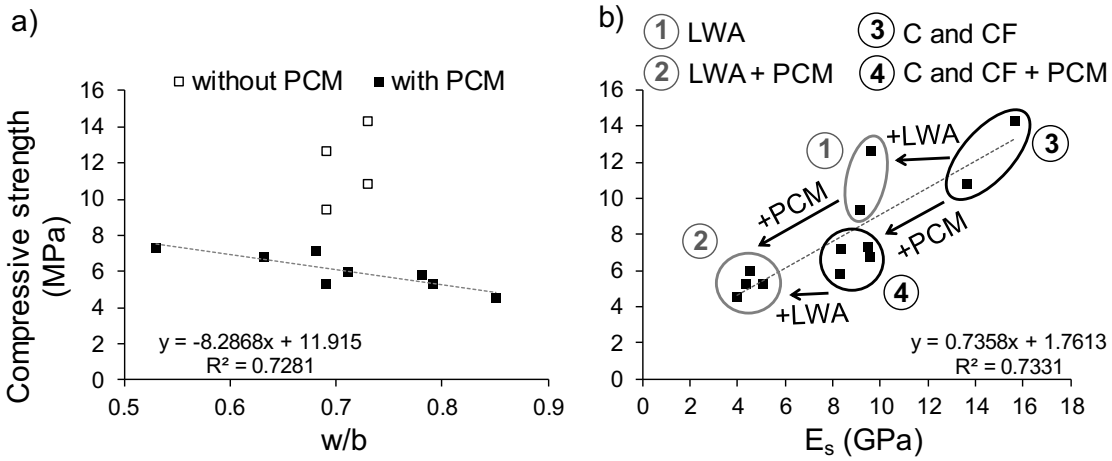

Figura 9. Efecto del PCM y áridos ligeros en la relación entre la resistencia a compresión y: (a) a/cg (b) Módulo de Young (E). (Sección 10.1.2)

3.3.2 Caracterización de propiedades térmicas e influencia del PCM y de las diferentes adiciones en el comportamiento térmico de los morteros.

La Tabla 4 presenta los valores obtenidos de conductividad térmica para cada una de las dosificaciones en ambos estados del PCM (sólido o líquido). λ_s (PCM sólido) presentó valores entre 0.17 W/mK (CL) y 0.40W/mK (CF_{10}) mientras que los valores de λ_l (PCM en estado líquido) variaron entre 0.15W/mK (CLF_{20}) y 0.32W/mK (C_{10}). En todos los casos el estado del PCM afectó en la conductividad térmica siendo los valores más elevados para λ_s (PCM en estado sólido) que para λ_l (PCM en estado líquido).

Tabla 4. Conductividad térmica de los morteros de cemento-cal con PCM en estado sólido y líquido.

	C	C_{10}	C_{20}	CF	CF_{10}	CF_{20}	CL	CL_{10}	CL_{20}	CLF	CLF_{10}	CLF_{20}
λ_s W/mK	0.23	0.26	0.20	0.29	0.40	0.30	0.17	0.27	0.29	0.22	0.25	0.23
λ_l W/mK	0.21	0.32	0.28	0.21	0.26	0.23	0.16	0.19	0.18	0.19	0.21	0.15

La Figura 10 muestra la relación entre la estructura porosa de los materiales y su comportamiento térmico dependiendo del estado del PCM y de los componentes que formaran el material.

Se puede ver como la perlita disminuyó la conductividad térmica a la par que aumentó la porosidad abierta de los morteros. Sin embargo, con la adición de fibras de celulosa no se observaron cambios significativos.

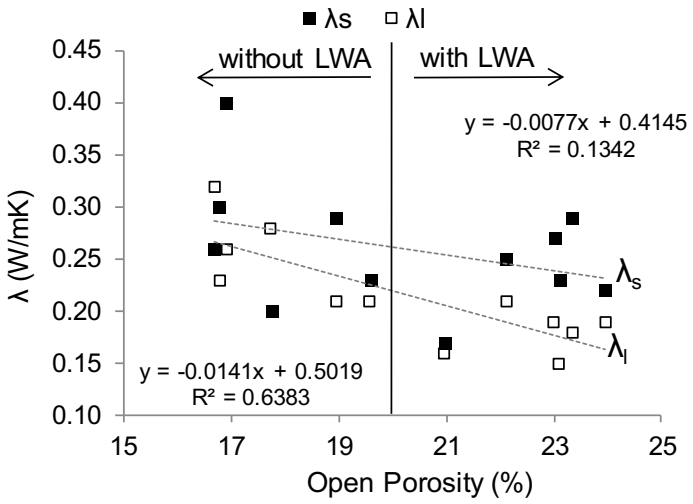

Figura 10. Conductividad térmica (λ) de los morteros con el PCM en estado líquido. (Sección 10.1.2)

La adición de fibras de celulosa, áridos ligeros y PCM influyó igualmente en la entalpía de los morteros (Figura 11). El PCM aumentó en todos los casos la entalpía de los morteros dentro del rango de temperatura ensayado (entre 10ºC y 28ºC).

Sin embargo, la cantidad de PCM añadida no mostró una relación lineal con el aumento de entalpía de los morteros. Más concretamente, C_{20} presentó los valores más bajos de entalpía entre las dosificaciones con 20% de PCM mientras que CL_{20} mostró los más altos. Estos resultados establecen que cuando la dosificación estuvo compuesta por áridos ligeros, la dosificación precisó de una mayor energía (mayor entalpía) para el

calentamiento del material consecuencia de la capacidad de aislante térmico de los áridos ligeros. la Tabla 4 muestra que las dosificaciones con áridos ligeros presentaron una conductividad térmica más baja que el resto de las dosificaciones. Por esta razón, la perlita redujo el flujo de calor a través del mortero hacia las cápsulas de PCM impidiendo el paso de calor. Por el contrario, las fibras de celulosa no aumentaron la entalpía de los morteros respecto al mortero de referencia.

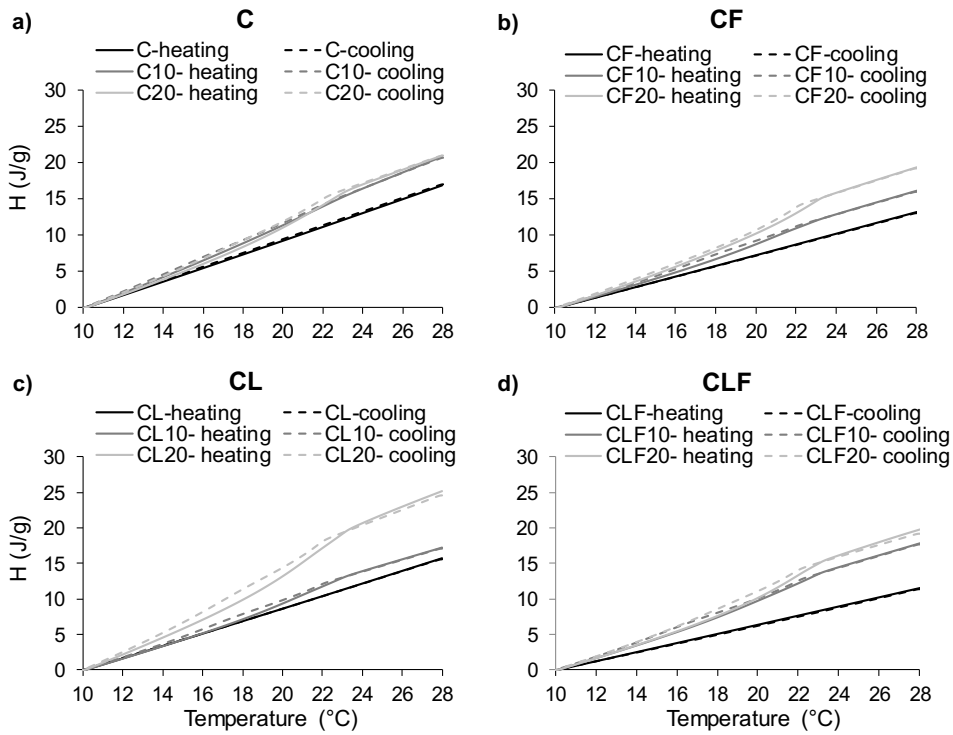

Figura 11. Efecto del PCM y de las adiciones (fibras de celulosa y áridos ligeros) en la entalpía de los morteros durante ciclos de calentamiento y enfriamiento (Sección 10.1.2).

3.3.3 Caracterización de la microestructura y comportamiento del PCM dentro de los morteros.

La Figura 12 muestra varias imágenes del mortero de referencia con 20 % de PCM (C_{20}) a una temperatura inferior a 23ºC. Es decir, el PCM en estado sólido. Estas imágenes fueron realizadas con microscopía electrónica de barrido durante la estancia en la

Technische Universität Darmstadt en el laboratorio del Insitut für Werkstoffe im Bauwesen. En ellas se muestran dos microcápsulas rotas (una en la Figura 12a y otra en la 12b y 12c) perfectamente integradas en la pasta de cemento-cal. Se puede observar que no existió dispersión de la parafina por la pasta (Drissi S., 2015, Jayalath A., 2016). Por esta razón, la rotura de las microcápsulas estuvo asociada a la preparación de la muestra para el propio ensayo, para el cual se utilizaron muestras de pequeño tamaño.

En las Figuras 12a y 12b se distinguen las diferentes partes que forman la microcápsula de PCM. Por un lado, se ve la cáscara que forma las microcápsulas (Shell) y es encargada de mantener la parafina encapsulada. Además, se observan dos tipos de esferas de parafina en el interior de las cápsulas. El primero, está formado por microesferas adosadas a la cáscara y el segundo trata de esferas de mayor tamaño que se encuentran en el centro de la microcápsula.

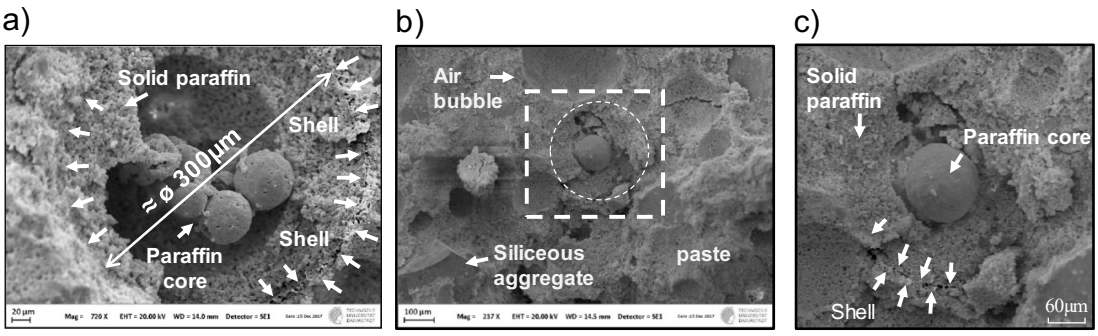

Figura 12. Imagen una microcápsula de PCM rota dentro del mortero de referencia (C) – Laboratorio de Institut für Wrkstoffe im Bauwesen de la Technische Universität Darmstadt (Alemania) (Sección 10.1.2).

A partir de estas imágenes se pudo determinar el proceso de solidificación de la parafina y su comportamiento en el interior de la microcápsula. La Figura 13 muestra un esquema de este proceso.

Se parte de la parafina en estado líquido en el interior de la cápsula, es decir el material está sometido a una temperatura superior a 23ºC (temperatura de fusión del PCM utilizado en este trabajo). Con la parafina en estado líquido comienza el descenso de la temperatura necesario para lograr el cambio de fase de la parafina. Una vez se alcanzada una temperatura igual o por debajo de 23ºC la parafina comienza el proceso de cambio de fase (de líquido a sólido), es decir, comienza la solidificación. Durante este proceso se libera la energía acumulada durante el proceso inverso de cambio de fase de sólido a líquido. Es en ese momento en el que la parafina más cercana a la cáscara de la cápsula comienza a agruparse y contraerse, solidificándose en forma de microesferas agrupadas alrededor de la cáscara.

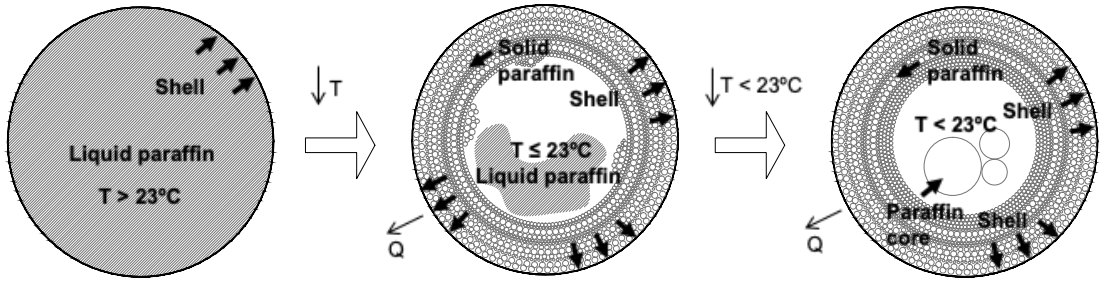

Figura 13. Proceso de solidificación en el interior de una cápsula de PCM durante el enfriamiento. (Sección 10.1.2).

Estas microesferas liberan espacio en el interior de la cápsula, dejando espacio libre para la parafina líquida restante. Esta parafina comienza a solidificarse (mientras la temperatura sigue bajando de 23ºC). Sin embargo, cambia de estado de una forma más lenta gracias al aire que se quedó libre en el interior de la cápsula. Este fenómeno es el causante de la agrupación de la parafina en esferas de mayor tamaño en el núcleo de la microcápsula de PCM. Finalmente, toda la parafina se solidifica habiendo liberado toda la energía acumulada durante el proceso sin aumentar la propia temperatura de la parafina (calor latente).

3.3.4 Simulación matemática de la absorción de agua por succión capilar a partir de resultados experimentales.

A partir de los resultados experimentales obtenidos de absorción de agua por succión capilar (AC) (Tabla 3) (**Secciones 10.1.1**. y **10.1.2**.) para cada una de las doce dosificaciones estudiadas en este trabajo, se realizó una simulación numérica de la evolución de este parámetro en el tiempo **(Sección 10.1.3).**

Se tomaron de referencia los valores obtenidos a lo largo del ensayo en laboratorio donde se tomaron medidas a los 10 minutos, 90 minutos y 24 horas según el ensayo normalizado para AC.

La Figura 14 muestra las imágenes del desarrollo del ensayo.

Figura 14. Ensayo de absorción de agua por succión capilar. – Laboratorio de Materiales de la Universidad de Alcalá. (Sección 10.1.3).

Los resultados experimentales obtenidos se utilizaron en un procedimiento de calibración inversa (Caggiano A. 2018). Se empleó un modelo basado en elementos finitos (FEM) no lineal para el cálculo del transporte de humedad a través de la microestructura porosa del material basándose en la Ley de Darcy.

Esta calibración inversa permitió entender de una manera más eficaz la influencia de cada uno de los componentes de los morteros, especialmente el PCM, en los parámetros de AC, así como la distribución de poro por el método Raleigh-Ritz.

Los resultados mostraron como los morteros con los valores más altos de Raleigh-Ritz tenían una baja absorción capilar. Además, la adición de PCM a las mezclas incrementaba el valor de Raleigh-Ritz obtenido y en consecuencia la permeabilidad de los morteros se veía reducida (Figura 15). **(Sección 10.1.3)**

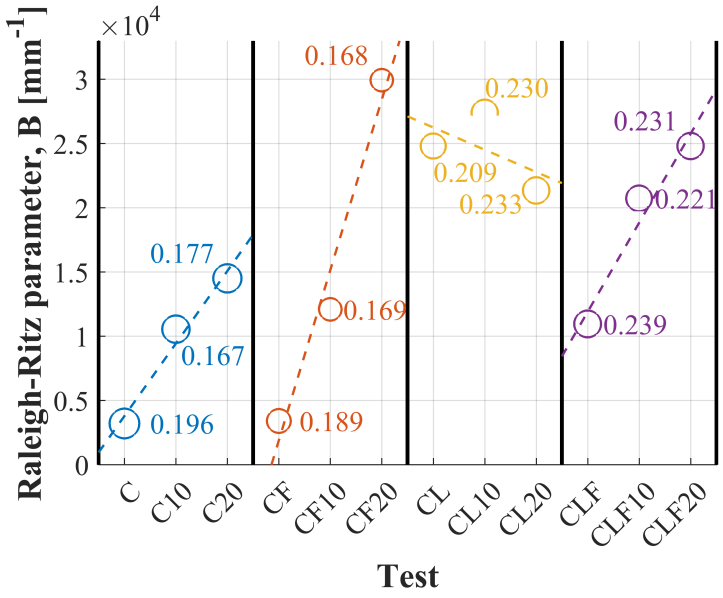

Figura 15. Relación entre el parámetro Raleigh-Ritz y la porosidad abierta. (Sección 10.1.3).

Todo el proceso de la simulación numérica y resultados están explicados y desarrollados en la **Sección 10.1.3**. Esta parte del trabajo se realizó en colaboración con el grupo de investigación de TU-Darmstadt que se estableció a través de la estancia de investigación realizada en el centro.

3.4 CONCLUSIONES

Este capítulo recoge la caracterización y análisis de las doce dosificaciones de cemento-cal con PCM y las diferentes adiciones planteadas. Para ello se realizó la evaluación física, mecánica y térmica de los distintos materiales diseñados. A partir de estos resultados se determinó la influencia del PCM sin otras adiciones y el efecto del PCM en combinación con otras adiciones en el comportamiento de los morteros. También se estudió la microestructura y el funcionamiento del material de cambio de fase en el interior de las microcápsulas. Por último, se realizó una simulación numérica de algunas de las propiedades obtenidas a partir de los resultados de los ensayos experimentales realizados. Las conclusiones más relevantes alcanzadas fueron las siguientes:

- El uso de fibras de celulosa, áridos ligeros, PCM y su combinación modifica las propiedades de un mortero del cemento-cal de referencia. Los áridos ligeros incrementan la porosidad abierta de los moteros mientras que reducen la conductividad térmica de los mismos. Las fibras de celulosa, sin embargo, no muestran cambios significativos en las propiedades. **(Secciones 10.1.1 y 10.1.2)**

- La adición de PCM a un mortero de referencia reduce la porosidad abierta, la resistencia a compresión y el módulo de Young. **(Secciones 10.1.1 y 10.1.2)**

- La conductividad térmica de los morteros con PCM es más baja con altas temperaturas (es decir PCM estado líquido). Por otro lado, la adición de PCM al mortero de referencia incrementa la entalpía de las mezclas. **(Sección 10.1.2)**

- La cantidad de PCM añadida (10% o 20%) no supone gran diferencia en las propiedades físicas o mecánicas de los morteros. **(Secciones 10.1.1 y 10.1.2)**

- Los morteros con áridos ligeros y PCM muestran grandes diferencias en las propiedades térmicas como la entalpía porque la menor conductividad suministrada por los áridos ligeros ralentiza el flujo de calor a través de los morteros hacia las cápsulas de PCM. **(Sección 10.1.2)**

- Los morteros con áridos ligeros y 20% de PCM muestran mejor comportamiento térmico por su baja conductividad térmica y mayor entalpía alcanzando el doble que la del mortero de referencia. **(Sección 10.1.2)**

- A partir de los resultados experimentales obtenidos de absorción capilar por succión de agua se pudo realizar una simulación numérica con un modelo no lineal de elementos finitos basado en la Ley de Darcy. El método de Raleigh-Ritz permitió evaluar la influencia del PCM en la capacidad de transporte de agua de cada una de las mezclas. **(Sección 10.1.3)**

- Un valor elevado de Raleigh-Ritz supone una reducción en la permeabilidad de los morteros. La adición de PCM aumenta ese valor y por lo tanto se puede decir que ayuda a la reducción de la permeabilidad de succión capilar de los morteros objetos de este estudio. **(Secciones 10.1.2 y 10.1.3)**

4. EVALUACIÓN TÉRMICA MEDIANTE TÉCNICAS NO DESTRUCTIVAS DE MORTEROS DE CEMENTO-CAL CON PCM DURANTE PROCESOS DE CALENTAMIENTO Y ENFRIAMIENTO.

4.1 INTRODUCCIÓN

En el capítulo anterior se describe la caracterización física, mecánica y térmica de los 12 morteros de cemento-cal con PCM y adiciones estudiados en este trabajo de investigación.

Los resultados obtenidos han demostrado que el comportamiento del PCM no sólo depende de los componentes que formen el mortero en el que se encuentre el material de cambio de fase si no también influyen las condiciones ambientales bajo las que se encuentre este. Esta diferencia se vio claramente reflejada en los valores obtenidos de conductividad térmica, los cuales dependían del estado (sólido o líquido) del PCM. **(Secciones 10.1.1 y 10.1.2)**

En este capítulo se realiza el estudio del comportamiento térmico de esos morteros durante diferentes condiciones ambientales: procesos de calentamiento y enfriamiento **(Sección 10.2).** Para este análisis se utilizaron técnicas no destructivas utilizadas por otros autores con anterioridad (Barluenga G. 2018).

Una de estas técnicas es la de transmisión de ondas de ultrasonidos (Popovics, S. 1990, Arizzi, A. 2013). Gracias a los ultrasonidos se pueden analizar, de una forma indirecta, los parámetros mecánicos y la estructura porosa de los materiales en diferentes estados (Zoubeir L. 2006, Palomar I., 2017), como ya se utilizó en el capítulo anterior para la evaluación de las constantes elásticas de los morteros (**Sección 10.1.2**). Además, a través de la atenuación y coeficientes de atenuación de la señal de ultrasonidos, puede determinarse la cantidad de energía absorbida por los materiales cementicios (sólidos o líquidos) u otros materiales (Philippidis T.P., 2005, Philippidis T.P., 2005b).

Otra técnica no destructiva útil para la caracterización de los morteros durante procesos de calentamiento y enfriamiento son los medidores de flujo de calor. Con estos medidores se puede determinar la cantidad de calor que es capaz de pasar por un material o de un material a otro y, por lo tanto, la capacidad de los materiales de intercambiar energía con su entorno (entalpía) (Günther E., 2009), sin la necesidad de romper el material para su evaluación como si ocurre con la Calorimetría Diferencial de Barrido (DSC).

4.2 METODOLOGÍA DE ENSAYO EN CÁMARA CLIMÁTICA Y NDT

Para la evaluación de la evolución térmica de los morteros de cemento-cal con PCM durante procesos de calentamiento y enfriamiento con técnicas no destructivas se utilizó una cámara climática para la simulación de las diferentes condiciones ambientales. A lo largo de la simulación de los ciclos, se midieron simultáneamente la temperatura, los ultrasonidos y el flujo de calor de la dosificación de referencia (C) y de las dosificaciones con 20% de PCM (C_{20}, CF_{20}, CL_{20} y CLF_{20}).

4.2.1 Montaje experimental en cámara climática para la simulación de ciclos de calentamiento y enfriamiento.

La Figura 16 muestra el esquema y fotografía del montaje de la cámara climática que se utilizó para llevar a cabo los ensayos de caracterización térmica de las placas realizadas con morteros de cemento-cal con PCM, fibras de celulosa y áridos ligeros (perlita) durante los procesos de calentamiento y enfriamiento.

La cámara climática fue programada para simular las dos condiciones climáticas en el interior que se programaron en el ensayo llevado a cabo en el capítulo anterior: un

proceso de calentamiento que pasaba de 15ºC -80% de humedad relativa (HR) a 30ºC-33% HR; y un proceso de enfriamiento que pasaba de 30ºC-33%HR a 15ºC-80%RH. Las condiciones ambientales del laboratorio se mantuvieron constantes en 20ºC y 60% de humedad relativa. La humedad relativa se calculó en cada caso para limitar el transporte de agua a través de los materiales por difusión del vapor. Sobre las muestras se midieron temperatura, ultrasonidos y flujo de calor a lo largo de ambos ciclos. Antes del comienzo de ambos ciclos, se aseguró que las condiciones de temperatura y humedad fueran estables y se mantuvieran sin variaciones.

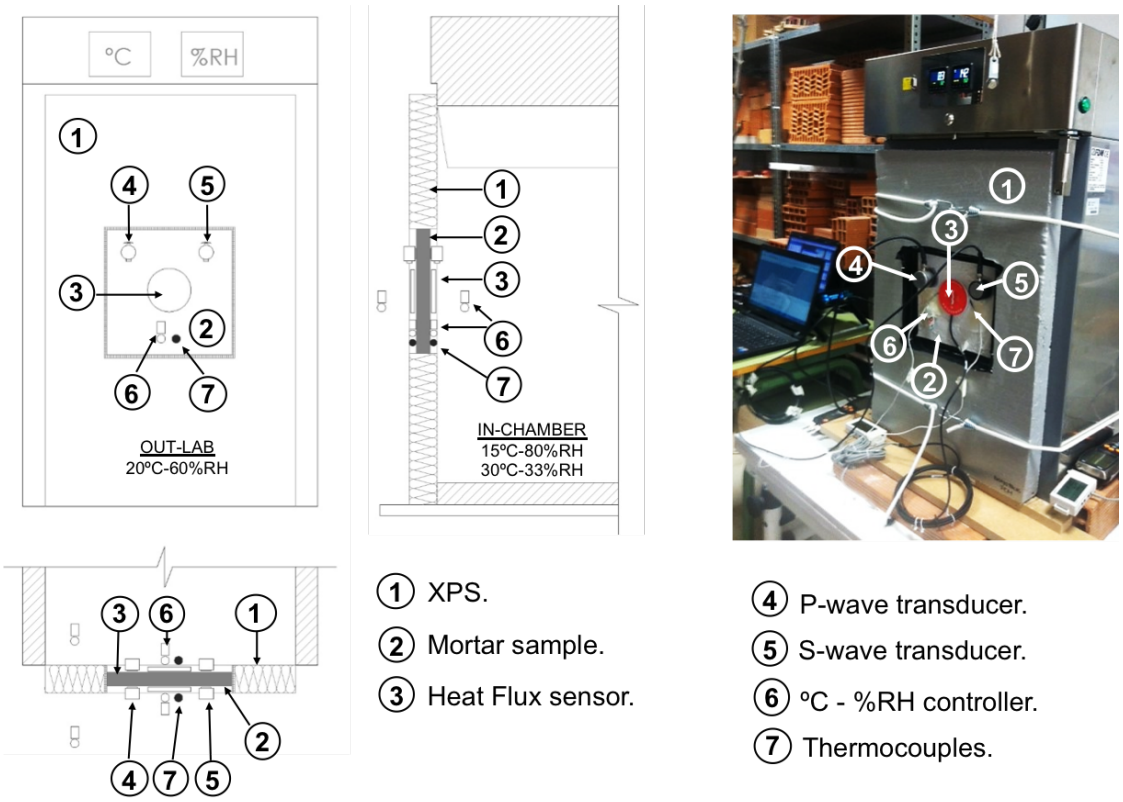

Figura 16. Ensayo para la evaluación, con técnicas no destructivas, del comportamiento térmico de los morteros de cemento-cal con PCM. Laboratorio de Materiales de la Universidad de Alcalá. (Sección 10.2.1 y 10.2.2)

El montaje y procedimiento del ensayo pueden encontrarse explicados más detalladamente en las **Secciones 10.2.1 y 10.2.2.**

4.2.2 Procedimiento de cálculo de medidas de atenuación de ultrasonidos.

Para el cálculo de los coeficientes de atenuación con el PCM en estado líquido (AT_L), estado líquido-sólido ($AT_{L\text{-}S}$) y estado sólido (AT_S) se utilizó la siguiente ecuación (Philippidis T.P, 2005):

$$AT_{PCM} = -(20/x)(\log(A_m/A_T)) \qquad \textit{(Eq. 1)}$$

Esta ecuación se determinó considerando la amplitud (A_M) de la onda de ultrasonidos en voltios (V) a través de las muestras. A_T corresponde a la amplitud de onda medida cuando ambos transductores se posicionan cara contra cara (V). Por último, x es la distancia entre los transductores en mm (24 ± 2mm).

Cuanto mayor sea el valor de AT_{PCM}, mayor será la cantidad de energía de ultrasonidos absorbida por la muestra. Por esta razón, se consigue evaluar la composición y el estado del material.

4.2.3 Procedimiento de cálculo de las entalpías a partir del flujo de calor a través de los morteros.

A partir de las medidas de temperatura y flujo de calor durante ambos procesos de calentamiento y enfriamiento se determinó el flujo total a través de las placas y la entalpía para cada una de las dosificaciones ensayadas.

La formulación utilizada para el cálculo de las entalpías de los morteros estudiados fue la siguiente:

$$\emptyset_T = \emptyset_{in} - \emptyset_{out} \quad \textit{(Eq. 2)}$$

$$\emptyset_Q = \int_{T0}^{Tf} \emptyset_T \, dT \quad \textit{(Eq. 3)}$$

$$H = \left[\emptyset_Q/(D_G \, e)\right]1000 \quad \textit{(Eq. 4)}$$

Donde,

$\emptyset_T$ (W/m^2) es la diferencia entre el flujo de calor en la cara interior ($\emptyset_{in}$)y la cara exterior ($\emptyset_{out}$)de las placas;

$\emptyset_Q$ es el sumatorio del flujo de calor en función de la temperatura en Jm^2;

H es la entalpía de cada una de las mezclas de los morteros en MJ/g obtenida a partir de la ecuación 3;

D_G es la densidad geométrica de cada una de las placas (obtenida a partir del peso de cada una de las muestras entre su volumen) representado en kg/m^3;

y *e* es el espesor de las muestras en mm.

4.3 RESULTADOS Y DISCUSIÓN DE LA EVALUACIÓN TÉRMICA DE MORTEROS

4.3.1 Identificación del estado del PCM y de la microestructura de los morteros de cemento-cal con PCM y adiciones con la técnica de ultrasonidos.

El uso de la técnica de ultrasonidos presentó resultados relevantes para la caracterización indirecta de materiales cementicios tanto en laboratorio como in-situ. A través de esta técnica se puede detectar no solo el tipo de estructura porosa del material si no también el estado en el que se encuentre el mismo (Palomar I. 2017, Barluenga G 2018).

Durante el ensayo en cámara climática se simularon procesos de calentamiento y enfriamiento para cada uno de los morteros analizados en esta sección. Durante estos ciclos, como se esperaba, el PCM añadido a las mezclas sufrió cambios de fase de sólido a líquido (calentamiento) y de líquido a sólido (enfriamiento).

La Figura 17 muestra la relación detectada entre los diferentes momentos de solidificación del PCM durante el proceso de enfriamiento respecto a la señal de onda registrada. Por un lado, se muestra el ejemplo de solidificación (cambio de fase de líquido a sólido) de una microcápsula de PCM (esquema explicado en el apartado 3.3.3 del capítulo 3). Por otro lado, junto con estos esquemas se presentan las señales de ondas ultrasónicas de cortante (S-wave) emitidas a una frecuencia de 250 kHz . Estas señales fueron registradas durante el ensayo del proceso de enfriamiento de la dosificación C_{20}. Cómo se puede ver en la Figura 17, se detectaron tres tipos de ondas coincidentes con cada uno de los estados del PCM. Además, se observa como todas las ondas presentaron el mismo patrón, así como tiempos de llegada (manteniéndose por tanto la velocidad de propagación de ultrasonidos - UPV). Sin embargo, dependiendo de la fase del PCM (líquido, sólido-líquido o sólido) el pico máximo de la onda no fue el mismo. Se puede apreciar cómo a medida que el PCM iba cambiando de fase, de líquido a sólido, el pico máximo de onda fue aumentando, pasando de 10V al comienzo del proceso y llegando a 70V con el PCM totalmente solidificado. **(Secciones 10.2.1 y 10.2.2)**

Por último, hay que destacar que esta técnica no destructiva permitirá evaluar el estado del PCM no solo en el laboratorio, sino también en inspecciones in-situ, es decir, una vez aplicados los materiales en los edificios existentes. Además, se podría comprobar la durabilidad del PCM en el interior del mortero. De esta forma, se puede verificar si el PCM sigue cambiando de fase y, por lo tanto, sigue funcionando durante los cambios de condiciones ambientales.

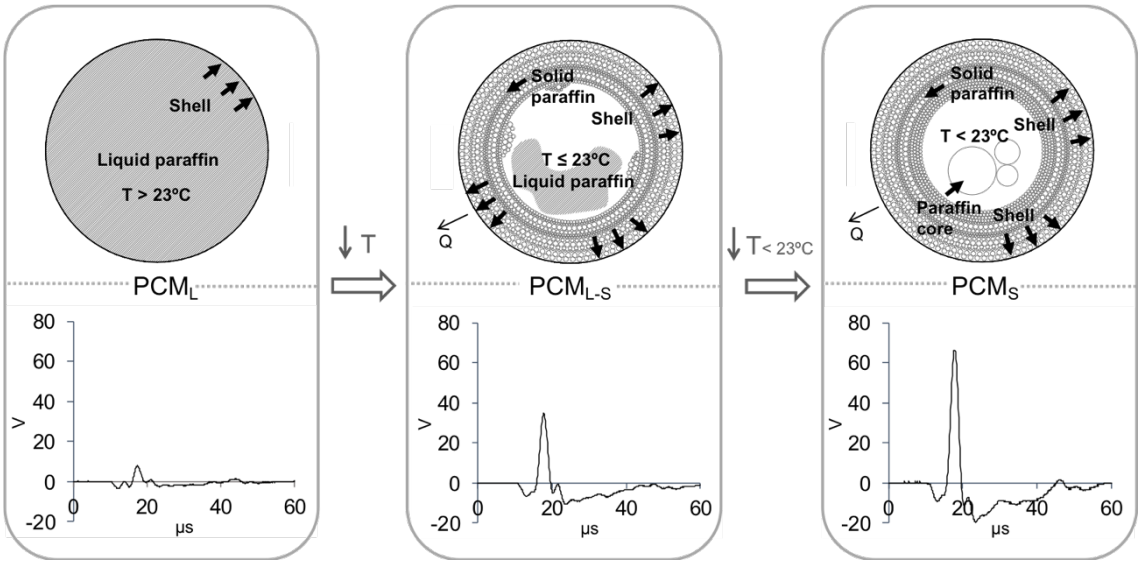

Figura 17. Esquema del proceso de solidificación en el interior de una microcápsula de PCM y detección del estado del PCM con ondas ultrasónicas de compresión (Sw). (Sección 10.2.2)

A partir de estos resultados fue posible evaluar el coeficiente de atenuación de las ondas para cada una de las dosificaciones ensayadas. Este coeficiente no solo permitió detectar el estado del PCM, sino que también permitió evaluar la capacidad de cada material para absorber la energía de ultrasonidos dependiendo de su composición.

La Tabla 5 muestra los AT_{PCM} obtenidos a partir de la ecuación 1 para cada una de las dosificaciones durante el cambio de fase del PCM.

Tabla 5. Coeficientes de atenuación de los morteros durante los diferentes estados de PCM

	C	**C_{20}**	**CF_{20}**	**CL_{20}**	**CLF_{20}**
Líquido (T> 23ºC)	0.99	0.84	0.57	1.33	1.29
Líquido-sólido (T≤ 23ºC)	0.92	0.30	0.46	1.13	1.02
Sólido (T< 23ºC)	0.86	0.05	0.42	1.05	0.96

Tal como se esperaba, la dosificación de referencia C (sin PCM), presentó valores de AT_{PCM} similares en cualquiera de los momentos del ciclo (diferentes temperaturas) variando entre 0.86dB/mm y 0.99dB/mm. Se considera que estas pequeñas variaciones

pueden estar asociadas al contenido de humedad de la propia mezcla que pudo evaporarse, dejando de esta forma huecos libres y haciendo que la señal tuviera cambios en su transmisión.

La Tabla 4 junto con la Figuras 18 y 19 muestra la variación en los valores de los AT_{PCM} dependiendo del estado del PCM. En todos los casos cuando las dosificaciones tenían un 20% de PCM, los valores disminuyeron a medida que el PCM se solidificó.

Sin embargo, la reducción de este coeficiente varió en función de los componentes que formaban la mezcla como se puede ver en la Figura 18 que muestra los valores relativos del coeficiente de atenuación para todas las dosificaciones. Todas las dosificaciones empezaron con el valor máximo (100%) estando el PCM en estado líquido. **(Sección 10.2.2)**

Los valores obtenidos de la dosificación de referencia (C), presentaron un descenso lineal desde el comienzo hasta el final del ciclo. Por el contrario, todas las dosificaciones, excepto la C_{20}, presentaron un descenso en estado sólido menor al 30% respecto al máximo obtenido en estado líquido. En el caso de la dosificación C_{20} la disminución del coeficiente de atenuación alcanzó casi un 90% para el PCM cuando éste se encontraba en estado sólido. Una de las posibles razones a este comportamiento es la capacidad del material de cambio de fase como transmisor de señal de ultrasonidos, la cual se ve modificada cuando este mismo PCM se encuentra dentro de una mezcla con otros componentes que dificultan la continuidad del paso de onda.

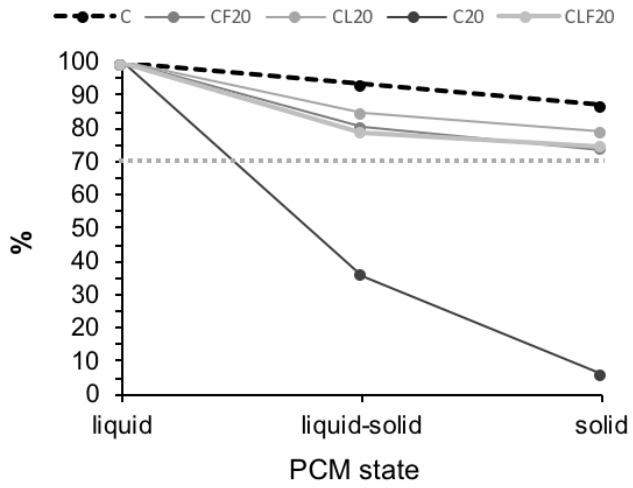

Figura 18. Atenuación relativa (%) en función del estado del PCM (Sección 10.2.2)

Los resultados obtenidos en la Tabla 5 y la figura 19 demuestran que los valores de los coeficientes dependieron de los componentes que conformaron las mezclas de los morteros.

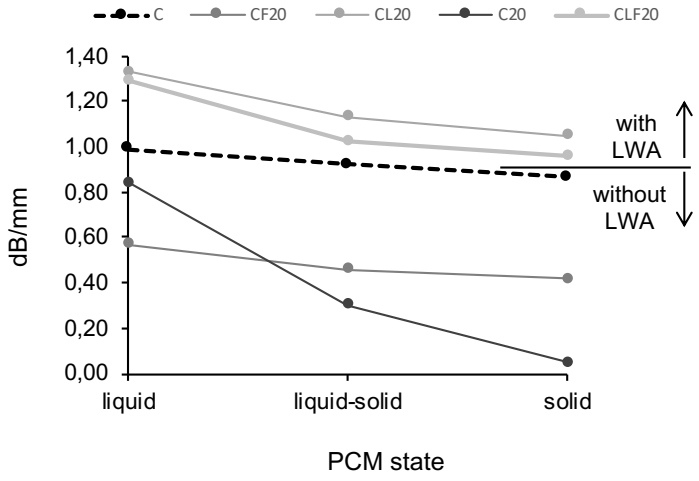

Figura 19. Coeficientes de atenuación en función del estado del PCM y de la composición del mortero (Sección 10.2.2)

Al igual que ocurría en la relación entre alguno de los parámetros evaluados en el capítulo anterior, se observa como existen dos grupos de valores en función de los componentes. Por un lado, se encuentran los que tienen áridos ligeros y, por el otro, los

que no tienen o tienen solo fibras de celulosa. Los primeros mostraron valores por encima de 1dB/mm, mientras que los segundos presentaron valores por debajo de 1dB/mm. Por el contrario, la dosificación de referencia mostro valores muy similares a 1dB/mm.

Las mezclas con áridos ligeros fueron las que absorbieron más la energía de ultrasonidos. Estos resultados pueden relacionarse con los obtenidos de densidad aparente y porosidad abierta (Capítulo 3.3.1,Tabla 3). Estas dosificaciones fueron las que presentaron los valores más bajos de densidad aparente y los más altos de porosidad abierta **(Sección 10.1.2, 10.2.1 y 10.2.2)**. Es decir, cuanto menor fue la densidad aparente mayor fue el coeficiente de atenuación y cuanto mayor fue la porosidad abierta mayor fue también el AT_{PCM}.

4.3.2. Evaluación de la temperatura media de los morteros de cemento-cal con PCM y adiciones bajo diferentes condiciones ambientales.

En las Figura 20a y 20b se muestran las temperaturas medias en el interior de las placas de mortero ensayadas durante un proceso de enfriamiento y de calentamiento. En ambas situaciones, se comenzó el ensayo una vez lograda la estabilización de las temperaturas iniciales. Se aseguró el cambio de fase del PCM, alcanzando y rebasando las temperaturas de fusión necesarias para tal fin (23ºC para el cambio de sólido a líquido y 21-22ºC para el cambio de líquido a sólido **(Sección 10.1.2).**

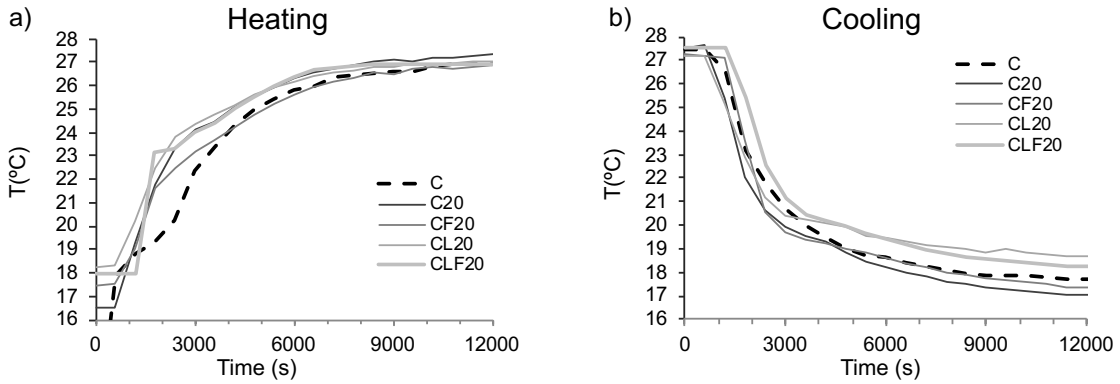

Figura 20. Temperatura media de las placas de mortero durante el proceso de calentamiento (a) y de enfriamiento(b).(Sección 10.2.2)

La Figura 20a muestra la evolución durante el proceso de calentamiento durante 120.000 segundos. Se puede ver como C (dosificación de referencia sin PCM) tuvo un comportamiento diferenciado al resto de dosificaciones, tardando más tiempo en aumentar la temperatura final hasta la estabilización. El resto de las dosificaciones (todas con la adición de PCM) mostraron un comportamiento similar entre ellas: un aumento notable de temperatura en un primer tramo hasta llegar a los 23ºC (temperatura de fusión del PCM) y, a partir de este momento, un segundo tramo donde la temperatura siguió aumentando, pero más lentamente, hasta llegar a la estabilización. Sin embargo, una de estas dosificaciones, CF_{20} tardó más tiempo en llegar a los 23ºC (al igual que ocurrió con C). Esta diferencia en la evolución de las temperaturas puede relacionarse con la diferencia en las densidades de los morteros. Ambos morteros, C y CF_{20} presentaron valores más elevados de densidad geométrica de las placas ensayadas (2376 kg/m^3 y 2091 kg/m^3 respectivamente **Sección 10.2.2**) no alcanzando ninguna de las otras mezclas los 2000 kg/m^3. Del mismo modo, la temperatura media final de estas dos dosificaciones se mantuvo 0.5ºC por debajo del resto.

La Figura 20b muestra la temperatura media de los morteros durante el proceso de enfriamiento. Al igual que ocurría en el ciclo de calentamiento se pueden apreciar dos comportamientos respecto a la evolución de las temperaturas.

Se observa un primer tramo donde las temperaturas descendieron hasta alcanzar la temperatura de fusión (21ºC -22ºC en el caso de la solidificación **(Sección 10.1.2)**. A partir de ese punto comenzó otro tramo donde la temperatura siguió disminuyendo en menor medida hasta alcanzar la estabilización. A lo largo de este ciclo, las dosificaciones con perlita (CL_{20} y CLF_{20}), se quedaron 1ºC por encima del resto de dosificaciones.

4.3.3. Evaluación del flujo de calor de los morteros de cemento-cal con PCM y adiciones bajo diferentes condiciones ambientales.

Las Figuras 21a y d muestran la evolución de la diferencia de flujo de calor entre ambos lados de las muestras estudiadas (ecuación 2), en relación con la temperatura media de las mezclas (anteriormente descrita) durante un proceso de calentamiento y enfriamiento respectivamente. El intervalo de temperaturas dentro del cual se evaluó el flujo de calor varió entre los 18ºC y los 27ºC.

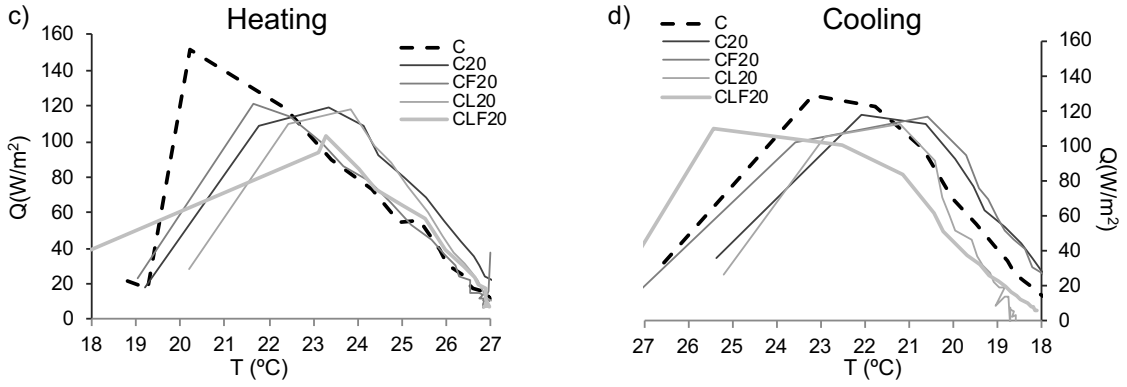

Figura 21. Flujo de calor durante el proceso de calentamiento (a) y de enfriamiento(b) en relación con la temperatura media de las placas de mortero (Sección 10.2.2)

En ambas situaciones, se comenzó el ensayo una vez alcanzada la estabilización del fuljo de calor. La Figura 21c muestra la evolución de la diferencia del flujo de calor ($\emptyset_T$) durante el proceso de calentamiento a una determinada temperatura. Se ven dos comportamientos claramente diferenciados:

1. La dosificación de referencia C sin PCM; y
2. El resto de las dosificaciones con 20% de PCM.

En el caso de C el flujo de calor comenzó a ascender hasta que alcanzó el pico máximo (151.41W/m^2) a 21ºC aproximadamente (cambio de dirección del flujo de calor a través de la muestra). Tras alcanzar el pico máximo, comenzó a descender hasta su estabilización, siendo $\emptyset_T$ próximo a 0W/m^2.

Sin embargo, el resto de las dosificaciones mostraron un desarrollo diferente. En el primer tramo ascendieron hasta alcanzar el pico máximo, alcanzando CLF_{20} 100W/m^2 y el resto de las dosificaciones 120W/m^2 aproximadamente. Estos puntos se alcanzaron entre los 21.5ºC y 24ºC. Al contrario que ocurrió con C, una vez alcanzados los puntos máximos no hubo un descenso directo del flujo de calor hacia la estabilización, si no que se produjo un flujo de calor constante entre los 21ºC y 24ºC. Una vez pasado este intervalo, los flujos descendieron hasta aproximarse, igual que C, a $\emptyset_T = 0$.

Los resultados obtenidos para C muestran como el valor de pico máximo de flujo de calor se relacionó con la densidad del material, siendo la de C la más elevada.

El flujo constante registrado para el resto de las dosificaciones esta directamente relacionado con el PCM y su cambio de fase, teniéndose que mantener el flujo de calor (en W/m^2) para conseguir el aumento de temperatura de la mezcla y experimentar el cambio de dirección del flujo de calor. CLF_{20} mostró un comportamiento algo diferente,

estando influenciado por el propio procedimiento del ensayo. Estos comportamientos no se vieron tan distintos en el proceso de enfriamiento. C siguió siendo la dosificación con el pico máximo de flujo de calor más elevado (130W/m^2). Esta disminución puede estar relacionada con el posible contenido en agua dentro del mortero, que en el proceso de enfriamiento (tras el de calentamiento) ya se hubo evaporado. El resto de las dosificaciones volvieron a mostrar un $\emptyset_T$ constante durante el intervalo de temperatura correspondiente al cambio de fase del PCM (entre 23ºC y 20ºC). Estos resultados sirvieron como punto de partida para poder cuantificar en el siguiente apartado la cantidad de energía que necesitó cada uno de los morteros para lograr aumentar su temperatura e intercambiar energía con el entorno, es decir, poder calcular la entalpía de los morteros.

4.3.4. Evaluación de las entalpías de los morteros de cemento-cal con PCM y adiciones bajo diferentes condiciones ambientales.

Las Figuras 22a y b muestran los resultados de entalpía obtenidos a partir de las Eq. 2-4 (tomando de referencia las temperaturas y los flujos de calor) para cada una de las dosificaciones ensayadas durante los procesos de calentamiento y enfriamiento.

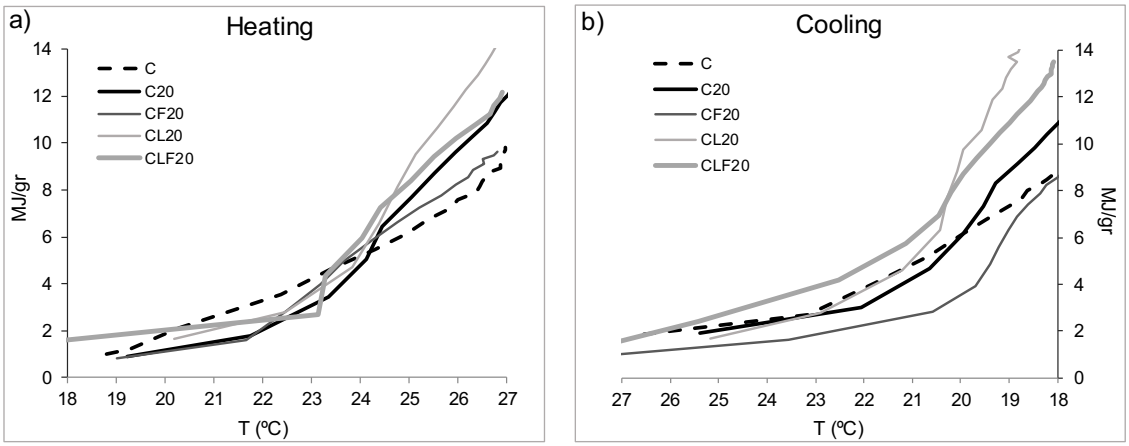

Figura 22. Entalpía de cada dosificación durante el proceso de calentamiento (a) y de enfriamiento (b), en relación a la temperatura media de las placas de mortero. (Sección 10.2.2)

La dosificación de referencia C (sin PCM) presentó una evolución lineal (sin cambios de tendencia) de la entalpía en relación con las temperaturas expuestas tal como se esperaba comparándolo con el obtenido con el ensayo de calorimetría diferencial de barrido – DSC, presentado en el capítulo anterior (cap. 3.3.3. y **Sección 10.1.2**).

Por otro lado, las dosificaciones con PCM mostraron una tendencia similar en los valores de entalpía variando éstos en función de los componentes de la mezcla. En todos los casos hubo dos tipos de comportamiento:

1. Al comienzo y final, donde la evolución fue lineal a medida que avanzó el ensayo y aumentó o disminuyó la temperatura de la muestra (calor sensible); y
2. En el tramo central, el cual se situó en el intervalo de temperatura entre 22ºC-24ºC durante el calentamiento y entre 22ºC-19ºC durante el enfriamiento. Precisamente, es en estos intervalos de temperatura, donde el PCM experimenta el cambio de fase al igual que ocurría en los resultados obtenidos en el DSC.

Sin embargo, la entalpía (MJ/g) que cada una de las dosificaciones necesitó para el aumento de temperatura durante el cambio de fase no fue la misma. Durante el proceso de calentamiento (Figura 22a) la mezcla que necesitó una mayor energía para conseguir aumentar la temperatura durante el cambio de fase fue CL_{20} necesitando 6MJ/g. Por el contrario, C_{20} y CF_{20} (4.5MJ/g) fueron las que menos energía necesitaron. **(Sección 10.2.2)**

Los resultados de entalpía durante el ciclo de enfriamiento (Figura 22b) mostraron que, al igual que para el calentamiento, la dosificación CL_{20} fue la que más energía necesitó para aumentar la temperatura de la mezcla (7MJ/g) y la CF_{20} la que menos (3.8MJ/g). Por lo tanto, durante ambos ciclos, tanto el de calentamiento como el de enfriamiento, CL_{20} fue la mezcla que más energía acumuló dado que fue la que más tardó en aumentar o disminuir su temperatura media. Este comportamiento viene asociado no solo a la adición de PCM, sino que también a su combinación con los áridos ligeros.

Mediante el flujo de calor y las temperaturas de las placas se pudo evaluar la cantidad de MJ/g necesarios para aumentar o disminuir la temperatura de cada una de las dosificaciones estudiadas durante un proceso de calentamiento y enfriamiento o, lo que es lo mismo, la capacidad de cada mortero de intercambiar energía (en este caso en forma de calor) con su entorno (entalpía). Estos resultados coinciden con los obtenidos a través de los ensayos realizados con el DSC (capítulo 3.3.2, Figura 11) con la virtud de que no fue necesaria la rotura de la probeta para su realización.

Además, estos ensayos, como en el caso de la técnica de ultrasonidos, permitirían en un futuro realizar mediciones in-situ una vez instalado el material. De esta manera, sería posible su evaluación, así como la comprobación de su durabilidad a lo largo del tiempo.

4.4 CONCLUSIONES

En este capítulo se han analizado cinco de los doce morteros estudiados en esta tesis (C, C_{20}, CF_{20}, CL_{20} y CLF_{20}) durante un ciclo de calentamiento y otro de enfriamiento.

Se midieron con técnicas no destructivas simultáneamente señales de onda de ultrasonidos, temperatura y el paso de flujo de calor por las muestras. Además, se evaluaron el cambio de fase del PCM y la capacidad de los morteros de acumulación térmica para cada una de las dosificaciones. Las conclusiones más significativas de esta parte del trabajo han sido las siguientes:

- A través del uso de ultrasonidos se pudo detectar el estado del PCM en cada momento de los ciclos de calentamiento y enfriamiento. Además, se evaluó el tipo de microestructura de cada una de las dosificaciones estudiadas en función de los coeficientes de atenuación obtenidos. **(Secciones 10.2.1 y 10.2.2)**

- Los valores del coeficiente de atenuación en una misma dosificación cuando el PCM se encontró en estado líquido fueron en todos los casos más elevados que cuando el PCM se encontró en estado sólido. **(Sección 10.2.2)**

- CL_{20} presentó los coeficientes de atenuación más elevados siendo, por esta razón, la dosificación con mayor capacidad de absorción de energía de la señal de onda. **(Sección 10.2.2)**

- Los ultrasonidos, como técnica no destructiva, permitieron la verificación del estado del PCM dentro de una mezcla cementicia., haciendo posible la comprobación del mantenimiento de la capacidad de acumulación del PCM en el interior de los morteros sin dañar el material una vez aplicado. **(Sección 10.2.2)**

- La adición de PCM proporcionó a los morteros la capacidad de acumulación, aumentando la entalpía de estos. **(Sección 10.2.2)**

- La dosificación que presentó el mejor comportamiento térmico y una mayor capacidad de acumulación térmica fue la $CL_{20.}$ **(Sección 10.2.2)**

5. SIMULACIÓN EXPERIMENTAL DE MODELOS DE CERRAMIENTO MULTICAPA INCLUYENDO MORTEROS DE CEMENTO-CAL CON PCM.

5.1 INTRODUCCIÓN

En los capítulos anteriores se han estudiado las propiedades físicas, mecánicas y térmicas de los doce morteros de cemento-cal con PCM y adiciones de fibras de celulosa y áridos ligeros analizados en este trabajo de investigación. Los resultados obtenidos determinaron que el comportamiento de los morteros se vio influenciado por la adición de fibras de celulosa, áridos ligeros y PCM y por la combinación de estos. Como se observó en otros estudios, para conocer el alcance real de las mejoras conseguidas en el laboratorio es necesario la evaluación de los materiales dentro de sistemas constructivos (Palomar I, 2019, Wi S., 2020). Dado que la evaluación a escala real de los materiales es en la mayoría de los casos complicada, muchos autores se limitan a simular en el laboratorio las condiciones climáticas reales y a analizar cómo afectan dichas condiciones a los morteros (Alonso C, 2016, Rathore, P.K.S, 2020). De esta forma, se considera eficiente la utilización de cámaras climáticas como medio para este tipo de simulaciones experimentales en laboratorio (Palomar I, 2019, Qiao, Y, 2019).

En este trabajo se han evaluado los diferentes morteros diseñados dentro de un cerramiento multicapa para su estudio bajo diferentes condiciones ambientales mediante una cámara climática **(Sección 10.3.1)** Se utilizó una cámara climática donde se simularon las mismas condiciones ambientales que en el capítulo anterior (capítulo 4.2). Se evaluó el comportamiento de un cerramiento incorporando estos morteros (mortero de referencia y el resto de los morteros con 20% de PCM) simulando un proceso de calentamiento y un proceso de enfriamiento. De esta forma, se evaluó la influencia, por un lado, del PCM (calor latente y acumulación térmica) y, por otro, del resto de las adiciones (calor sensible y aislamiento térmico) en el propio funcionamiento del cerramiento. Las muestras se ensayaron con técnicas no destructivas como son los medidores de temperatura y de flujo de calor. Además, se evaluó la influencia del PCM

en el comportamiento térmico de los morteros y se observó la capacidad de acumulación térmica de los diferentes morteros en función de sus componentes. A partir de estos resultados, se consideró necesario evaluar la aplicabilidad y el comportamiento de estos morteros dentro de un sistema de cerramiento multicapa real. **(Sección 10.3.1)**

5.2 METODOLOGÍA PARA SIMULACIÓN EN CÁMARA CLIMÁTICA DE CERRAMIENTO MULTICAPA

Como se señaló anteriormente, este capítulo de la tesis aborda la evaluación del comportamiento térmico de los morteros estudiados dentro de un modelo de cerramiento multicapa durante un proceso de calentamiento y enfriamiento aplicado en una de sus caras mediante una cámara climática.

Para este ensayo se programaron las mismas condiciones de temperatura y humedad que en el capítulo anterior (capítulo 4.2) para cada uno de los ciclos (Figura 23).

Se tomó como referencia un muro simple con hoja de ladrillo de hueco doble, que correspondería a un tipo de muro construido en España a finales del siglo XX (Terés-Zubiaga, J. 2013, 2015). A éste se le adosó una capa de mortero de cemento-cal con PCM y una capa de aislamiento térmico tipo XPS (poliestireno extruido), simulando una rehabilitación energética (Figura 23). Como revestimiento de la cara interior del cerramiento se instaló una placa de yeso.

Las condiciones ambientales en el interior de la cámara simularon el exterior del edificio, es decir, condiciones de ambiente exterior y las condiciones de ambiente del laboratorio se consideraron equivalentes al interior de un edificio de viviendas.

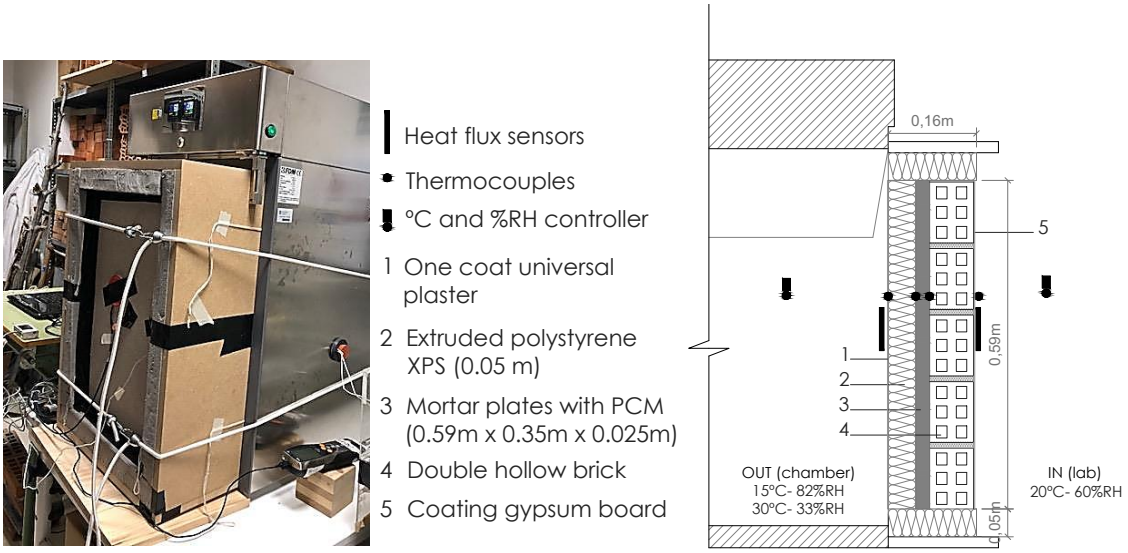

Figura 23. Ensayo de simulación de un cerramiento multicapa mejorado con cámara climática durante procesos de calentamiento y enfriamiento.

(Sección 10.3.1)

Durante los ensayos se midió la temperatura simultáneamente entre las diferentes capas de material, así como en las caras interior y exterior del cerramiento. Además, se midió el flujo de calor en ambas caras del cerramiento. Se pueden consultar más detalles del montaje y procedimiento del ensayo en la **Sección 10.3.1.**

5.3 RESULTADOS Y DISCUSIÓN

En los capítulos anteriores se han analizado y discutido las propiedades físicas, mecánicas y térmicas de los morteros observando la influencia de la adición del PCM en el comportamiento y propiedades de las mezclas, así como la influencia de la combinación de las adiciones con el PCM en las propiedades de éstos.

A continuación, se evaluó el comportamiento térmico bajo diferentes condiciones ambientales de cinco de esas dosificaciones, más concretamente la dosificación de referencia C y el resto de las dosificaciones con 20% de PCM (C_{20}, CF_{20}, CL_{20} y CLF_{20}). Por último, se analizó el comportamiento térmico de un cerramiento multicapa con cada

uno de estos cinco morteros en su interior durante procesos de calentamiento y enfriamiento.

En este apartado se describen y analizan los resultados obtenidos en la simulación del cerramiento multicapa con morteros de cemento-cal con PCM **(Sección 10.3.1)**. Se midieron las temperaturas en cada una de las capas que formaban los cerramientos estudiados y el flujo de calor en las caras interior y exterior de cada uno de ellos.

5.3.1 Evaluación del comportamiento térmico del cerramiento multicapa durante el ciclo de calentamiento.

5.3.1.1 Evolución de las temperaturas de las placas de mortero de cemento-cal con PCM en el interior del cerramiento multicapa.

Tabla 6. Temperaturas a ambos lados de las placas de motero de cemento-cal con PCM durante el proceso de calentamiento.

	C	**C_{20}**	**CF_{20}**	**CL_{20}**	**CLF_{20}**
Temperatura Inicial (T_i) (°C)					
Cara XPS	19.60	19.00	20.80	19.00	20.30
Cara B	21.40	20.60	21.30	20.70	20.60
Temperatura Final (T_f) (°C)					
Cara XPS	24.23	23.50	25.50	23.40	25.20
Cara B	22.22	21.60	25.00	21.30	24.80
Temperatura media placas (°C)					
Temp. media placa (T_i)	20.50	19.80	21.05	19.85	20.45
Temp. media placa (T_f)	23.23	22.55	25.25	22.35	25.00
Diferencia de Temperaturas (°C)					
Diferencia de T inicial (T_i)	1.80	1.60	1.30	1.70	0.30
Diferencia de T final (T_f)	2.01	1.90	0.50	2.10	0.40

Las temperaturas a ambos lados de las placas de los morteros de cemento-cal con PCM (lado junto al aislamiento térmico - XPS y lado junto al muro de ladrillo – B) y las temperaturas medias de las placas están resumidas en la Tabla 6.

La tabla 6 también muestra los valores de diferencia de temperatura entre ambos lados de las placas de mortero. Todos estos valores corresponden al inicio (15ºC -82% HR) y al final del ciclo (30ºC – 33% HR).

Por otro lado, la Figura 24 muestra la evolución de las temperaturas desde el inicio hasta el final del ensayo durante todo el ciclo de calentamiento.

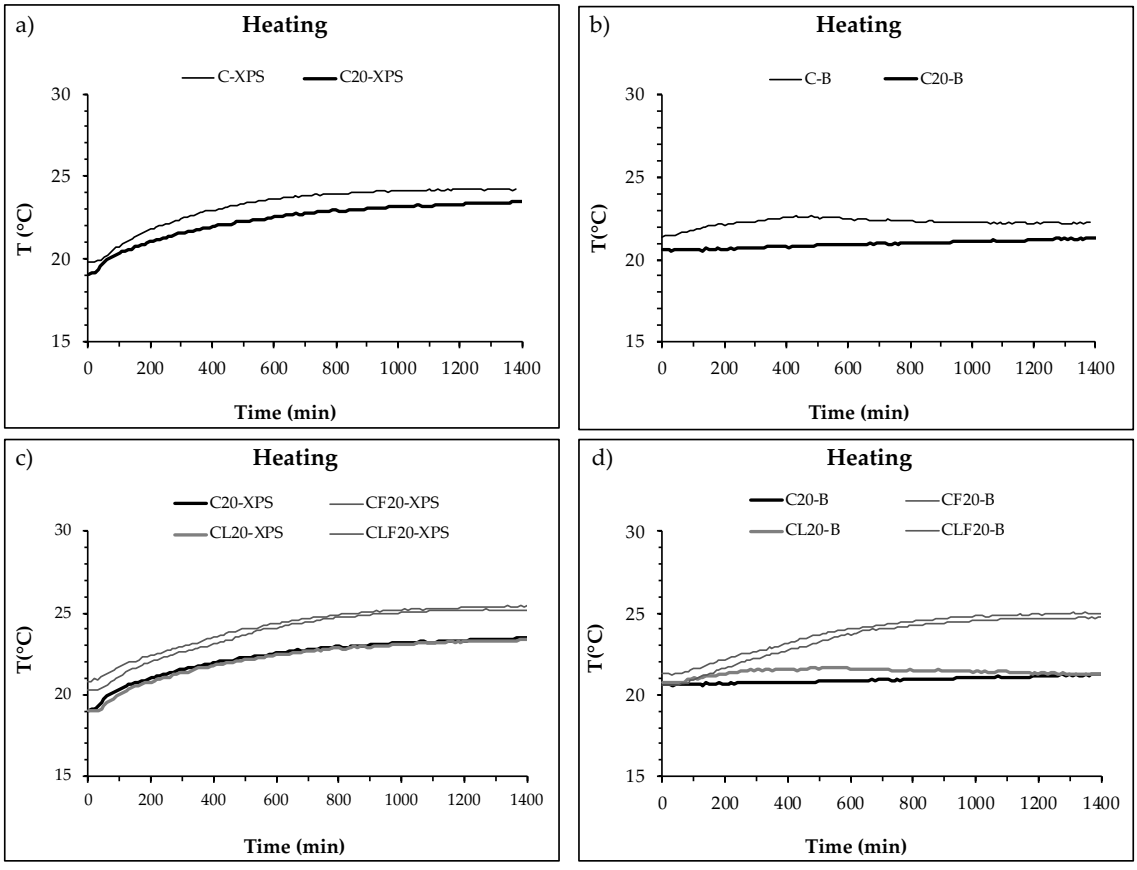

Figura 24. Temperaturas a ambos lados de las placas de los morteros de cemento-cal con PCM durante el proceso de calentamiento. (Sección 10.3.1)

Las Figuras 24a y 24b muestran la evolución de las temperaturas a ambos lados de las placas del mortero de referencia C y con 20% de PCM. Las figuras 24c y 24d muestran el mismo proceso, pero de todas las dosificaciones con 20% de PCM a ambos lados de las placas respectivamente.

Los resultados obtenidos en la Tabla 6 y Figura 24 de las temperaturas al inicio y al final del ensayo permitieron la comprobación del estado del PCM dentro de cada una de las dosificaciones tanto al inicio (15ºC - 82% HR) como al final (30ºC – 33% HR) del proceso de calentamiento, respectivamente. Se constató que al inicio todas las placas se encontraron a una temperatura por debajo de 22ºC (por debajo de la temperatura de fusión del PCM), por lo que en todos los casos el PCM comenzó el ensayo en estado sólido. Por el contrario, al final del ciclo, las temperaturas medias de las placas de morteros se situaron por encima de los 22ºC, por lo que el PCM finalizó en estado líquido. Por lo tanto, el PCM sufrió un cambio de fase de sólido a líquido en todas las dosificaciones.

En la Figura 24a se ve que la temperatura por el lado del XPS aumentó de manera continua hasta el final del ciclo (estabilización del cerramiento). Sin embargo, se observa como la adición del PCM redujo la inclinación de la curva de temperatura reduciendo a su vez la temperatura final en casi 0.5ºC respecto a C (Tabla 6). Este mismo efecto se produjo en el lado B (lado de la placa junto al ladrillo). Por lo tanto, se pude decir que la adición de 20% de PCM redujo el incremento de temperatura a ambos lados de la placa.

La evolución de la temperatura de las placas con la adición de PCM (C_{20}) y fibras de celulosa y áridos ligeros con PCM (CF_{20}, CL_{20} y CLF_{20}) que se muestra en la figura 24b también mostró un incremento de las temperaturas asociado a las condiciones ambientales de calentamiento programadas en el interior de la cámara climática. Sin embargo, se diferenciaron dos grupos de mezclas en función de su evolución. El

primero, C_{20} y CL_{20} dado que no alcanzaron los 23ºC, siendo la diferencia de temperatura al final del ciclo de 2ºC. El segundo, CF_{20} y CLF_{20} que llegaron a los 25ºC con una diferencia de temperatura en este caso de 0.5ºC y 0.4ºC respectivamente. Por todo ello, se puede decir que la adición de fibras de celulosa aumentó la temperatura global de las placas de mortero.

5.3.1.2 Efecto del mortero de cemento-cal con PCM en el interior del cerramiento multicapa.

Simultáneamente a las mediciones de temperatura en el interior del cerramiento, se midieron las temperaturas a ambos lados del cerramiento (en la cara interior y exterior de este) y el flujo de calor para cada una de las dosificaciones. **(Sección 10.3.1)**

La Figura 25 y la Tabla 7 presentan los resultados obtenidos para ambas mediciones.

Las Figuras 25a y 25c muestran la evolución de las temperaturas y las Figuras 25b y 25d muestran la evolución del flujo de calor a través de las caras interior y exterior del cerramiento multicapa.

En la Figura 25a se presentan las temperaturas de las dosificaciones C y C_{20} y la Figura 24b agrupa las temperaturas en el interior y exterior de las dosificaciones con 20% de PCM, C_{20}, CF_{20}, CL_{20} y CLF_{20}. Como se esperaba, todas las dosificaciones muestraron el mismo comportamiento en la cara exterior, la directamente expuesta a las condiciones de la cámara climática.

Se observa como la temperatura por la cara exterior del cerramiento (en contacto con la cámara climática) aumentó hasta los 30ºC durante los primeros 200 minutos hasta llegar a su estabilización durante el resto del ensayo.

En cuanto a las temperaturas en la cara interior del cerramiento (cara expuesta a las condiciones del laboratorio, 20ºC – 60% HR) para las dosificaciones C y C_{20} se mantuvieron constantes hasta los 200 minutos a partir de los cuales la temperatura aumentó levemente correspondiendo con la llegada de calor del otro lado del cerramiento. En este caso se puede ver como la adición de PCM a la mezcla supuso la disminución de 1ºC respecto a la dosificación sin PCM en la cara interior del muro. Esta disminución se puede asociar directamente a la adición de un 20% PCM a la mezcla.

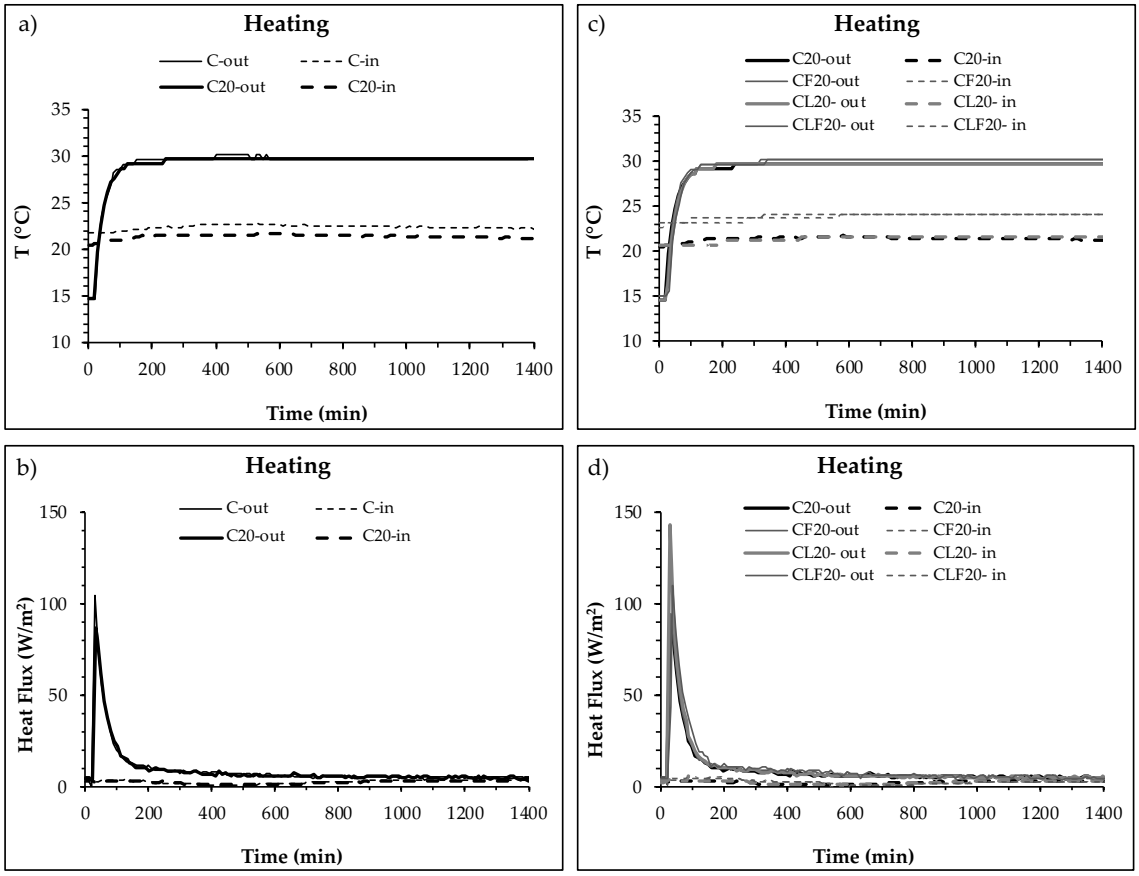

Figura 25. Temperaturas y flujos de calor a ambos lados del cerramiento multicapa mejorados con placas de los morteros estudiados a lo largo del proceso de calentamiento. (Sección 10.3.1)

Por otro lado, la Figura 25c muestra dos grupos de dosificaciones en función de la temperatura en la cara interior del cerramiento. El primer grupo, las dosificaciones con fibras de celulosa, CF_{20} y CLF_{20} y, el segundo grupo, las dosificaciones sin fibras de

celulosa C_{20} y CL_{20}. Las dosificaciones con fibras de celulosa se situaron 2-3ºC por encima de las dosificaciones sin fibras que como muestra la Tabla 7 rondaron los 21ºC. Por lo tanto, las dosificaciones con fibras de celulosa presentaron peor comportamiento dado que las mezclas sin fibras tuvieron una temperatura final inferior.

Las Figuras 25b y 25d muestran la evolución del flujo de calor en ambos lados del cerramiento comparando C y C_{20} en la Figura 25b, y C_{20}, CF_{20}, CL_{20} y CLF_{20} en la Figura 25d.

En ambas figuras todas las dosificaciones estudiadas presentaron tanto para el flujo de calor a través de la cara exterior como para el flujo de calor a través de la cara interior del cerramiento una tendencia similar para cada una de las caras. Sin embargo, los valores de pico máximo en el caso del flujo de calor por la cara exterior y el punto de inflexión en el flujo de calor por la cara interior fueron diferentes. Estos valores se pueden ver numéricamente en la tabla 7, la cual acompaña a la Figura 25 anteriormente descrita.

Tabla 7. Resumen de las temperaturas y flujos de calor a ambos lados del cerramiento multicapa mejorado con morteros de cemento-cal con PCM durante el proceso de calentamiento.

	C	**C_{20}**	**CF_{20}**	**CL_{20}**	**CLF_{20}**
Temp. interior inicial (T_i) (°C)	21.13	20.50	23.11	20.63	22.61
Temp. interior final (T_f) (°C)	22.63	21.20	24.11	21.63	24.11
Diferencia de tempertaruras interiores (T_{in}) (°C)	1.5	0.7	1	1	1.5
FC máx. exterior (W/m^2)	105	90	95	140	110
Punto de inflexión interior (min)	370	400	580	440	540
FC final exterior (W/m^2)	3.24	4.60	3.92	3.15	4.47
FC final interior (W/m^2)	1.82	3.15	3.15	2.55	2.55

Como se puede ver, la dosificación con el valor de pico máximo de flujo de calor fue la mezcla con áridos ligeros CL_{20} (140W/m^2). Este valor está relacionado directamente con los valores de conductividad térmica obtenidos en el capítulo 3.3 (Tabla 4), los cuales fueron más bajos con la adición de la perlita. Por todo ello, la dosificación CL_{20} fue la que presentó un comportamiento más favorable en tanto en cuanto fue necesaria más energía para el paso del calor por el cerramiento en comparación con el resto de las dosificaciones.

Por otro lado, la Tabla 7 también muestra los tiempos de llegada de la onda de calor, identificada por el punto de inflexión por la cara interior del cerramiento, para cada una de las dosificaciones estudiadas. Si se compara la dosificación C (sin PCM) con la C_{20} (con 20% de PCM) se observa como la adición del PCM origina un retraso del paso del flujo de calor por el punto de inflexión de 30 minutos. Este retraso viene originado por la capacidad de acumulación térmica que aporta el PCM a la mezcla. A partir de este punto, los retrasos en el paso del flujo de calor por el punto de inflexión se asocian directamente a los otros componentes que forman las dosificaciones, siendo las fibras las que aportan más retraso en este punto.

5.3.2 Evaluación del comportamiento térmico del cerramiento multicapa durante el ciclo de enfriamiento.

5.3.2.1 Evolución de las temperaturas de las placas de mortero de cemento-cal con PCM en el interior del cerramiento multicapa.

En este aparatado a diferencia del anterior, se evalúan las temperaturas a ambos lados de las placas de los morteros de cemento-cal con PCM (lado junto al aislamiento térmico - XPS y lado junto al muro de ladrillo – B) y las temperaturas medias de las placas durante el proceso de enfriamiento. **(Sección 10.3.1)** La tabla 8 muestra un resumen de

los valores obtenidos y los valores de diferencia de temperatura entre ambos lados de las muestras. Todos estos valores corresponden al inicio (30ºC -33% HR) y al final del ciclo (15ºC – 82% HR).

Tabla 8. Temperaturas a ambos lados de las placas de motero de cemento-cal con PCM durante el proceso de enfriamiento.

	C	C_{20}	CF_{20}	CL_{20}	CLF_{20}
Temperatura Inicial (T_i) (°C)					
Cara XPS	24.10	23.90	25.60	23.90	25.40
Cara B	22.30	21.60	25.20	21.50	23.80
Temperatura Final (T_f) (°C)					
Cara XPS	21.50	19.80	21.40	19.70	21.00
Cara B	21.50	20.90	21.70	20.90	21.40
Temperatura media placas (°C)					
Temp. media placa (T_i)	23.20	22.75	25.40	22.70	24.60
Temp. media placa (T_f)	21.50	20.35	21.55	20.30	21.20
Diferencia de Temperaturas (°C)					
Diferencia de T inicial (T_i)	1.80	2.30	0.40	2.40	1.60
Diferencia de T final (T_f)	0	1.10	0.30	1.20	0.40

La Figura 26 muestra la evolución de las temperaturas desde el inicio hasta el final del ensayo durante todo el proceso de enfriamiento.

Las Figuras 26a y 26b muestran la evolución de las temperaturas a ambos lados de las placas del mortero de referencia C y la dosificación C_{20} con 20% de PCM. Las figuras 26c y 26d muestran el mismo proceso para todas las dosificaciones con 20% de PCM a ambos lados de las placas respectivamente.

Al igual que se explicó en el apartado 5.3.1.1 de este mismo capítulo, a partir de las temperaturas obtenidas tanto al inicio como al final del ensayo a ambos lados de las placas de mortero se pudo comprobar si el estado del PCM sufrió cambios. La tabla 8

muestra los valores de temperatura media de cada placa obtenidos a partir de las temperaturas iniciales y finales de estas.

Como se esperaba, en el caso de las temperaturas medias iniciales se pudo comprobar como todas ellas superaron los 22ºC confirmando que el PCM en ese momento se encontraba en estado líquido. En el caso de las temperaturas finales, todas las placas finalizaron con una temperatura por debajo de los 22ºC, encontrándose por lo tanto PCM en estado sólido.

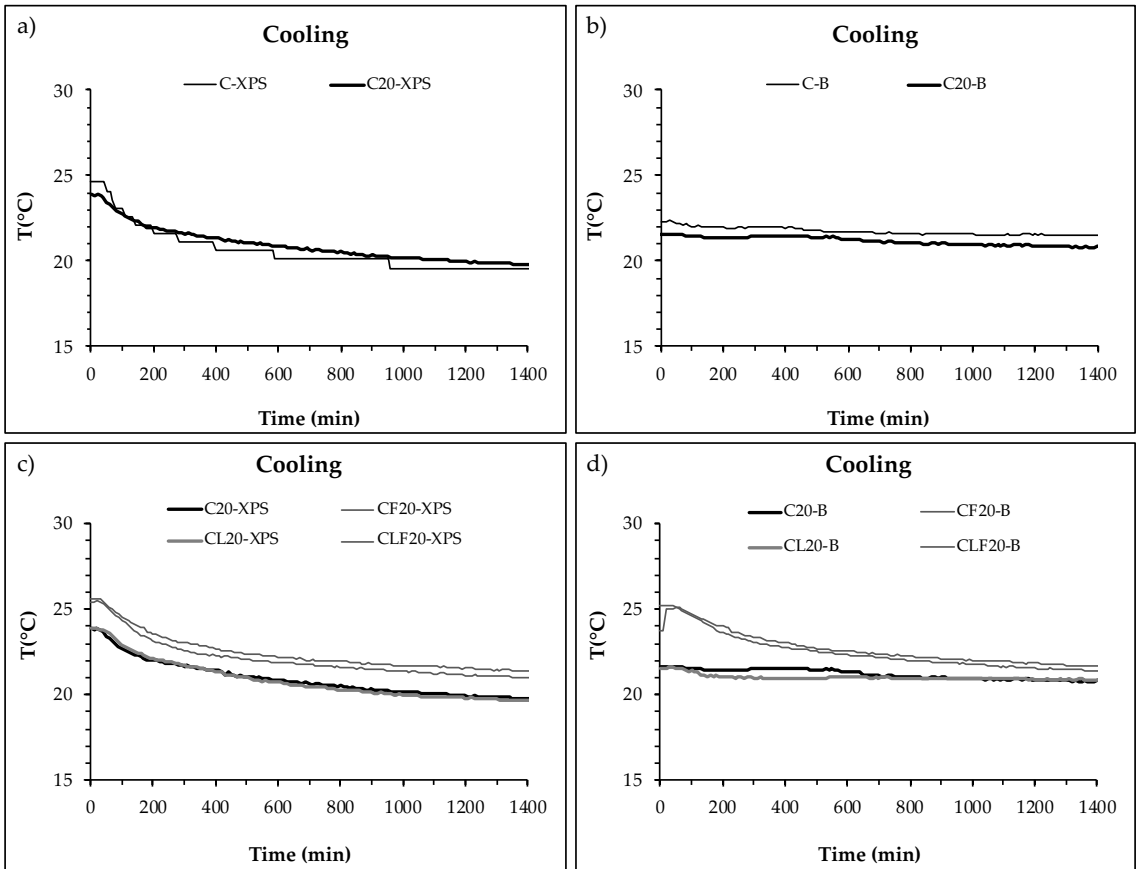

Figura 26. Temperaturas a ambos lados de las placas de los morteros de cemento-cal con PCM durante el proceso de enfriamiento. (Sección 10.3.1)

En cuanto a la evaluación de las temperaturas a ambos lados de las placas de mortero, la Figura 26a y 26b muestran las dosificaciones C y C_{20} mientras que las figuras 26c y

26d el resto de las dosificaciones con 20% de PCM. Comparando C y C_{20} no se observaron grandes diferencias. Sin embargo, sí se observaron diferencias en las dosificaciones con fibras y áridos ligeros. Las Figuras 26 y la tabla 8 muestran como el PCM incrementó en este caso la diferencia de temperatura entre ambos lados de los morteros.

La dosificación con áridos ligeros no mostró grandes diferencias en los valores de diferencia de temperaturas finales obtenidos, respecto a la de referencia con 20% de PCM, siendo esta diferencia en ambos casos por encima de 1ºC. Sin embargo, las fibras de celulosa redujeron esta diferencia final, encontrándose el valor de diferencia de temperaturas finales por debajo de 0.5ºC.

5.3.1.2 Efecto del mortero de cemento-cal con PCM en el interior del cerramiento multicapa.

Se evaluó el efecto del mortero de cemento-cal con PCM y diferentes adiciones en el comportamiento térmico de un cerramiento multicapa durante un ciclo de enfriamiento. Para ello se han analizado los resultados de temperatura y el flujo de calor a ambos lados de este cerramiento. **(Sección 10.3.1)**

Las Figuras 27a y 27c muestran la evolución de la temperatura a ambos lados del cerramiento mientras que b y d muestran el flujo de calor que pasa por la cara interior del cerramiento (condiciones del laboratorio 20ºC – 60% HR) y exterior (condiciones dentro de la cámara climática pasando en este ciclo de 30ºC – 33% HR a 15ºC -82% HR). La tabla 9 muestra de una forma numérica el resumen de los resultados plasmados en la figura 27.

Respecto a los resultados obtenidos de temperatura, en las Figuras 27a (para las dosificaciones C y C_{20}) y 27b (resto de dosificaciones con 20% de PCM) se observó la misma tendencia que para el ciclo de calentamiento. La temperatura en la cara exterior (la expuesta a las condiciones ambientales) alcanzó los 15ºC pasados 200 minutos desde el comienzo del ensayo. Tuvo temperaturas similares a las de la dosificación de referencia manteniendo durante todo el proceso 1ºC menos que la dosificación sin PCM. Por esta razón, se puede afirmar que el PCM disminuyó la temperatura.

Al igual que ocurrió en el ciclo de calentamiento, la Figura 27c muestra dos grupos diferenciados en función de los componentes que formen la mezcla. En esta ocasión, las dosificaciones con fibras (CF_{20} y CLF_{20}), se encontraron 2ºC por encima de la temperatura del resto de dosificaciones, (C_{20} y CL_{20}).

Las figuras 27b y 27d muestran los valores de flujo de calor tanto al interior como al exterior del cerramiento multicapa objeto de este trabajo. En los flujos de calor registrados en la cara exterior del cerramiento se observan las mismas tendencias que las expuestas en el proceso de calentamiento a pesar del cambio en la dirección en el flujo de calor, observando un pico máximo de flujo de calor con una posterior caída hasta su estabilización junto con el flujo de calor por la cara interior. En esta cara interior también se mantiene la misma tendencia que para el ciclo de calentamiento dando lugar un punto de inflexión el cual dependiendo de la dosificación sufrió un retraso en el tiempo o no.

La **sección 10.3.1** muestra con más detalle este proceso.

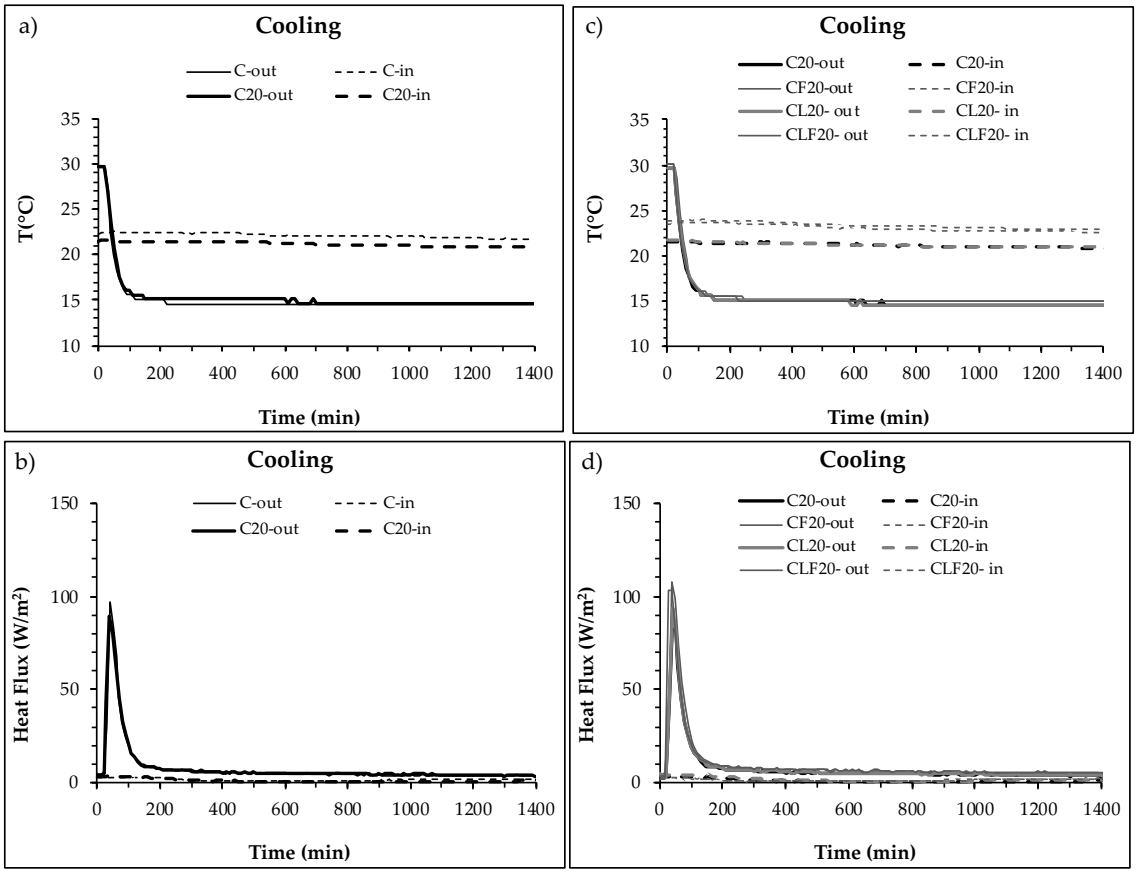

Figura 27. Temperaturas y flujos de calor a ambos lados del cerramiento multicapa mejorados con placas de los morteros estudiados a lo largo del proceso de enfriamiento. (Sección 10.3.1).

La tabla 9 muestra como la dosificación con el valor de pico máximo de flujo de calor por la cara exterior del cerramiento lo presentó CF_{20} con 110 W/m^2. Esta pequeña diferencia respecto al valor de pico máximo del resto de dosificaciones se asoció a la temperatura inicial de esta cara, la cual fue ligeramente superior en comparación con el resto de las dosificaciones.

Con respecto al tiempo que fue necesario para alcanzar el punto de inflexión para cada una de las dosificaciones se observaron varias diferencias las cuales están expuestas en la Tabla 9.

Tabla 9. Resumen de las temperaturas y flujos de calor a ambos lados del cerramiento multicapa mejorado con morteros de cemento-cal con PCM durante el proceso de calentamiento.

	C	**C_{20}**	**CF_{20}**	**CL_{20}**	**CLF_{20}**
Temp. interior inicial (T_i) (°C)	22.63	22.13	24.11	21.63	24.11
Temp. interior final (T_f) (°C)	21.63	21.13	23.61	20.63	23.11
Diferencia de tempertaruras interiores (T_{in}) (°C)	1	1	0.5	1	1
FC máx. exterior (W/m^2)	100	90	110	95	105
Punto de inflexión interior (min)	320	450	270	540	270
FC final exterior (W/m^2)	3.24	3.24	3.92	4.47	5.13
FC final interior (W/m^2)	1.82	1.32	1.82	1.87	1.87

Nuevamente, como ocurrió en el proceso de calentamiento, C_{20} y CL_{20} fueron las dosificaciones que presentaron mayor retardo en el paso por el punto de inflexión respecto a la dosificación de referencia C. En este caso, C_{20} muestra un retardo de 130 minutos respecto a C. Además, los áridos ligeros añadieron 90 minutos más a este retraso inicial haciendo un total de 220 minutos respecto a C.

Sin embargo, las dosificaciones con fibras de celulosa no presentaron ningún retardo respecto a C, acelerando incluso la llegada. En todos los casos el flujo de calor tendió a la estabilización no observando apenas diferencia entre los flujos en la cara interior y exterior del cerramiento al final del ensayo.

5.4 CONCLUSIONES

En este capítulo, con el fin de dar continuidad al estudio realizado en los capítulos anteriores de la tesis y, se ha realizado una evaluación del comportamiento térmico de un cerramiento multicapa con placas de mortero de cemento-cal con PCM y adiciones de fibras de celulosa y áridos ligeros durante un ciclo de calentamiento y enfriamiento, cumpliendo así el tercer objetivo de la tesis. Para ello se midió la temperatura a ambos lados de cada una de las placas de mortero y simultáneamente, la temperatura y el como el flujo de calor en ambas caras del cerramiento. Los hallazgos más destacados se exponen a continuación:

- El comportamiento térmico de los morteros de cemento-cal con PCM dependió no solo de su composición si no que también de las condiciones climáticas a las que estuvieran expuestos. **(Secciones 10.2.3 y 10.3.1)**
- La adición de fibras de celulosa a la mezcla produjo un incremento o disminución de las temperaturas de las placas debido a su facilidad de transmisión de calor o frío por el material. **(Sección 10.3.1)**
- La combinación de fibras de celulosa con PCM mostró un leve efecto sinérgico en el comportamiento térmico durante el proceso de calentamiento. **(Sección 10.3.1)**
- La adición de PCM retrasó el flujo de calor respecto a la dosificación de referencia sin PCM, tanto en calentamiento como en enfriamiento otorgando a los morteros con PCM la capacidad acumuladora de energía en forma de calor. Este retardo fue más acentuado en el proceso de enfriamiento que en el de calentamiento. Por lo tanto, el PCM mostró mayor influencia sobre las capacidades térmicas de los morteros durante el ciclo de enfriamiento que durante el de calentamiento. **(Sección 10.3.1)**

- Los áridos ligeros aumentaron la capacidad de aislamiento térmico de los morteros y en conjunto con los PCM pueden mejorar aún más las capacidades de los morteros. **(Sección 10.1.2, 10.2.2 y 10.3.1)**

6. SUMARIO Y CONCLUSIONES FINALES

El objetivo principal de esta tesis es el diseño y caracterización experimental de morteros de cemento-cal con PCM y adición de fibras de celulosa y áridos ligeros para la mejora del comportamiento térmico de las fachadas de los edificios existentes. Para dicho fin se ha realizado:

1. Un plan experimental para evaluar las propiedades físicas, mecánicas, térmicas y de microestructura de los morteros. **(Secciones 10.1.1, 10.1.2)**
2. Una simulación numérica de los resultados experimentales obtenidos de absorción capilar por succión de agua a partir de la propuesta de un nuevo modelo. **(Sección 10.1.3)**
3. Una evaluación del comportamiento térmico de los morteros bajo diferentes condiciones ambientales durante procesos de calentamiento y enfriamiento, realizando un análisis cualitativo de la capacidad de aislamiento y acumulación de los morteros. **(Secciones 10.2.1 y 10.2.3)**
4. Una identificación mediante ensayos no destructivos con ondas de ultrasonidos del estado del PCM para cada temperatura, así como su microestructura. **(Sección 10.2.3)**
5. Una simulación de cerramientos multicapa con las mezclas estudiadas en su interior y se han evaluado durante procesos de calentamiento y enfriamiento. **(Sección 10.3.1)**

Las conclusiones más significativas obtenidas a partir de los resultados experimentales se exponen a continuación:

- Las propiedades físicas, mecánicas y térmicas de un mortero de referencia en base cemento-cal variaron con la adición de fibras de celulosa, áridos ligeros, PCM y la combinación de estos.

- Los áridos ligeros influyeron notablemente incrementando la porosidad abierta mientras que redujeron la densidad aparente, las propiedades mecánicas y la conductividad térmica de los morteros. Sin embargo, las fibras de celulosa no mostraron cambios significativos en las propiedades de las dosificaciones estudiadas.

- La adición de PCM disminuyó la densidad aparente, la porosidad abierta y las propiedades mecánicas tales como resistencias a compresión y flexo tracción de los morteros de cemento-cal. La conductividad térmica dependió del estado del PCM, disminuyendo cuando este se encontró en estado líquido.

- Los morteros de referencia adquirieron la capacidad de acumulación térmica con la adición de PCM, aumentando la entalpía de estos. La combinación PCM y áridos ligeros (CL, CL_{10} y CL_{20}) fue la que mostró el valor más elevado de entalpía.

- Fue posible la realización de una simulación numérica con un modelo de elementos finitos de los resultados experimentales obtenidos para el coeficiente de absorción capilar por succión de agua.

- A partir de un modelo no lineal de elementos finitos y de un modelo basado en Raleigh-Ritz se pudo evaluar la influencia del PCM en la permeabilidad de los morteros, más concretamente en la absorción capilar de los mismos. La adición de PCM aumento el valor de Raleigh-Ritz para todas las dosificaciones reduciendo en consecuencia la permeabilidad de todas las mezclas con PCM.

- La adición de 10% o 20% de PCM no supuso grandes cambios en las propiedades físicas y mecánicas de los morteros.

- Las ondas de ultrasonidos, a través del coeficiente de atenuación, permitieron detectar el estado del PCM (líquido-sólido) durante la simulación de diferentes condiciones ambientales. En todos los casos, los valores más bajos de coeficiente de atenuación los presentó el PCM en estado líquido respecto al PCM en estado sólido. También pudo detectarse la microestructura siendo el coeficiente de atenuación más elevado para las dosificaciones con áridos ligeros y 20% de PCM (CL_{20}).

- A partir de los valores de flujo de calor se pudieron evaluar las entalpías de los morteros durante los procesos de calentamiento y enfriamiento sin necesidad de romper el material para su evaluación. La combinación de áridos ligeros y 20% de PCM (CL_{20}) fue la dosificación que presentó mayor capacidad de intercambio de energía por gramo de material con su entorno y tuvo los valores de entalpía más elevados.

- La densidad y la porosidad abierta de los morteros sin PCM influyó en la cantidad total de flujo de calor que es capaz de pasar por el material debido a su inercia térmica. Sin embargo, la adición de PCM retrasó el paso del flujo de calor por el cerramiento multicapa, haciendo efecto, por lo tanto, la capacidad de acumulación térmica adquirida por los materiales con el PCM.

- El cerramiento multicapa con mortero de cemento-cal con 20% de PCM y áridos ligeros (CL_{20}) es el que mejor comportamiento térmico presentó, ralentizando el paso del flujo de calor por la muestra, es decir, quedándose con una cantidad más elevada de calor en su interior aprovechando la capacidad acumuladora del material.

7. SUMMARY AND CONCLUSIONS

The main objective of this PhD thesis was the design and characterization of cement-lime mortars with the addition of PCM and cellulose fibers and lightweight aggregates to improve the thermal behavior of the existing buildings façades. To achieve this aim, some studies were carried out, as summarized next:

1. An experimental plan to evaluate the physical, mechanical and thermal properties of twelve cement-lime mortars. (Sections 10.1.1 and 10.1.2)
2. A numerical simulation from the capillary absorption results with a FEM model. (Section 10.1.3)
3. A thermal evaluation of the mortars under heating and cooling processes. A qualitative analysis has been carried out in order to know the thermal insulation and heat storage capacity of the mortars. **(Sections 10.2.1 y 10.2.3)**
4. Non-destructive techniques such as ultrasonic waves were used in order to identify the PCM states inside mortars and their microstructure. **(Section 10.2.3)**
5. A simulation of enhanced multilayered building enclosures during heating and cooling processes. **(Section 10.3.1)**

The main conclusions of the study were:

- Physical, mechanical and thermal properties of the reference cement-lime mortar varied with the addition of cellulose fibers, lightweight aggregates and Phase Change Material and the combination of both.

- Lightweight aggregates increased the open porosity while decreased the apparent density, the mechanical properties and the thermal conductivity of the mortars. However, cellulose fibers did not influence significantly on the studied properties.

- PCM decrease the apparent density, the open porosity and the compressive and flexural strength of the mortars. Thermal conductivity depended on the PCM state, being lower at liquid state.

- PCM gave the reference mortars heat storage capacity producing an increase of mortar enthalpy. Mixtures with lightweight aggregates (CL, CL_{10} and CL_{20}) showed the highest enthalpy values.

- A numerical simulation with a FEM model adjusted using capillary absorption results was done.

- With a non-lineal Finite Element Method and a model based in Raleigh-Ritz, the influence of PCM on the capillary absorption rate was evaluated. In all cases, the addition of PCM increased Raleigh-Ritz parameter, which meant a capillary absorption decrease of the mixtures with PCM.

- The addition of 10% or 20% of PCM, did not produce significant changes on the physical and mechanical properties of the mortars.

- The attenuation coefficient allowed the PCM physical state (liquid – solid) identification during heating or cooling cycles. In all cases, liquid PCM showed lower attenuation coefficient values. Mixtures' microstructure was also detected analysed and it was found that higher attenuation coefficient corresponded to mixtures with lightweight aggregates and 20% of PCM (CL_{20}).

- Enthalpy of mortars during heating and cooling cycles were evaluated using heat flux measurement devices (Non-destructive technique),. The mixture with lightweight aggregate and 20% of PCM showed the highest energy exchange capacity with the environment per gram of material (higher enthalpy).

- Apparent density and open porosity of mortars without PCM influenced the total amount of heat flux that was able to cross through the material due to its thermal inertia. However, the addition of PCM delayed the heat flow crossing through the enhanced multilayered building enclosures (due to PCM's heat storage capacity).

- The multilayered building enclosure enhanced with a layer of CL20 mortar (20% of PCM and lightweight aggregates) was the enclosure with the best thermal behavior due to the highest thermal insulation capacity and the highest heat storage capacity of the mortar.

7. SCHLUSSFOLGERUNGEN

Das Hauptziel dieser Arbeit ist das Design und die experimentelle Charakterisierung von Zement-Kalk-Mörteln mit PCM, Cellulosefasern und leichten Aggregaten zur Verbesserung des thermischen Verhaltens der Fassaden der Gebäude. Zu diesem Zweck wurde Folgendes durchgeführt:

1. Ein Versuchsplan zur Bewertung der physikalischen, mechanischen, thermischen und mikrostrukturellen Eigenschaften von Mörteln. **(10.1.1, 10.1.2)**
2. Eine numerische Simulation der experimentellen Ergebnisse der Kapillarabsorption aus dem Vorschlag eines neuen Modells. **(10.1.3)**
3. Eine Bewertung des thermischen Verhaltens von Mörteln während Heiz- und Kühlprozesse, wobei eine qualitative Analyse der Isolations- und Akkumulationskapazität von Mörteln durchgeführt wird. **(10.2.1, 10.2.3)**
4. Identifizierung des Zustands des PCM für jede Temperatur sowie seiner Mikrostruktur mit der *Non-Destructive Technique* (Ultraschallwellen). **(10.2.3)**
5. Eine Simulation einer *multilayered enclosure* mit den untersuchten Mörteln, die während der Heiz- und Kühlprozesse ausgewertet wurden. **(10.3.1)**

Die wichtigsten Schlussfolgerungen aus den experimentellen Ergebnissen sind:

- Die physikalischen, mechanischen und thermischen Eigenschaften eines Zement-Kalk-Mörtels variierten mit der Zugabe von Cellulosefasern, leichten Aggregaten, PCM und deren Kombination.

- Leichte Aggregate haben einen Einfluss, indem sie die offene Porosität erhöhten. Gleichzeitig verringerten sie die Dichte, die mechanischen Eigenschaften und die Wärmeleitfähigkeit der Mörtel. Die Cellulosefasern zeigten jedoch keine signifikanten Änderungen in den Eigenschaften der untersuchten Mörtel.

- Die Referenzmörtel erlangten die thermische Akkumulationskapazität durch die Zugabe von PCM, wodurch ihre Enthalpie erhöht wurde. Die Kombination von PCM und leichten Aggregaten (CL, CL_{10} und CL_{20}) zeigte die höchste Enthalpie.

- Aus den experimentellen Ergebnissen, die für den Kapillarabsorptionskoeffizienten erhalten wurden, konnte eine numerische Simulation mit einem Finite-Elemente-Modell durchgeführt werden.

- Mit einem nichtlinearen Finite-Elemente-Modell und einem auf Raleigh-Ritz basierenden Modell konnte der Einfluss von PCM auf die Kapillarabsorption bewertet werden. Die Zugabe von PCM erhöhte den Raleigh-Ritz Parameter für alle Mörtel, wodurch die Permeabilität aller Mörteln mit PCM verringert wurde.

- Die Zugabe von 10% oder 20% PCM führte zu keinen großen Änderungen der physikalischen und mechanischen Eigenschaften der Mörtel.

- Durch den Dämpfungskoeffizienten konnte der Zustand des PCM während der Simulation verschiedener Umgebungsbedingungen erfasst werden. In allen Fällen wurden die niedrigsten Werte des Dämpfungskoeffizienten für flüssiges PCM im Vergleich zu festen PCM ermittelt. Die Mikrostruktur konnte ebenfalls nachgewiesen werden. Den höchsten Dämpfungskoeffizient für die Mörteln hatten die Mörtel mit leichten Aggregaten und 20% PCM (CL_{20}).

- Die Enthalpien der Mörtel während der Heiz- und Kühlprozesse konnten mithilfe der Wärmeflusswerten bewertet werden, ohne dass das Material für die Bewertung zerbrochen werden musste. Die Kombination von leichten Aggregaten und 20% PCM (CL20) war die Dosierung, die mit ihrer Umgebung die höchste Energieaustauschkapazität pro Gramm Material aufwies und somit auch die höchsten Enthalpiewerte aufzeigte.

- Die Dichte und offene Porosität der Mörtel ohne PCM beeinflussten die Gesamtmenge des Wärmeflusses, der aufgrund seiner thermischen Trägheit durch das Material fließen kann. Die Zugabe von PCM verzögerte jedoch den Durchgang des Wärmeflusses durch die Mehrschichtummantelung, wodurch die Wärmespeicherkapazität beeinflusst wurde, die durch die Materialien mit dem PCM erhalten wurde.

- Die mehrschichtige Ummantelung mit Zement-Kalk-Mörtel mit 20% PCM und leichten Zuschlagstoffen (CL20) zeigte das beste Wärmeverhalten und verlangsamte den Durchgang des Wärmeflusses durch die Probe. Daher blieb eine höhere Wärmemenge im Inneren zurück, wobei die Akkumulationskapazität des Materials ausgenutzt wurde.

8. FUTURAS LINEAS DE INVESTIGACIÓN

Con este trabajo se ha intentado dar respuesta a la problemática encontrada a partir del desarrollo de los objetivos planteados al inicio de la investigación. Sin embargo, se detectó la posibilidad de optimizar las prestaciones de los materiales y la mejora de su aplicabilidad. A continuación, se resumen algunas de las propuestas de futuras líneas de investigación:

- Se propone realizar un análisis cuantitativo de la repercusión de la mejora de la eficiencia energética de los cerramientos multicapa con morteros de cemento-cal con PCM en el usuario de los edificios residenciales.

- Se propone también realizar un estudio para el ajuste en la cantidad y proporción de los componentes que conforman las mezclas con el objetivo de optimizar los parámetros térmicos como la reducción de la conductividad térmica sin menoscabar otras propiedades como, por ejemplo, físico- mecánicas. También se podrían añadir otros componentes que favorezcan a parámetros no estudiados en este trabajo como los de aislamiento acústico.

- Se propone hacer un estudio para la optimización del cerramiento multicapa mejorado con morteros de cemento-cal con PCM. Podría estudiarse un cambio en el espesor de la muestra y alargar los procesos de evaluación con la simulación de diferentes condiciones ambientales.

- Se propone llevar a cabo una evaluación de la durabilidad de los morteros. Del mismo modo sería interesante una evaluación del comportamiento del PCM y su posible degradación dentro de las mezclas a lo largo del tiempo. Dicho estudio se podría llevar a cabo con técnicas no destructivas como las ondas de ultrasonidos.

- Se propone diseñar sistemas de cerramiento multicapa más complejos, incorporando morteros de cemento-cal y nuevos materiales que mejoren las propiedades acústicas, que sirvan como revestimiento y puedan ser pigmentados.

9. BIBLIOGRAFÍA

Ali Memon S., (2014) Phase change materials integrated in building walls: A state of the art review, Renewable and Sustainable Energy Reviews, 31 870-906, https://doi.org/10.1016/j.rser.2013.12.042.

Aligizaki, K. (2005). Pore Structure of Cement-Based Materials. London: CRC Press.

Alibakhsh K, Leyli b, Fathollah P, Erfan K, Wei-Mon Y, (2017) Experimental studies on the applications of PCMs and nano-PCMs in buildings: A critical review, Energy and Buildings, Volume 154, 96-112, ISSN 0378-7788, https://doi.org/10.1016/j.enbuild.2017.08.037.

Alonso C., Oteinza I., García-Navarro J., Martín-Consuegra F., (2016) Energy consumption to cool and heat experimental modules for the energy refurbishment of façades. Three case studies in Madrid. Energy and Buildings 126 252-262, https://dx.doi.org/10.1016/j.enbuild.2016.04.034.

Arici M., Bilgin F., Nizetic S., Karabay H., (2020) PCM integrated to external building walls: An optimization study on maximum activation of latent heat, Applied Thermal Engineering 165 114560, https://doi.org/10.1016/j.applthermaleng.2019.114560.

Arizzi, A., Martínez-Martínez, J., & Cultrone, G. (2013) Ultrasonic wave propagation through lime mortars: an alternative and non-destructive tool for textural characterization. Materilas and Structures, 46, 1321-1335.

Anant Kishore R., Bianchi,M. Booten C., Vidal J. and Jackson R., (2020) Optimizing PCM-integrated wall for potential energy savings in U.S, Energy&Buildings 226 110355, https://doi.org/10.1016/j.enbuild.2020.110355.

Banu, D., Feldman, D., Haghighat, F., Paris, J., & Hawes, D. (1998). Energy-storing wallboard: flammability tests. Journal of Materials in civil Engineering, 10(2), 98-105.

G. Barluenga, F. Hernández-Olivares, (2007) Cracking control of concretes modified with short AR-glass fibers at early age. Experimental results on standard concrete and SCC, Cement and Concrete Research, Volume 37, Issue 12, Pages 1624-1638, ISSN 0008-8846, https://doi.org/10.1016/j.cemconres.2007.08.019.

Barluenga G., Palomar I., Puentes J., (2013) Early age and hardened performance of cement pastes combing mineral additions. Material and Structures, 46 921–41, https://doi.org/10.1617/s11527-012-9944-9.

Barluenga G. Puentes, J., Palomar I., Guardia C., (2018) Methodology for monitoring Cement Based Materials at Early Age combining NDT techniques, Construction and Building Materials, Volume 193, 373-383, ISSN 0950-0618, https://doi.org/10.1016/j.conbuildmat.2018.10.205.

Bary B, Sellier A. (2004) Coupled moisture-carbon dioxide-calcium transfer model for carbonation of concrete. Cem Concr Res ;34(10):1859–72.

Bentchikou, M., Guidoum, A., Scrivener, K., Silhadi K., & Hanini, S., (2012) Effect of recycled cellulose fibres on the properties of lightweight cement composite matrix, Construction and Building Materials, 34 451-456, https://doi.org/10.1016/j.conbuildmat.2012.02.097.

Birgül, R. (2009), Hilbert transformation of waveforms to determine shear wave velocity in concrete. Cement and Concrete Research, 39(8), 696-700.

Cabeza L.F., Barreneche C., Castell A., de Garcia A., et al., (2011) Materials used as PCM in thermal energy storage in building: A review, Renewable and Sustainable Energy Reviews, 15 1675-1695, https://doi.org/10.1016/j.rser.2010.11.018.

Caggiano, A., Schicchi, D. S., Mankel, C., Ukrainczyk, N., & Koenders, E. A. (2018). A mesoscale approach for modeling capillary water absorption and transport phenomena in cementitious materials. Computers & Structures, 200, 1-10.

Chaube, Rajesh, Toshiharu Kishi, and Koichi Maekawa (2014). Modelling of concrete performance: Hydration, microstructure and mass transport. CRC Press.

Cui, H., Memon, S. A., & Liu, R. (2015). Development, mechanical properties and numerical simulation of macro encapsulated thermal energy storage concrete. Energy and buildings, 96, 162-174.

Cunha S., Aguiar J., Pacheco-Torgal F., (2015) Effect of temperature on mortars with incorporation of phase change materials, Construction and Building Materials, 98 89-101, https://doi.org/10.1016/j.conbuildmat.2015.08.077.

Cunha S., Lima M. , Aguiar J.B. (2016) Influence of adding phase change materials on the physical and mechanical properties of cement mortars, Construction and Building Materials, 127 1-10, https://doi.org/10.1016/j.conbuildmat.2016.09.119

De Freitas JT, Cuong P, Faria R. (2017). Hybrid finite elements for nonlinear thermal and hygral problems. Comput Struct; 182:14–25.

Drissi S., Eddhahak A., Caré S., Neji J.,(2015) Thermal analysis by DSC of Phase Change Materials, study of the damage effect, Journal of Building Engineering, 1 13-19, https://doi.org/10.1016/j.jobe.2015.01.001.

Edsjø Kalnæs, S., Petter Jelle, B. (2015) “Phase change materials and products for building applications: A state-of-the-art review and future research opportunities.” Energy and Buildings 94 (2015) 150–17.

Erlbeck, L., Schreiner, P., Schlachter, K., Dörnhofer, P., Fasel, F., Methner, F. J., & Rädle, M. (2018). Adjustment of thermal behavior by changing the shape of PCM inclusions in concrete blocks. Energy Conversion and Management, 158, 256-265.

Fachinotti V., Bre F., Mankel C., Koenders E. and Caggiano A., (2020) Optimization of multilayered Walls for Building Envelopes including PCM-Based Composites, Materials 13, 2787, https://doi.org/10.3390/ma13122787.

Günther E., Hiebler S., Mehling H. , Redlich R. , (2009) Enthalpy of phase change materials as a function of temperature: required accuracy and suitable measurement methods, Int J Thermophys, 30 1257-1269, https://doi.org/10.1007/s10765-009-0641-z.

Gschwander S., Haussmann T., Hagelstein G., Sole A., Cabeza LF., Diarce G. et al., (2015) Standardization of PCM characterization via DSC. 13th international conference on energy storage. 19–21.

Guardia, C., Barluenga, G., & Palomar, I. (2017). Phase Change Material cement-lime mortars for thermal retrofitting of façades. 2nd International Conference on Bio-based Buildung Materials & 1st Conference on ECOlogical valorisation of GRAnular and Fibrous materials. (RILEM PRO 119). RILEM Publications SARL. Clermont-Ferrand, France.

Guardia, C., Barluenga, G., & Palomar, I. (2018). *Thermal Evaluation of Cement-Lime Based Materials with PCM*. 4th International Conference on Service Life Design for Infrastructures (SLD4), RILEM PRO 125, RILEM Publications SARL Delft, Netherlands. E-ISBN: 978-2-35158-213-8

Guardia, C., Barluenga, G., & Palomar, I. Diarce G., (2019) Thermal enhanced cement-lime mortars with phase change materials (PCM), lightweight aggregate and cellulose fibers, Construction and Building Materials, Volume 221, 586-594, ISSN 0950-0618, https://doi.org/10.1016/j.conbuildmat.2019.06.098.

Guardia, C., Schicchi, D.S., Caggiano, A. et al. (2020) On the capillary water absorption of cement-lime mortars containing phase change materials: Experiments and simulations. Build. Simul. 13, 19–31, https://doi.org/10.1007/s12273-019-0556-y

Guardia, C.; Barluenga, G.; Palomar, I. (2020) PCM Cement-Lime Mortars for Enhanced Energy Efficiency of Multilayered Building Enclosures under Different Climatic Conditions. Materials, 13, 4043. https://doi.org/10.3390/ma13184043.

Halamickova, P., Detwiler, R. J., Bentz, D. P., & Garboczi, E. J. (1995). Water permeability and chloride ion diffusion in Portland cement mortars: relationship to sand content and critical pore diameter. Cement and concrete research, 25(4), 790-802.

Hall, Christopher (2007). "Anomalous diffusion in unsaturated flow: Fact or fiction?" Cement and Concrete Research 37.3: 378-385.

Haurie L., Serrano S., Bosch M., A. Fernandez,L. Cabeza, (2016) Single layer mortars with microencapsulated PCM: Study of physical and thermal properties, and fire behaviour, Energy and Buildings, 111 393-400, https://doi.org/10.1016/j.enbuild.2015.11.028.

Herrero S., Mayor P., Hernández-Olivares F., (2013) Influence of proportion and particle size gradation of rubber from end-of-life tires on mechanical, thermal and acoustic properties of plaster–rubber mortars, Materials & Design, 47, 633-642, https://doi.org/10.1016/j.matdes.2012.12.063.

Hunger, M., Entrop, A. G., Mandilaras, I., Brouwers, H. J. H., & Founti, M. (2009). The behavior of self-compacting concrete containing micro-encapsulated phase change materials. Cement and Concrete Composites, 31(10), 731-743.

Isgor OB, Razaqpur A. (2004). Finite element modeling of coupled heat transfer, moisture transport and carbonation processes in concrete structures. Cem Concr Compos; 26(1):57–73.

Jahangir Khan R., Zubayer Md. Bhuiyan H., Hasan Ahmed D., (2020) Investigation of heat transfer of a building wall in the presence of phase change material (PCM), Energy and Built Environment 1, 199-206, https://doi.org/10.1016/j.enbenv.2020.01.002.

Jayalath A, San Nicolas R., Sofi M., Shanks R., Ngo T., Aye L., Mendis P., Properties of cementitious mortar and concrete containing micro-capsulated phase change materials, Construction and Building Materials, 120 (2016) 408-417, https://doi.org/10.1016/j.conbuildmat.2016.05.116.

Jin X., Xu X., Zhang X., Yin Y., (2014) Determination of the PCM melting temperature range using DSC, Thermochimica Acta, 595, 17-21, https://doi.org/10.1016/j.tca.2014.09.004.

Jeon, J., Lee, J. H., Seo, J., Jeong, S. G., & Kim, S. (2013). Application of PCM thermal energy storage system to reduce building energy consumption. Journal of thermal analysis and calorimetry, 111(1), 279-288.

Juárez D., Balart R, Ferrándiz S., García D. (2012) “Classification of phase change materials and his behaviour in SEBS/PCM blends”, 3Ciencias.

Kim, H. K., Jeon, J. H., & Lee, H. K. (2012). Workability, and mechanical, acoustic and thermal properties of lightweight aggregate concrete with a high volume of entrained air. Construction and Building Materials, 29, 193-200.

Khudhair, A. M., & Farid, M. M. (2004). A review on energy conservation in building applications with thermal storage by latent heat using phase change materials. Energy conversion and management, 45(2), 263-275.

Kumar Singh Rathore P., Kumar Shukla S., (2020) An experimental evaluation of themal behavior of the building envelope using macroencapsulated PCM for energy saving, Renewable Energy 149, 1300-1313, https://doi.org/10.1016/j.renene.2019.10.130.

Lafhaj Z, Goueygou M., Djerbi A., Kaczmarek M., (2006) Correlation between porosity, permeability and ultrasonic parameters of mortar with variable water/cement ratio and water content, Cement and Concrete Research, Volume 36, Issue 4, 625-633, ISSN 0008-8846, https://doi.org/10.1016/j.cemconres.2005.11.009.

Lucas S., Ferreira V.M., (2010) Selecting insulating building materials trough an assessment tool. In CIB ed. Portugal SB10. Sustainable Building Affordable to All, 745-752.

Lucas S., L. Senff L, Ferreira V.M. V.M, J.L. (2010) Barroso de Aguiar et al., Fresh state Characterization of lime mortars with PCM addition, Applied Rheology, 20, 63162 1-7, http://doi.org/10.3933/ApplRheol-20-63162

Lucas S., Ferreira V.M., Barroso de Aguiar J.L. (2013) Latent heat storage in PCM containing mortars—Study of microstructural modifications, Energy and Buildings, 66 724-731, https://doi.org/10.1016/j.enbuild.2013.07.060.

Lucas, S.S. & Barroso de Aguiar, J.L. (2019) Heat Mass Transfer 55: 2429. https://doi.org/10.1007/s00231-019-02594-1.

Martın-Pérez B, Pantazopoulou S, Thomas M. (2001) Numerical solution of mass transport equations in concrete structures. Comput Struct;79 (13):1251–64.

Mankel C., Caggiano A., Ukrainczyk N., Koenders E., (2019) Thermal energy storage characterization of cement-based systems containing microencapsulated-PCMs, Construction and Building Materials, Volume 199, 307-320, ISSN 0950-0618, https://doi.org/10.1016/j.conbuildmat.2018.11.195.

Oliver, A. (2009) Integración de materiales de cambio de fase en placas de yeso reforzadas con fibras de polipropileno. Aplicación a sistemas de refrigeración y calefacción pasivos para almacenamiento de calor latente en edificios. Junio, Madrid.

Oria, A. (2011) La evolución de las fachadas ventiladas, nuevos materiales y sistemas constructivo. Universidad de Valencia. Escuela Técnica Superior de Ingeniería de Edificación.

Palomar I., G. Barluenga, J. Puentes, (2015) Lime–cement mortars for coating with improved thermal and acoustic performance, Construction and Building Materials, 75, 306-314, https://doi.org/10.1016/j.conbuildmat.2014.11.012

Palomar I., Barluenga G., (2017) Assessment of lime-cement mortar microstructure and properties by P- and S- ultrasonic waves, Construction and Building Materials, 139, 334-341, https://doi.org/10.1016/j.conbuildmat.2017.02.083.

Palomar I. (2017b) Desarrollo y caracterización de morteros de revestimiento para la mejora acústica y térmica en construcción, rehabilitación o restauración del patrimonio edificado. Universidad de Alcalá.

Palomar I., Barluenga G., (2018) A multiscale model for pervious lime-cement mortar with perlite and cellulose fibers, Construction and Building Materials, 160, 136-144, https://doi.org/10.1016/j.conbuildmat.2017.11.032.

Palomar I., G. Barluenga, R.J. Ball, M. Lawrence, (2019) Laboratory characterization of brick walls rendered with a pervious lime-cement mortar, Journal of Building Engineering, Volume 23, 241-249, ISSN 2352-7102, https://doi.org/10.1016/j.jobe.2019.02.001.

Pavlík, Z., Vejmelková,E., Fiala,L.,& Černý, R. (2009). Effect of moisture on thermal conductivity of lime-based composites. International Journal of Thermophysics, 30 (6) 1999-2014

Pavlík Z., Fořt J., Pavlíková M., Pokorný J., Trník A., Černý R., (2016) Modified lime-cement plasters with enhanced thermal and hygric storage capacity for moderation of interior climate, Energy and Buildings, 126, 113-127, https://doi.org/10.1016/j.enbuild.2016.05.004.

Philippidis, T.P., & Aggelis, D.G. (2005). Experimental study of wave dispersion and attenuation in concrete. Ultrasonics, 43 (7), 584-595.

Popovics, S., Rose, J.L., & Popovics, J.S (1990). The behavior of ultrasonic pulses in concrete. Cement and Concrete Reasearch, 20 (2), 259-270.

Qiao Y., Yang L., Bao J., Liu Y. and Liu J., (2019) Reduced-scale experiments on the thermal performance of phase change material wallboard in different climate conditions, Building and Environment 160, 106191, https://doi.org/10.1016/j.buildenv.2019.106191.

Ristić A., Furbo S., Moser C., Schranzhofer H., et al., (2016) IEA SHC Task 42 / ECES Annex 29 WG A1: Engineering and Processing of PCMs, TCMs and Sorption Materials, Energy Procedia, 91, 207-217, https://doi.org/10.1016/j.egypro.2016.06.205.

Ryms M., Klugmann-Radziemska E., (2019) Possibilities and benefits of a new method of modifying conventional building materilas with phase-change materials (PCMs), Construction and Building Materials.211, 1013-1024, https://doi.org/10.1016/j.conbuildmat.2019.03.277.

Ryms M., Januszewicz K., Kazimierski P., Luczak J., et al., (2020) Post-Pyrolytiz Carbon as a Phase Change Materials (PCMs) Carrier for Application in Building Materials, Materials 13 , 1268, https://goi.org/10.3390/ma13061268.

Sala E., Zanotti C., Passoni C., Marini A., (2016) Lightweight natural lime composites for rehabilitation of Historical Heritage, Construction and Building Materials, 125 , 81-93, https://doi.org/10.1016/j.conbuildmat.2016.08.033.

Samson E, Marchand J. (2007). Modeling the transport of ions in unsaturated cementbased materials. Comput Struct; 85(23):1740–56.

Schlangen E, Koenders E, van Breugel K. Influence of internal dilation on the fracture behaviour of multi-phase materials. Eng Fract Mech 2007;74:18–33.

Schiavoni S., D'Alessandro F., Bianchi F., Asdrubali F., (2016) Insulation materials for the building sector: A review and comparative analysis, Renewable and Sustainable Energy Reviews, 62, 988-1011, https://doi.org/10.1016/j.rser.2016.05.045.

Sharifi N. P., Sakulich A., (2015) Application of phase change materials to improve the thermal performance of cementitious material, Energy and Buildings, 103 , 83-95, https://doi.org/10.1016/j.enbuild.2015.06.040.

Sharma A., V.V. Tyagi, C.R. Chen, D. Buddhi, (2009) Review on thermal energy storage with phase change materials and applications, Renewable and Sustainable Energy Reviews, 13, 318-345, https://doi.org/10.1016/j.rser.2007.10.005.

Sharma R.K., Ganesan P., Tyagi V.V., Metselaar H.S.C., Sandaran S.C., (2015) Developments in organic solid–liquid phase change materials and their applications in thermal energy storage, Energy Conversion and Management, Volume 95, 193-228, ISSN 0196-8904, https://doi.org/10.1016/j.enconman.2015.01.084.

Segura J, Carol I. On zero-thickness interface elements for diffusion problems. Int J Nmer Anal Methods Geomech 2004;28(9):947–62.

Shin, K. J., Bae, W., Choi, S. W., Son, M. W., & Lee, K. M. (2017). Parameters influencing water permeability coefficient of cracked concrete specimens. Construction and Building Materials, 151, 907-915.

Silva L.M., Ribeiro R.A., Labrincha J.A., Ferreira V.M., (2010) Role of lightweight fillers on the properties of a mixed-binder mortar, Cement and Concrete Composites, 32, 19-24, https://doi.org/10.1016/j.cemconcomp.2009.07.003.

Soongswang, P., Tia, M., & Bloomquist, D. (1991). Factors affecting the strength and permeability of concrete made with porous limestone. Materials Journal, 88(4), 400-406.

Stefanidou M., (2014) Cement-based renders with insulating properties, Construction and Building Materials, 65, 427-431, https://doi.org/10.1016/j.conbuildmat.2014.04.062.

Terés-Zubiaga J., Martín K., Erkoreka A., Sala J.M., (2013) Field assessment of thermal behaviour of social housing apartments in Bilbao, Northern Spain, Energy and Buildings, 67, 118-135, https://doi.org/10.1016/j.enbuild.2013.07.061.

Terés-Zubiaga J., Campos-Celador A., González-Pino I., Escudero-Revilla C., (2015) Energy and economic assessment of the envelope retrofitting in residential buildings in Northern Spain, Energy and Buildings, 86, 194-202, https://doi.org/10.1016/j.enbuild.2014.10.018.

Veiga R., (2017) Air lime mortars: What else do we need to know to apply them in conservation and rehabilitation interventions? A review, Construction and Building Materials, 157, 132-140, https://doi.org/10.1016/j.conbuildmat.2017.09.080.

Venkateswara Rao V., Parameshwaran R., Vinayaka Ram V., (2018) PCM-mortar based construction materials for energy efficient buildings: A review on research trends, Energy and Buildings, 158, 95-122, https://doi.org/10.1016/j.enbuild.2017.09.098.

Wang L, Ueda T. (2011) Mesoscale modeling of water penetration into concrete by capillary absorption. Ocean Eng;38(4):519–28.

Warda, B. A., & Munaz, A. N. (2012). Effects of aggregate gradation on water permeability of concrete. In Advanced Materials Research (Vol. 488, pp. 248-252). Trans Tech Publications.

Weinläder, H., Beck, A., & Fricke, J. (2005). PCM-facade-panel for daylighting and room heating. Solar Energy, 78(2), 177-186.

Wi S., Yang S., Hun Park J. et al. (2020) Climatic cycling assessment of red clay/perlite and vermiculite composite PCM for improving thermal inertia in buildings, Building and Enviroment 167, 106464, https://doi.org/10.1016/j.buildenv.2019.106464.

Zhou D., Zhao C.Y., Tian Y., (2012) Review on thermal energy storage with phase change materials (PCMs) in building applications, Applied Energy, 92, 593-605, https://doi.org/10.1016/j.apenergy.2011.08.025.

Zhou, Jian (2011). Performance of engineered cementitious composites for concrete repairs.

AA.VV. Código Técnico de la Edificación. Documento Básico HE Ahorro de energía. B.O.E: 27/12/2019.

BASF, Datasheet Micronal PCM DS 5040 X, (11/2013).

Omya Clariana S.L, Datasheet Fibracel® BC-1000 (Ø20µm).

UNE 80305:2012. Cementos blancos.

UNE-EN 197-1:2011. Cemento. Parte 1: Composición, especificaciones y criterios de conformidad de los cementos comunes.

UNE-EN 459-1:2011. Cales para la construcción. Parte 1: Definiciones, especificaciones y criterios de conformidad.

UNE-EN 998-1:2010. Especificaciones de los morteros para albañilería. Parte 1: Morteros para revoco y enlucido.

UNE-EN 1015-3:1999. Métodos de ensayo para morteros de albañilería. Parte 3: Determinación de la consistencia del mortero fresco (por la mesa de sacudidas).

UNE-EN 1015-6:1998. Métodos de ensayo de los morteros para albañilería. Parta 6: Determinación de la densidad aparente del mortero fresco.

UNE-EN 1015-10:1999. Métodos de ensayo de los morteros para albañilería. Parte 10: Determinación de la densidad aparente en seco del mortero endurecido.

UNE-EN 1015-11:1999. Métodos de ensayo de los morteros para albañilería. Parte 11: Determinación de la resistencia a flexión y a compresión del mortero endurecido.

UNE-EN 1015-12:2000. Métodos de ensayo de los morteros para albañilería. Parte 12: Determinación de la resistencia a la adhesión de los morteros de revoco y enlucido endurecidos aplicados sobre soportes.

UNE-EN 1015-18:2002. Métodos de ensayo de los morteros para albañilería. Parte 18: Determinación del coeficiente de absorción de agua por capilaridad del mortero endurecido.

UNE-EN 1015-18:1999. Métodos de ensayo de los morteros para albañilería. Parte 19: Determinación de la permeabilidad al vapor de agua de los morteros endurecidos de revoco y enlucido.

Nearly-Zero-Energy-Buildings, *https://ec.europa.eu/energy/topics/energy-efficiency/energy-efficient-buildings/nearly-zero-energy-buildings_en*

10. RESULTADOS DE INVESTIGACIÓN

10.1. Publicaciones sobre el diseño y caracterización de los morteros.

10.1.1 Phase Change Material cement-lime mortars for thermal retrofitting of facades.

Guardia, C., Barluenga, G., & Palomar, I. (2017). *Phase Change Material cement-lime mortars for thermal retrofitting of façades*. 2nd International Conference on Bio-based Buildung Materials & 1st Conference on ECOlogical valorisation of GRAnular and Fibrous materials. (RILEM PRO 119). RILEM Publications SARL. Clermont-Ferrand, France. e- ISBN 978-2-35158-192-6.

2nd International Conference on Bio-based Building Materials &
1st Conference on ECOlogical valorisation of GRAnular and FIbrous materials

June 21th - 23th 2017
Clermont-Ferrand, France

PHASE CHANGE MATERIAL CEMENT-LIME MORTARS FOR THERMAL RETROFITTING OF FACADES

C. Guardia*, G. Barluenga, I. Palomar
Department of Architecture, University of Alcalá, Madrid, Spain
*Corresponding author; e-mail: cynthia.guardia@edu.uah.es

Abstract
The poor thermal performance of many dwelling units built from 1940 to 1980 produces a low energy efficiency under the present thermal standards. In order to fulfil comfort and energy efficiency requirements, these facades need to be retrofitted. In many cases, External Thermal Insulation Composite System (ETICS) are used to increase thermal insulation, although this solution does not consider the thermal inertia. New mortars with improved thermal insulation and inertia are investigated as an innovative solution. Twelve cement-lime mortars were designed, using: white cement, air lime, siliceous aggregate (0-4 mm), lightweight aggregate (LWA) (expanded perlite), short cellulose fibres and 10 and 20% of a Phase Change Material (PCM) - microencapsulated paraffin wax. PCM's nominal melting temperature was 23 ± 1 °C. An experimental program was carried out to assess the effect of PCM on the physical and thermal performance of the mortars. Two different scenarios were considered to evaluate the temperature effect on the PCM-mortar performance. Bulk density, open porosity, capillary absorption, vapour permeability, thermal conductivity and compressive strength were characterized. PCM produced significant changes on the mortar thermal properties and a synergetic effect of PCM and LWA was identified.

Keywords:
Phase Change Material, cement mortar, experimental characterization, thermal inertia, facades' thermal retrofitting.

1 INTRODUCTION

Many dwelling units in Spain built from 1940 to 1980 present a large energy consumption due to their poor thermal performance, when compared to present thermal standards. These façades have also a low thermal inertia which further reduce their thermal properties. Nowadays, façade retrofitting solutions are designed to improve energy efficiency primarily through thermal insulation. The most common solutions are ventilated façade systems and External Thermal Insulation Composite System (ETICS) [Lucas 2010b]. However, those solutions have shown a poor performance in summer conditions [Schiavoni 2016] and do not consider the façade thermal inertia and its influence on energy efficiency. Besides, some issues arise on both systems due to their low adaptability and the thickness increase of the façade.

The design of new mortars with improved thermal properties is an alternative solution for façade retrofitting [Stefanidou 2014, Palomar 2015b]. The former mortars only considered thermal insulation, but thermal inertia is increasing interest in the last years. Phase Change Materials (PCM) have shown to be a very effective solution as mortar components due to their capacity as thermal accumulators without needing active systems [Pavlík 2016]. PCM have a large thermal accumulation capacity during the change from solid to liquid state and vice versa (latent heat), while the material absorbs or releases energy, respectively. The latent heat transfer by the PCM fusion occurs at a certain temperature designated as phase change temperature [Cabeza 2011].

Due to wide variations in their compositions, PCMs can show different characteristics and thermal performance. The most common PCMs are organic because of their low price and commercialization and a higher thermal and chemical stability. Moreover, organic PCMs do not require additives for long-term use and are non-corrosive and recyclable materials. Organic microencapsulated PCMs as paraffin waxes can be mixed with common binders (cement, lime, gypsum) [Lucas 2010a].

This paper presents an experimental program on a PCM cement-lime mortar for thermal retrofitting of façades with an external thermal insulation under specific climatic conditions. The mortars would be placed in the inner side of the insulation (hot side). The effect of a microencapsulated paraffin wax on early age dimensional stability and hardened properties was assessed, measuring free shrinkage, physical and mechanical properties and thermal parameters of twelve cement-lime mixtures.

2 EXPERIMENTAL PROGRAM

2.1 Materials and mortars compositions

The components used in the study were:

- A white cement type BLII/B-L 32.5N (UNE-EN 197-1) supplied by Readymix- Asland S.A.
- An air lime class CL 90-S, designated according to the European standard (UNE-EN 459-1).
- A normal-weight siliceous aggregate (0-4mm).
- A lightweight aggregate (LWA): expanded perlite (L).
- Short cellulose fibres (F) of 1mm length - Fibracel® BC-1000 (Ø20µm) – supplied by Omya Clariana S.L.
- A microencapsulated paraffin wax (Phase Change Material - PCM) with particle size ca. 50-300 µm and a melting point of ca. 23ºC – Micronal® DS 5040 X – supplied by BASF Construction Chemicals Company. Fig. 1 shows an image of PCM.

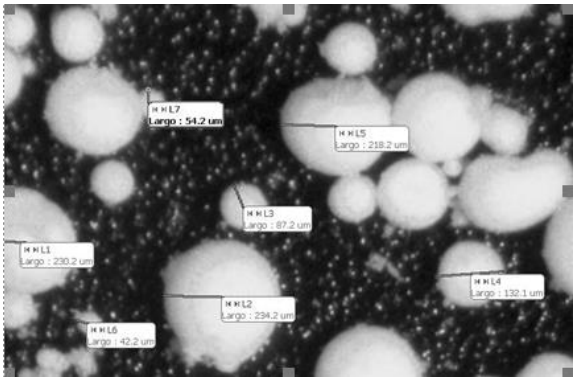

Fig. 101 : Optical micrographs of PCM

Fig. 2 shows a scheme for the mixture composition. A reference cement-lime mixture was designed (C). Then, 10% and 20% by volume of PCM (C_{10} and C_{20}) was added. Afterwards, 1.5% of dry cellulose fibres was added (CF, CF_{10} and CF_{20}). On the other hand 50% of the siliceous aggregate was replaced by perlite (CL, CL_{10} and CL_{20}). Finally a mixture was made adding both fibres and perlite (C, CLF_{10} and CLF_{20}).

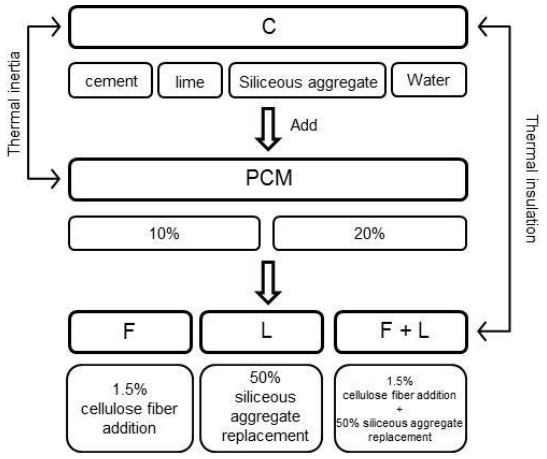

Fig. 102 : Mixture design of PCM cement-lime mortars.

Tab. 1 summarizes the compositions of the twelve mortars of this study. The binder to aggregate ratio was 1: 0.5: 4.5 (cement: lime: aggregate) by volume in all cases. The water to binder ratio (w/b) varied between 0.63 and 0.85 to get a plastic consistency and similar fresh workability for all the mixtures. The dry components, included the fibres and PCM, were mixed first and water was added afterwards. The total mixing time did not exceed 5 min in any case.

2.2 Experimental methods

The experimental program assessed the early age shrinkage (free shrinkage and initial time), physical properties (bulk density, open porosity, capillarity water absorption coefficient and water vapour diffusion resistance factor), mechanical performance (compressive strength and compressive modulus by ultrasonic pulse) and thermal properties of twelve cement-lime mixtures.

Free shrinkage

Early age free shrinkage was monitored on 500 x 100 x 50 mm samples subjected to an airflow of 3 m/s during the first 6 h to force drying shrinkage. The experimental set-up have been previously published [Barluenga 2013]. Only the mixtures without PCM and with 20% of PCM were tested.

Hardened performance

The characterization in the hardened state was done on 40 x 40 x 160 mm specimens. The samples were demoulded at 24h and cured until tested at 28 days (21± 3ºC and 95±5%RH).

The bulk density and open (accessible to water) porosity were calculated using a hydrostatic balance (UNE-EN 1015-10). Capillary water absorption coefficient and, water vapour diffusion resistance factor were measured according to UNE-EN 1015-18 and UNE-EN 1015-19, respectively.

Compressive strength (UNE-EN 1015-11) and ultrasonic pulse velocity propagation (UPV) were tested at 28 days. The compressive modulus (M) was also assessed at 28 days [Palomar 2015a].

Thermal performance

Thermal gradient, T_G (ºC/mm), was measured on 210 x 210 mm and 24 ± 2 mm thick plate samples. A thermally insulated box, with sample openings on its sides, was used. A heat source, connected to a thermal regulator, was located inside the box. Temperature (°C) and humidity (%) sensors were place on the inner and outer surface of the sample and inside and outside the box [Palomar 2015b]. Two temperature scenarios were set in the box: one at 25ºC (5h) and the other one at 40ºC (16h). The laboratory conditions were 20 ± 1^{0}C and 50 ±5% RH during the test (Fig.3).

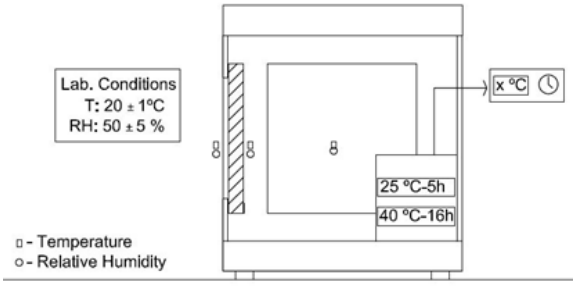

Fig. 103. Scheme of the insulated box.

Tab. 56 : Compositions of the lime-cement mortars (components in Kg).

	Cement	Air lime	Perlite*	Cellulose fibres	Sand 0-4	PCM	Water**	w/b***
C	348	55	-	-	1403	-	220	0.73
C_{10}	348	55	-	-	1403	42.3	140	0.53
C_{20}	348	55	-	-	1403	84.6	200	0.68
CF	348	55	-	0.40	1403	-	220	0.73
CF_{10}	348	55	-	0.62	1403	42.3	180	0.63
CF_{20}	348	55	-	0.66	1403	84.6	240	0.78
CL	348	55	94	-	702	-	240	0.69
CL_{10}	348	55	94	-	702	42.3	240	0.69
CL_{20}	348	55	94	-	702	84.6	250	0.71
CLF	348	55	94	0.49	702	-	240	0.69
CLF_{10}	348	55	94	0.62	702	42.3	305	0.85
CLF_{20}	348	55	94	0.59	702	84.6	380	0.79

** 50% of volume of the siliceous aggregate was replaced by perlite.*

*** Liquid water added.*

**** The amount of water included in the components (sand) was also taken into account. Sand 0–4: Humidity 5.3%.*

3 EXPERIMENTAL RESULTS AND ANALYSIS

Phase change material (PCM) cement-lime mortars for thermal retrofitting of facades were evaluated using the properties summarized in Tab. 2, as maximum free early age shrinkage (S_{FREE}) and initial time (S_{TIME}); bulk density (D), open porosity (P), capillary water absorption coefficient (CC), water vapour diffusion resistance factor (VD); and compressive strength (CS) and modulus (M) at 28 days. The thermal gradient (T_G) is reported in Fig. 4. The influence of the fibres (F) and lightweight aggregates (L) on the properties of the reference cement-lime mortar (C) and the effect of PCM are also discussed.

Tab. 57 : PCM cement-lime mortars' properties

	Shrinkage parameters		Mechanical properties*		Physical properties*			
	S_{FREE} (mm/m)	S_{TIME} (h min)	CS (MPa)	M (GPa)	D (Kg/m^3)	P (%)	CC ($Kg/m^2min^{0.5}$)	VD (-)
C	1.30	2h10min	13.7	18.65	1900	19.56	1.02	4.13
C_{10}	-	-	7.7	11.99	1690	16.68	0.48	4.02
C_{20}	1.94	2h00min	7.3	10.66	1600	17.72	0.48	4.29
CF	0.98	2h10min	10.3	19.27	1960	18.93	1.08	3.85
CF_{10}	-	-	6.7	11.83	1720	16.90	0.45	3.57
CF_{20}	0.66	1h50min	6.0	10.23	1660	16.77	0.28	3.47
CL	0.24	2h40min	9.3	11.14	1430	20.95	0.35	3.54
CL_{10}	-	-	5.3	6.49	1180	22.99	0.52	3.63
CL_{20}	0.42	2h00min	6.0	6.35	1270	23.33	0.53	3.62
CLF	0.16	3h10min	13.0	10.92	1430	23.94	0.72	3.80
CLF_{10}	-	-	5.0	4.63	1110	22.10	0.53	3.12
CLF_{20}	0.74	1h40min	5.3	5.61	1160	23.09	0.45	3.26

* *The mechanical and physical characterization were done at 28 days.*

3.1 Early age shrinkage

Tab. 2 records the maximum free early age shrinkage (S_{FREE}) and initial time (S_{TIME}). All the samples shrank, reaching values from 0.15 to 2.00 mm/m. C_{20} showed the highest value (1.94 mm/m) and CLF the lowest one (0.16 mm/m).The start of shrinkage ranged between 1 h 40 min and 3 h 10 min. The mixture CLF shrank the latest, whereas CLF_{20} sample began the first.

As can be observed, the free shrinkage was larger on the reference mixture (C) than on samples with cellulose fibres and perlite (CF, CL and CLF). On the other hand, these components slowed down the initial time, especially CLF. Adding PCM (C_{20}, CF_{20}, CL_{20} and CLF_{20}) increased the value of S_{FREE}, except CF_{20}, and accelerated the initial time, especially CLF_{20}.

3.2 Physical and mechanical characterization in the hardened state

Physical characterization

Bulk density (D), open porosity (P), capillary water absorption coefficient (CC) and water vapour diffusion resistance factor (VD) are summarized in Tab. 2.

Bulk density varied between 1100 and 2000 kg/m^3. The maximum D was measured for CF (1960 Kg/m^3), and the minimum for CLF_{10} (1110 Kg/m^3). It was observed that fibres (CF) increased D, whereas perlite reduced it, even when was combined with fibres (CL and CLF). In addition, the compositions with PCM reduced the bulk density around 300 kg/m^3. However, CL_{20} and CLF_{20} had larger D than CL_{10} and CLF_{10}. Other authors have been reported a decrease of bulk density if PCM was added [Pavlík 2016].

Open porosity varied from 16 to 24 %. CLF had the highest P (23.94%) and C_{10} the lowest (16.68%). As expected, perlite increased the open porosity [Palomar 2015b]. On the other hand, fibres reduced P. The PCM effect on open porosity showed two different trend: compositions with lightweight aggregates (CL_{10} and CL_{20}) increased P, whereas C, CL and CLF mortars had a decrease of open porosity as PCM particles tend to fill the larger pores [Lucas 2013]. Slightly differences were found between 10% and 20% of PCM samples.

The mixtures had capillarity water absorption coefficient ranging from 0.25 to 1.10 $kg/m^2min^{0.5}$. CF showed the largest value (1.08 $Kg/m^2min^{0.5}$) and CF_{20} the lowest one (0.28 $Kg/m^2min^{0.5}$). Perlite mixtures (CL and CLF) reduced the capillarity water absorption coefficient of the reference mixture (C), especially CL. As it can be seen in Tab. 2, there were two groups of PCM mixtures: PCM decreased CC in C, CF and CLF while increased in CL. Therefore, CC followed a trend similar to P [Palomar 2015b]. The amount of PCM did not vary significantly P.

The water vapour diffusion resistance factor oscillated between 4.30 and 3.10. CLF_{10} exhibited the lowest VD (3.12) value, while C_{20} (4.29) showed the highest one. In general terms, fibres, perlite and PCM reduced VD, which means more vapour permeable mortars. Slightly differences were found between 10% and 20% of PCM samples, except for C_{20} and CLF_{20}.

Mechanical characterization

Tab. 2 reports compressive strength (CS) and ultrasonic compressive modulus (M) at 28 days. CS varied between 5 and 14 MPa and M ranged from 4 to 20 GPa. CLF_{10} showed the lowest values of CS and M. On the other hand, the reference mixture (C) exhibited the largest compressive strength and the reference mixture with fibres (CF) the highest ultrasonic modulus values.

As expected, perlite (L) reduced the compressive strength and fibres (F) increased the ultrasonic compressive modulus [Palomar 2015b]. The composition with PCM decreased both parameters, as it has been previously described for compressive strength [Sakulich 2012, Pavlík 2016]. However, there is not a linear relationship between the amount of PCM and the effect on mechanical performance. Adding 10% of PCM meant a higher decrease of compressive strength and ultrasonic compressive modulus than adding 20%.

3.3 Thermal performance

Fig. 4 plots thermal gradient (T_G) at 25 °C ($T_{G,25}$) and at 40 °C ($T_{G,40}$). It can be observed that $T_{G,40}$ was higher (0.2-0.5 °C/mm) than $T_{G,25}$ (0.05-0.15 °C/mm) for all the mortars.

In both temperature scenarios, CLF_{20} sample showed the highest thermal gradient (T_G).

Under 25ºC scenario, CF and CFL without and with 10% of PCM had a very similar T_G. C_{10} and CL_{10} samples had a lower T_G than the reference samples. However, all 20%PCM mixtures showed the highest value.

On the other hand, 40ºC scenario, C and CL, thermal gradient was under 0.3ºC/mm and CF and CFL thermal gradient was 0.3ºC/mm or higher. When PCM was added (C_{10} and C_{20}) TG increased regarding to C.

On the opposite site, the reference mixture combined with perlite and with PCM (CL_{10} and CL_{20}) decreased T_G regarding to CL.

CF mixtures with PCM had different behaviour depending on the amount: CF_{10} showed the same value than CF; and CF_{20} increased T_G.

In CLF mixtures, the more the PCM content the larger the thermal gradient.

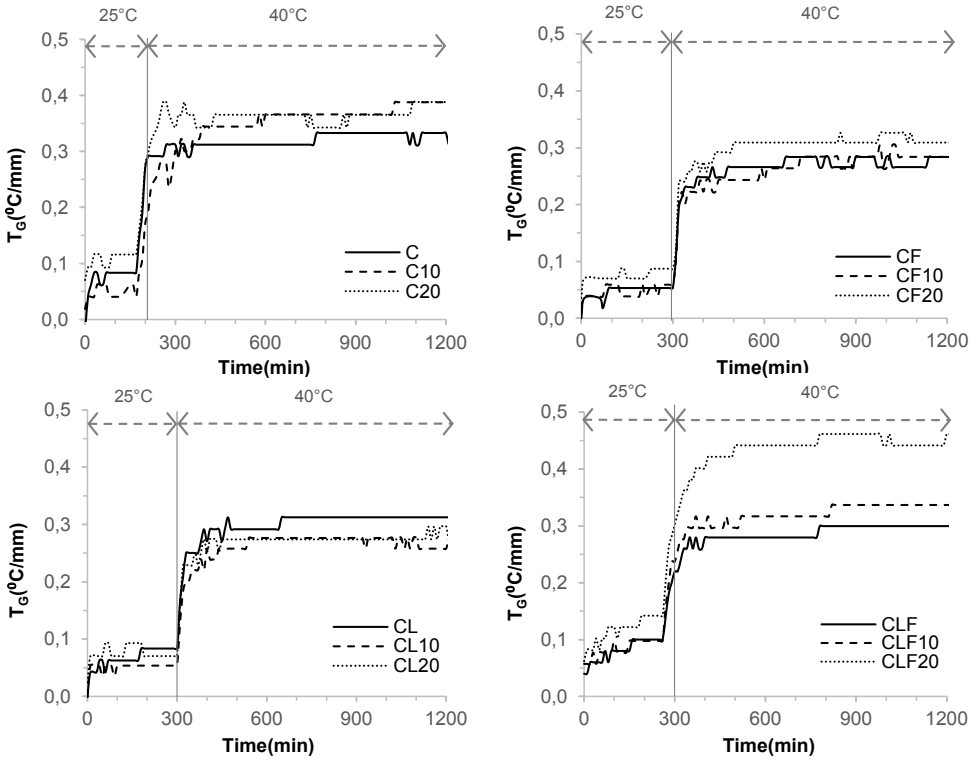

Fig. 104 : Thermal gradient, T_G, (°C/mm of mortar thickness) between inner and outer sample surface at 25 ºC and 40 ºC.

4 SUMMARY

This paper presents the effect of a Phase Change Material (PCM) on cement-lime mortars properties. Short cellulose fibres (F) and a lightweight aggregate (L) (expanded perlite) were also added. The experimental program assessed the early age shrinkage, hardened physical and mechanical properties and thermal behaviour.

The main findings of the study can be summarized as:

- The use of FC, L and PCM modified the properties of a reference cement-lime mortar. The water to binder ratio (w/b) varied slightly to get a similar consistency and workability.
- Compositions with LWA (CL) reduced and slowed down the early age shrinkage, especially with fibres (CLF). On the other hand, PCM had the opposite effect.
- Adding FC, L and PCM affected the pore structure parameters - open porosity (P), capillary water absorption coefficient (CC) and water vapour diffusion resistance factor (VP) – and mechanical properties. PCM modified the pore structure reducing P, CC and VP on C, CF and CLF samples, but increasing them on CL mixtures. Regarding mechanical performance, PCM reduced both parameters, compressive strength and ultrasonic compressive modulus.
- In general, the amount of PCM did not affect significantly the pore structure and mechanical performance.
- Thermal performance of PCM cement-lime mortars was affected by temperature scenario and components as cellulose fibres and expanded perlite. Thermal gradient at 25 °C ($T_{G,25}$) was lower than 40 °C ($T_{G,40}$).
- The 10% PCM samples had a different thermal gradient ($T_{G,25}$ and $T_{G,40}$) depending on the reference mixture. On the other hand, a larger amount of PCM (20%) increased the thermal gradient (T_G), especially on CLF_{20} at 40ºC scenario. However, PCM decreased $T_{G,40}$, on CL mixture.

5 ACKNOWLEDGMENTS

The authors want to acknowledge the help of Prof. Consuelo Cid of UAH. Some of the components were supplied by BASF Construction Chemicals España S.L., Omya Clariana S.L. and Readymix-Asland S.A.

6 REFERENCES

[Barluenga 2013] Barluenga, G.; Palomar, I.; Puentes, J.; Early age and hardened performance of cement pastes combing mineral additions. Material and Structures, 2013, 46, 921–41, ISSN 1871-6873.

[Cabeza 2011] Cabeza, L.F.; Barreneche, C.; Castell, A.; de Garcia, A. et al.; Materials used as PCM in thermal energy storage in building: A review. Renewable and Sustainable Energy Reviews, 2011, 15, 3, 1675-1695, ISSN 1364-0321.

[Lucas 2010a] Lucas S.; Senff L.; Ferreira V.M.; Barroso de Aguiar J.L. et al.; Fresh state Characterization of lime mortars with PCM addition. Applied Rheology, 2010, 20, 6, 63162 1-7.

[Lucas 2010b] Lucas, S.; Ferreira, V.M.; Selecting insulating building materials trough an assessment tool. In CIB ed. Portugal SB10. Sustainable Building Affordable to All, Vilamoura 2010, 745-752.

[Lucas 2013] Lucas, S.S.; Ferreira; Barroso, J.L.; Latent heat storage in PCM containing mortars-Study of microstructural modifications. Energy and Buildings, 2013, 66, 724-731, ISSN 0378-7788.

[Palomar 2015a] Palomar, I.; Barluenga, G.; Puentes, J.; Assessment by non-destructive testing of new mortar coatings for retrofitting the Architectural Heritage. WIT Transactions on the Built Environment, 2015, 153, 357-366, ISSN 1743-3509.

[Palomar 2015b] Palomar, I.; Barluenga, G.; Puentes, J.; Lime-cement mortars for coating with improved thermal and acoustic performance. Construction and Building Materials, 2015, 75, 306-314, ISSN 0950-0618.

[Pavlík 2016] Pavlík, Z. ; Fořt, J. ; Pavlíková, M. ; Pokorný, J. et al. ; Modified lime-cement plasters with enhanced thermal and hygric storage capacity for moderation of interior climate, Energy and Buildings, 2016, 126, 113-127, ISSN 0378-7788.

[Sakulich 2012] Sakulich, A.R.; Bentz, D.P.; Incorporation of Phase Change Materials in Cementitious Systems via Fine Lightweight Aggregate. Construction and Building Materials, 2012, 35, 483-490, ISSN 0950-0618.

[Schiavoni 2016] Schiavoni, S.; D'Alessandro, F.; Bianchi, F.; Asdrubali, F.; Insulation materials for the building sector: A review and comparative analysis. Renewable and Sustainable Energy Reviews, 2016, 62, 988-1011.

[Stefanidou 2014] Stefanidou, M.; Cement-based renders with insulating properties. Construction and Building Materials, 2014, 65, 427-431, ISSN 0950-0618.

10.1.2 Thermal enhanced cement-lime mortars with phase change materials (PCM), lightweight aggregate and cellulose fibers

Guardia, C., Barluenga, G., & Palomar, I. Diarce G., (2019) *Thermal enhanced cement-lime mortars with phase change materials (PCM), lightweight aggregate and cellulose fibers*, Construction and Building Materials, Volume 221, 586-594, ISSN 0950-0618, https://doi.org/10.1016/j.conbuildmat.2019.06.098.

Construction and Building Materials 221 (2019) 586–594

Contents lists available at ScienceDirect

Construction and Building Materials

journal homepage: www.elsevier.com/locate/conbuildmat

Thermal enhanced cement-lime mortars with phase change materials (PCM), lightweight aggregate and cellulose fibers

Cynthia Guardia [a,*], Gonzalo Barluenga [a], Irene Palomar [a], Gonzalo Diarce [b]

[a] Department of Architecture, University of Alcala, Madrid 28801, Spain
[b] ENEDI Research Group, Dpto. de Máquinas y Motores Térmicos, Escuela Universitaria de Ingeniería Técnica de Minas y Obras Públicas, University of the Basque Country UPV/EHU, Bilbao 48013, Spain

HIGHLIGHTS

- Twelve cement-lime mortars with PCM, LW aggregates and cellulose fibers characterized.
- Physical, mechanical and thermal properties were measured.
- PCM increased enthalpy and reduced porosity and strength.
- LWA increased porosity and reduced strength and thermal conductivity.
- LWA increased the enthalpy of PCM cement-lime mortars.

ARTICLE INFO

Article history:
Received 14 March 2019
Received in revised form 26 April 2019
Accepted 12 June 2019
Available online 19 June 2019

Keywords:
Phase Change Material (PCM)
Cement-lime mortar
Lightweight aggregate
Cellulose fibers
Experimental characterization
Thermal properties

ABSTRACT

The influence of a microencapsulated phase change material (PCM), a lightweight aggregate (LWA) and cellulose fibers on the behavior of cement-lime mortar was investigated. Lightweight aggregates and cellulose fibers were added in order to reduce thermal conductivity. PCM in two different amounts, 10% and 20%, was included to increase thermal inertia of mortars, taking advantage of its heat storage capacity. An experimental program was carried out to assess the effect on physical, mechanical and thermal properties of the different additions and combinations. Thermal conductivity of mortars with PCM at solid and liquid states were measured and Differential Scanning Calorimetry (DSC) was used to evaluate mortars' enthalpy.

Twelve cement-lime mortars designed for rendering applications, were studied and the experimental results were compared. It was observed that the type and amount of component affected physical, mechanical and thermal mortar properties. Lightweight aggregates increased porosity while reduced strength and thermal conductivity. Cellulose fibers did not modify significantly mortar properties. PCM increased mortar enthalpy while acted as a filler, reducing porosity and strength. However, enthalpy was not linearly related only to the amount of PCM and also depended on mortar composition. LWA increased the enthalpy of PCM cement-lime mortars.

1. Introduction

Phase Change Materials (PCM) have become materials with a great potential for construction and building rehabilitation due to the thermal properties supplied by their phase change capacity at a certain temperature. During phase change, the material absorbs or release heat while temperature remains constant (latent heat), acting as a heat storage [1,2] Depending on their nature, there are two main groups of PCM, organic and inorganic [3]. Organic PCM are usually paraffin waxes, fatty acids, and mixtures of both. Organic PCM are characterized by their chemical and thermal stability, melting and solidifying without suffering disaggregation or changes on their properties, and are not corrosive. Their main disadvantages are their low thermal conductivity and their low phase change enthalpy [3].

Accordingly, the use of PCM in construction materials is seen as a promising solution for the improvement of thermal behaviour of both new and existing buildings [4]. Nowadays, there is a great interest in the development of new construction materials to improve energy efficiency of buildings. Many dwelling units have

* Corresponding author at: Department of Architecture, University of Alcala, C/ Santa Ursula, 8. Alcalá, de Henares, 28801 Madrid, Spain.
E-mail address: cynthia.guardia@edu.uah.es (C. Guardia).

https://doi.org/10.1016/j.conbuildmat.2019.06.098
0950-0618/

envelopes (mainly façades) with poor thermal insulation [5] which leads to high energy costs [6]. The most common solutions to improve energy efficiency are ventilated façades and External Thermal Insulation Composite Systems (ETICS) [7]. However, those solutions do not consider the façade thermal inertia and have shown a poor performance in summer conditions [8]. Besides, these solutions have a low adaptability to existing buildings due to the increase of the façades thickness. PCM are proposed as a solution that overcomes these limitations.

The incorporation of PCM in construction can be done by encapsulating organic PCM, avoiding leakages while it is in liquid state. Then PCM can be mixed into other materials in microcapsules or placed in layered building elements by macro-encapsulation [9]. Micro-encapsulation consists in coating small portions of PCM with a solid spherical plastic capsule (1–1000 μm) to facilitate material dispersion. Microencapsulated paraffin waxes are the most used in construction due to their high adaptability, commercial availability and competitive price [10,11].

Microencapsulated PCM can be mixed in building materials, as pastes and mortars for rendering and plastering applications [12–18]. The most common binder of PCM modified mortars has been usually cement, followed by gypsum [19]. Very few studies combined cement and lime with PCM [12,15].

The most common solution to improve thermal properties of mortars has been the reduction of thermal conductivity by the addition of different components. New thermally enhanced cement and cement-lime mortars have been investigated and their physical, mechanical and thermal properties have been characterized [20 –23]. Lightweight aggregates (LWA) and fibres have been added to improve mortar thermal properties. It has been described that LWA reduced mortar density, and thermal conductivity [21,24]. On the other hand, the addition of cellulose fibres decreased thermal conductivity [21,25]

This paper presents a study on cement-lime mortars with LWA (expanded perlite) and cellulose fibres with PCM (microencapsulated paraffin wax). The aim of the study was to design mortars useful for rendering applications with improved thermal behaviour taking advantage of both the reduction of thermal conductivity provided by LWA and fibres and the thermal storage capacity of PCM.

2. Materials and experimental methods

In this study twelve different cement- lime mixtures were analyzed. Fig. 1 shows the design criteria followed to produce the mortar compositions with LWA, fibers and PCM and a combination of all those components. The experimental program assessed early age shrinkage, physical and mechanical hardened properties, thermal conductivity and enthalpy (DSC) and hardened microstructure observed by Scanning Electron Microscopy (SEM) images of the cement-lime mixtures with and without the addition of PCM.

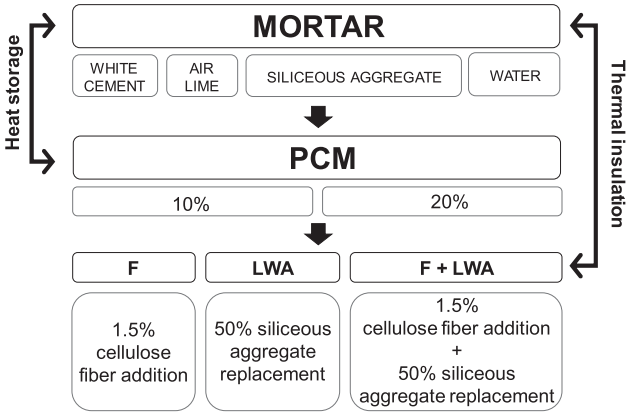

Fig. 1. Composition design of PCM lime-cement mortars.

2.1. Materials and mixtures compositions

The components used in the mortars are listed below:

- A white cement type BLII/B-L 32.5N (UNE-EN 197-1) supplied by Cementos Portland Valderrivas.
- An air lime class CL 90-S, designated according to the European standard (UNE-EN 459-1).
- A normal-weight siliceous aggregate (0–4 mm).
- A lightweight aggregate (LWA): expanded perlite (L).
- Short cellulose fibers (F) of 1 mm length- Fibracel® BC-1000 (ø20μm) – supplied by Omya Clariana S.L.
- A microencapsulated paraffin wax (Phase Change Material – PCM) with particle size ca. 50–300 μm, bullk density ca. 300–400 Kg/m^3 and a melting point of ca. 23 °C ± 1 - Micronal® DS 5040X – supplied by BASF Construction Chemicals Company. Fig. 2 shows the DSC curves achieved to ensure the melting point of the PCM (23 °C ± 1).

Table 1 summarizes the compositions of the twelve mortars evaluated in this study. A reference cement-lime mortar with a binder to aggregate ratio by volume of 1: 0.5: 4.5 (cement: lime: aggregate) was designed (C). Then, 10% and 20% by fresh mortar volume of PCM (C_{10} and C_{20}) was added. Afterwards, 1.5% of the total fresh mortar's volume (considering both the reference components and the LWA) of dry cellulose fibers were added (CF, CF_{10} and CF_{20}). 50% of the siliceous aggregate was replaced by perlite (CL, CL_{10} and CL_{20}). Finally, a mixture was made adding both fibers and perlite (C, CLF_{10} and CLF_{20}).

Water to binder ratio (w/b) was adjusted to get a plastic consistency and similar fresh workability for all the mixtures. Plastic consistency was selected because it is adequate for façade renderings. The target minimum compressive strength value was 3.5 MPa, which corresponds to a CS-III grade rendering mortar, according to UNE-EN 998-1. The mixing procedure took two stages. First, the dry components, included the fibers and PCM, were mixed and water was added afterwards. The total mixing time did not exceed 5 min in any case.

2.2. Workability and free shrinkage testing methods

The fresh mortar consistency was measured using the flow table test, according to the European standard (UNE-EN 1015-

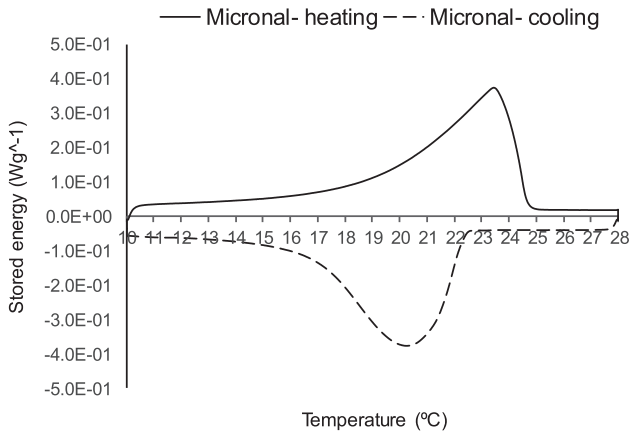

Fig. 2. Differential Scanning Calorimetry of the PCM under study (Micronal® DS 5040X).

Table 1
Compositions of PCM lime-cement mortars (components in kg).

	C	C_{10}	C_{20}	CF	CF_{10}	CF_{20}	CL	CL_{10}	CL_{20}	CLF	CLF_{10}	CLF_{20}
BLII/B-L 32.5N	348	348	348	348	348	348	348	348	348	348	348	348
CL 90-S	55	55	55	55	55	55	55	55	55	55	55	55
Sand (0–4)	1403	1403	1403	1403	1403	1403	702	702	702	702	702	702
Cellulose fibres	–	–	–	0.40	0.62	0.66	–	–	–	0.49	0.62	0.59
Perlite*	–	–	–	–	–	–	94	94	94	94	94	94
PCM	–	42.3	84.6	–	42.3	84.6	–	42.3	84.6	–	42.3	84.6
Water**	220	140	200	220	180	240	240	240	250	240	305	380
w/b***	0.73	0.53	0.68	0.73	0.63	0.78	0.69	0.69	0.71	0.69	0.85	0.79
D_{dry} (kg/m^3)	1400	1448	1357	1387	1260	1440	845	964	868	822	–	–
D_{wet} (kg/m^3)	2264	1857	1937	2165	1904	1885	1711	1682	1562	1854	1433	1561

Cement:Lime:Aggregates = 1:0.5:4.5 by volume.
* 50% of volume of the siliceous aggregate was replaced by perlite.
** Liquid water added. The amount of water included in the components (sand) was also taken into account. Sand 0–4: Humidity 5.3%. The water was adjusted to get a plastic consistency and similar workability for all the fresh samples.
*** 50% of volume of the siliceous aggregate was replaced by perlite. Liquid water added. The amount of water included in the components (sand) was also taken into account. Sand 0–4: Humidity 5.3%.

3:2000). The water to binder ratio was fixed to achieve the plastic consistency required for coating mortars. Early age free shrinkage was monitored on 500 × 100 × 50 mm samples subjected to an airflow of 3 m/s during the first 6 h to force drying shrinkage. The experimental set-up has been previously published [26]. In order to evaluate the effect of PCM on shrinkage, only mixtures without PCM and with 20% of PCM were tested.

2.3. Hardened properties testing procedures

The characterization in the hardened state was carried out on 40 × 40 × 160 mm specimens, according to the European standard (UNE-EN 101-11). The samples were demolded at 24 h and cured until tested at 28 days (21 ± 3 °C and 95 ± 5%RH).

Bulk density and open (accessible to water) porosity were calculated by using a hydrostatic scale (UNE-EN 101-10). Capillary water absorption coefficient and water vapor diffusion resistance factor (VD) were measured according to UNE-EN 1015-18 and UNE-EN 1015-19, respectively. Capillary water absorption was measured on 40 × 40 × 160 cm samples in contact with water by their bottom side. Capillary water absorption coefficient was calculated weighing the 40 × 40 × 160 mm specimens at 10 and 90 min and at 24 h. The weight gain corresponded to the water absorbed through the bottom face of the samples in contact with water. VD was determined by wet – cup method containing a saturated saline dissolution (75%RH) and using cylindrical specimens with 35 mm diameter and 40 ± 2 mm thick.

Regarding mechanical properties, compressive and flexural strength (UNE-EN 1015–11:2000) were tested at 28 days on standard specimens. Ultrasonic pulse velocity propagation (UPV) was also tested at 28 days. A PUNDIT LAB ® Ultrasonic device using P- and S-wave 250 kHz transducers was used to evaluated the samples. Transmission times were identified using the Hilbert transform algorithm [27] and Ultrasonic Young modulus (E), bulk modulus (K) and Poisson ratio (υ) were calculated, according to Eqs. (1)–(3) respectively:

$$E = 2\left(\rho \cdot V_s^2\right)(1+\upsilon)/10^6 \quad (1)$$

$$K = \rho \cdot \left(V_p^2 - 4/3V_s^2\right)/10^6 \quad (2)$$

$$\upsilon = \left(0.5 \cdot V_p^2 - V_s^2\right)/\left(V_p^2 - V_s^2\right) \quad (3)$$

where ρ is the apparent (bulk) density (g/cm^3) and V_P and V_S are the P- and S- wave velocity (m/s), respectively.

2.4. Thermal conductivity testing procedure

A thermally insulated box, with sample openings on its sides, was used for the measurement of the Thermal Conductivity (λ) on 210 × 210 mm and 24 ± 2 mm thick plate samples. The laboratory conditions were 20 ± 1 °C and 50 ± 5% RH during the test. A heat source was located inside the box and connected to a thermal regulator. Temperature and relative humidity (RH) were monitored with sensors placed at the inner and outer surface of the sample and inside and outside the box [28]. When a steady thermal state was reached, both with PCM in solid or liquid state and thermal conductivity was calculated (λ_s and λ_l for PCM in solid and liquid state respectively) according to Fourier's Law [28].

Two different temperature conditions were set inside the box, 25 °C and 40 °C, to calculate λ of mortars with and solid (λ_s) and liquid (λ_l) PCM. For 25 °C inside the box, the internal temperature of the samples was below 23 °C (melting point) and PCM was in a solid state. At the other condition of 40 °C, the internal temperature of the plates was well above melting point (ca. 30 °C) so the PCM was in a liquid state.

2.5. Differential Scanning Calorimetry (DSC)

DSC was used to determine the thermal properties of the cement-lime mixtures investigated. The apparatus used was a Mettler Toledo DSC1. Both heat flow and temperature calibrations were performed with gallium and indium. Aluminum crucibles of 25 ml were used, and dry nitrogen (99.999% pure) was employed as a purge gas. The phase change enthalpies were determined by integration of the phase transition peaks of the thermograms. Accordingly, the enthalpies reported throughout the article consider only latent heat unless otherwise indicated. An integral tangential interpolated baseline was used for this purpose. In order to obtain the DSC samples, the cement-lime materials were gently ground by mortar and pestle and introduced into the aluminum crucibles. Three fresh samples were prepared for each cement-lime material evaluated; thus, a total of 12 samples were measured.

The DSC measurements performed to achieve the enthalpy vs. temperature were carried out following the standardized PCM characterization procedure developed under the IEA Task 42 - Annex 29 [29,30]. This procedure includes a preliminary step for the determination of a suitable measurement rate. The heating/-cooling rate obtained for the present case was 1 K/min. The minimum and maximum temperatures selected for the temperature program were 10 and 28 °C with isothermal segments of 5 min between each consecutive heating/cooling ramp. As recommended

by the procedure, each measurement (fresh sample) was comprised of 3 consecutive heating and cooling cycles. The results for the different heating (or cooling) cycles of each sample showed negligible differences; accordingly, only those data of the second heating and cooling cycles of each sample will be used along the article.

2.6. Scanning Electron Microscopy

A direct observation of the microstructure morphology with scanning electron microscopy (SEM) was done. The apparatus used was a Zeiss EVO LS25 (provided by Institut für Werkstoffe im Bauwesen - TU- Darmstadt). Small specimen fragments of previously tested specimen (compressive strength test) of the mixtures C_{20}, CF_{20}, CL_{20} and CLF_{20} were analyzed. The fragments were in solid state, under the melting temperature of the Phase Change Material. Samples were metalized with gold powder, following the standard procedure for inorganic materials.

3. Experimental results

3.1. Fresh state and early age shrinkage characterization

Table 2 summarizes the fresh state and workability values, as consistency and water to binder ratio (w/b), which was fixed with the flow table test. W/b ratio to get a plastic consistency ranged between 0.53 and 0.85.

The maximum free early age shrinkage (S_{FREE}) and shrinkage initial time (S_T) are also reported in Table 2. All the samples shrank, reaching values from 0.16 (CLF) to 1.94 mm/m (C_{20}). The mixture that shrank the first was CLF (1 h 40 min) while the latest was CLF_{20} (3 h 10 min). It can be seen that free shrinkage was larger for the reference mixture (C) than on samples with cellulose fibers and perlite (CF, CL and CLF). When fibers and perlite were added, the initial time of shrinkage was delayed, especially for CLF. This behavior is probably related to the water content of the mortar's pore network and the water absorption capacity of the fibers and LWA. Adding 20% PCM accelerated the initial time, especially CLF_{20}, and increased the value of S_{FREE}, except for CF_{20}. This fact is probably related to the retained water around the PCM shell, creating small and thin pores filled with water.

3.2. Physical characterization

Table 2 also presents the experimental results of mortars' physical properties: bulk density (D), open porosity (OP), capillary water absorption coefficient (CC) and water vapor diffusion resistance factor (VD).

Regarding density, CF was the mixture with the maximum D value (1960 Kg/m^3) whereas CLF_{10} presented the lowest (1110 Kg/m^3). As expected perlite reduced D [24], also combined with fibers, while fibers (CF) increased D. Compositions with PCM reduced D around 300 Kg/m^3, according to the results reported by other authors [12]. However, CL_{20} and CLF_{20} showed larger D than CL_{10} and CLF_{10}.

The values of open porosity varied from 16.68% (C_{10}) to 23.94% (CLF). As other authors have already pointed out, perlite increased OP [21,24] whereas fibers reduced OP. The effect of PCM on OP showed two different trends: compositions with lightweight aggregates (CL_{10} and CL_{20}) increased OP. On the other hand, C, CL and CLF mortars with PCM reduced OP, due to the filler effect of PCM particles [15]. Only slight differences between 10% and 20% of PCM samples on OP were found.

Capillary water absorption coefficient (CC) ranged from 0.28 Kg/m^{2}min$^{0.5}$ (CF_{20}) to 1.08 Kg/m^{2}min$^{0.5}$ (CF). It was observed that mixtures with perlite (CL and CLF) reduced the CC of the reference mixture (C), especially CL. Two groups of PCM mixtures were identified: PCM increased CC in CL mortars, whereas decreased C, CF and CLF. As reported previously [21], capillary water absorption coefficient followed a trend similar to OP.

Water vapour diffusion resistance factor (VF) varied between 4.30 and 3.10. C_{20} presented the largest VD value (4.29), while CLF_{10} (3.12) showed the lowest. Fibers, perlite and PCM reduced VD, which means highly vapor permeable mortars. Slight differences were found between 10% and 20% of PCM samples except, for C_{20} and CLF_{20}.

3.3. Mechanical characterization

The experimental results of compressive and flexural strength, Ultrasonic Young modulus (E), bulk modulus (K) and Poisson ratio (υ) at 28 days are summarized in Table 2 reports.

Compressive strength varied between 4.6 MPa, corresponding CLF_{10}, and 14.33 MPa to the reference mixture C. Accordingly, all

Table 2
Physical and mechanical properties of PCM cement-lime mortars.

	C	C_{10}	C_{20}	CF	CF_{10}	CF_{20}	CL	CL_{10}	CL_{20}	CLF	CLF_{10}	CLF_{20}
Workability												
Consistency mm	178	170	166	160	173	170	195	173	170	170	180	170
w/b	0.73	0.53	0.68	0.73	0.63	0.78	0.69	0.69	0.71	0.69	0.85	0.79
Early Age Shrinkage parameters												
Free Shr. mm/m	1.30	–	1.94	0.98	–	0.66	0.24	–	0.42	0.16	–	0.74
Initial time h min	2 h10	–	2 h00	2 h10	–	1 h50	2 h40	–	2 h00	3 h10	–	1 h40
Phy. Prop.												
Bulk density kg/m^3	1900	1690	1600	1960	1720	1660	1430	1180	1270	1430	1110	1160
O.Porosity %	19.56	16.68	17.72	18.93	16.90	16.77	20.95	22.99	23.33	23.94	22.10	23.09
Capillary kg/m^{2}min$^{0.5}$	1.02	0.48	0.48	1.08	0.45	0.28	0.35	0.52	0.53	0.72	0.53	0.45
VD (–)	4.13	4.02	4.29	3.85	3.57	3.47	3.54	3.63	3.62	3.80	3.12	3.26
Mech. Prop												
Com. Str. MPa	14.33	7.30	7.17	10.83	6.83	5.83	9.40	5.33	6.00	12.67	4.60	5.33
Flexural Str. MPa	3.36	2.26	2.40	2.66	1.98	2.20	3.18	2.24	1.79	3.46	1.84	2.16
E GPa	15.67	9.44	8.31	13.59	9.55	8.25	9.13	5.02	4.48	9.57	3.96	4.29
K GPa	8.59	6.29	6.46	9.29	6.44	4.62	5.85	2.94	3.23	6.06	2.49	2.77
ν	0.19	0.25	0.29	0.26	0.25	0.20	0.24	0.22	0.27	0.23	0.23	0.24

the mixtures reached the target minimum compressive strength value of 3.5 MPa, which corresponds to a CS-III grade rendering mortar, according to UNE-EN 998-1. As expected, mortars with perlite (L) showed lower compressive strength values [12,13,21]. The addition of PCM also decreased the compressive strength [13,17,18]. Furthermore, adding 10% of PCM, regarding the mixture without PCM meant a higher decrease of compressive strength than adding 20% of PCM regarding the mixture with 10% PCM. This fact is probably related to the amount of water necessary to achieve the target plastic consistency, that is not either proportional to the amount of PCM.

Flexural strength varied between 1.79 MPa (CLF_{10}) and 3.46 MPa (CLF). The results showed that the mixtures with perlite presented values slightly lower than the rest of mixtures. Flexural strength decreased when PCM was added, although there was no linear relationship between the amount of PCM and the reduction of compressive and flexural strength.

Young modulus (E) was calculated from the ultrasonic pulse velocity (UPV) measured at 28 days. CLF_{10} showed the lowest E value (3.96 GPa), while C showed the highest one (15.67GPa). As other authors reported, mixtures with the addition of perlite decreased the values of E [24,27]. The same behavior was observed with the addition of PCM. Slight differences were found between 10% and 20% of PCM samples. This trend occurred in all the mixtures except in CLF_{20}, where E increased slightly regarding to CLF_{10}, which can be considered insignificant, because these values were obtained using an indirect testing technique (UPV).

Bulk Modulus (K) values varied between 2.49 GPa, corresponding to CLF_{10} and 9.29 GPa, corresponding to CF. As expected, the addition of perlite decreased K modulus [27]. On the other hand, the addition of PCM caused also a decrease of K for the reference mixture C and CF, whereas it increased from 10% to 20% of PCM. However, it was observed that there was no linear relationship between the amount of PCM and K.

Poisson ratio values obtained at 28 days with UPV varied between 0.19 and 0.29. C presented the lowest value of Poisson ratio, while C_{20} showed the highest one. In this case, there was not a big difference between mixtures without PCM and mixtures with PCM.

3.4. Thermal characterization

Table 3 reports thermal conductivities for solid PCM (λ_s) and liquid PCM (λ_l) calculated by using the insulated box. These results were obtained after the samples reached a thermally steady state. Therefore, only sensible heat of the material was taken into account, but not the latent heat (enthalpy), which was analyzed with another experimental setup (DSC) [31].

The lowest λ_s value was obtained for CL (0.17 W/m K), while CF_{10} showed the highest one (0.40 W/mK). λ_l values varied between 0.15 W/mK (CLF_{20}) and 0.32 W/mK (C_{10}). In general, λ_l showed lower values than λ_s, except for C_{10} and C_{20}, probably due to the water content in the mortar's pore network. Differences in λ_s between adding 10% or 20% of PCM were observed for mixtures C and CF, and in lower degree for CL and CLF. Mixtures with lightweight aggregates (LWA) showed lower λ_l. All mixtures with 10% of PCM increased both thermal conductivities λ_s and λ_l, while 20% PCM trend to reduce them.

Fig. 3 shows the enthalpy for each mixture in heating and cooling cycles within a temperature interval between 10 °C and 28 °C. During the heating cycle enthalpy increased with temperature, while decreased in cooling cycles. As expected, mixtures without PCM showed a linear enthalpy increase with temperature. However, it can be seen that enthalpy varied among mixtures: CF and CLF showed values at 28 °C below 15 J/g (Fig. 3b and d); the reference mixture C showed the highest enthalpy value above 15 J/g (Fig. 3a) and CL (Fig. 3c) an enthalpy around 15 J/g. It must be highlighted that the enthalpy of these compositions without PCM depends only on the specific heat, related to mortar density.

Fig. 3 shows the effect of PCM on enthalpy. The addition of PCM showed slight differences between heating and cooling cycles for samples with PCM, according to the lag observed in Fig. 2. The inflection point of the curve corresponded to the melting point of the PCM, located at 23 °C for heating cycles and at 22 °C for cooling cycles (Fig. 2).

Mixtures with 10% of PCM CF_{10}, CL_{10} and CLF_{10} presented similar values at heating cycles as well as cooling cycles with an enthalpy between 15 and 20 J/g. However, reference mixture C_{10} showed values above 20 J/g.

When 20% of PCM was added larger differences were observed, depending on the mortar composition. Reference mortar showed the smallest difference (Fig. 3a), followed by mortar with LWA and fibers (CLF) (Fig. 3d) and mortar with fibers (CF) (Fig. 3b). Fig. 3c plots the highest difference on enthalpy when PCM was added to mortars with LWA, reaching 25 J/g for 28 °C. It was observed that enthalpy depends not only on the amount of PCM, but also on the other components added to the mixtures.

3.5. Microstructural characterization

The microstructure of a sample extracted from a specimen of the reference mixture with PCM (C_{20}) is shown in Fig. 4. During the preparation of the samples for Scanning Electron Microscopy (SEM), a few microcapsules where broken, allowing to see the solid paraffin wax contained inside the capsules [10,11,18], which are surrounded by cement-lime paste. As far as the paste was not contaminated by paraffin, it can be assumed that the microcapsule was intact when the specimen was thermally tested, which confirms that the capsule was broken during the preparation for SEM analysis. The external plastic shell, highlighted in the images with white arrows (Fig. 4a and c), can be identified because it creates a clear limit between the paste and the solid paraffin. The distribution of the solid paraffin inside the shell was not homogeneous. Small paraffin microspheres were located bonded to the shell and larger spheres can be seen at the core of the capsule [10].

Fig. 5 presents the paraffin wax solidification process inside a PCM microcapsule during cooling. When the temperature is over 23 °C, the paraffin is in a liquid state completely filling the capsule. Then, the temperature of the surrounding paste decreases till it reaches the solidification point (23 °C according to the manufacturer and 22 °C when measured with DSC). At this moment, the paraffin wax begins to change its phase from liquid to solid state (releasing energy). As the heat transfer from the interior of the capsule happens through the external shell, the paraffin next to it solidifies the first, shrinking and forming solid microspheres, leav-

Table 3
Thermal conductivity of cement-lime mortars with PCM in solid and liquid states.

	C	C_{10}	C_{20}	CF	CF_{10}	CF_{20}	CL	CL_{10}	CL_{20}	CLF	CLF_{10}	CLF_{20}
Ther. Prop												
λ_s W/mK	0.23	0.26	0.20	0.29	0.40	0.30	0.17	0.27	0.29	0.22	0.25	0.23
λ_l W/mK	0.21	0.32	0.28	0.21	0.26	0.23	0.16	0.19	0.18	0.19	0.21	0.15

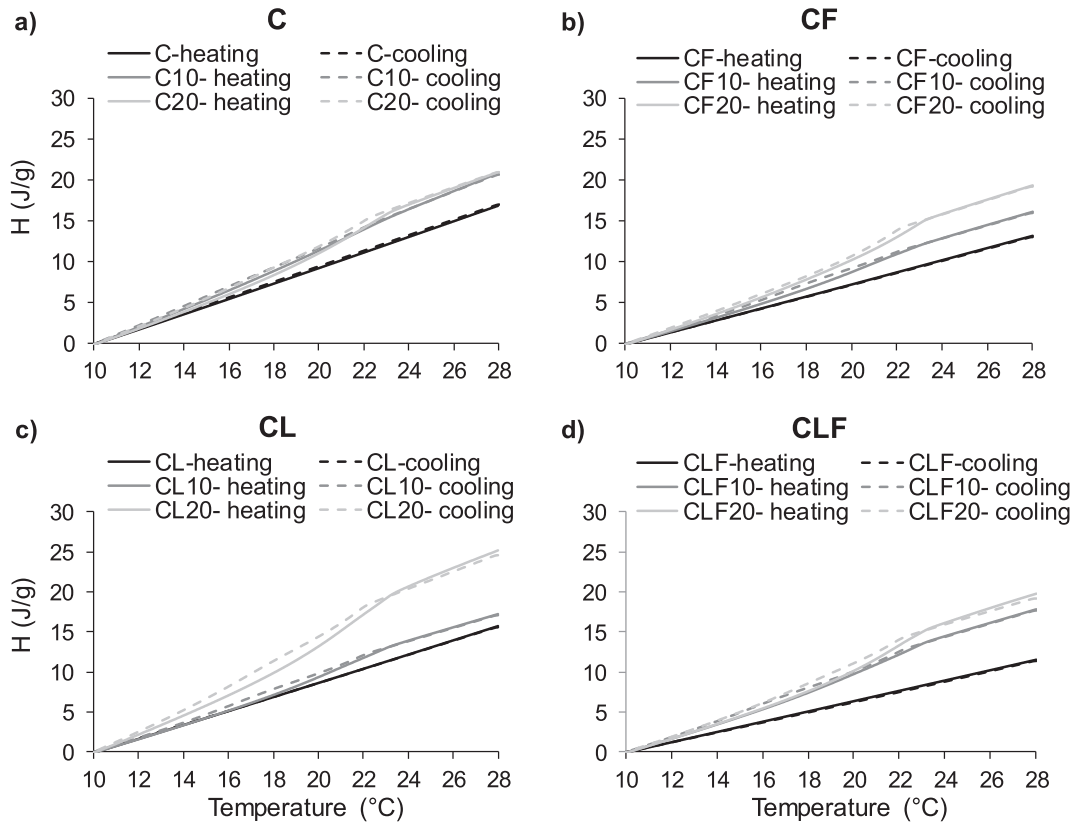

Fig. 3. Enthalpy measured in DSC of the PCM lime-cement mortars during heating and cooling cycles. (a) Reference mortars; (b) Mortars with cellulose fibers; (c) Mortars with LWA; (d) mortar with cellulose fibers and LWA.

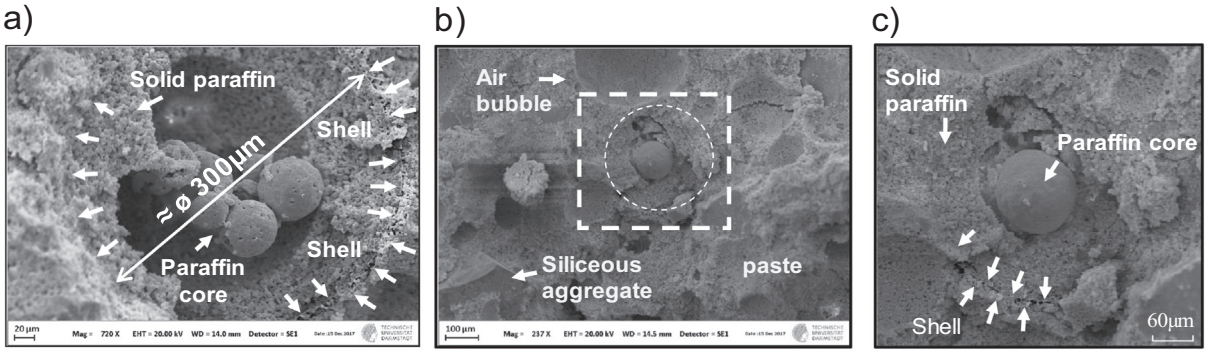

Fig. 4. SEM images of PCM microcapsules in lime-cement mortar C_{20}. (a) A PCM microcapsule broken during sample preparation for SEM allows to see the solid paraffin and the external microcapsule shell. (b) cement-lime mortar matrix with a PCM broken microcapsule. (c) Detail of the paraffin core of microcapsule in 4b.

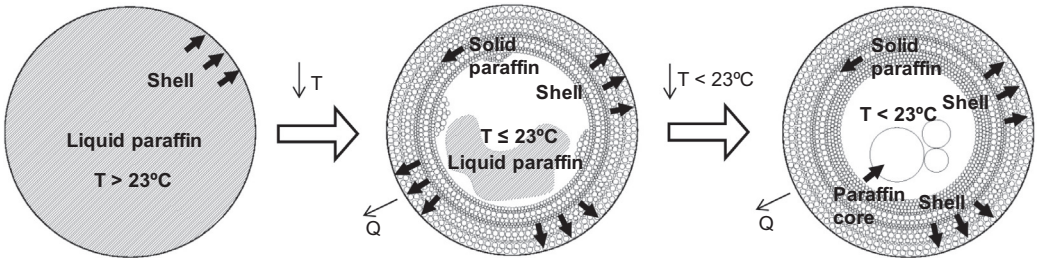

Fig. 5. Paraffin wax solidification process inside a PCM microcapsule during cooling.

ing free space inside the capsule. The paraffin that is still liquid only fills a portion of the space available. The air surrounding it reduces the heat transfer, allowing a slower solidification, forming spheres of larger size at the core of the capsule, as seen in the images of Fig. 4.

4. Analysis of results and discussion

The experimental results pointed out that fibers, lightweight (LWA), and Phase Change materials varied the physical, mechanical and thermal properties of a cement-lime mortar. The different properties and particle size of the components jointly with the w/b required to obtain plastic consistency of the fresh mortars are behind those changes on properties. This section analyzes the effects of the mortar compositions on porosity and mass transfer (physical properties), on compressive strength (mechanical properties) and on thermal conductivity and enthalpy (thermal performance).

4.1. Effect of mortar composition on porosity and transport properties

Fig. 6 relates open porosity (OP) and capillary water absorption coefficient (CC) were evaluated. A linear relationship can be observed, as capillary water absorption increased with the increase of the open porosity, as expected [21,24]. Besides, two groups of mixtures were identified: with and without LWA. The former showed OP higher than 20% (Table 2), while the mixtures without LWA showed values lower than 20%. Therefore, two linear equations could be drawn, as the addition of LWA did not increase CC as much as OP. It can be explained because LWA pores are coarser than capillary pores.

On the other hand, PCM reduced both OP and CC of mixtures without LWA, due to the filler effect of the micrometric size of the PCM particles. This effect was not observed for mortars with LWA as PCM did only modify paste porosity and not LWA porosity. Cellulose fibres did not produce significant effects either on OP nor CC, as expected [21].

Summarizing, LWA had a large impact on the pore structure, due to its own large porosity, while PCM behaves as a filler, reducing the capillary pores of the mortar paste.

4.2. Effect of mortar composition on mechanical properties

Fig. 7 plots the effect of composition on compressive strength, related to open porosity (OP). The inclusion of LWA produced a slight decrease of compressive strength and a large increase of OP, while CF did not modify significantly strength as expected [21]. On the other hand, PCM slightly reduced OP but produced a large impact on compressive strength. This apparently divergent behavior can be explained if the w/b of the mixture is considered (Table 1). The amount of water required to achieve a plastic consistency for mixtures with PCM was larger for larger amount of PCM, and the increase of w/b reduced compressive strength, as can be observed in Fig. 8a. Consequently, the reduction on compressive strength was produced by the inclusion of PCM micro-particles and is enlarged by the extra water demanded by PCM. This effect could be reduced if water reducing admixtures were added to improve the flowability of PCM mortars instead of adding more water.

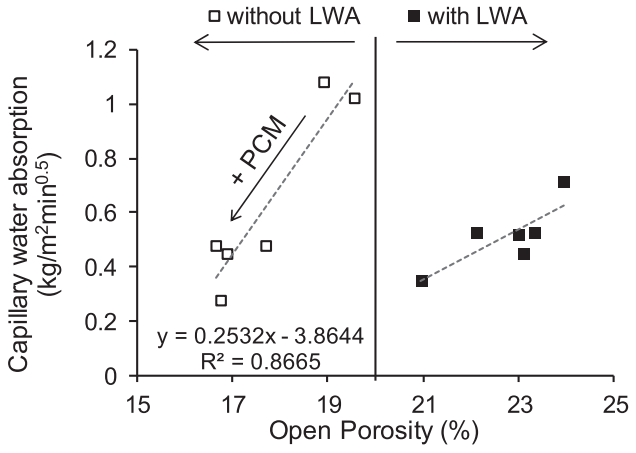

Fig. 6. Effect of PCM and LWA content on Capillary water absorption and open porosity of PCM lime-cement mortars.

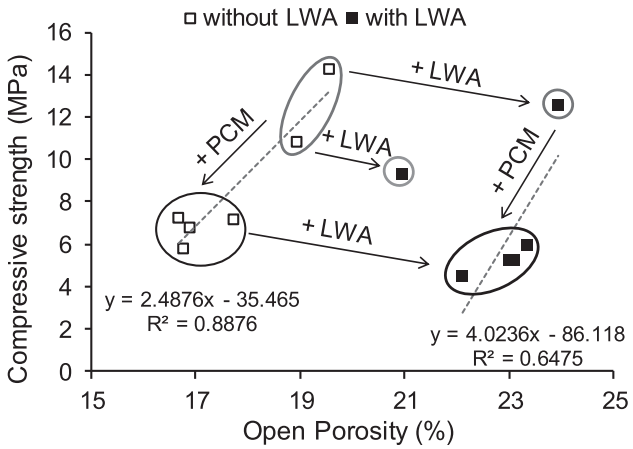

Fig. 7. Effect of PCM and LWA content on Compressive strength and open porosity of PCM lime-cement mortars.

Fig. 8b relates compressive strength to Ultrasonic Young Modulus (E_s) measured with Ultrasonic pulse velocity at 28 days. Again, the effect of components on properties can be evaluated, as Compressive strength can be easily related and a fairly correlation coefficient can be obtained. It can be observed that LWA slightly reduced compressive strength while PCM showed a larger effect. It can be highlighted that US can be used as NDT quality control technique to evaluate lime-cement mortars with different compositions.

4.3. Effect of mortar composition on thermal performance: conductivity and enthalpy.

The thermal properties as thermal conductivity and enthalpy were also influenced by the mortar components, as can be observed in Table 2.

Fig. 9 relates thermal conductivity to open porosity of mortars with and without LWA, CF and PCM. The inclusion of LWA reduced significantly conductivity both at low temperature (solid PCM (λ_s)) and at higher temperature (liquid PCM (λ_l)), due to the increase of mortar open porosity (Table 2). PCM physical state also affected thermal conductivity, as λ_l was lower than λ_s in all cases. Mixtures with cellulose fibers did not showed significant changes in the steady state thermal conductivity, although they could be expected at least for mortars with discontinuous aggregates [21,32]. It can be explained because the fibers would only modify the thickness of paste surrounding gap-graded aggregates [32], which is not the case on the mortars under study.

On the other hand, the addition of cellulose fibers, LWA and PCM also impacted the mortar enthalpy (Fig. 3). As expected, the addition of PCM increased enthalpy in the temperature range

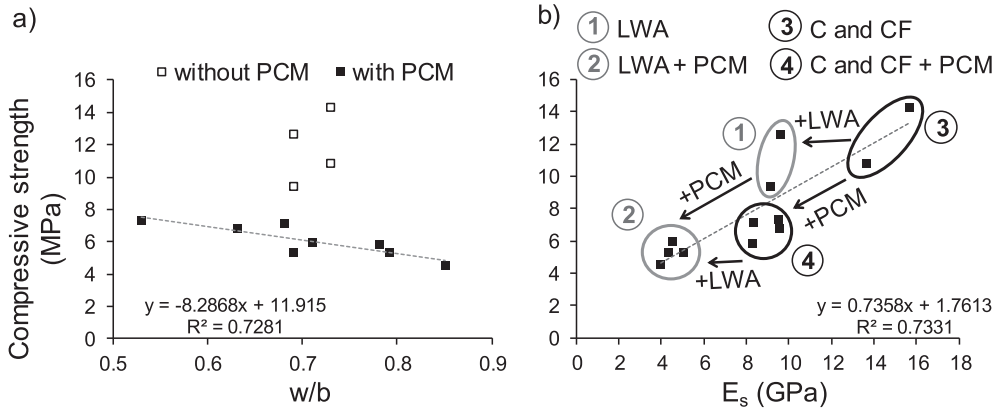

Fig. 8. Effect of PCM and LWA content on Compressive strength related to: (a) water to binder ratio (w/b); (b) 28 days Ultrasonic Young Modulus (E_s).

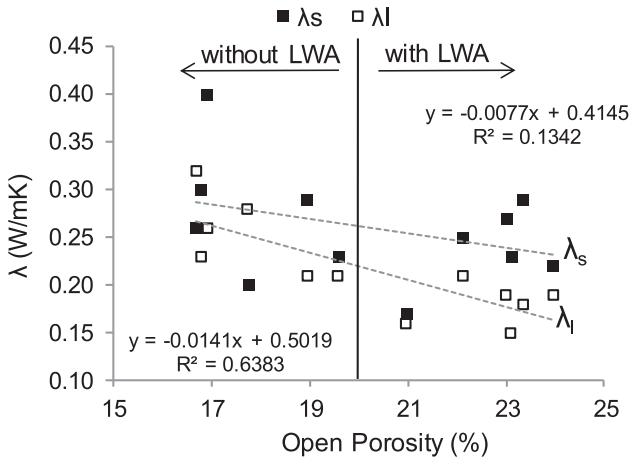

Fig. 9. Thermal conductivity of PCM lime-cement mortars at 40 °C (melted paraffin) vs. open porosity.

tested, as PCM melted at 23 °C and solidified at 22 °C (Fig. 2). However, the amount of PCM did not show a linear relationship to enthalpy in most of the cases but mortars with cellulose fibers. The largest differences were identified between C_{20} (Fig. 3a) and CL_{20} (Fig. 3c). C_{20} presented the lowest enthalpy value for mortars with 20% of PCM, while CL_{20} showed the largest value. Accordingly, the mixture with LWA requires more energy (larger enthalpy) because LWA increases the thermal insulation (reducing thermal conductivity), slowing down the heat flow through the mortar to the PCM capsules. In the case of cellulose fibers, the mortars did not show a significant enthalpy increase because cellulose fibers did not behave as a thermal insulator as effective as LWA for the mortars under study.

5. Conclusions

An experimental study to analyze the effect of the addition of LWA, cellulose fibers and different amounts (10% and 20%) of a microencapsulated Phase Change Material (PCM) on cement-lime mortar properties was carried out. The experimental program assessed workability, free shrinkage and hardened physical, mechanical and thermal properties. The main conclusions of this study were:

- The addition of PCM to a reference cement-lime mortar reduced open porosity, compressive strength and ultrasonic Young modulus. It was the combined effect of the filler effect of PCM and by the extra water to binder ratio (w/b) required to achieve plastic fresh consistency.
- The addition of PCM increased the enthalpy values of the cement-lime mortars. Thermal conductivity of mortars with PCM was lower at higher temperature when PCM is melted.
- Lightweight aggregates increased porosity while reduced compressive strength and thermal conductivity.
- The addition of cellulose fibres did not affect significantly the properties of the cement-lime mortars with or without PCM.
- Adding 10% or 20% of PCM did not mean a significant difference in physical and mechanical mortar properties. However, the differences in thermal properties such as enthalpy were remarkable for mortars with LWA, because the lower conductivity supplied by LWA slowed down the heat flow through the mortar to the PCM capsules.
- The mortar with LWA and 20% of PCM showed the best thermal performance, with low conductivity and the largest enthalpy, reaching twice the reference mortar enthalpy.

Declaration of Competing Interest

The authors declared that there is no conflict of interest.

Acknowledgements

The authors want to acknowledge the help of Prof. Consuelo Cid of UAH and Prof. Dr.ir. Eddie Koenders and the Institut für Werkstoffe im Bauwesen – Technische Universität Darmstadt for the SEM images.

Some of the components were supplied by BASF Construction Chemicals España S.L., Omya Clariana S.L. and Cementos Portland Valderrivas.

References

[1] A. Sharma, V.V. Tyagi, C.R. Chen, D. Buddhi, Review on thermal energy storage with phase change materials and applications, Renew. Sustain. Energy Rev. 13 (2009) 318–345, https://doi.org/10.1016/j.rser.2007.10.005.
[2] E. Günther, S. Hiebler, H. Mehling, R. Redlich, Enthalpy of phase change materials as a function of temperature: required accuracy and suitable measurement methods, Int J Thermophys 30 (2009) 1257–1269, https://doi.org/10.1007/s10765-009-0641-z.
[3] L.F. Cabeza, C. Barreneche, A. Castell, A. de Garcia, et al., Materials used as PCM in thermal energy storage in building: a review, Renew. Sustain. Energy Rev. 15 (2011) 1675–1695, https://doi.org/10.1016/j.rser.2010.11.018.
[4] D. Zhou, C.Y. Zhao, Y. Tian, Review on thermal energy storage with phase change materials (PCMs) in building applications, Appl. Energy 92 (2012) 593–605, https://doi.org/10.1016/j.apenergy.2011.08.025.

[5] J. Terés-Zubiaga, K. Martín, A. Erkoreka, J.M. Sala, Field assessment of thermal behaviour of social housing apartments in Bilbao, Northern Spain, Energy and Buildings 67 (2013) 118–135, https://doi.org/10.1016/j.enbuild.2013.07.061.
[6] J. Terés-Zubiaga, A. Campos-Celador, I. González-Pino, C. Escudero-Revilla, Energy and economic assessment of the envelope retrofitting in residential buildings in Northern Spain, Energy Build. 86 (2015) 194–202, https://doi.org/10.1016/j.enbuild.2014.10.018.
[7] S. Lucas, V.M. Ferreira, Selecting insulating building materials trough an assessment tool. In: CIB (Ed.), Portugal SB10. Sustainable Building Affordable to All, 2010, pp. 745–752.
[8] S. Schiavoni, F. D'Alessandro, F. Bianchi, F. Asdrubali, Insulation materials for the building sector: a review and comparative analysis, Renew. Sustain. Energy Rev. 62 (2016) 988–1011, https://doi.org/10.1016/j.rser.2016.05.045.
[9] S. Ali Memon, Phase change materials integrated in building walls: a state of the art review, Renew. Sustain. Energy Rev. 31 (2014) 870–906, https://doi.org/10.1016/j.rser.2013.12.042.
[10] A. Jayalath, R. San Nicolas, M. Sofi, R. Shanks, T. Ngo, L. Aye, P. Mendis, Properties of cementitious mortar and concrete containing micro-capsulated phase change materials, Constr. Build. Mater. 120 (2016) 408–417, https://doi.org/10.1016/j.conbuildmat.2016.05.116.
[11] S. Drissi, A. Eddhahak, S. Caré, J. Neji, Thermal analysis by DSC of phase change materials, study of the damage effect, J. Build. Eng. 1 (2015) 13–19, https://doi.org/10.1016/j.jobe.2015.01.001.
[12] Z. Pavlík, J. Fořt, M. Pavlíková, J. Pokorný, A. Trník, R. Černý, Modified lime-cement plasters with enhanced thermal and hygric storage capacity for moderation of interior climate, Energy Build. 126 (2016) 113–127, https://doi.org/10.1016/j.enbuild.2016.05.004.
[13] N.P. Sharifi, A. Sakulich, Application of phase change materials to improve the thermal performance of cementitious material, Energy Build. 103 (2015) 83–95, https://doi.org/10.1016/j.enbuild.2015.06.040.
[14] S. Lucas, L. Senff, V.M. Ferreira, J.L. Barroso de Aguiar, et al., Fresh state Characterization of lime mortars with PCM addition, Appl. Rheol. 20 (63162) (2010) 1–7, https://doi.org/10.3933/ApplRheol-20-63162.
[15] S. Lucas, V.M. Ferreira, J.L. Barroso de Aguiar, Latent heat storage in PCM containing mortars—study of microstructural modifications, Energy Build. 66 (2013) 724–731, https://doi.org/10.1016/j.enbuild.2013.07.060.
[16] S. Cunha, J. Aguiar, F. Pacheco-Torgal, Effect of temperature on mortars with incorporation of phase change materials, Constr. Build. Mater. 98 (2015) 89–101, https://doi.org/10.1016/j.conbuildmat.2015.08.077.
[17] S. Cunha, M. Lima, J.B. Aguiar, Influence of adding phase change materials on the physical and mechanical properties of cement mortars, Constr. Build. Mater. 127 (2016) 1–10, https://doi.org/10.1016/j.conbuildmat.2016.09.119.
[18] L. Haurie, S. Serrano, M. Bosch, A. Fernandez, L. Cabeza, Single layer mortars with microencapsulated PCM: study of physical and thermal properties, and fire behaviour, Energy Build. 111 (2016) 393–400, https://doi.org/10.1016/j.enbuild.2015.11.028.
[19] V. Venkateswara Rao, R. Parameshwaran, V. Vinayaka Ram, PCM-mortar based construction materials for energy efficient buildings: a review on research trends, Energy Build. 158 (2018) 95–122, https://doi.org/10.1016/j.enbuild.2017.09.098.
[20] E. Sala, C. Zanotti, C. Passoni, A. Marini, Lightweight natural lime composites for rehabilitation of historical heritage, Constr. Build. Mater. 125 (2016) 81–93, https://doi.org/10.1016/j.conbuildmat.2016.08.033.
[21] I. Palomar, G. Barluenga, J. Puentes, Lime–cement mortars for coating with improved thermal and acoustic performance, Constr. Build. Mater. 75 (2015) 306–314, https://doi.org/10.1016/j.conbuildmat.2014.11.012.
[22] M. Stefanidou, Cement-based renders with insulating properties, Constr. Build. Mater. 65 (2014) 427–431, https://doi.org/10.1016/j.conbuildmat.2014.04.062.
[23] R. Veiga, Air lime mortars: what else do we need to know to apply them in conservation and rehabilitation interventions? A review, Constr. Build. Mater. 157 (2017) 132–140, https://doi.org/10.1016/j.conbuildmat.2017.09.080.
[24] L.M. Silva, R.A. Ribeiro, J.A. Labrincha, V.M. Ferreira, Role of lightweight fillers on the properties of a mixed-binder mortar, Cem. Concr. Compos. 32 (2010) 19–24, https://doi.org/10.1016/j.cemconcomp.2009.07.003.
[25] M. Bentchikou, A. Guidoum, K. Scrivener, K. Silhadi, S. Hanini, Effect of recycled cellulose fibres on the properties of lightweight cement composite matrix, Constr. Build. Mater. 34 (2012) 451–456, https://doi.org/10.1016/j.conbuildmat.2012.02.097.
[26] G. Barluenga, I. Palomar, J. Puentes, Early age and hardened performance of cement pastes combing mineral additions, Mater. Struct. 46 (2013) 921–941, https://doi.org/10.1617/s11527-012-9944-9.
[27] I. Palomar, G. Barluenga, Assessment of lime-cement mortar microstructure and properties by P- and S- ultrasonic waves, Constr. Build. Mater. 139 (2017) 334–341, https://doi.org/10.1016/j.conbuildmat.2017.02.083.
[28] S. Herrero, P. Mayor, F. Hernández-Olivares, Influence of proportion and particle size gradation of rubber from end-of-life tires on mechanical, thermal and acoustic properties of plaster–rubber mortars, Mater. Des. 47 (2013) 633–642, https://doi.org/10.1016/j.matdes.2012.12.063.
[29] A. Ristić, S. Furbo, C. Moser, H. Schranzhofer, et al., IEA SHC task 42/ECES Annex 29 WG A1: engineering and processing of PCMs, TCMs Sorpt. Mater. Energy Procedia 91 (2016) 207–217, https://doi.org/10.1016/j.egypro.2016.06.205.
[30] S. Gschwander, T. Haussmann, G. Hagelstein, A. Sole, L.F. Cabeza, G. Diarce, et al., Standardization of PCM characterization via DSC, in: 13th International Conference on Energy Storage, 2015, pp. 19–21.
[31] X. Jin, X. Xu, X. Zhang, Y. Yin, Determination of the PCM melting temperature range using DSC, Thermochimica Acta 595 (2014) 17–21, https://doi.org/10.1016/j.tca.2014.09.004.
[32] I. Palomar, G. Barluenga, A multiscale model for pervious lime-cement mortar with perlite and cellulose fibers, Constr. Build. Mater. 160 (2018) 136–144, https://doi.org/10.1016/j.conbuildmat.2017.11.032.

10.1.3 On the capillary water absorption of cement-lime mortars containing phase change materials: Experiments and simulations

Guardia, C., Schicchi, D.S., Caggiano, A. et al. (2020) *On the capillary water absorption of cement-lime mortars containing phase change materials: Experiments and simulations.* Building Simulations 13, 19–31, https://doi.org/10.1007/s12273-019-0556-y

Build Simul
https://doi.org/10.1007/s12273-019-0556-y

On the capillary water absorption of cement-lime mortars containing phase change materials: Experiments and simulations

Cynthia Guardia[1], Diego Said Schicchi[2], Antonio Caggiano[3,4] (✉), Gonzalo Barluenga[1], Eddie Koenders[3]

1. Department of Architecture, University of Alcalá, Madrid, Spain
2. Leibniz-Institut für Werkstofforientierte Technologien - IWT, Bremen, Germany
3. Institut für Werkstoffe im Bauwesen, Technische Universität Darmstadt, Germany
4. CONICET, LMNI, INTECIN, Facultad de Ingeniería, Universidad de Buenos Aires, Argentina

Abstract

Nowadays, the use of phase change materials (PCMs) represents a novel technique employed for retrofitting facades in existing buildings, mainly to fulfil temperature comfort and building energy efficiency requirements. The present study summarizes the results of a wide series of permeability tests carried out for understanding the moisture transport phenomena by capillary action in microencapsulated-PCM (MPCM) porous cementitious composites. Particularly, twelve MPCM cement-lime mortars are analyzed, which were cast with white cement, air lime, siliceous and lightweight aggregates (LWAs), short cellulose fibers and microencapsulated paraffin waxes. A total amount of 10% and 20% of MPCM by volume was added to the plain mixtures, and physical, mechanical and thermal properties of the composites were characterized. The experimental results are employed in an inverse identification procedure aimed at unveiling the key features of the capillary action in these partly saturated MPCM porous systems. A nonlinear FEM-based model for moisture transport phenomena is used with this purpose by adopting an extended Darcy's law. The capillary pressure is considered to control the overall diffusion-driven mechanism. The outcome of the inverse calibration allows to better understand the influence of each material component (and specially focusing on the MPCM volume fraction) on the resulting diffusion parameters, capillary pressure and the Raleigh-Ritz pore size distribution of the analyzed porous cementitious composites. The inverse calibration procedure showed that MPCM mortars with high values of the Raleigh-Ritz (*B*) parameter exhibit a low capillary permeability performance. Particularly, it was observed that when MPCMs are added into the analyzed mortars, an increment of the B value is numerically obtained and a subsequent reduction of the permeability performance of the composites is obtained.

Keywords

thermal-energy storage,
MPCM,
paraffin waxes,
capillary water absorption,
diffusion,
moisture,
transport phenomena

Article History

Received: 26 October 2018
Revised: 23 April 2019
Accepted: 6 May 2019

1 Introduction

The realization of energy efficient buildings, characterized by a low energy consumption, can be supported by employing smart materials and novel technologies (Weinläder et al. 2005). In this context energy storage cementitious composites, with an enhanced thermal storage capacity through using phase change materials (PCMs), are worth of investigation (Khudhair and Farid 2004). In contrast to sensible thermal heat storages, PCMs can store and release a significantly higher amount of (thermal) energy in a relatively smaller volume and at almost constant temperature (Erlbeck et al. 2018). Since the construction sector in Europe is responsible for a huge energy consumption (buildings are responsible for approximately 40% of such energy demand and 36% of CO_2 EU emissions (Jeon et al. 2013)), innovation in new materials is asked to reduce environmental impact and carbon footprint.

In the last two decades, the interest in developing new cementitious systems to improve energy efficiency of new or retrofitted buildings has considerably increased. To enhance the thermal properties of such composites, several

E-mail: caggiano@wib.tu-darmstadt.de

additions in mixtures have been proposed in the literature. Authors recognized that the addition of fibers, like cellulose or polypropylene ones, leads to remarkable improvements on the thermal and acoustic properties of the composite (Palomar et al. 2015). The use of lightweight aggregates (LWAs), like expanded perlites, has been also investigated with the same purpose (Kim et al. 2012). As a matter of fact, both fiber reinforced mortars and concrete with LWAs are widely employed for retrofitting of existing facades since they can improve energy efficiency by providing higher thermal insulation. The investigation of PCM-concrete started from the same energy-saving idea but following a completely different concept. PCM-based composites do not deal with insulation phenomena but contribute to the capacity of a material to store and release energy while conducting a phase change. Actually, a good PCM-composite should have poor insulation characteristics and rather large thermal energy storage (TES) capacity, being able to store/release high amounts of energy during temperature fluctuations, efficiently and with a low thermal inertia. Papers on this matter have been published in the last years investigating, among others, the mechanical properties of PCM-cement based composites (Cui et al. 2015), high temperature responses (Banu et al. 1998), freeze-thaw cycles (Sakulich and Bentz 2012), hydration effects on early age PCM-concretes (Hunger et al. 2009) and PCM effects in geopolymer applications (Shadnia et al. 2015).

Permeability tests for concrete specimens have been widely used to characterize the moisture transport capacity and its connectivity in cement-based materials (Shin et al. 2017). On this regard, several works are available studying the key parameters affecting the transport phenomena of a cementitious system and its durability performance. For example, the effects of maximum aggregate size, cement type, water-cement ratio and curing, affecting the concrete permeability, were discussed in Soongswang et al. (1991). The effects of sand content which modified the transition zones formed at the aggregate-paste interfaces were studied by Halamickova et al. (1995). The incidence of aggregate gradation on concrete permeability was deeply investigated for two different cement types and for a total of twenty mixtures by Warda and Munaz (2012).

Some theoretical proposals are also available for describing moisture phenomena and diffusion processes in concrete at a macroscopic level (Martín-Pérez et al. 2001; Bary and Sellier 2004; Isgor and Razaqpur 2004; Samson and Marchand 2007; de Freitas et al. 2017). Moreover, some of the numerical tools aim at performing lower scale observations and descriptions of this problem. For example, a mesoscopic approach was proposed by Schlangen et al. (2007) to investigate the influence of the water content on the effect of drying shrinkage, cracking response, tensile strength and ductility issues. The simulations were performed through a meso-level lattice model, explicitly considering the formation of (micro-) cracks in concrete. Segura and Carol (2004) proposed a zero-thickness interface formulation for diffusion problems through discontinuities. Other models for mesoscale modeling of water penetration into concrete by capillary absorption were proposed by Wang and Ueda (2011) and Caggiano et al. (2018).

In this context, the present research is mainly intended at investigating the capillary water absorption of cement-lime mortars containing MPCMs. Main scope of the study is to examine the effects of MPCM, at both experimental and numerical standpoint, on the resulting transport mechanisms of the composites under investigation. The results of a wide series of permeability tests, carried out on plain mortars, mortars with LWAs, short cellulose fiber reinforced mortars and mixed LWA-fiber ones, are summarized. All mixtures were also cast with and without MPCM: a dosage of 10% and 20% of the microencapsulated paraffin wax was alternatively considered. Then, the achieved experimental results are employed in an inverse identification procedure for unveiling the key parameters that drive the absorption capacity of the mixtures. It is worth mentioning that this field of research, dealing with the capillary water absorption of cement-based systems containing MPCMs, from both experimental and numerical standpoints, has not been investigated yet in the scientific literature. This article represents a significant contribution to the current state-of-the-art in this research topic.

After this general introduction about the state-of-the-art and motivations of this research, the paper is organized as follows. Section 2 reports the employed materials, mixtures and methods, highlighting and discussing the investigated experimental results of twelve MPCM cement-lime mortar systems. After that, in Section 3 a comparison between the experimental results and the corresponding numerical simulations is presented. Transport simulations were done to analyze moisture diffusion and capillary water absorption phenomena, and were based on an available model recently proposed by the authors. Finally, some concluding remarks and future research lines are described in Section 4.

2 Experimental procedure and results

The results reported in this section were obtained from experimental tests performed on twelve MPCM cement-lime mortars. The section deals with an overview of the physical, mechanical and thermal characterization of the analyzed composites.

2.1 Materials and mixtures

MPCM cement-lime mortars were prepared using the

components listed below:

- White cement BLII/B-L 32.5N (UNE-EN 2000).
- Air lime CL90-S, designated according to UNE-EN (2011).
- Siliceous aggregates (range size: 0–4 mm).
- Short cellulose fibers of 1 mm length - Fibracel® BC-1000 (Ø20 μm) by Omya Clariana S.L.
- LWAs: expanded perlites (range size: 0–2 mm).
- MPCM - Micronal® DS 5040X (BASF 2013), with particle sizes in the range of ca. 50–300 μm and a melting point of about 23 °C.

The MPCM mortars compositions (twelve different in total) used in this study are summarized in Table 1. The reason for choosing MPCM particles with a melting point of 23 °C was because this value stands close to the comfort temperature required inside residential buildings (which normally ranges between 19 °C and 27 °C).

A cement-lime mortar, in Table 1 labeled as C, represents the reference mixture. It has been designed by a binder to aggregates ratio of "1: 0.5: 4.5" (i.e., cement-lime-aggregate) in volume. Then:

- 1.5% of short Cellulose Fibers (having the label CF) was added in terms of the total fresh mortar volume;
- 50% of siliceous aggregates were replaced by expanded perlites (this mortar was labeled as CL); lastly
- mortars with both short cellulose fibers and expanded perlites were also produced (labelled as CLF).

Afterwards, 10% and 20% of MPCM in volume were added to the mixtures. The water to binder ratio (w/b) was adjusted to get similar plastic consistency and fresh workability for all mixtures. Particularly, w/b varied between 0.63 and 0.85 (see Table 1).

Regarding the mixing procedure: firstly, all the dry components, included fibers and MPCM, were mixed for 2 minutes; afterwards, water was incorporated. The total mixing time did not exceed 5 min.

2.2 Experimental methods

The experimental program was realized for evaluating the physical properties of the aforementioned mixtures. Particularly, bulk density, open porosity, capillary water absorption coefficients, mechanical characterization (flexural and compressive strengths) and thermal performance (e.g., thermal conductivity at 25 °C and 40 °C, indicated as λ_{25} and λ_{40}, respectively) of the twelve cement-lime mixtures were investigated.

Prismatic 40 mm × 40 mm × 160 mm specimens were used for characterizing the mortars in hardened state. The samples were demolded at 24 h and stored at 21 °C ± 3 °C and 95% ± 5% RH until testing, after 28 days. The bulk density and open porosity (accessible to water) were calculated using a hydrostatic balance according to UNE-EN (2007b) standard. Then, capillary water absorption coefficients were measured according to UNE-EN (2003) and the procedure described in Palomar et al. (2015). The absorbed water under capillary action was obtained by leaving the bottom part of the specimens (having a cross section of 40 mm × 40 mm) in direct contact with water (Fig. 1). The immersion depth was 10 mm. The capillary water absorption coefficient was estimated weighing the 40 mm × 40 mm × 160 mm specimens at 10 minutes, 90 minutes and 24 hours. No sealant was used in these tests (Palomar et al. 2015). Flexural and compressive strengths were evaluated according to UNE-EN (2007a).

Thermal conductivity (λ) of all mixtures was measured by means of a thermally insulated box (Guardia et al. 2018). This box has a 210 mm × 210 mm opening on one side

Table 1 MPCM cement-lime mortars compositions

	Cement-lime			With cellulose fibers (CFs)			With lightweight aggregates (LWAs)			With LWA and CFs		
Mortars	C	C10	C20	CF	CF10	CF20	CL	CL10	CL20	CLF	CLF10	CLF20
BLII/B-L 32.5N	348	348	348	348	348	348	348	348	348	348	348	348
CL 90-S	55	55	55	55	55	55	55	55	55	55	55	55
Sand (0–4)	1403	1403	1403	1403	1403	1403	702	702	702	702	702	702
Cellulose fibers	—	—	—	0.40	0.62	0.66	—	—	—	0.40	0.62	0.66
Perlite*	—	—	—	—	—	—	94	94	94	94	94	94
PCM	—	42.3	84.6	—	42.3	84.6	—	42.3	84.6	—	42.3	84.6
Water**	220	140	200	220	180	240	240	240	250	240	305	380
D_{dry}[kg/m^3]	1400	1448	1357	1387	1260	1440	845	964	868	822	—	—
D_{wet}[kg/m^3]	2264	1857	1937	2165	1904	1885	1711	1682	1562	1854	1433	1561
w/b	0.73	0.53	0.68	0.73	0.63	0.78	0.69	0.69	0.71	0.69	0.85	0.79
Consistency [mm]	178	170	166	160	173	170	195	173	170	170	180	170

Cement: lime: aggregates = 1: 0.5: 4.5 by volume.

* 50% of volume of the siliceous aggregate was replaced by perlite.

** Added water: the amount of water included in the components (sand) was also taken into account. Sand 0–4: humidity 5.3%.

All components in kg (when no specified).

Fig. 1 Experimental setup for measuring capillary water absorption coefficients

where the 210 mm × 210 mm × 24 mm thick plate must be positioned for testing. A heat source, connected to a thermal regulator, was placed inside the box. Temperature (°C) and relative humidity (%) sensors were placed on the inner and outer surfaces of the sample as well as inside and outside the box. Subsequently, two temperature conditions were set inside (for each specimen): namely, 25 °C and 40 °C. Once the steady-state was reached, thermal conductivity (λ) was calculated from the recorded data. Laboratory conditions during testing were 20 °C ± 1 °C and 50% ± 5% RH. Further test details (set-up, geometries, sensor positions and numbers) can be found in Herrero et al. (2013).

2.3 Experimental results

The experimental results are next summarized and discussed. Particularly, Table 2 shows the values of the physical, mechanical and thermal characterization of the twelve different MPCM paste mixtures. Physical properties are the density (D), the open porosity (OP) and the capillary water absorption coefficient (CC). Mechanical results are given in terms of Compressive (CS) and flexural strengths (FS). Lastly, the thermal conductivity at two different temperatures (λ_{25} and λ_{40}) is reported. Three samples of each mixture were tested to obtain D, OP, CC and FS; CS was measured on six samples of each mixture; while λ_{25} and λ_{40} were measured once per mixture. The table shows the tests' mean values, while their scatters are available (as error bars) in Figs. 2 to 5.

From the experimental results, bulk density (D) varied between approximately 1100 and 2000 kg/m^3. CF mixtures presented the maximum D value of 1960 kg/m^3, and CLF10 the minimum one of 1110 kg/m^3. It was observed that mixtures with LWAs had a reduced D in comparison with fiber-reinforced mixtures, which were characterized by an increased D. The same trend observed for CL was also recognized in mixtures where LWAs were combined with fibers (i.e., CLF mixtures). Moreover, the compositions with MPCMs showed a decrease of bulk density. However, CL10 and CLF10 had lower bulk densities than CL20 and CLF20.

On the other hand, the values of open porosity (OP) varied from 16% to 24% in volume. Particularly, the addition of LWA to the mixtures mainly increased the open porosity values, while fibers reduce them (Palomar et al. 2015; Silva et al. 2010). It can also be observed that C10 had the lowest OP (16.68%) while CLF the highest one (23.94%). As general trend the addition of MPCMs decreased the OP of C, CF and CLF mortars: MPCM particles tend to fill the smaller pores producing a reduction of the OP (Palomar and

Table 2 Physical, mechanical and thermal characterization of the MPCM cement-lime mortars

	Cement-lime			With cellulose fibers (CFs)			With lightweight aggregates (LWAs)			With LWA and CFs		
Mortars	C	C10	C20	CF	CF10	CF20	CL	CL10	CL20	CLF	CLF10	CLF20
Phy. prop.												
D [kg/m^3]	1900	1690	1600	1960	1720	1660	1430	1180	1270	1430	1110	1160
OP [%]	19.56	16.68	17.72	18.93	16.90	16.77	20.95	22.99	23.33	23.94	22.10	23.09
CC at 24h [kg/m^2]	25.91	10.43	11.81	26.54	12.28	8.82	10.99	12.98	14.85	20.34	14.18	12.57
Mech. prop.												
CS [MPa]	14.33	7.33	7.17	10.83	6.83	5.83	9.40	5.33	6.0	12.67	4.60	5.33
FS [MPa]	3.36	2.26	2.40	2.66	1.98	2.20	3.18	2.24	1.79	3.44	1.84	2.16
Therm. prop.												
λ_{25} [W/(m·K)]	0.23	0.26	0.20	0.29	0.40	0.30	0.17	0.27	0.29	0.22	0.25	0.23
λ_{40} [W/(m·K)]	0.21	0.32	0.28	0.21	0.26	0.23	0.16	0.19	0.18	0.19	0.21	0.15

Barluenga 2018). Moreover, mortar mixtures with LWAs (CL10 and CL20) had increased OPs in comparison with the other samples when MPCM were added: slight differences were found between 10% and 20% of MPCM samples this time.

Figure 2 presents the capillarity water absorption coefficient of the twelve MPCM cement-lime mortar mixtures at 24h (additional measurements in time are reported in Section 3). All measured values have been normalized by multiplying them by a factor accounting for the different *w*/*b* values. Specifically, this factor is defined as the ratio between *w*/*b* of the C mixture, chosen as reference, and the *w*/*b* value of each one of the remaining eleven mixtures (see Table 1). In the following Section 3, numerical calculations are performed based on the actual experimental determinations, leaving the normalization procedure only to perform a better comparison of the mechanical and thermal properties.

The normalized CC values ranged from 8.25 to 26.54 kg/m^2. CF20 showed the lowest value (8.25 kg/m^2) while CF the largest (26.54 kg/m^2). The addition of MPCM led to decrease the CC at 24h for all mixtures, except for CL for which the CC value increased: this trend is registered in both normalized and non-normalized values. Therefore, it can be concluded that CC values followed a similar trend of the OP results (Palomar and Barluenga 2018).

All capillarity results here presented were obtained under same laboratory conditions (i.e., 20 °C ± 1°C and 50% ± 5% RH) and following the procedure described in Palomar et al. (2015), in which the specimens were not sealed. In this regard, it is important to remark that under these laboratory conditions (with controlled temperature and humidity) a very low loss of water due evaporation is to be expected. This has been experimentally confirmed in the abovementioned research (Palomar et al. 2015), and also (experimentally and numerically, see Section 3) in this work.

Compressive (CS) and flexural strengths (FS) are reported in Figs. 3 and 4, respectively. The measured values

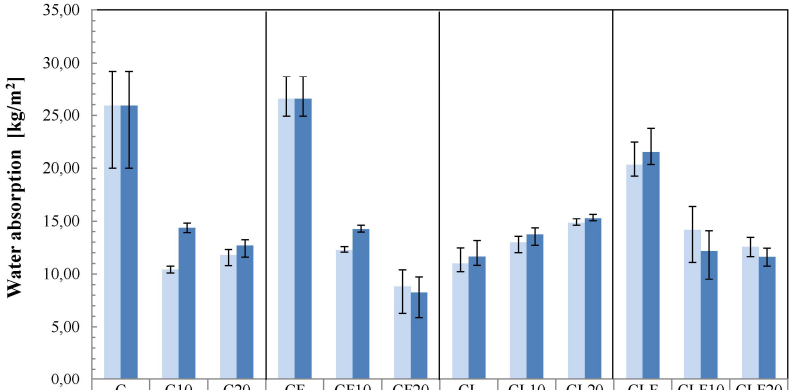

	C	C10	C20	CF	CF10	CF20	CL	CL10	CL20	CLF	CLF10	CLF20
CC at 24 h	25,91	10,43	11,81	26,54	12,28	8,82	10,99	12,98	14,85	20,34	14,18	12,57
Normalized CC	25,91	14,36	12,68	26,54	14,23	8,25	11,62	13,73	15,26	21,51	12,17	11,62

Fig. 2 Capillarity water absorption coefficient of the mixtures. The error bars represent the range between the minimum and the maximum value of the repeated tests

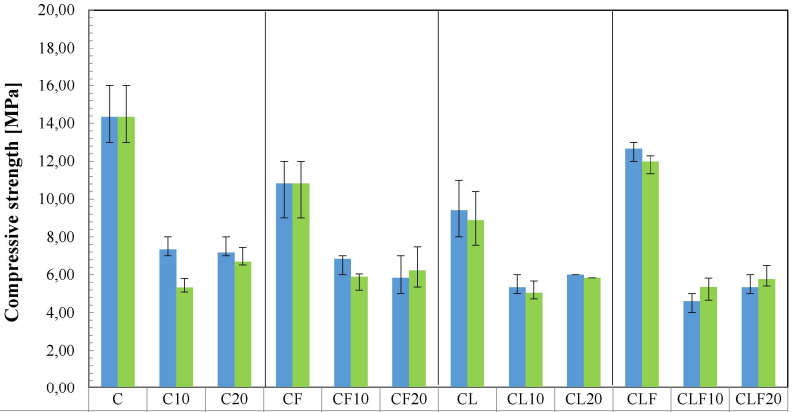

	C	C10	C20	CF	CF10	CF20	CL	CL10	CL20	CLF	CLF10	CLF20
CS at 28 days	14,33	7,33	7,17	10,83	6,83	5,83	9,40	5,33	6,00	12,67	4,60	5,33
Normalized CS	14,33	5,32	6,68	10,83	5,90	6,23	8,88	5,04	5,84	11,97	5,36	5,77

Fig. 3 Compressive strengths of the mixtures. The error bars represent the range between the minimum and the maximum value of the repeated tests

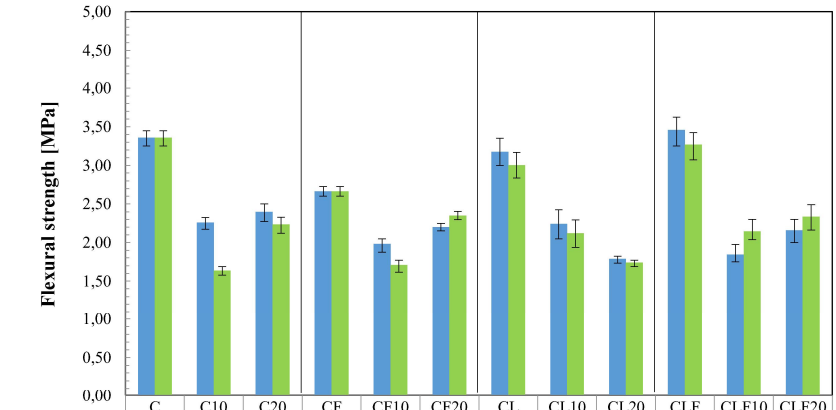

	C	C10	C20	CF	CF10	CF20	CL	CL10	CL20	CLF	CLF10	CLF20
FS at 28 days	3,36	2,26	2,40	2,66	1,98	2,20	3,18	2,24	1,79	3,46	1,84	2,16
Normalized FS	3,36	1,64	2,24	2,66	1,71	2,35	3,00	2,12	1,74	3,27	2,14	2,34

Fig. 4 Flexural strengths of the mixtures. The error bars represent the range between the minimum and the maximum value of the repeated tests

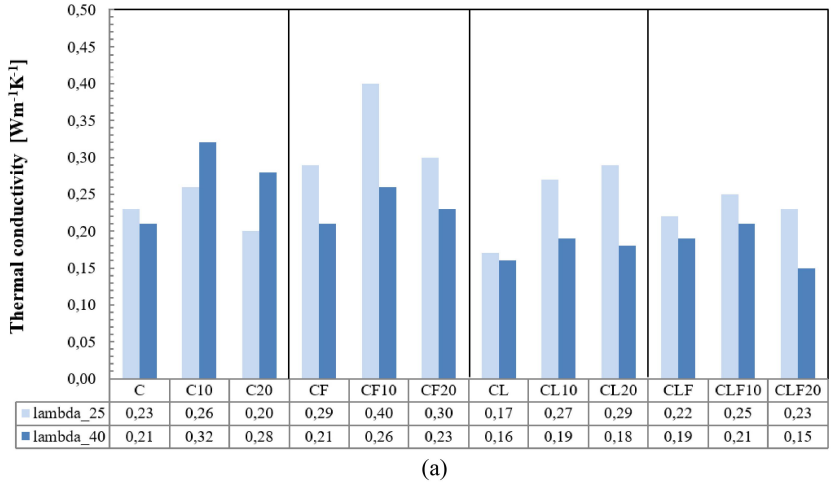

	C	C10	C20	CF	CF10	CF20	CL	CL10	CL20	CLF	CLF10	CLF20
lambda_25	0,23	0,26	0,20	0,29	0,40	0,30	0,17	0,27	0,29	0,22	0,25	0,23
lambda_40	0,21	0,32	0,28	0,21	0,26	0,23	0,16	0,19	0,18	0,19	0,21	0,15

(a)

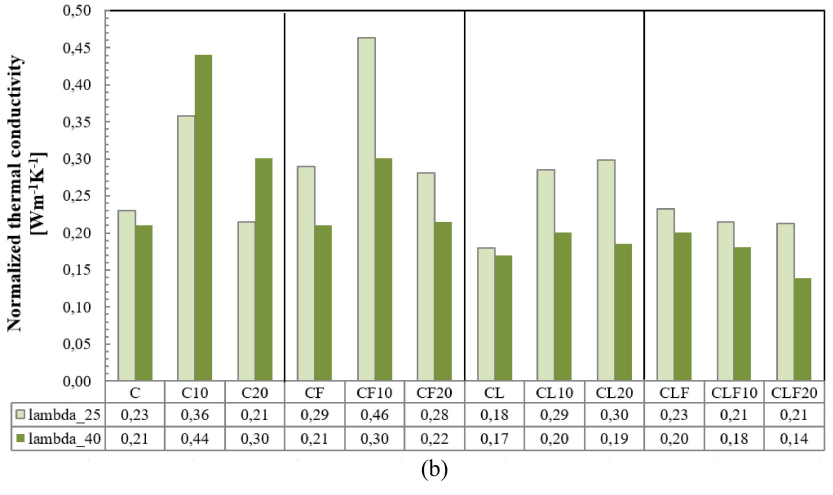

	C	C10	C20	CF	CF10	CF20	CL	CL10	CL20	CLF	CLF10	CLF20
lambda_25	0,23	0,36	0,21	0,29	0,46	0,28	0,18	0,29	0,30	0,23	0,21	0,21
lambda_40	0,21	0,44	0,30	0,21	0,30	0,22	0,17	0,20	0,19	0,20	0,18	0,14

(b)

Fig. 5 Thermal conductivity at two steady state conditions of the mixtures (λ_{25} and λ_{40}): (a) measured values and (b) normalized ones

have been also normalized by dividing them by the same factor employed in the CC calculations. This accounts for the different *w*/*b* ratios of the mixtures to give an objective understanding of the results. The normalized CS varied between 5.04 and 14.33 MPa. It can be observed that the reference mixture (C) exhibited the largest compressive strength. As expected, perlite (L) additions mainly produce a reduction of the CS. Moreover, the addition of MPCM

generates, as well, a CS reduction. This fact is also confirmed in other studies, e.g. Lucas et al. (2013); Pavlík et al. (2016). Furthermore, adding 10% of MPCM meant a higher decrease of (both normalized and non-normalized) CS than adding 20% (Fig. 3). On the other hand, the normalized FS values of the different mixtures varied between 1.64 and 3.36 MPa. The lowest value corresponded to C10 while the highest to C. When MPCMs were added, the FSs (both normalized and non-normalized) were considerably affected, as it happened with the CS (Fig. 4). However, no linear dependency was appreciated between the amount of MPCM and the reduction of compressive and flexural strength.

Finally, MPCM cement-lime mixtures were thermally characterized by measuring the thermal conductivity (λ) at 25 and 40 °C. All measured values were then normalized as described above, by multiplying all results by the unifying w/b factor. Particularly, Fig. 5(a) reports such thermal conductivities of the mixtures at different temperatures (λ_{25} and λ_{40}), while the normalized values are shown in Fig. 5(b). For the lower temperature, λ_{25} varied between 0.17 W m^{-1} K^{-1} (CL) (0.18 when normalized) and 0.40 (0.46 normalized) W m^{-1} K^{-1} (CF10). For the higher temperature, the lowest λ_{40} value was obtained for the CL mixture with 0.15 W m^{-1} K^{-1} (0.14 normalized) while C10 showed the highest one with 0.32 W m^{-1} K^{-1} (0.44 normalized). It can be finally observed that λ_{25} values of all mixtures were higher than λ_{40} (for both normalized and non-normalized values), except for C10 and C20. For both conditions, λ increased when 10% of MPCM was added. On the contrary, λ decreased when 20% MPCM was considered. For λ_{25}, the difference between adding 10% or 20% of MPCM to the mixtures C and CF was larger than for those mixtures with LWAs. Finally, mixtures with LWAs (CL) showed lower λ than mixtures without them.

Further thermal analyses are currently ongoing. They are aimed at investigating the temperature-dependent specific heat capacity and thermal conductivity (or in more general sense the thermal energy storage capacity of the mixtures) in a wider temperature range for transient heat conduction conditions, both during heating and cooling cycles. These activities are out of the scope of this paper and will be available soon in next stages of this research.

3 Capillary water absorption and numerical simulations

3.1 Overview of the moisture diffusion model

This section presents the basic equations of the moisture diffusion approach proposed by Caggiano et al. (2018), which are considered in this work for simulating the capillary water absorption in MPCM-mortar materials.

Governing equations ruling the drying/wetting behavior of MPCM cement-lime mortars assume a strong nonlinearity of material parameters depending on the water content and the local porosity.

Richards equation, establishing the transport of water for unsaturated materials, in the unsteady state form is employed as follows

$$\frac{\partial \theta}{\partial t} = \nabla \cdot \left(K_\theta \nabla p \right) \tag{1}$$

where θ represents the water content [m^3/m^3], K_θ is the unsaturated water permeability [m^4 N^{-1} s^{-1}] and p is the pore pressure [N m^{-2}]; $\nabla\cdot$ and ∇ are the divergence and gradient tensor operators, respectively.

Equation (1) represents the so-called "mixed form" of Richards equation containing both pressure and water content. When $p(\theta)$ is known, a saturation-based expression can be formulated as follows:

$$\frac{\partial \theta}{\partial t} = \nabla \cdot \left(D_\theta \nabla \theta \right) \tag{2}$$

being D_θ the capillary diffusivity [m^2 s^{-1}] (Hall 2007):

$$D_\theta = K_\theta \frac{\partial p}{\partial \theta} \tag{3}$$

The capillary (pore) pressure takes the form (Aligizaki 2005):

$$p = \frac{2CB\gamma_{lv}\cos\theta_c}{\ln\left(1-\frac{\theta}{\phi}\right)} \tag{4}$$

where B is the Raleigh-Ritz pore size distribution constant [m^{-1}], γ_{lv} [N m^{-1}] is the liquid-vapor interfacial energy (surface tension), θ_c is the equilibrium contact angle between the liquid and the solid [deg.], C is an empirical constant [—] and ϕ the open porosity [m^3/m^3].

Zhou (2011) proposal of the unsaturated water permeability was adopted in this study:

$$K_\theta = \frac{\phi^2}{50B^2\mu}\left[1-\left[1-\ln\left(1-\frac{\theta}{\phi}\right)\right]\times\left(1-\frac{\theta}{\phi}\right)\right]^2 \tag{5}$$

being μ the dynamic viscosity of water.

Finally, replacing Eqs. (4) and (5) into Eq. (3) leads to the following relation for the diffusivity rule:

$$D_\theta = \frac{C\gamma_{lv}\cos\theta_c}{25B\mu}\frac{\phi^2}{(\phi-\theta)\ln^2\left(1-\frac{\theta}{\phi}\right)}\left[1-\left[1-\ln\left(1-\frac{\theta}{\phi}\right)\right]\times\left(1-\frac{\theta}{\phi}\right)\right]^2 \tag{6}$$

Further details and the extension of the model for a mesoscale approach are available in Caggiano et al. (2018).

3.2 Model assumptions and analyzed cases

The finite element method (FEM) is employed to implement the capillary transport in cement-lime mortars specimens described in Section 2. The twelve cases discussed in the previous section represent the experimental benchmark for the inverse calibration next presented.

The following model characteristics were considered:

- Double symmetry is assumed for the (40 mm × 40 mm × 160 mm) prismatic specimens. Therefore, (i) only a quarter of the geometry was modeled seeking to minimize the computational cost of the analyses and (ii) the corresponding null Neumann boundary conditions (BCs) were imposed on the symmetry faces.
- Specimens were partially immersed in a container, where a constant level of water of 10 mm depth was maintained by means of a tank water system. The corresponding Dirichlet BCs were applied on the inferior region of the model.
- Adiabatic conditions were implemented in the external (not immersed) surfaces to suppress the interaction with the environment (i.e., evaporation, humidity transfer, etc.) in the form of null Neumann BCs.

It is worth mentioning that, even though assuming adiabatic conditions does not exactly represent the experimental set-up, from an engineering and practical point of view, neglectable differences might derive when the evaporable water loss is considered taking into account the controlled laboratory conditions of this experimental campaign, especially during the first half (12 hours) of the simulated tests. Only for higher elapsed times (e.g. 24 hours) the results could be affected by this adiabatic assumption. However, the numerical results introduced in the following section 3.3, demonstrated that good predictions were obtained over the whole test duration. Hence, the validity of the null moisture exchange with the environment is verified and the outcome of the numerical results are valid and accurate for the environmental conditions of this work. Figure 6 exhibits the BCs abovementioned and the FE discretization. 3D first order brick elements were employed for this moisture transfer analysis, where the water content represents the one and only nodal degree of freedom. A total of 31311 nodes and 28000 elements formed the mesh. The number of nodes/elements was chosen after a sensitivity study of the FEM problem. The diffusive law for unsaturated porous concrete, outlined in Section 3.1 was implemented and considered.

Material properties were chosen according to both literature and experimental evidence. Particularly, the adopted parameters were (Caggiano et al. 2018):

- $\gamma_{lv} = 7.2 \times 10^{-5}$ N mm^{-1},
- $\mu = 1.002 \times 10^{-9}$ N s mm^{-2},
- $\cos\theta_c = 0.94$ and
- $C = 2.15$.

The open porosity for each one of the twelve cases ϕ [mm^3/mm^3] (see Table 2) is listed below:

C	C10	C20	CF	CF10	CF20
0.1956	0.1668	0.1772	0.1893	0.169	0.1677
CL	CL10	CL20	CLF	CLF10	CLF20
0.2095	0.2299	0.2333	0.2394	0.221	0.2309

and lastly, the calibrated Raleigh-Ritz pore size distribution B is:

C	C10	C20	CF	CF10	CF20
3.23	10.56	14.52	3.42	12.10	29.95
CL	CL10	CL20	CLF	CLF10	CLF20
24.80	27.47	21.34	10.96	20.74	24.86

It is remarked that Eq. (2) represents the governing equation of this moisture transport problem. Considering the diffusivity coefficient of Eq. (6), the known material properties were γ_{lv}, μ, θ_c and C, while the only unknown of the problem was the Raleigh-Ritz parameter B, which deals with key information of the micro/meso-porostructure of the composite. B values were calibrated upon the experimental results and the corresponding predictions are presented and discussed in the following Section 3.3.

Many of the above parameters are related to well-known physical and/or mechanical values of the materials under consideration (cement, lime, siliceous aggregate, water, etc.). Zhou (2011) and Maekawa et al. (2014) are referred on this regard; while, the open porosity ϕ was experimentally

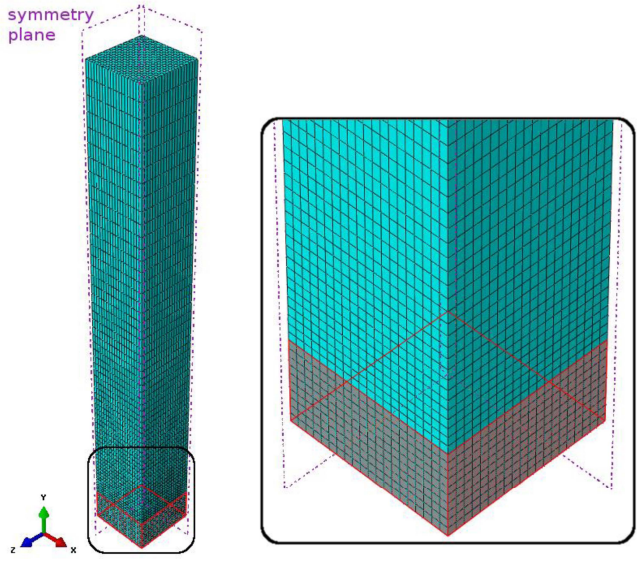

Fig. 6 FE discretization of the testing specimen

determined and reported in the previous section.

3.3 Numerical results and comparisons

In this section, the predictions of the diffusive model are compared against the results of the specimens subjected to capillary transport tests. Figures 7 to 18 compare the behavior in terms of water absorption vs. time. Three specimens per mixture were tested, with data available at three different times: 10 min, 90 min and 24 hours. In addition, the water absorption in the middle section (symmetry plane) of the simulated FE meshes (shown in Fig. 6) is incorporated in these figures for the three different time steps to complement and graphically clarify the curve results. These are aimed at easing the visualization of the level of capillarity absorption at different elapsed times.

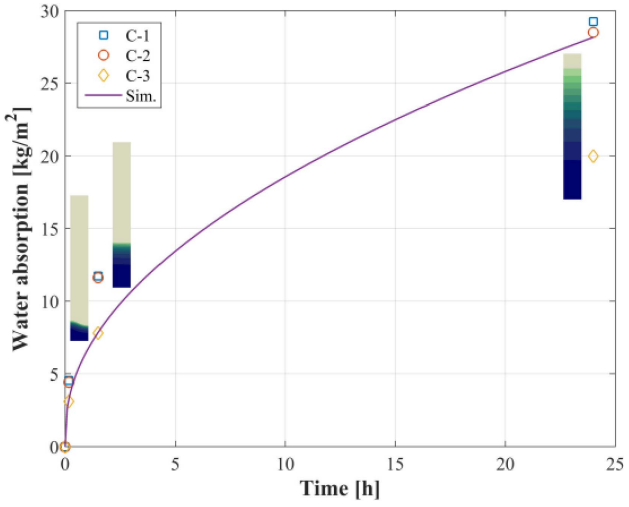

Fig. 7 Water absorption for the reference mortar: experimental results against numerical simulation

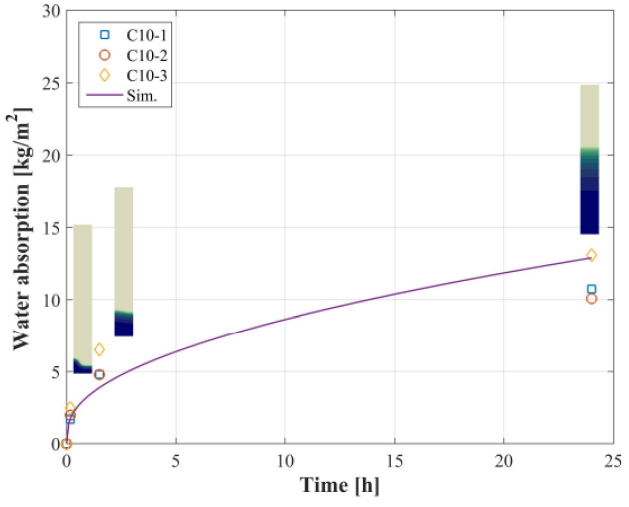

Fig. 8 Water absorption for the reference mortar with 10% MPCM: experimental results against numerical simulation

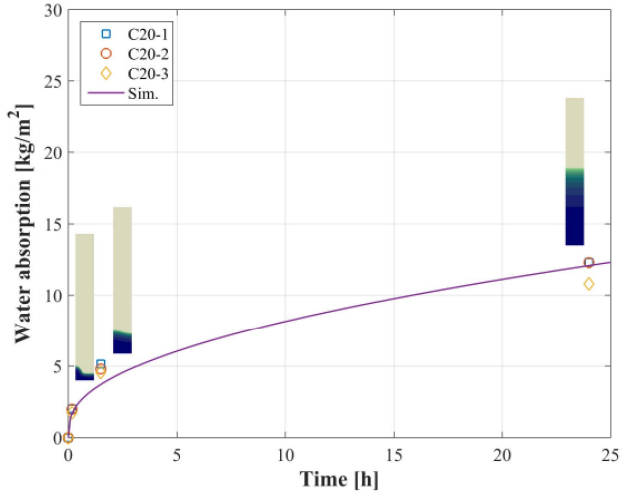

Fig. 9 Water absorption for the reference mortar with 20% MPCM: experimental results against numerical simulation

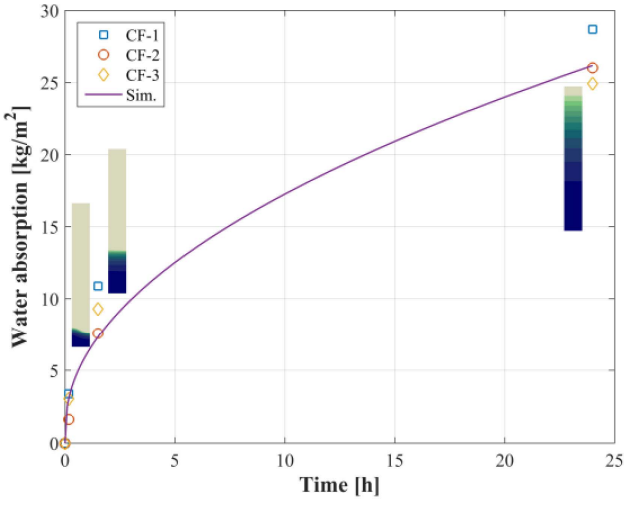

Fig. 10 Water absorption for the mortar with dry cellulose fibers with no MPCM: experimental results against numerical simulation

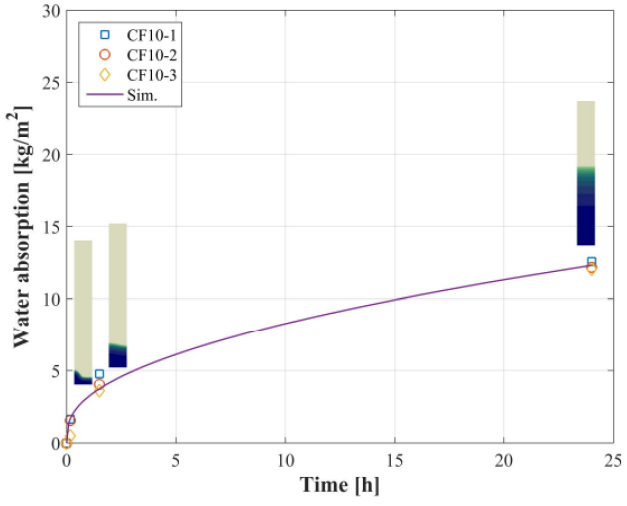

Fig. 11 Water absorption for the mortar with dry cellulose fibers with 10% MPCM: experimental results against numerical simulation

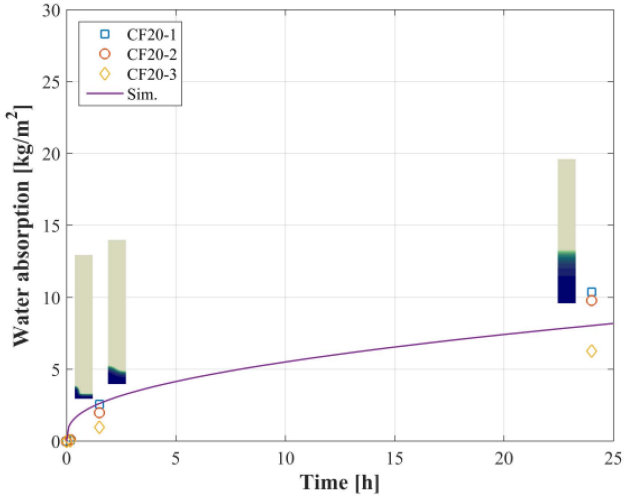

Fig. 12 Water absorption for the mortar with dry cellulose fibers with 20% MPCM: experimental results against numerical simulation

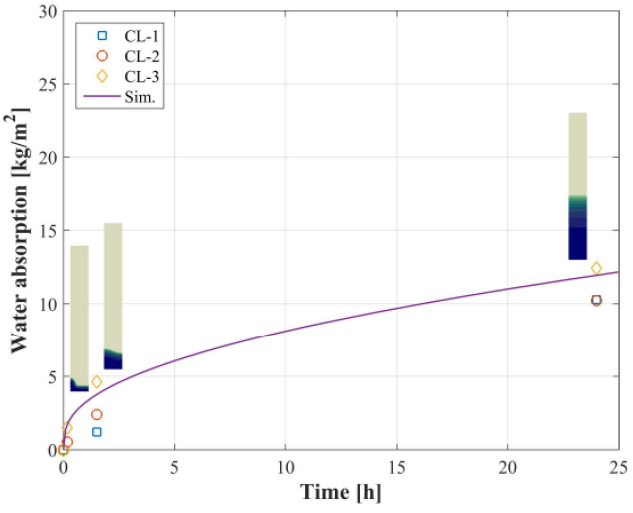

Fig. 13 Water absorption for the mortar with 50% perlite and no MPCM: experimental results against numerical simulation

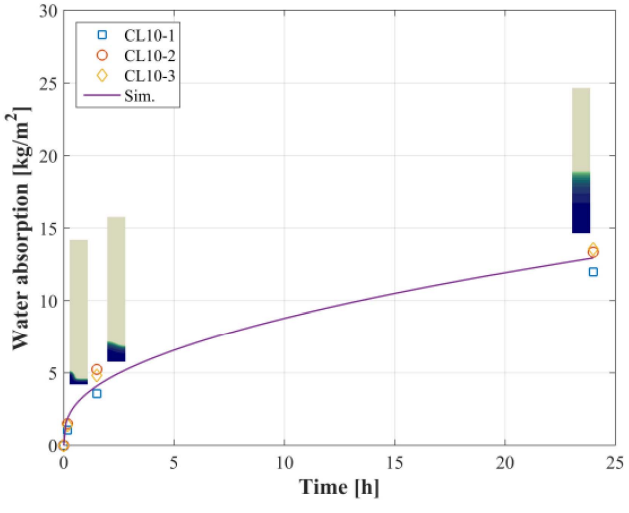

Fig. 14 Water absorption for the mortar with 50% perlite and 10% MPCM: experimental results against numerical simulation

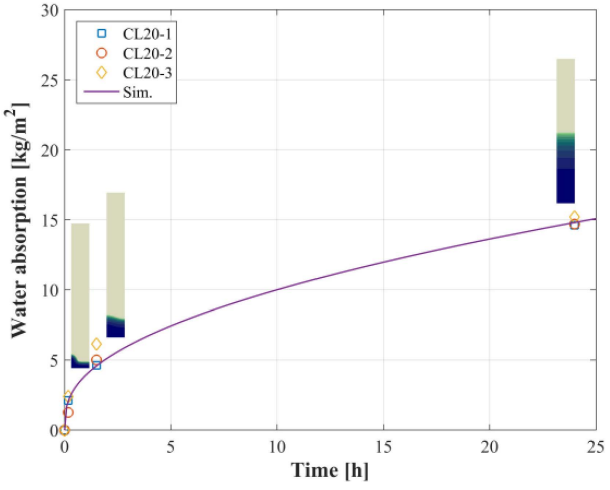

Fig. 15 Water absorption for the mortar with 50% perlite and 20% MPCM: experimental results against numerical simulation

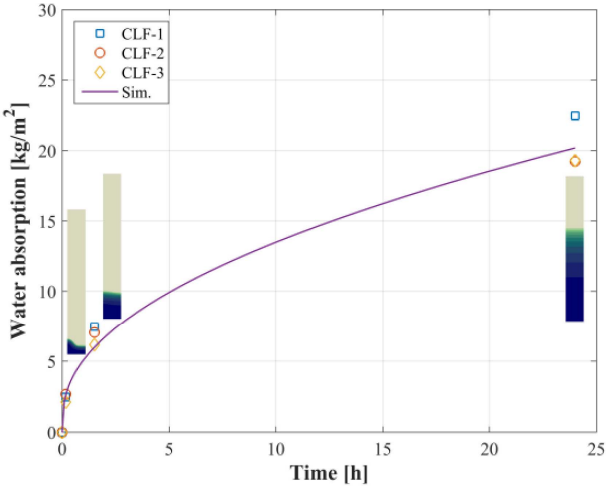

Fig. 16 Water absorption for the mortar with dry cellulose fibers plus 50% perlite and no MPCM: experimental results against numerical simulation

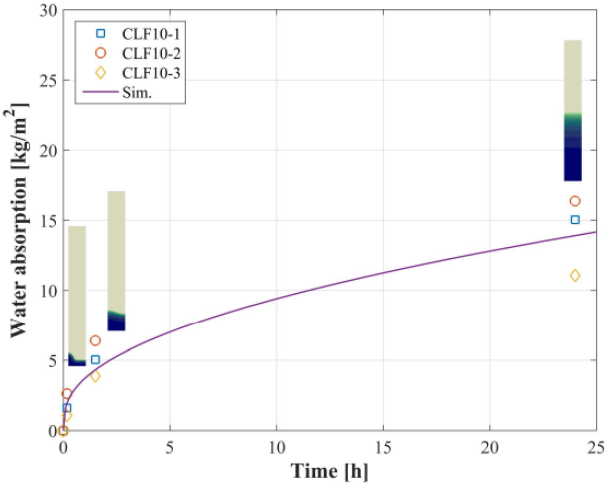

Fig. 17 Water absorption for the mortar with dry cellulose fibers plus 50% perlite and 10% MPCM: experimental results against numerical simulation

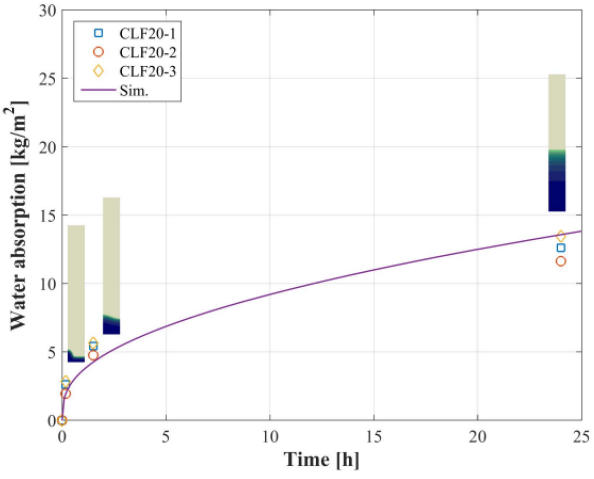

Fig. 18 Water absorption for the mortar with dry cellulose fibers plus 50% perlite and 20% MPCM: experimental results against numerical simulation

It can be generally observed that the absorption responses were very well captured by this approach based on the proposed nonlinear diffusive model. The model predicted quite well the capillary absorption for all mixtures. Figures 7 to 18 also highlight, for each one of the three mentioned elapsed times, the numerically predicted moisture level by means of the FEM procedure. Complete saturation was not reached after 24 h of any of the specimens. The reference mortar (C) and that with dry cellulose fibers added (CF), both with no MPCM, exhibited the closest to the fully saturation behavior.

The Raleigh-Ritz parameter values, introduced in Section 3.2, have been evaluated from these calibrated curves. This parameter is fundamental for understanding the permeability issues for each one of the composites. Particularly, the highest level of capillary absorption can be directly correlated to lowest value of *B* for the analyzed mixtures (and not with the OP). For example, MPCM mortars with high values of *B* are characterized by a low capillary permeability (even though they have a high OP). Figure 19

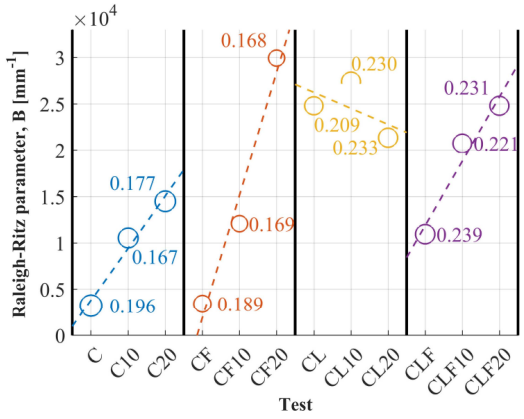

Fig. 19 Raleigh-Ritz parameter and open porosity for the twelve tested conditions

compares the Raleigh-Ritz parameter for each mixture. Moreover, the marker size reflects the relative magnitude of the OP for each specimen (also reported in Section 3.2). It is clearly seen how *B* increases with the MPCM contents, except for the case of perlite aggregates where the trend is not hold for the 20% MPCM scenario. Furthermore, a smaller dispersion is observed for the *B* values in this latter group (CL), suggesting a lower influence of the MPCM material in the permeability when perlite is incorporated as aggregate material.

4 Conclusions

This work aimed at investigating the effect of MPCMs mixed into several cement-based mortars on the capillary water absorption, which represents one of the main feature controlling the durability design of constructions and buildings made of MPCM-concrete materials.

The following main points can be highlighted:

- Experimental tests performed on 8 MPCM cement-lime mortars plus 4 reference ones (for a total of twelve mixtures), were outlined. These results were intended at investigating the effect of MPCM on several mortars produced with either short cellulose fibers, LWAs, and a combination of them. A total amount of 10% and 20% of MPCM by volume was added to the plain mixtures. Physical, mechanical and thermal characterization of the composites under discussion were summarized in this paper.
- A nonlinear FEM-based model, with material parameters depending on the water content and the local porosity, was employed for modelling the moisture diffusion phenomena and reproducing the experimental observations.
- The inverse calibration procedure demonstrated the model capability in identifying the Raleigh-Ritz pore size distribution parameter which represents a key variable for determining the permeability characteristics of a cementitious composite.
- These results provide relevant insights for understanding the effect of MPCM into the modification of the porosity structure of the material, which mainly affects the overall water absorption capillarity permeability.
- MPCM mortars with high values of the Raleigh-Ritz parameter exhibit a low capillary permeability performance. The inverse calibration allows to observe that when MPCM are added into the analyzed mortars there is an increase of the B value, in other words, MPCMs help to reduce the permeability of the composites.

Further developments are currently ongoing for better understanding other relevant aspects and coupling phenomena of MPCMs when added to cementitious mortars having LWAs and short cellulose fibers. Particularly a

multi/micro-scale framework is currently under development for investigating such phenomena by adopting lower scale effects of each one of the components of the mortars. This is a straightforward evolution of the presented work which was only limited to study the capillary diffusion mechanisms at the macroscale.

Acknowledgements

Dr. Caggiano wishes to acknowledge the Alexander von Humboldt-Foundation for funding his position at the WiB – TU Darmstadt under the research grant ITA-1185040-HFST-P (2CENERGY project).

References

Aligizaki K (2005). Pore Structure of Cement-Based Materials. London: CRC Press.

Banu D, Feldman D, Haghighat F, Paris J, Hawes D (1998). Energy-storing wallboard: Flammability tests. *Journal of Materials in Civil Engineering*, 10: 98–105.

Bary B, Sellier A (2004). Coupled moisture–carbon dioxide–calcium transfer model for carbonation of concrete. *Cement and Concrete Research*, 34: 1859–1872.

BASF (2013). BASF Datasheet. Micronal PCM DS 5040 X, 11/2013.

Caggiano A, Schicchi DS, Mankel C, Ukrainczyk N, Koenders EAB (2018). A mesoscale approach for modeling capillary water absorption and transport phenomena in cementitious materials. *Computers & Structures*, 200: 1–10.

Cui H, Memon SA, Liu R (2015). Development, mechanical properties and numerical simulation of macro encapsulated thermal energy storage concrete. *Energy and Buildings*, 96: 162–174.

de Freitas JAT, Cuong PT, Faria R (2017). Hybrid finite elements for nonlinear thermal and hygral problems. *Computers & Structures*, 182: 14–25.

Erlbeck L, Schreiner P, Schlachter K, Dörnhofer P, Fasel F, Methner FJ, Rädle M (2018). Adjustment of thermal behavior by changing the shape of PCM inclusions in concrete blocks. *Energy Conversion and Management*, 158: 256–265.

Guardia C, Barluenga G, Palomar I (2018). Thermal evaluation of cement-lime based materials with PCM. In: RILEM week 2018 Conference, TU-Delft, the Netherlands.

Halamickova P, Detwiler RJ, Bentz DP, Garboczi EJ (1995). Water permeability and chloride ion diffusion in portland cement mortars: Relationship to sand content and critical pore diameter. *Cement and Concrete Research*, 25: 790–802.

Hall C (2007). Anomalous diffusion in unsaturated flow: Fact or fiction? *Cement and Concrete Research*, 37: 378–385.

Herrero S, Mayor P, Hernández-Olivares F (2013). Influence of proportion and particle size gradation of rubber from end-of-life tires on mechanical, thermal and acoustic properties of plaster–rubber mortars. *Materials & Design*, 47: 633–642.

Hunger M, Entrop AG, Mandilaras I, Brouwers HJH, Founti M (2009). The behavior of self-compacting concrete containing micro-encapsulated Phase Change Materials. *Cement and Concrete Composites*, 31: 731–743.

Isgor OB, Razaqpur AG (2004). Finite element modeling of coupled heat transfer, moisture transport and carbonation processes in concrete structures. *Cement and Concrete Composites*, 26: 57–73.

Jeon J, Lee JH, Seo J, Jeong SG, Kim S (2013). Application of PCM thermal energy storage system to reduce building energy consumption. *Journal of Thermal Analysis and Calorimetry*, 111: 279–288.

Khudhair AM, Farid MM (2004). A review on energy conservation in building applications with thermal storage by latent heat using phase change materials. *Energy Conversion and Management*, 45: 263–275.

Kim HK, Jeon JH, Lee HK (2012). Workability, and mechanical, acoustic and thermal properties of lightweight aggregate concrete with a high volume of entrained air. *Construction and Building Materials*, 29: 193–200.

Lucas SS, Ferreira VM, de Aguiar JLB (2013). Latent heat storage in PCM containing mortars—Study of microstructural modifications. *Energy and Buildings*, 66: 724–731.

Maekawa K, Chaube R, Kishi T, (2014). Modelling of Concrete Performance: Hydration, Microstructure and Mass Transport. London: CRC Press.

Martín-Pérez B, Pantazopoulou SJ, Thomas MDA (2001). Numerical solution of mass transport equations in concrete structures. *Computers & Structures*, 79: 1251–1264.

Palomar I, Barluenga G (2018). A multiscale model for pervious lime-cement mortar with perlite and cellulose fibers. *Construction and Building Materials*, 160: 136–144.

Palomar I, Barluenga G, Puentes J (2015). Lime–cement mortars for coating with improved thermal and acoustic performance. *Construction and Building Materials*, 75: 306–314.

Pavlík Z, Fořt J, Pavlíková M, Pokorný J, Trník A, Černý R (2016). Modified lime-cement plasters with enhanced thermal and hygric storage capacity for moderation of interior climate. *Energy and Buildings*, 126: 113–127.

Sakulich AR, Bentz DP (2012). Increasing the service life of bridge decks by incorporating phase-change materials to reduce freeze-thaw cycles. *Journal of Materials in Civil Engineering*, 24: 1034–1042.

Samson E, Marchand J (2007). Modeling the transport of ions in unsaturated cement-based materials. *Computers & Structures*, 85: 1740–1756.

Schlangen E, Koenders EAB, van Breugel K (2007). Influence of internal dilation on the fracture behaviour of multi-phase materials. *Engineering Fracture Mechanics*, 74: 18–33.

Segura JM, Carol I (2004). On zero-thickness interface elements for diffusion problems. *International Journal for Numerical and Analytical Methods in Geomechanics*, 28: 947–962.

Shadnia R, Zhang L, Li P (2015). Experimental study of geopolymer mortar with incorporated PCM. *Construction and Building Materials*, 84: 95–102.

Shin KJ, Bae W, Choi SW, Son MW, Lee KM (2017). Parameters influencing water permeability coefficient of cracked concrete specimens. *Construction and Building Materials*, 151: 907–915.

Silva LM, Ribeiro RA, Labrincha JA, Ferreira VM (2010). Role of lightweight fillers on the properties of a mixed-binder mortar. *Cement and Concrete Composites*, 32: 19–24.

Soongswang P, Tia M, Bloomquist D (1991). Factors affecting the strength and permeability of concrete made with porous limestone. Materials Journal, 88: 400–406.

UNE EN (2000). UNE EN 197-1. Cement - Part 1: Composition, specifications and conformity criteria for common cements. AENOR.

UNE-EN (2003). UNE-EN 1015-18. Methods of test for mortar for masonry - Part 18: Determination of water absorption coefficient due to capillary action of hardened mortar, AENOR.

UNE-EN (2007a). UNE-EN 1015-1:1999/A1. Methods of test for mortar for masonry - Part 1: Determination of particle size distribution (by sieve analysis), AENOR.

UNE-EN (2007b). UNE-EN 1015-10:2000/A1. Methods of test for mortar for masonry - Part 10: Determination of dry bulk density of hardened mortar, AENOR.

UNE EN (2011). UNE EN 459-1. Building lime - Part 1: Definitions, specifications and conformity criteria. AENOR.

Wang L, Ueda T (2011). Mesoscale modeling of water penetration into concrete by capillary absorption. *Ocean Engineering*, 38: 519–528.

Warda BA, Munaz AN (2012). Effects of aggregate gradation on water permeability of concrete. *Advanced Materials Research*, 488–489: 248–252.

Weinläder H, Beck A, Fricke J (2005). PCM-facade-panel for daylighting and room heating. *Solar Energy*, 78: 177–186

Zhou J (2011). Performance of engineered cementitious composites for concrete repairs. PhD Thesis, Delft University of Technology, the Netherlands.

10.2. Publicaciones sobre la evaluación térmica con NDT (técnicas no destructivas) de morteros durante procesos de calentamiento y enfriamiento.

10.2.1 Thermal Evaluation of Cement-lime Based Materials with PCM

Guardia, C., Barluenga, G., & Palomar, I. (2018). *Thermal Evaluation of Cement-Lime Based Materials with PCM*. 4th International Conference on Service Life Design for Infrastructures (SLD4), RILEM PRO 125, RILEM Publications SARL Delft, Netherlands. E-ISBN: 978-2-35158-213-8

4th International Conference on Service Life Design for Infrastructures (SLD4) –
27-30 August 2018 – Delft, Netherlands

THERMAL EVALUATION OF CEMENT-LIME BASED MATERIALS WITH PCM

C. Guardia[(1)], G. Barluenga[(1)] and I. Palomar[(1)]

(1) University of Alcalá, Madrid, SPAIN

Abstract

Phase Change Materials (PCM) are characterized by their heat storage capacity and have arisen as an innovative opportunity for developing new energy efficiency building materials which can fulfil comfort and energy efficiency requirements satisfying nowadays thermal standards. This study investigates the influence of adding PCM to cement-lime based mortars on thermal properties. PCM cement-lime mortars were designed, using white cement, air lime, siliceous aggregate (0-4 mm), lightweight aggregate (LWA) (expanded perlite), short cellulose fibres and 10 and 20% of a PCM -microencapsulated paraffin wax. PCM's nominal melting temperature was 23 ± 1 °C. An experimental program was carried out to assess the thermal behaviour of 9 mixtures at different temperature conditions. DSC measurements were done to analyse the heat storage capacity of the mixtures. Besides, PCM-cement-lime plates were placed on a climatic chamber at two different temperature (15ºC and 30ºC) to produce the phase change from solid to liquid states of the PCM. Ultrasonic Pulse Velocity, heat flux and temperature differences between both sides of the plates were measured. Hardened properties of the mixtures were also evaluated. Some differences in the thermal behaviour of the samples, according to the amount of PCM were observed. The experimental results would allow to optimize the mixtures for specific building applications.

1. INTRODUCTION

Nowadays, there is an interest in the development of new mortars to improve energy efficiency of buildings. The main advantage of these materials is the ease of modifying their composition for their property optimization. The mixture of cement-lime as a basic composition is frequently used for these materials. To enhance the mixture's properties, other components such as fibres (cellulose or polypropylene fibres) and lightweight aggregates (for example expanded perlite) are included. Some authors have already pointed out the improvement on thermal and acoustic properties when fibres or lightweight aggregates were added [1, 2]. These mixtures were designed for building retrofitting of existing façades. This mortars can improve energy efficiency through thermal insulation, although the thermal inertia and heat storage capacity of façades is not usually considered. Phase Change Materials (PCM) have been used for designing new cement-lime mortars, because PCM can storage or release energy at a certain temperature (nominal melting point) while the material changes from liquid to solid state and vice versa (latent heat) [3]. PCM commonly used in construction are organic (for example, paraffin waxes) due to their chemical and thermal stability [4]. In addition, micro-encapsulation of those PCM is frequently used due to its facility to be mixed with inorganic binders [5]. These mixtures with PCM can be characterized applying different temperature conditions to analyse their behaviour both at liquid and solid states.

Differential Scanning Calorimetry (DSC) is the main technique used to analyse this materials in laboratory. DSC allows to measure the heat storage capacity of mixtures during

the phase change of the PCM [6]. However, DSC does not consider the time for changing from solid to liquid states and vice versa under specific climatic conditions. Besides this technique can be only used in the laboratory but not in the field. To overcome this limitations, heat flux plates and Ultrasonic Pulse (US) transducers (compressive and shear waves) are proposed for the analysis of this materials at a larger scale [7, 8]. Heat flux plates can detect the peak of heat flux due to their capacity of measure the heat flux between both sides of a cement-based material during temperature differences, and can be used to evaluate the energy consumption of a certain building envelope during a period of time [9]. US have already shown their effectiveness as non-destructive technique for the characterization of building materials [8]. Through the wave transmission (P- and S-waves) it is possible to detect the solid and pore structure of a material as well as their stiffness or elasticity [8]. Wave amplitude increase or decrease according to the difficulty of wave transmission through a liquid or solid material. Accordingly, US is proposed in this study as a NDT testing technique to detect the phase change of PCM in cement-lime mixtures.

This paper presents an experimental program on a PCM cement-lime mortar under specific climatic conditions. The aim of the study was to investigate new cement-lime mortars that could be used to improve the thermal behaviour of building façades through both thermal insulation and thermal inertia through the energy storage. Cellulose fibres and lightweight aggregates were used as well as microencapsulated paraffin wax (PCM). The effect of the PCM on hardened properties and thermal performance was assessed, measuring, physical and mechanical properties and thermal parameters of 9 cement-lime mixtures with PCM. Non-destructive testing techniques based on Heat Flux and Ultrasonic Pulse transmission were also used to analyse the behaviour of heat plates placed on a climatic chamber simulating different climatic conditions.

2. EXPERIMENTAL PROCEDURE

2.1 Materials and compositions

The components used in the study are listed below:

- A white cement type BLII/B-L 32.5N (UNE-EN 197-1) supplied by Cementos Portland Valderrivas.
- An air lime class CL90-S, according to the European standard (UNE-EN 459-1).
- A siliceous aggregate (0-4 mm).
- Short cellulose fibres of 1 mm length -Fibracel® BC-1000 (Ø20µm) – supplied by Omya Clariana S.L.
- A lightweight aggregate (LWA): expanded perlite (0-2 mm).
- A microencapsulated paraffin wax (Phase Change Material) with a particle size ca. 50-300µm and a melting point of ca. 23ºC – Micronal® DS 5040X supplied by BASF Construction Chemicals Company.

The compositions of the PCM cement-lime mortars are described in Table 1: A reference cement-lime mortar (C); a cement-lime mixture with the addition of 1.5% of the total fresh mortar's volume of short cellulose fibres (CF) and a cement-lime mortar with a 50%

replacement of the siliceous aggregate by expanded perlite (CL). Afterwards, 10% and 20% of PCM by volume was added to all mixtures (C_{10}, CF_{10}, CL_{10} and C_{20}, CF_{20}, CL_{20}). The binder to aggregate ratio was 1: 0.5: 4.5 (cement: lime: aggregate) by volume in all cases.

The mixing process had two stages: firstly, all the dry components, included fibres and PCM, were mixed and, then, water was added. The total mixing time did not exceed 5 min in any case. The water to binder ratio (w/b) was changed to get a plastic consistency and similar fresh workability for all the mixtures.

Table 1: PCM cement-lime mortars compositions (Components in Kg).

	C	**C_{10}**	**C_{20}**	**CF**	**CF_{10}**	**CF_{20}**	**CL**	**CL_{10}**	**CL_{20}**
BLII/B-L 32.5N	348	348	348	348	348	348	348	348	348
CL 90-S	55	55	55	55	55	55	55	55	55
Sand (0-4)	1403	1403	1403	1403	1403	1403	702	702	702
Cellulose fibres	-	-	-	0.40	0.62	0.66	-	-	-
Perlite*	-	-	-	-	-	-	94	94	94
PCM	-	42.3	84.6	-	42.3	84.6	-	42.3	84.6
Water**	220	140	200	220	180	240	240	240	250
w/b***	0.73	0.53	0.68	0.73	0.63	0.78	0.69	0.69	0.71
Consistency (mm)	178	170	166	160	173	170	195	173	170

Cement: Lime: Aggregates = 1: 0.5: 4.5 by volume.
** 50% of volume of the siliceous aggregate was replaced by perlite.*
*** Liquid water added. The amount of water included in the components (sand) was also taken into account. Sand 0–4: Humidity 5.3%. The water was adjusted to get a plastic consistency and similar workability for all the fresh samples.*

2.2 Experimental methods

2.2.1 Hardened properties

The characterization in the hardened state was done on 40 x 40 x 160 mm specimens. The samples were demoulded at 24h and cured until tested at 28 days (21± 3ºC and 95± 5% RH). A hydrostatic balance was used to calculate the bulk density and open (accessible to water) porosity (UNE-EN 1015-10). Regarding mechanical performance, compressive and flexural strength (UNE-EN 1015 -11:2000) were tested at 28 days.

2.2.2 Thermal properties

Thermal Conductivity (λ) was measured on 210 x 210 mm and 24 ± 2 mm thick plates in a thermally insulated box [10]. A heat source was placed inside the box and connected to a thermal regulator. On the inner and outer surface of the samples and inside and outside the box, temperature (ºC) and relative humidity (%) sensors were placed. Two temperature

conditions inside the box (25 and 40ºC) were considered and λ was calculated after a steady state was reached, to ensure the complete phase change of the PCM, either liquid or solid. The laboratory conditions were 20 ± 1ºC and 50 ± 5% RH during the test.

Differential Scanning Calorimetry (DSC) was used to determine the thermal properties of the cement-lime mixtures investigated. A Mettler Toledo DSC1 was used to do the measurements. In order to obtain the DSC samples, the cement-lime materials were softly milled by a pestle and introduced into the aluminium crucibles. Three samples were prepared and evaluated for each mixture under the IEA Task 42-Annex 29 [11]. The heating/cooling rate obtained for the present case was 1K/min. The minimum and maximum temperatures selected for the temperature program were 10 and 28ºC with isothermal segments of 5 min between each consecutive heating/cooling ramp.

2.2.3 Heat flux plate test setup (Climatic Chamber)

Figure 1 presents the experimental setup for the test. The door of a climatic chamber FDM-C140SX (0-70ºC temperature and 10-98% of relative humidity ranges) was replaced by a 50 mm expanded polystyrene (XPS) frame and 220 x 240 mm a mortar plate was placed in a central hole, completely covering the opening of a climatic chamber, to produce a unidimensional heat flux.

Two different temperatures inside the chamber, 15ºC and 30ºC, were tested. The relative humidity was 80% and 33% respectively to reduce the effect of mass transfer on the energy transport between both sides of the plates. The laboratory conditions remained constant at 20ºC and 60% RH.

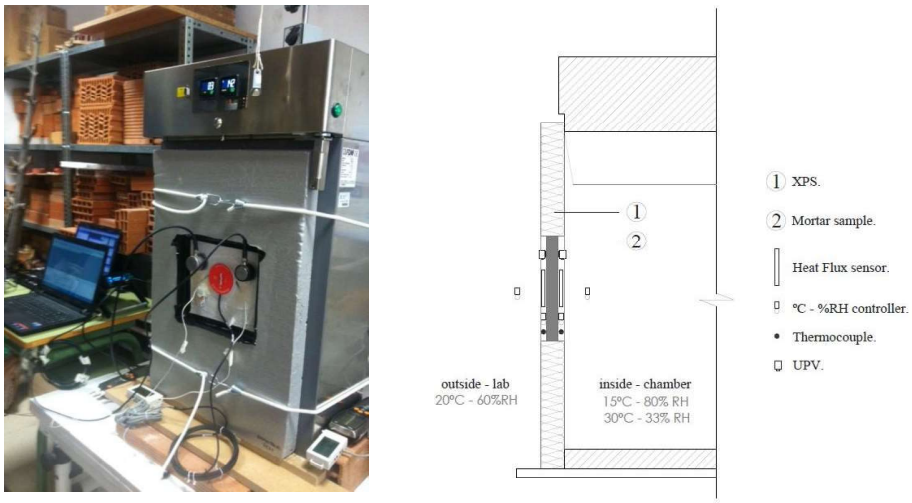

Figure 1. Experimental set up of the samples at different temperature conditions.

2.2.4 Laboratory characterization under different temperature scenarios

Heat flux sensors and temperature (ºC) and relative humidity (%) sensors were located on both sides of the mortars plates and extra temperature and relative humidity sensors were also placed in and outside the chamber to record the environmental conditions.

Ultrasonic Pulse propagation S-wave transducers (250 kHz) were also placed on the inner and outer surface of the plates as shown in Figure 1. Amplitude transmission values were calculated using the Hilbert transformation algorithm [12].

3. EXPERIMENTAL RESULTS AND ANALYSIS

3.1 Physical and mechanical characterization

Table 2 shows the values of the physical and mechanical characterization of the different PCM cement-lime mixtures.

Table 2: Physical and mechanical characterization of PCM cement-lime mortars under study.

		C	C_{10}	C_{20}	CF	CF_{10}	CF_{20}	CL	CL_{10}	CL_{20}
Phy. Prop.	Bulk density (Kg/m^3)	1900	1690	1600	1960	1720	1660	1430	1180	1270
	O.Porosity (%)	19.56	16.68	17.72	18.93	16.90	16.77	20.95	22.99	23.33
Mech. Prop.	Com. Str. (MPa)	13.7	7.7	7.3	10.3	6.7	6.0	9.3	5.3	6.0
	Flexural Str. (MPa)	3.36	2.26	2.40	3.18	2.24	1.79	2.66	1.98	2.20

It can be seen that bulk density decreased when PCM was added. The mixtures with the lowest bulk density values were those containing lightweight aggregates. The sample with the highest bulk density value was CF (1960 kg/ m^3) and the mixture with the lowest was CL_{10} with 1180 kg/m^3. On the other hand, open porosity (OP) presented a trend for C and CF mixtures as OP decreased with the addition of PCM. However for CL, CL_{10} and CL_{20}, the OP values increase. CL_{20} showed the highest value of OP (23.33%) and C_{10} presented the lowest with 16.68%.

Table 2 also summarizes the mechanical properties of the different PCM cement-lime mortars. Compressive strength varied between 5.3 MPa (CL_{10}) and 13.7 MPa (C). As expected, the addition of PCM reduced compressive strength [3, 13]. For the flexural strength the same trend can be observed, as PCM addition produced a decrease. Mixture C had the highest value (3.36 MPa) and CF_{20} the lowest (1.79 MPa). The main difference occurred when PCM was included, although the amount of PCM was not so significant.

3.2 Thermal characterization

PCM cement-lime mixtures were thermally characterized by measuring the thermal conductivity (λ) at two steady states corresponding to PCM in solid or liquid states [13]. The heat storage capacity of each mixture during the phase change (heating and cooling) was also measured by a Differential Scanning Calorimetry (DSC).

Table 3 reports thermal conductivity of the mixtures at different temperature scenarios (25° C and 40° C) where the PCM was either solid (λ_{25}) or liquid (λ_{40}). For the solid state it was ensured that the inner temperature of the sample was under 23ºC (the nominal melting point

of PCM) setting the insulated box at 25ºC. On the other hand, to achieve a liquid state of the PCM inside the sample (more than 23ºC), 40ºC was selected.

Table 3: Thermal conductivity (after reaching a steady state) at 25ºC and 40ºC.

	C	**C_{10}**	**C_{20}**	**CF**	**CF_{10}**	**CF_{20}**	**CL**	**CL_{10}**	**CL_{20}**
λ_{25} (W/mK)	0.23	0.26	0.20	0.29	0.40	0.30	0.17	0.27	0.29
λ_{40} (W/mK)	0.21	0.32	0.28	0.21	0.26	0.23	0.16	0.19	0.18

Table 3 shows that the mixture with the lowest value at λ_{25} was CL (0.17 W/mK) while CF_{10} showed the highest one (0.40 W/mK). At λ_{40} the values varied between 0.16W/mK (CL) and 0.32 W/mK (C_{10}). Generally speaking, λ_{40} showed lower values than λ_{25}, except for C_{10} and C_{20}. At both conditions, when 10% of PCM was added the thermal conductivity increased. On the other hand, λ decreased when 20% PCM was added when compared to 10% of PCM. At λ_{25}, it can be seen that the difference between adding 10% or 20% of PCM for the mixtures C and CF was larger than for CL. At λ_{40} the mixtures with lightweight aggregates showed lower thermal conductivity than mixtures without LWA.

Figure 2 records the heat storage capacity (stored energy) of mixtures C, C_{20}, CF_{20} and CL_{20}. The curves over the horizontal axis correspond to heating cycles and the curves under the temperature axis to the cooling cycles. Three samples of each mixture were measured showing high reproducibility.

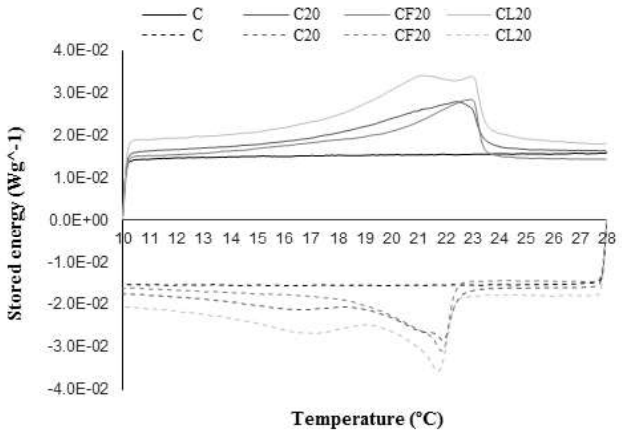

Figure 2: DSC measurements of the cement-lime mortars C and C_{20}, CF_{20} and CL_{20}.Heating and cooling cycles (1 K/min).

As expected, mixture C presented an almost horizontal line both for heating and cooling cycles, which corresponded to its lack of heat storage capacity. All the other mixtures showed heat storage capacity due to the addition of PCM [14]. The mixtures with PCM reached the melting point between 22 and 23ºC in the heating cycles and 21-22 ºC in the cooling cycles.

This difference agrees with data previously reported by other authors [6], where the melting point at the cooling cycles were around 1ºC lower than the melting point at heating cycles.

Mixtures C_{20} y CF_{20} showed a similar curve for both heating and cooling cycles, while CL_{20} showed a different behaviour for the heating cycle. The total heat storage of CL_{20} (heating and cooling cycle) was higher than the heat storage of C_{20} and CF_{20}. Besides, two different peaks can be seen in de CL_{20} heating curve, probably due to the moisture inside the pores of lightweight aggregates as this mixture showed the highest open porosity accessible to water (23.33%). On the other hand, all the PCM samples produced a two-peak curve for the cooling cycle, as expected according to other authors [15].

The different slope of the plot before and after the phase change of the PCM (10 and 28 ºC respectively) indicates that the sensible heat (specific heat) at 28ºC is lower than at 10ºC. This change could be related to the different thermal conductivity values observed at the steady state in the insulated box test.

3.3 Evaluation at different temperature conditions (heat flux plate test)

Figure 3 plots the heat flux and the surface temperature of C, C_{20}, CF_{20} and CL_{20} measured in- and outside the climatic chamber under different conditions.

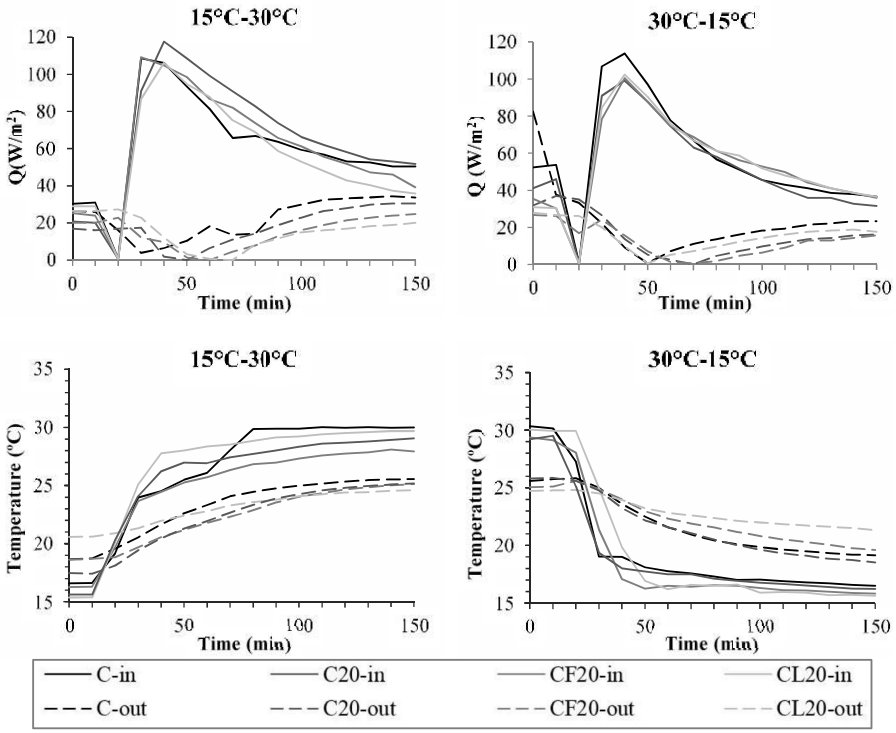

Figure 3: Heat flux and surface temperatures of the mixtures inside (-in) and outside (-out) the climatic chamber at different temperature conditions.

The test procedure of PCM melting can be followed by the temperature curves. Firstly, the samples were placed in the climatic chamber at 15ºC (Time = 0 minutes) until reaching a constant temperature and heat flux to ensure the solid state of the phase change material. After the steady state was reached (Time = 10 minutes), a temperature of 30ºC was programmed

inside the chamber to heat the sample. It can be seen that after 10 minutes from the steady-state point (Time = 20 minutes), all the heat flux values of the plate surface inside the chamber fell to zero. This point corresponded with the time when no temperature difference between both sides of the samples was measured (crossing point in the temperature plot). During this first period the outer heat fluxes values for all samples slightly decreased.

Subsequently, the heat flux through the inner surface of the plates reached the maximum values. The maximum heat flux depended on the different mixtures as Figure 3 indicates. Mixture C showed the maximum inner heat flux when the outer one fell to zero. At this point, the inner surface temperature was 23.8ºC and the outer surface temperature was 20.5ºC. As Figure 3 shows, this situation only happened for the reference mixture without PCM. When 20% PCM was added, the maximum heat flux values inside the chamber did not corresponded to the zero point of the outer heat flux values. As observed, the addition of PCM delayed the heat flux values passing through 0 over time. Consequently, the time to go through zero depended on the other components of the mixtures.

For cooling setup (PCM solidification), the climatic chamber was set at 30ºC to ensure a steady state of liquid PCM (Time = 0 minutes). Once the steady state was reached (Time = 10 minutes), a temperature of 15ºC inside the chamber was programmed to produce the phase change from liquid to solid. All the mixtures followed the same pattern described for the heating case. As the inner heat fluxes fell to zero, the temperature differences between both sides of the plates were zero. Then the maximum heat flux value was reached. For Mixture C (without PCM), the maximum value corresponded to the zero point of the outer heat flux sensor. However, as occurred in the phase change from solid to liquid, these two points did not match for the mixtures with PCM due to the delay for the outer zero point.

Ultrasonic Pulse Transmission (S- waves) measurements were recorded simultaneously to the heat flux measurements for the mixtures C, CF_{20} and CL_{20}. Figure 4 shows the Hilbert transformed s-waves transmitted through the mixtures at different temperatures.

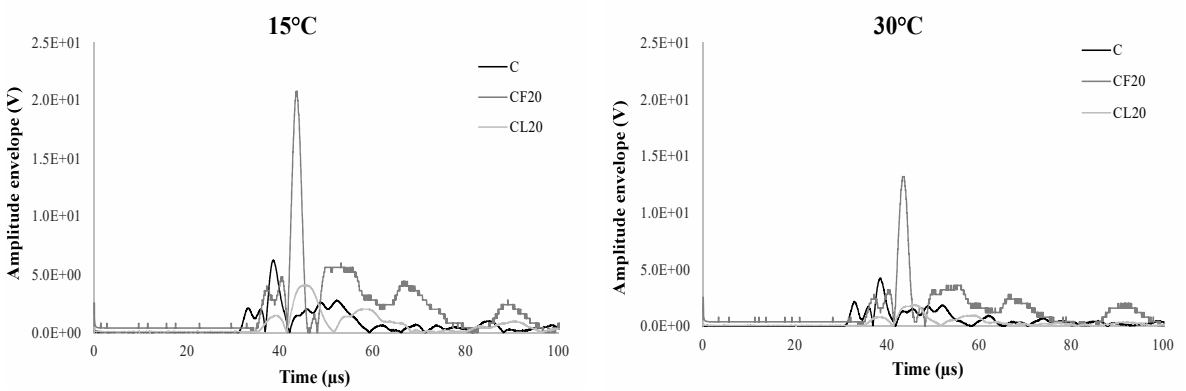

Figure 4: UPV measurements of the samples at different temperature conditions using Hilbert transform algorithm.

Amplitude differences between s-wave signals related to the different components of mixtures can be identified in Figure 4. As other authors already discovered, this behaviour is related to the composition and microstructure of the mixtures [8]. It can be observed that for

CL_{20} (with lightweight aggregates and 20% of PCM) s-waves were more attenuated than the rest. This behaviour can be associated with the larger open porosity of the mixture (23.33%). On the other hand, CF_{20} showed the highest maximum peak of the s-waves (Figure 4). It can be related to the microstructure produced by the cellulose fibres and their s-wave transmission capacity [8]. The same trend for both 15 and 30 ºC scenarios was observed.
The phase change of the PCM can be followed using transmitted US s-wave (15ºC - solid state- and 30ºC – liquid state-). At 15ºC the waves showed different peak points for each mixture when compared to 30ºC. At 30ºC, the peak value is remarkably lower than at 15ºC, which can be explained considering the physical state of the PCM, as it transmits s-waves better in a solid state than in a liquid state. Accordingly, the phase change of PCM can be detected with s-wave US transmission.

4. CONCLUSIONS

The effect of the addition of PCM to a cement-lime mortar with fibres and lightweight aggregates under different temperatures was evaluated. Hardened properties and thermal parameters (thermal conductivity, heat storage and heat flux) were measured. Ultrasonic Pulse Transmission (s-wave) was also evaluated. The main findings of the study can be summarized as:

- The cement-lime based mortars developed heat storage capacity with the addition of PCM.
- The addition of PCM influenced not only the thermal parameters but also the physical and mechanical properties of the cement-lime materials.
- Thermal conductivity, heat flux and s-wave ultrasonic transmission depended not only on the mixture components but also on the PCM state (liquid or solid).
- The thermal conductivity increased when the PCM was in a liquid state.
- The heat flux plate test identified the effect of PCM at different temperature conditions detecting the time it takes to the heat flux to pass through the materials.
- Ultrasonic Pulse Transmission (Non-Destructive Technique) identified not only the structure of the material but also the phase change of de PCM inside the mixture at different environmental conditions.

ACKNOWLEDGEMENTS

The authors acknowledge the assistance of Prof. C. Cid of UAH and Dr. G. Diarce of ENEDI, UPV/EHU. Some of the components were supplied by Cementos Portland Valderrivas, Omya Clariana S.L. and BASF Construction Chemicals España S.L.

REFERENCES

[1] Palomar, I.; Barluenga, G.; Puentes, J.; Lime-cement mortars for coating with improved thermal and acoustic performance. Construction and Building Materials, 2015, 75, 306-314, ISSN 0950-0618.

[2] Stefanidou, M.; Cement-based renders with insulating properties. Construction and Building Materials, 2014, 65, 427-431, ISSN 0950-0618.
[3] Lucas, S.S.; Ferreira; Barroso, J.L.; Latent heat storage in PCM containing mortars-Study of microstructural modifications. Energy and Buildings, 2013, 66, 724-731, ISSN 0378-7788.
[4] Cabeza, L.F.; Barreneche, C.; Castell, A.; de Garcia, A. et al.; Materials used as PCM in thermal energy storage in building: A review. Renewable and Sustainable Energy Reviews, 2011, 15, 3, 1675-1695, ISSN 1364-0321.
[5] Simen Edsjø Kalnæs, Bjørn Petter Jelle; Phase change materials and products for building applications: A state-of-the-art review and future research opportunities, Energy and Buildings, Volume 94, 2015, Pages 150-176, ISSN 0378-7788, https://doi.org/10.1016/j.enbuild.2015.02.023.
[6] Xing Jin, Xiaodong Xu, Xiaosong Zhang, Yonggao Yin; Determination of the PCM melting temperature range using DSC, Thermochimica Acta, Volume 595, 2014, Pages 17-21, ISSN 0040-6031, https://doi.org/10.1016/j.tca.2014.09.004
[7] Kyoung Ok Lee, Mario A. Medina, Erik Raith, Xiaoqin Sun; Assessing the integration of a thin phase change material (PCM) layer in a residential building wall for heat transfer reduction and management, Applied Energy, Volume 137, 2015, Pages 699-706, ISSN 0306-2619, https://doi.org/10.1016/j.apenergy.2014.09.003.
[8] I. Palomar, G. Barluenga; Assessment of lime-cement mortar microstructure and properties by P- and S- ultrasonic waves, Construction and Building Materials, Volume 139, 2017, Pages 334-341, ISSN 0950-0618,https://doi.org/10.1016/j.conbuildmat.2017.02.083.
[9] Denholm P, Ong S, Booten C.; Using utility load data to estimate demand for space. Denver, CO: Pub. No.: NREL/TP-6A20-5450.9, 2012.
[10] Herrero S, Mayor P, Hernández-Olivares F.; Influence of proportion and particle size gradation of rubber from end-of-life tires on mechanical, thermal and acoustic properties of paster-rubber mortars. Mater Des 2013;47:633–42.
[11] Gschwander, Stefan et al. (2015). ; Standardization of PCM Characterization via DSC. SHC 2015 International Conference on Solar Heating and Cooling for Buildings and Industry.
[12] Recep Birgül ; Hilbert transformation of waveforms to determine shear wave velocity in concrete, Cement and Concrete Research, Volume 39, Issue 8, 2009, Pages 696-700, ISSN 0008-8846, https://doi.org/10.1016/j.cemconres.2009.05.003.
[13] Pavlík, Z. ; Fořt, J. ; Pavlíková, M. et al. ; Modified lime-cement plasters with enhanced thermal and hygric storage capacity for moderation of interior climate, Energy and Buildings, 2016, 126, 113-127, ISSN 0378-7788.
[14] Amitha Jayalath, Rackel San Nicolas, Massoud Sofi, et al.; Properties of cementitious mortar and concrete containing micro-encapsulated phase change materials, Construction and Building Materials, Volume 120, 2016, Pages 408-417, ISSN 0950-0618, https://doi.org/10.1016/j.conbuildmat.2016.05.116.
[15] Lu Li, Hang Yu, Xu Wang, Shiling Zheng; Thermal analysis of melting and freezing processes of phase change materials (PCMs) based on dynamic DSC test, Energy and Buildings, Volume 130, 2016, Pages 388-396, ISSN 0378-7788, https://doi.org/10.1016/j.enbuild.2016.08.058.

10.2.2 Novel thermal characterization with Non-destructive techniques of PCM cement-lime mortars with lightweight aggregates and cellulose fibers.

Guardia, C., Barluenga, G., & Palomar, I. *Novel thermal characterization with Non-destructive techniques of PCM cement-lime mortars with lightweight aggregates and cellulose fibers.* Artículo enviado para próxima publicación.

Novel thermal characterization with NDT of PCM cement-lime mortars with lightweight aggregate and cellulose fibers.

Cynthia Guardia[a*], Gonzalo Barluenga[a], Irene Palomar[a]

[a]Department of Architecture, University of Alcala, Madrid-28801 (Spain)

Abstract

Nowadays, there is an interest in development of new mortars to improve energy efficiency of buildings through retrofitting of façades. The mixture of microencapsulated Phase Change Materials (paraffin wax) with cement-lime and the addition of cellulose fibres and lightweight aggregates (LWA) are presented as a solution for this purpose. This study evaluates the thermal performance of 5 different cement-lime mortars with 20% of PCM and the addition of cellulose fibres and LWA (perlite) under different climatic conditions. A sample plate for each mortar was placed in a climatic chamber where heating and cooling cycles were set up. Non-destructive techniques, such as temperature and humidity sensors, Ultrasonic Pulse Velocity transducers and heat flux plates were used in order to evaluate (in- and outside the chamber) the thermal performance of the mortars. Different attenuation coefficients for each mixture were analysed and the PCM states (liquid, liquid-solid, solid) at different temperature conditions were identified. Heat flux differences during heating and cooling cycles between both sides of the plates (in and out) were also evaluated. Due to the heat flux and temperatures results, enthalpies of the mixtures were also analysed. Mixtures with LWA and PCM showed the best thermal performance achieving higher heat storage capacity than mortars with fibres or the combination of both additions.

Keywords

Phase Change Materials (PCM); cement-lime mortars; experimental characterization; Ultrasonic testing; Heat Flux; Different climatic conditions.

Highlights

- Five cement-lime mortars with PCM, Lightweight aggregates and cellulose fibres were characterized under different climatic conditions.
- Climatic chamber set-up for the simulation of different climatic conditions.

- Ultrasonic wave transmission (NDT) detected the phase change of PCM inside cement-lime mortars.
- UPV as a technique for the PCM durability control.
- The combination of PCM and LWA increased the enthalpy of the mortar.

1. Introduction

Phase Change Materials (PCM) are proposed as a solution for the improvement of energy efficiency of buildings **[1-3]** The main characteristic of these materials is their phase change capacity at a certain temperature. During phase change, the material absorbs or release heat while temperature remains constant (latent heat), acting as a heat storage **[4,5].** Organic PCM, such as microencapsulated paraffin wax, are the most PCM used in construction, due to their high adaptability, commercial availability and competitive price **[6].** Some authors have already studied the thermal behaviour of PCM inside cement-based mortars with addition of other components (fibres and Lightweight aggregates LWA) **[7-12]**. These studies pointed out that the PCM behaviour changed depending on the mixture where it was included.

For mortars characterization different techniques (destructive and non-destructive) can be used **[9, 13, 14].** Ultrasonic pulse transmission is a powerful non-destructive technique tool for construction and building materials indirect characterization **[14-17]** With Ultrasonic pulse transmission tool some mechanical parameters and pore microstructure of the materials at different states can be analysed. Additionally, US is affected by the ultrasonic frequency. The raw US signal attenuation has also been used for cement mortar and concrete samples characterization **[15,17].** With the attenuation coefficients the US energy absorbed by cement-based materials can be evaluated **[15, 16]**. This technique can be used both in the lab and in on-site applications.

On the other hand, several techniques can be used for thermal performance of mortars (for example, insulated box for thermal conductivity measurements) **[9, 13, 18].** However, when PCM is added, the use of a Differential Scanning Calorimetry (DSC) for measuring the latent heat (enthalpy) of the material is used **[4, 6, 8, 9].**

However, this test is not enough for the thermal characterization when mortars with PCM are under different environmental conditions because temperature development is not the same over a certain time. For this purpose, the measurement of heat flux is needed. For heat flux measurements, Heat flux plates can be used **[19, 20]**. They can measure

the total amount of heat that is able to pass through a material with a determined thickness.

The aim of this study is to evaluate five different cement-lime mortars with PCM and different additions such as cellulose fibres and lightweight aggregates under different climatic conditions. Temperature and humidity sensors, Ultrasonic Plus transducers (at 250kHz frequency) and heat flux plates were placed on mortars samples in a climatic chamber set-up (Figure 2). Heating and a cooling cycles inside the chamber were set-up and the thermal performance of the different mortars was evaluated.

2. Materials and Experimental methods

Five different cement-lime mortars were studied. Figure 1 shows the composition design criteria followed using a reference cement-lime mortar and the combination of the referent mortar with fibers (F), lightweight aggregates (LWA) and 20% fresh mortar volume of PCM. On one hand, the experimental program assessed the physical, mechanical and thermal hardened properties of the five cement-lime mortars. On the other hand, a climatic chamber was used in order to evaluate simultaneously the development of average temperature, ultrasonic pulse propagation and heat flux difference between in and outside the chamber, at different temperature conditions.

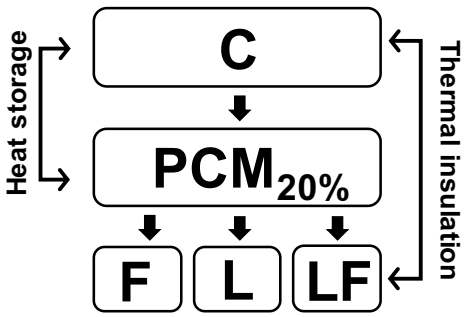

Figure 1. Composition design of the 5 PCM cement-lime mortars under study.

2.1 Materials and mixtures compositions

The five different cement-lime mortars were prepared using the components listed below:

- A white cement type BLII/B-L 32.5N (UNE-EN 197-1) supplied by Cementos Portland Valderrivas.

- An air lime class CL90-S designated according to the European standard (UNE-EN 459-1).
- A normal weight siliceous aggregate (0-4mm).
- A lightweight aggregate (LWA): expanded perlite (L).
- Short cellulose fibres (F) of 1mm length - Fibracel® BC-1000 (Ø 20μm)- supplied by Omya Clariana S.L.
- A microencapsulated paraffin wax (Phase Change Material PCM) with a particle size ca. 50-300μm, bulk density ca. 300-400 kg/m^3 and a melting point of ca. 23º C ± 1 – Micronal® DS 5040X- supplied by BASF Construction Chemicals Company.

Table 1 summarizes the compositions of the five mortars evaluated in this study.

Table 1
Compositions of PCM lime-cement mortars (components in kg).

	Cement	CL 90-S	Sand (0-4)	Fibres	Perlite (A)	PCM	Water (B)	w/b (C)	D_{dry} (kg/m^3)	D_{wet} (kg/m^3)
C	348	55	1403	-	-	-	220	0.73	1400	2264
C_{20}	348	55	1403	-	-	84.6	200	0.68	1357	1937
CF_{20}	348	55	1403	0.66	-	84.6	240	0.78	1440	1885
CL_{20}	348	55	702	-	94	84.6	250	0.71	868	1562
CLF_{20}	348	55	702	0.59	94	84.6	380	0.79	-	1561

Cement: Lime: Aggregates = 1: 0.5: 4.5 by volume.
A) 50% of volume of the siliceous aggregate was replaced by perlite.
B) Liquid water added. The amount of water included in the components (sand) was also taken into account. Sand 0–4: Humidity 5.3%. The water was adjusted to get a plastic consistency and similar workability for all the fresh samples.
C) 50% of volume of the siliceous aggregate was replaced by perlite. Liquid water added. The amount of water included in the components (sand) was also taken into account. Sand 0–4: Humidity 5.3%.

A reference cement-lime mortar with a binder to aggregate ratio by volume of 1: 0.5: 4.5 (cement: lime: aggregate) was designed. Then, 20% by fresh mortar volume of PCM was added. Afterwards, 1.5% of the total fresh mortar's volume (considering the reference components) of dry cellulose fibres were added (CF_{20}) 50% of the siliceous aggregate was replaced by perlite (CL_{20}). Finally, a mixture was made adding both fibres (considering both the reference components and the LWA) and perlite (CLF_{20}). Water to binder ratio (w/b) was adjusted to get a plastic consistency and a similar fresh workability for all the mixtures. The consistency was selected due to the adaptability for façade renderings. According to UNE-EN 998-1, the target minimum compressive strength value was 3.5MPa, corresponding to a CS-III grade rendering mortar. The mixing process had two stages: firstly, all the dry components, included fibres, LWA and PCM

were mixed and water was added afterwards. The total mixing process did not exceed 5 minutes in any case.

2.2 Mortars properties testing procedures

The five different mixtures were characterised in the fresh and hardened state. The fresh mortar consistency was measured using the flow table test, according to the European standard UNE-EN 1015-3:2000.

Several physical and mechanical parameters were characterised on 40x40x160mm specimens, according to the European standard (UNE-EN 101-11). For thermal characterization, 210mm x 210mm and 24 ± 2mm thick plate samples were used. The samples were demoulded at 24h and cured until tested at 28 days.

The experimental set-up and test procedures have been previously published **[9].** Geometrical density (D_g) of the sample plates was calculated using the plates weight divided by the area of each mixture. Open (accessible to water) porosity (OP) was calculated complying with UNE-EN 101-10. Water vapour diffusion resistance factor (VD) was determined by wet-up method containing a saturated saline dissolution (75% RH) and using cylindrical specimens with 35mm diameter and 40± 2mm thick (UNE-EN 1015-19). Compressive and flexural strength were tested according to UNE-EN 1015-11:2000 at 28 days in standard specimens. Thermal conductivities (λ_S, λ_L) and Differential Scanning Calorimetry (DSC) were calculated according to the methods previously described **[9].** A thermally insulated box for the measurement of thermal conductivities at liquid and solid PCM steady state was used. 210 x 210 mm and 24±2mm thick plate samples for each mixture were tested. Temperature and relative humidity were monitored with sensors placed at the inner and outer surface of the sample and inside and outside the box. Thermal conductivity (λ_S, λ_L) was calculated according to Fourier's Law **[9, 13, 18].**

DSC measurements were performed following the standardized PCM characterization procedure developed under the IEA Task 42- Annex 29 **[21, 22].** The selected temperatures were 10ºC and 28ºC with isothermal segments of 5 minutes between each consecutive heating and cooling ramp. 1k/min was the heating and cooling rate obtained for this case.

Figure 2 presents the experimental set-up for the climatic chamber test. A climatic chamber, FDM C140SX (0-70ºC temperature and 10-98% of relative humidity ranges) was used. The door of the chamber was replaced by a 50mm expanded polystyrene (XPS) frame completely covering the opening of the climatic chamber door to produces a unidimensional heat flux. The different mortars plates (210mm x 210mm x 24±2 mm

thickness) were replaced in a central hole (Figure 2) in the middle of the XPS frame. Several temperature (ºC) and relative humidity (%) sensors were located on both sides of the mortar plates.

In order to record the environmental conditions, extra temperature and relative humidity sensors were placed in- and outside the climatic chamber.

Two different temperatures inside the chamber, 15ºC and 30ºC, were tested. The relative humidity was 80% and 33% respectively to reduce the effect of mass transfer on the energy transport between both sides of the plates. The laboratory conditions remained constant at 20ºC and 60%RH.

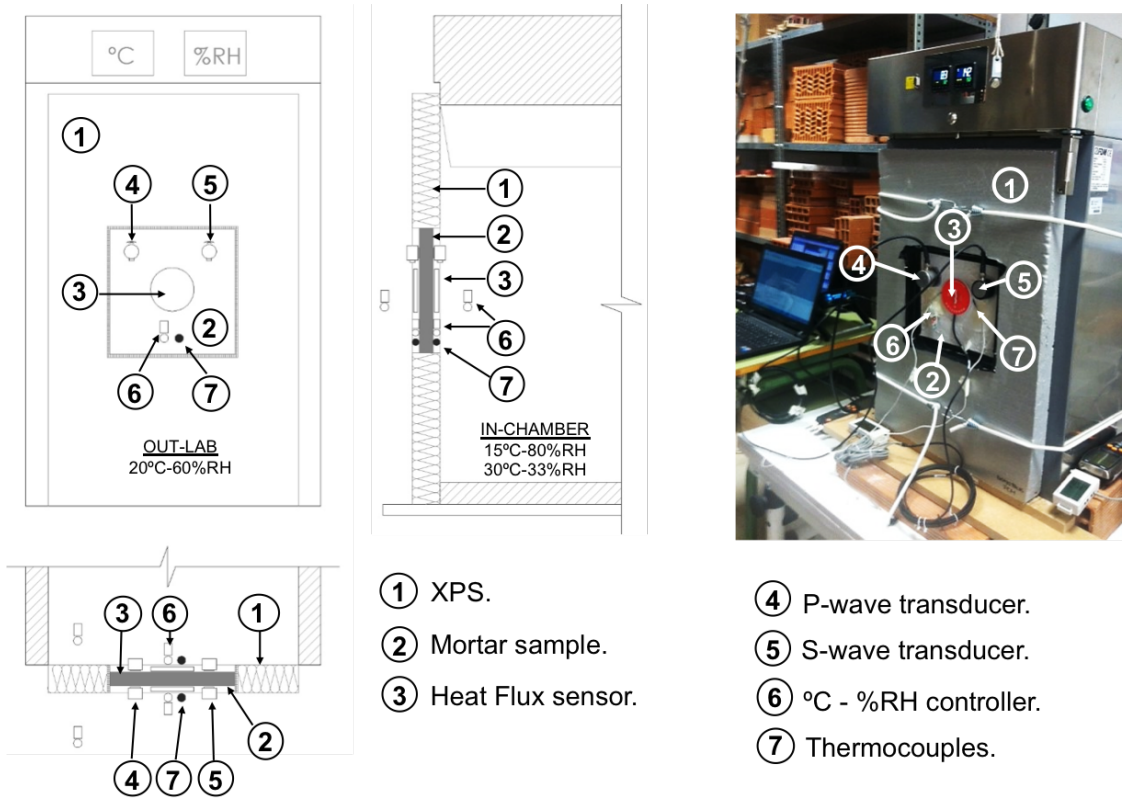

Figure 2. Climatic Chamber set up for monitoring the samples at different temperature conditions.

Ultrasonic Pulse Propagation transducers (P-waves 54kHz and S-waves 250kHz) were also placed on the inner and outer surface of the plates as shown in Figure 2. The signal was recorded in computer with an oscilloscope connected to the US device.

The attenuation coefficients (AT_{PCM} in dB/mm), for liquid PCM state (AT_L), liquid-solid PCM state (AT_{L-S}) and solid PCM state (AT_S) were determined considering the amplitude (A_m) of the raw US signal in Volts trough the samples and calculated according to Eq. **[16]**:

$$AT_{PCM} = -(20/x)(\log(A_m/A_T)) \quad \textit{(Eq. 1)}$$

where AT is the amplitude measured when both transducers (transmitter and reciver) were placed face and x is the distance between them in a specific specimen (24±2mm). This approach points out that the larger the attenuation coefficient AT_{PCM}, the higher the US energy absorbed by the sample.

Two heat flux sensors were also placed in the middle of both sides of the mixtures samples to evaluate the heat flux at any time during the test at a certain temperature. The enthalpies of the sample's plates were calculated according to:

$$\emptyset_T = \emptyset_{in} - \emptyset_{out} \quad \textit{(Eq. 2)}$$

$$\emptyset_Q = \int_{T0}^{Tf} \emptyset_T \, dT \quad \textit{(Eq. 3)}$$

$$H = \left[\emptyset_Q/(D_G \, e)\right]1000 \quad \textit{(Eq. 4)}$$

Where $\emptyset_T$,in W/m^2, was the heat flux differences between in and outside the climatic chamber. $\emptyset_{in}$ and $\emptyset_{out}$ are the heat fluxes registered on the surface sample plates in- and outside the climatic chamber respectively. $\emptyset_Q$ (Jm^2) was the heat flux summatory related to the sample average temperature. Finally, *H* is the enthalpy of the mortar in MJ/g obtained from Eq.3 where D_G (kg/m^3) is the geometrical density of the plates (weight per volume) and *e* was the sample plates thickness represented in mm. In all cases, before the measurements began, constant temperatures and relative humidity (RH) conditions were set in the chamber. It was waited until all the plates reached an average temperature steady state. Thus, it was ensured that the initial point was the same for all the mixtures.

3. Experimental results

3.1 Hardened state

Table 2 summarizes the results obtained of physical, mechanical and thermal properties of the 5 different cement-lime mortars under study. Some correlations among the compositions parameters and properties have been described and discussed in a previous work **[9].**

Table 2 presents D_g of the mortar plates used for this study. As expected, C (mixture without PCM) presents the highest D_g value (2376 kg/m^3), while CLF20 showed the lowest, 1432 kg/m^3. Open porosity (OP) values varied between 16.77% and 23.33%.

CF_{20} presented the lowest value of Open Porosity, while CLF_{20} showed the highest one. Water vapour diffusion resistance factor (VD) varied between 3.26 (CLF_{20}) and 4.29 (C_{20}). Table 2 also reports the compressive (CS) and flexural (FS) strength results. The lowest CS value was obtained for CLF_{20} (5.33MPa), while C showed the highest one (14.33MPa). Accordingly, all the mixtures reached the target minimum compressive strength value of 3.5Mpa, which corresponds to a CS-III grade rendering mortar, according to UNE-EN 998-1. Flexural strength varied between 1.79MPa (CL_{20}) and 3.36 MPa (C). Table 2 shows thermal conductivities for solid PCM (λ_S) and liquid PCM (λ_L) calculated after the samples reached a thermally steady state. λ_S values varied between 0.20 W/mK (C_{20}) and 0.30 W/mK (CF_{20}) and λ_L varied between 0.15 W/mK (CLF_{20}) and 0.28 W/mK (C_{20}). Therefore, only sensible heat of the material was taken into account, but not the latent heat (enthalpy), which was analysed with other experimental setups (DSC and Climatic Chamber set-up).

Table 2
Physical, mechanical and thermal properties of PCM cement-lime mortars.

	Workability	**Physical properties**			**Mechanical properties**		**Thermal properties**	
	Consistency mm	D_g* kg/m^3	OP %	VD -	CS MPa	FS MPa	λ_S W/mK	λ_L W/mK
C	178	2376	19.56	4.13	14.33	3.36	0.23	0.21
C_{20}	166	1924	17.72	4.29	7.17	2.40	0.20	0.28
CF_{20}	170	2091	16.77	3.47	5.83	2.20	0.30	0.23
CL_{20}	170	1541	23.33	3.62	6.0	1.79	0.29	0.18
CLF_{20}	170	1432	23.09	3.26	5.33	2.16	0.23	0.15

**Geometrical Density obtained according to weight of plate samples divided by samples volume (kg/m^3)*

3.2 Identification of PCM states using UPV at different temperature conditions.

Figure 3 presents the paraffin wax solidification process inside a PCM microcapsule and the obtained s-wave signal at 250kHz frequency during a cooling cycle of C_{20}. This process has been already explained in a previously work **[9].** Firstly, the liquid paraffin filled the whole capsule (T<23ºC). Then, temperature began to drop, and the phase change of the paraffin occurred (liquid-solid). Finally, as the temperature dropped under 23ºC all the paraffin was a solid state.

These three PCM states were recognized with the climatic chamber set up using UPV technique. In all cases, similar wave arrival pattern was observed. 10x gain was set up at the oscilloscope in order to obtain the signal clearly. All the signals showed the

maximal voltage peak value at 18μm, although the peak values were different. Figure 3a) presents the wave signal when the average temperature of the sample was over 23ºC (liquid PCM). At liquid state the maximum voltage peak achieved 10V. Afterwards, the temperature decreased (T≥23ºC) corresponding with the PCM phase change (Figure 3b)). The s-wave presented an increased maximum voltage peak, 35V. Finally, as the temperature decreased under 23ºC (PCM in a solid state), the us signal presented the lowest attenuation in comparison with the other signals (Figure 3c)). The maximum peak of V was 70V. It can be observed that although the arrival time (μm) was the same for all PCM states, the waves amplitudes were different, depending on the PCM state. When PCM was in a liquid state, the transmitted s-wave was attenuated regarding to the s-wave received when PCM was in a solid state.

Consequently, when PCM was in a liquid state, the signal transmission was softer than the one for solid state. It can be said that with UPV, was possible to recognize the PCM state although it was inside a cement-lime mixture. Therefore, this technique not only allows to check if PCM is changing its phase, but it can be used as a control non-destructive technique to check the durability of PCM inside the mortar after a certain time.

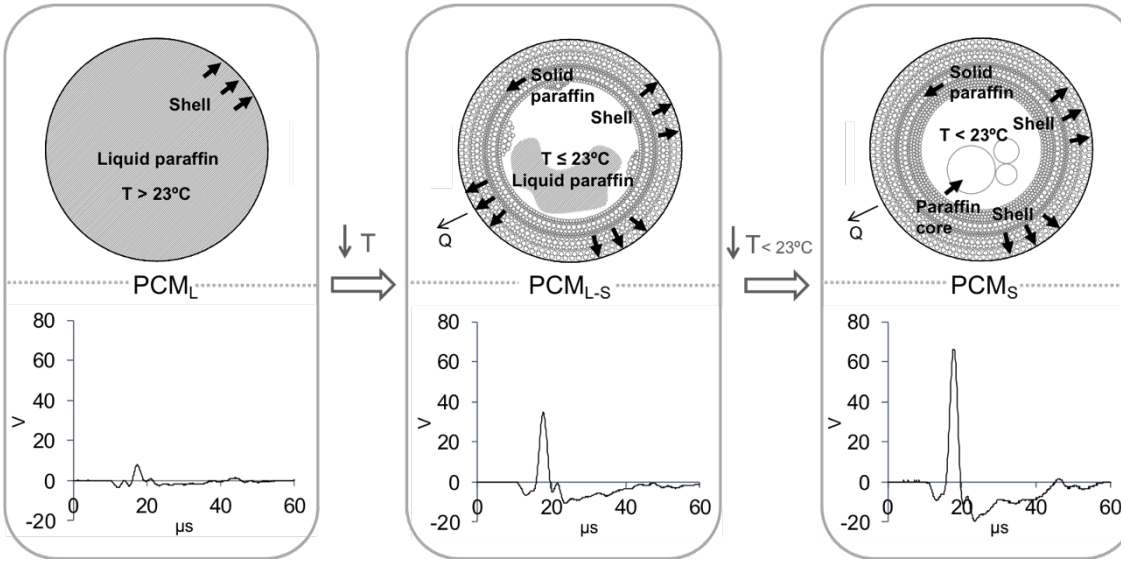

Figure 3. (a) A PCM microcapsule and US signal at liquid state (T>23ºC) of C_{20}. (b) A PCM microcapsule and US signal at liquid/solid state (T≥23ºC) of C_{20}. (c) A PCM microcapsule and US signal at solid state (T<23ºC) of C_{20}.

3.3 Attenuation coefficients depending on the PCM state.

Table 3 presents the attenuation coefficients obtained after using Eq.1. As expected, the mixture without PCM (C) showed a linear trend close to 1 dB/mm for all temperatures. AT_L showed a coefficient of 0.99 dB/mm while AT_S was 0.86 dB/mm. This slightly variation can be assumed as the relative humidity content inside the pore microstructure of the material. As water evaporates, pores were released, and US presented difficult wave transmission. However, when PCM was added AT_{PCM} values varied depending not only on PCM states but on the components of the mortars. When PCM was in liquid state (T>23ºC), AT_L values varied between 1.33 dB/mm (CL_{20}) and 0.57 dB/mm (CF_{20}). As temperature decreased (T≥23ºC), phase change began and AT_{PCM} decreased (US absorption decreased). CL_{20} showed the highest AT_{L-S} value (1.13 dB/mm) while C_{20} presented the lowest one (0.30 dB/mm). Finally, temperature decreased until PCM was completely in solid state (AT_S).

AT_S values decreased regarding to AT_{L-S} values. CL_{20} presented the highest value (1.05 dB/mm) and C_{20} the lowest one (0.05 dB/mm).

Table 3
Attenuation coefficients (dB/mm) for 250 kHz frequencies at different PCM states

	C	**C_{20}**	**CF_{20}**	**CL_{20}**	**CLF_{20}**
Liquid (T> 23ºC)	0.99	0.84	0.57	1.33	1.29
Liquid-solid (T≤ 23ºC)	0.92	0.30	0.46	1.13	1.02
Solid (T< 23ºC)	0.86	0.05	0.42	1.05	0.96

3.4 Heat Flux DSC

The enthalpy for the 5 mixtures under study during heating and cooling cycles measured with Differential Scanning Calorimetry are presented in Figure 4. A temperature interval between 10ºC and 28ºC was configured. During the heating cycle, enthalpy increased with temperature while decreased in cooling cycles. As expected, C, the mixture without PCM, showed a linear enthalpy increase with temperature. Besides, figure 4 shows enthalpy behaviour of the different mixtures with 20% of PCM. The addition of PCM showed slight differences between heating and cooling cycles. It can be seen an inflection point of the curve. This point appeared for each mixture with PCM. This point corresponded to the melting point of the PCM, located at 23ºC for heating cycles and at

22ºC for cooling cycles **[9].** It was observed that all the mixtures showed different enthalpy values depending on the mortar composition. As can be seen, C (without PCM) presented the lowest enthalpy value (15J/g) for 28ºC. Regarding to the mixtures with PCM, the mixtures with cellulose fibres (CF_{20} and CLF_{20}) showed a similar enthalpy value at 28ºC, 20 J/g. C_{20} presented an enthalpy value somewhat above 20 degrees. Finally, CL_{20} was the mixture with the highest enthalpy value at 28ºC, reaching 25J/g. As concluded in a preciously work (REF CBM), the enthalpy of the mixtures depends not only on PCM but also on the other components added to mixtures. Mixtures with LWA showed higher enthalpy than mixtures without LWA or with the addition of fibres.

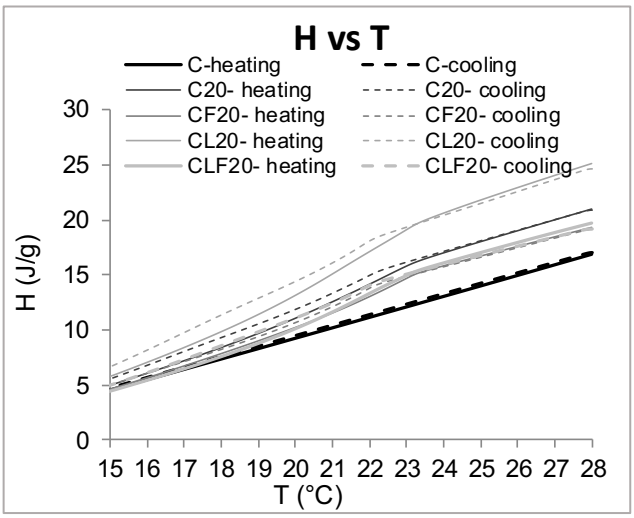

Figure 4. Cement-lime mortars enthalpy measured in DSC during heating and cooling cycles.

3.5 Average sample temperatures and heat flux differences between in- and outside the climatic chamber at different temperature conditions.

Figure 5. plots the average temperature and heat flux differences between inner and outer sample sides of the five different mortars under study during heating and cooling processes. In all cases, the same test procedure was followed. In order to ensure a liquid or solid PCM steady state, a constant temperature and heat flux were reached. For all the heating cycles the climatic chamber was set at 15ºC (time= 0s). After the steady state was reached (time= 600s), a temperature of 30ºC was programmed inside the chamber to heat the sample. For the cooling cycle (PCM solidification), the climatic chamber was set at 30ºC to ensured steady state of liquid PCM (Time = 0 seconds). Once the steady state was reached (time= 600 s), a temperature of 15ºC inside the chamber was programmed to produce the phase change from liquid to solid.

Figure 5a and figure 5b show the average temperature between inner and outer sides of the plate samples related to time of the heating and cooling cycles. Figure 5a shows that C, mixture without PCM, presented a different behaviour comparing with the other mixtures (all with PCM). During the first 3600 seconds, C average temperature was lower than the other temperatures. It took longer to achieve the PCM melting temperature (23ºC). On the other hand, Figure 5a shows that C_{20}, CL_{20} and CLF_{20} reached 23ºC between 2400s and 1800s. For CF_{20} lasted 3000 seconds to achieve the PCM melting temperature. This behaviour can be related to the density of the mixtures (Table 2). C was the mixture with the highest value of D_G (2376 kg/m^3). As expected, the higher D_G was, the longer took the temperature to pass through the material. Once 23ºC was reached, the increase of the average temperature was softer until a steady state at 27ºC was reached. It can be seen that C and CF_{20} showed an average temperature 0.5ºC lower than the other mixtures.

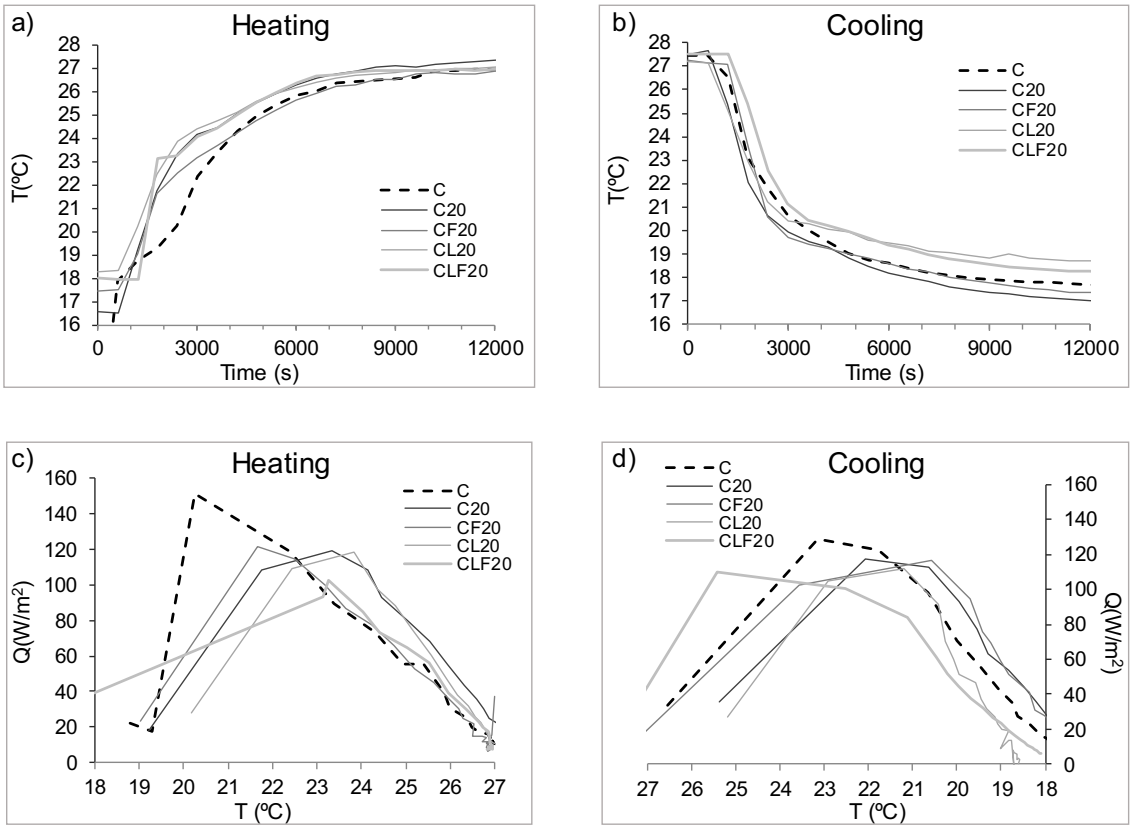

Figure 5. a) and b): samples average temperature during heating and cooling cycles. C) and d): Heat flux differences related to an average temperature during heating at cooling cycles.

In Figure 5b can be observed two behaviours depending on the mixture composition (with or without LWA). The development of the temperatures was similar, C, C_{20}, CF_{20}

and CL_{20} reached 21ºC (melting temperature of PCM for solidification [9]) after 2200-2400 seconds. CLF_{20} reached the melting temperature at 3000s. 4200 seconds after the test began, CL_{20} and CLF_{20} (mixtures with LWA) showed an average temperature 1ºC higher than the other mixtures under study. In this case, LWA worked as thermal insulator and did not allow the heat passing though the mixtures samples. At the end of the test, C_{20} presented the lowest temperature (17ºC), 2ºC below CL_{20}, the mixture with the highest temperature (19ºC). In all cases, the average temperature was under the melting temperature of PCM (21ºC) ensuring the solid state of the PCM. Figures 5c and 5d present the heat flux difference between in- and outside the climatic chamber, related to the average temperature (showed in Fig. 5a and 5b) at different temperature conditions. In both cases (heating and cooling cycles), a similar behaviour was observed. It can be differentiating two development stages: Firstly, an increase of the heat flux until maximum peak was reached and afterwards a decrease until 0 W/m^2 were reached (steady state). These maximum peaks, which corresponded with the heat flux inflection point, were related with the temperature in- and outside the different mixtures. Figure 5c showa the heat flux differences between in- and outside plates surfaces related to the average sample temperatures during heating process (Eq.2). C showed the highest maximum peak of heat flux (151.41 W/m^2) at 20ºC, while CLF20 (102.95 W/m^2 at 23ºC) presented the lowest. It can be assumed that C was the mixture with the highest on because of its high density regarding to the other mortars' density. It can be observed that C showed a different behaviour than the other mixtures with 20% of PCM. C heat flux measurements achieved lineally the maximum peak, then, it began to fell down until steady state was reached (approaching 0 W/m^2). In this case, only the sensible heat affected the mixture. However, mixtures with PCM showed a different behaviour. All mixtures began with the heat flux measurements between 19ºC and 20ºC. Afterwards the heat flux began to rise up to a maximum peak (sensible heat). Once the maximum peak was reached, instead falling down, the heat flux value stayed constant. This trend kept constant during 2ºC, specifically between 22ºC and 24ºC, which corresponds with the melting temperature of the PCM (latent heat). After this temperature was achieved, the heat fluxes began to fall down until a steady state was reached (27ºC-30ºC). Figure 5d presents the heat flux differences between in and out plates surfaces, related to the average temperature during the cooling process. A similar trend as the on presented, during heating process was showed. C was the mixture with the highest maximum peak (130.00 W/m2), reached at 23.5ºC. CLF_{20} presented the lowest one with 110.05 W/m^2 at 25.5ºC. In this case, there was no big differences between C and mixtures with PCM. However, it can be observed that mixtures with PCM showed again a constant heat flux value between solidification melting temperature **[9],** 23ºC- 21ºC, corresponding with the

phase change of the PCM (latent heat). Afterwards, as occurred in heating process, heat flux fell down to a steady state where the differences between in and out were nearly 0 W/m^2.

4. Analysis and discussion

The experimental results pointed out that the thermal behaviour of mortars with PCM depends not only on PCM but also on the mixtures components. The attenuation coefficient with 250kHz frequency for each mixture at different PCM states was evaluated. In addition, the capacity of mortars to absorb or release energy (enthalpy) at different temperature conditions was also discussed.

4.1 Attenuation coefficients regarding to microstructure of mortars.

Figure 6 presents the results of AT_{PCM} at different PCM states showed in Table 3.

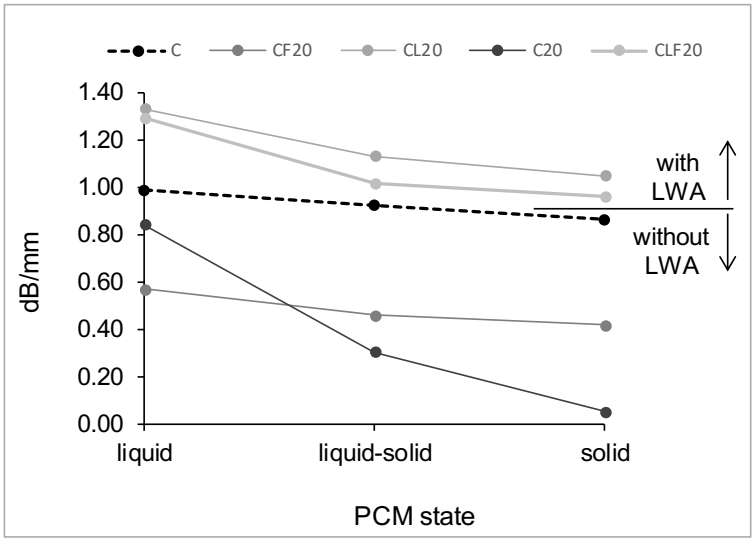

Figure 6. Attenuation coefficients at different PCM states.

It can be differentiated two different groups: mortars with LWA and mortars without LWA. Mortars with LWA showed AT_{PCM} values for all PCM states higher than 1 dB/mm. These values pointed out that lightweight aggregates were able to absorb US energy **[15].** On the other hand, figure 6 shows that mixtures without LWA presented AT_{PCM} values under 1 dB/mm. It can be appreciated that C_{20} showed higher differences between AT_L, AT_{L-S} and AT_S. These AT_{PCM} results can be also related with the results obtained for D_G and

OP (Table 2). Mixtures with LWA had lower D_G than mixtures without LWA. Besides, OP values were higher for mixtures with LWA than for mixtures without LWA. Accordingly, it can be said that the lower the density of the mixture the higher is the attenuation coefficient. On the other hand, high Open Porosity meant in this case high attenuation coefficient.

Some authors have already explained that there is a relationship between attenuation coefficient at 250kHz and the pore microstructure of the mortars in hardened state **[15].**

4.2 Attenuation coefficients depending on PCM state.

Figure 7 shows relative AT_{PCM} values (%) for each mixture from results described in Table 3.

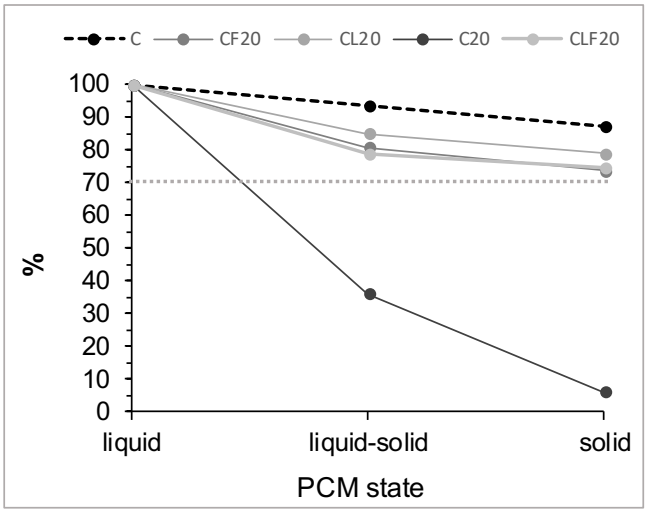

Figure 7. Relative attenuation values (%) related to PCM states.

The 100% corresponds with the maximum AT_{PCM} obtained. In all cases it corresponded with T> 23ºC (PCM in liquid state). 100% was the maximum US signal that the mortar was able to absorb. It can be observed that for all mixtures, except for C_{20}, the percentage varied between 100% and 70% regarding to PCM state. 100% corresponded for liquid PCM (T>23ºc) and 70% for solid PCM (T<23ºC).

As expected, the mixture without PCM (C) was the mixture that presented a slightly variation regarding to temperature. A linear development of AT_{PCM} can be observed. Values stayed in an interval of 15% between T>23ºC (liquid PCM) and T<23ºC (solid PCM). These results can be related to the water content inside the mixture, taking into account that water is also a PCM (liquid-solid-gas).

On the other hand, mixtures with the addition of PCM presented a similar pattern between each mixture depending on the PCM states. Two different AT_{PCM} behaviors can be observed. Firstly, a decrease of AT_{PCM} occurred. Afterwards a AT_{PCM} decrease happened again but softer than the first one. When PCM is in liquid-solid state (T≥23ºC), CL_{20}, CF_{20} and CLF_{20} presented a decrease between15%-20%, while C_{20} presented a decrease of 65% for AT_{PCM}. Finally, as PCM was in solid state (T<23ºC), AT_{PCM} suffered a decrease of 10% approximately regarding to values obtained for the liquid-solid state. C_{20} presented a decreased of 40% regarding to the value for AT_{L-S}.

Accordingly, C_{20} was the mixture that presented big differences between the different states of the PCM. It can be assumed that PCM is a good US signal transmitter when it is not mixed with other additions that hinder the US signal transmission.

4.3 Enthalpies for each mortar during heating and cooling cycles.

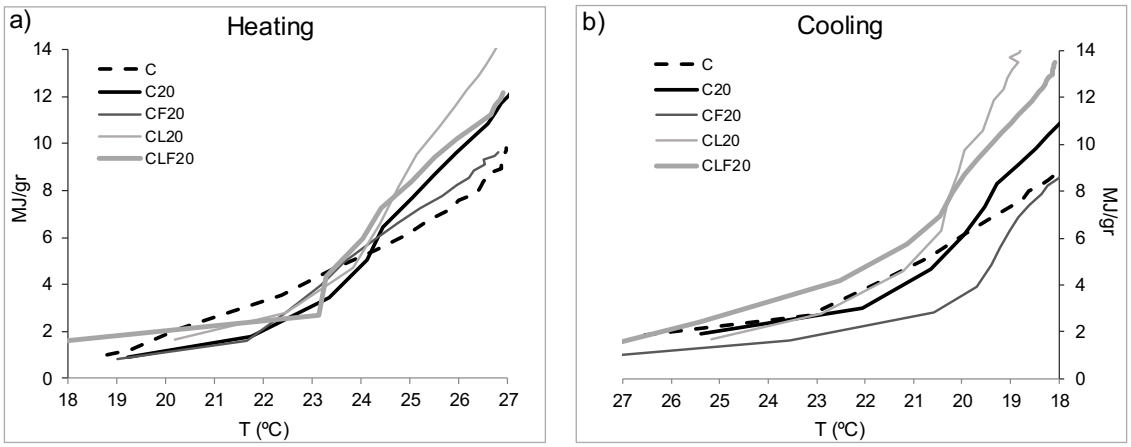

Figure 8. PCM cement-lime mortars enthalpy during heating and cooling cycles.

Figures 8a) and 8b) present enthalpy values regarding to sample average temperatures during heating and cooling cycles. The enthalpies were obtained according to Eq. 2-4.

As expected, C (mixture without PCM) presented a lineal enthalpy increase/decrease with temperature. These results corresponded with the results obtained with the Differential Scanning Calorimetry (Figure 3). On the other hand, mixtures with PCM showed a similar trend. Figure 8a) shows an inflection point for mixtures with PCM at a certain temperature. The inflection point of the curves corresponded to the melting point of the PCM **[9] and** was located for heating cycles between 22ºC and 24.5ºC. The inflection point during cooling cycle is shown in Figure 8b). In this case, it was located between 22ºC and 19ºC corresponding with the melting point of the PCM **[9].** Both intervals corresponded with the results obtained with DSC test and presented in Figure

3. Figure 8a) presented the enthalpy values obtained during a heating cycle between 18ºC and 27ºC (from solid to liquid PCM state). The values at 27ºC varied between 13.77 MJ/gr (CL_{20}) and 9.6 MJ/gr (CF_{20}). CLF_{20} and C_{20} showed the same enthalpy value, 11.93 MJ/gr. Figure 8b) presented the enthalpy values obtained during a cooling cycle between 27ºC and 18ºC (from liquid to solid PCM state). Values at 18ºC varied between 14MJ/gr (CL_{20}) and 8.5MJ/gr (CF_{20}). CLF_{20} showed an enthalpy value at 18ºC of 13.5 MJ/gr while C_{20} showed 11 MJ/gr.

The amount of energy that was necessary to increase/decrease the temperature (sensible heat) during heating and cooling cycles for each mixture can be determinate in Figures 8a) and 8b). As observed, the temperature interval during the phase change of the PCM was different for both cycles. During the heating cycle, the increase of temperature during the phase change was 2.5ºC. C_{20} and CF_{20} were the mixtures that needed less energy to increase 2.5ºC. These mixtures needed 4.5 MJ/gr to increase from 22ºC to 24.5ºC the mortar temperature. On the other hand, CLF_{20} needed 5 MJ/gr. Finally, CL_{20} was the mixture that needed more energy to increase its temperature (6 MJ/gr).

Consequently, CL_{20} was he mixture that absorbed more energy (more heat storage capacity) comparing with other mixtures for heating process.

During the cooling cycle, differences between the energy needed to decrease temperature were also observed. In this case, 3ºC was the temperature decrease during the phase change of the PCM. CF_{20} was the mixture that needed less energy to decrease the temperature (3.8 MJ/gr). C_{20} needed 5.3 MJ/gr and CLF_{20}, 6.5MJ/gr. Finally, CL_{20} was the mixture that needed more energy to decrease temperature, 7 MJ/gr. Accordingly, CL_{20} was de mixture with the highest latent heat storage capacity. In both cases, CL_{20} was the mixture that presented a better thermal performance due to its heat storage (larger enthalpy) capacity and its thermal insulation (low conductivity) capacity. In the case of cellulose fibres, the mortars did not show as effective as the mixture with only LWA and PCM. These results corresponded with the results obtained in Figure 3.

5. Conclusions

An experimental study to analyse the thermal performance of 5 different mortar with the addition of 20% of PCM, lightweight aggregates (LWA) and fibres at different temperature conditions. Us signal and heat flux measurements were evaluated. The main conclusions of this study were:

- With US signal the different microstructures of the mortars and PCM states were detected.

- US needs to be calibrated depending on the components of the mixtures.
- US is a non-destructive technique that allows the verification of the PCM behaviour inside a cement-lime mortar. Accordingly, the durability of the PCM inside the mortars can be proved.
- The addition of PCM increased the enthalpy values of the cement-lime mortars. - The enthalpy can be evaluated with the combination of temperatures and heat flux at different temperatures in- and outside a climatic chamber.
- CL_{20} showed the best thermal performance with largest enthalpy values and with low conductivity.

7. References

[1] Alibakhsh Kasaeian, Leyli bahrami, Fathollah Pourfayaz, Erfan Khodabandeh, Wei-Mon Yan, Experimental studies on the applications of PCMs and nano-PCMs in buildings: A critical review, Energy and Buildings, Volume 154, (2017) 96-112, ISSN 0378-7788, https://doi.org/10.1016/j.enbuild.2017.08.037.

[2] L.F. Cabeza, C. Barreneche, A. Castell, A. de Garcia, et al., Materials used as PCM in thermal energy storage in building: A review, Renewable and Sustainable Energy Reviews, 15 (2011) 1675-1695, https://doi.org/10.1016/j.rser.2010.11.018.

[3] D. Zhou, C.Y. Zhao, Y. Tian, Review on thermal energy storage with phase change materials (PCMs) in building applications, Applied Energy, 92 (2012), 593-605, https://doi.org/10.1016/j.apenergy.2011.08.025.

[4] E. Günther, S. Hiebler, H. Mehling, R. Redlich, Enthalpy of phase change materials as a function of temperature: required accuracy and suitable measurement methods, Int J Thermophys, 30 (2009) 1257-1269, https://doi.org/10.1007/s10765-009-0641-z.

[5] R.K. Sharma, P. Ganesan, V.V. Tyagi, H.S.C. Metselaar, S.C. Sandaran, Developments in organic solid–liquid phase change materials and their applications in thermal energy storage, Energy Conversion and Management, Volume 95, (2015) 193-228, ISSN 0196-8904, https://doi.org/10.1016/j.enconman.2015.01.084.

[6] S. Drissi, A. Eddhahak, S. Caré, J.Neji, Thermal analysis by DSC of Phase Change Materials, study of the damage effect, Journal of Building Engineering, 1 (2015) 13-19, https://doi.org/10.1016/j.jobe.2015.01.001.

[7] V. Venkateswara Rao, R. Parameshwaran, V. Vinayaka Ram, PCM-mortar based construction materials for energy efficient buildings: A review on research trends, Energy and Buildings, 158 (2018) 95-122, https://doi.org/10.1016/j.enbuild.2017.09.098.

[8] Christoph Mankel, Antonio Caggiano, Neven Ukrainczyk, Eddie Koenders, Thermal energy storage characterization of cement-based systems containing microencapsulated-PCMs, Construction and Building Materials, Volume 199 (2019) 307-320, ISSN 0950-0618, https://doi.org/10.1016/j.conbuildmat.2018.11.195.

[9] Cynthia Guardia, Gonzalo Barluenga, Irene Palomar, Gonzalo Diarce, Thermal enhanced cement-lime mortars with phase change materials (PCM), lightweight aggregate and cellulose fibers, Construction and Building Materials, Volume 221, (2019) 586-594, ISSN 0950-0618, https://doi.org/10.1016/j.conbuildmat.2019.06.098.

[10] A. Jayalath, R. San Nicolas, M. Sofi, R. Shanks, T. Ngo, L.Aye, P. Mendis, Properties of cementitious mortar and concrete containing micro-capsulated phase change materials, Construction and Building Materials, 120 (2016) 408-417, https://doi.org/10.1016/j.conbuildmat.2016.05.116.

[11] S. Lucas, V.M. Ferreira, J.L. Barroso de Aguiar; Latent heat storage in PCM containing mortars—Study of microstructural modifications, Energy and Buildings, 66 (2013) 724-731, https://doi.org/10.1016/j.enbuild.2013.07.060.

[12] S. Cunha, M. Lima, J.B. Aguiar; Influence of adding phase change materials on the physical and mechanical properties of cement mortars, Construction and Building Materials, 127 (2016) 1-10, https://doi.org/10.1016/j.conbuildmat.2016.09.119.

[13] I. Palomar, G. Barluenga, J. Puentes, Lime–cement mortars for coating with improved thermal and acoustic performance, Construction and Building Materials, 75 (2015) 306-314, https://doi.org/10.1016/j.conbuildmat.2014.11.012.

[14] G. Barluenga, J. Puentes, I. Palomar, C. Guardia, Methodology for monitoring Cement Based Materials at Early Age combining NDT techniques, Construction and Building Materials, Volume 193 (2018), 373-383, ISSN 0950-0618, https://doi.org/10.1016/j.conbuildmat.2018.10.205.

[15] I. Palomar, G. Barluenga, Assessment of lime-cement mortar microstructure and properties by P- and S- ultrasonic waves, Construction and Building Materials, Volume 139, (2017) 334-341, ISSN 0950-0618, https://doi.org/10.1016/j.conbuildmat.2017.02.083.

[16] T.P. Philippidis, D.G. Aggelis, Experimental study of wave dispersion and attenuation in concrete, Ultrasonics, Volume 43, (2005) 584-595, ISSN 0041-624X, https://doi.org/10.1016/j.ultras.2004.12.001.

[17] Zoubeir Lafhaj, Marc Goueygou, Assia Djerbi, Mariusz Kaczmarek, Correlation between porosity, permeability and ultrasonic parameters of mortar with variable water/cement ratio and water content, Cement and Concrete Research, Volume 36, Issue 4 (2006) 625-633, ISSN 0008-8846, https://doi.org/10.1016/j.cemconres.2005.11.009.

[18] S. Herrero, P. Mayor, F. Hernández-Olivares, Influence of proportion and particle size gradation of rubber from end-of-life tires on mechanical, thermal and acoustic properties of plaster–rubber mortars, Materials & Design, 47, (2013) 633-642, https://doi.org/10.1016/j.matdes.2012.12.063.

[19] I. Palomar, G. Barluenga, R.J. Ball, M. Lawrence, Laboratory characterization of brick walls rendered with a pervious lime-cement mortar, Journal of Building Engineering, Volume 23, (2019) 241-249, ISSN 2352-7102, https://doi.org/10.1016/j.jobe.2019.02.001.

[20] Lucas, S.S. & Barroso de Aguiar, J.L. Heat Mass Transfer (2019) 55: 2429. https://doi.org/10.1007/s00231-019-02594-1.

[21] A. Ristić, S. Furbo, C.Moser, H. Schranzhofer, et al., IEA SHC Task 42 / ECES Annex 29 WG A1: Engineering and Processing of PCMs, TCMs and Sorption Materials, Energy Procedia, 91 (2016) 207-217, https://doi.org/10.1016/j.egypro.2016.06.205.

[22] S. Gschwander, T. Haussmann, G. Hagelstein, A.Sole, LF. Cabeza, G. Diarce et al., Standardization of PCM characterization via DSC. 13th international conference on energy storage. (2015),19–21.

10.2.3 Thermal evaluation of cement-lime materials with PCM

Guardia, C., *Thermal evaluation of cement-lime based materials with PCM. Ponencia invitada durante el V Congreso Hispano-Luso de cerámica y vidrio, LVI Congreso Nacional de la SECV, 8-10 de octubre de 2018.*

V Congreso Hispano-Luso de cerámica y vidrio
LVI Congreso Nacional de la SECV
Barcelona 2018

Thermal evaluation of cement-lime based materials with PCM

C. Guardia[1]*, G. Barluenga[1] & I. Palomar[1]
[1] *Department of Architecture, University of Alcalá, Madrid.*
* *cynthia.guardia@edu.uah.es*

October 8th - 10th 2018
Barcelona, Spain

Background | PCM | Aims | Compositions | Results | Conclusions | …

Dwelling units in Spain (1940-1980) present poor thermal performance:

- Loss of aestethic and operating properties of existing façades.
- Low energy efficiency.
- High energetic costs.

Fig.1

Fig.2

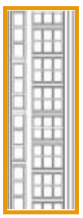

Fig.3

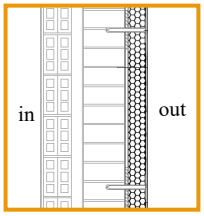

Present solutions:

- Energy efficiency = thermal insulation not considering thermal inertia.
- Cement-lime based mortars with additions (I.Palomar 2015):

  Cellulose fibres. Lightweight Aggregates (perlite).

Fig.1, Fig.3 : J. Terés-Zubiaga et al. " Field assessment of thermal behaviour of social housing apartments in Bilbao, Northern Spain." Energy and Buildings. 2013. Vol. 67. p. 118-135. Fig 2: Edificio de viviendas en Bilbao, España.

Universidad de Alcalá

Thermal evaluation of cement-lime based materials with PCM

SOCIEDAD ESPAÑOLA DE CERAMICA Y VIDRIO

Background | **PCM** | Aims | Compositions | Results | Conclusions | …

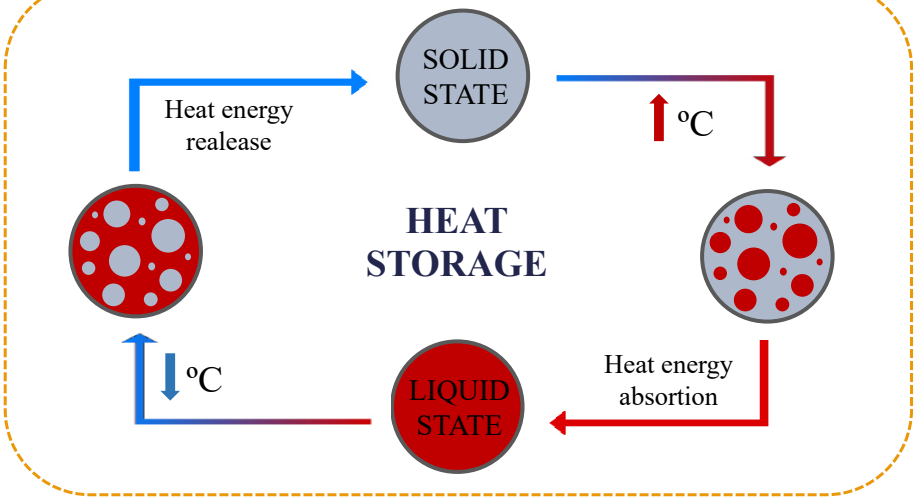

Universidad de Alcalá

Thermal evaluation of cement-lime based materials with PCM

SOCIEDAD ESPAÑOLA DE CERAMICA Y VIDRIO

Background | **PCM** | Aims | Compositions | Results | Conclusions | …

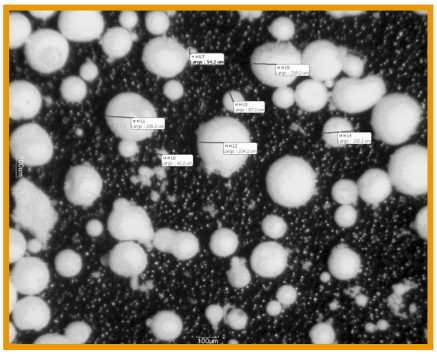

ORGANIC

- Low price.
- High thermal and chemical stability.
- Not require additives for long-term-use.
- Non corrosive.
- Recyclable.

MICROENCAPSULATED

- Can be mixed with common binders.
- Commercially developed.

MICROENCAPSULATED PARAFFIN WAX

Particle size ca. 50-300 µm
Melting point of ca. 23ºC

Aims and Scope

- Design of PCM cement-lime mortars for thermal retrofitting of façades.
- New constructive solutions for façades including PCM.
- Improvement of the energy efficiency of buildings through retrofitting of façades.

Universidad de Alcalá
Thermal evaluation of cement-lime based materials with PCM
SOCIEDAD ESPAÑOLA DE CERAMICA Y VIDRIO
Background | PCM | Aims | Compositions | Results | Conclusions | …

Material evaluation at 3 levels:

L_1 Physical, mechanical and thermal characterization of PCM cement-lime mortars.

L_2 Evaluation of the thermal behavior of PCM cement-lime mortars under different climatic conditions.

L_3 Evaluation of PCM cement-lime mortars on a façade brick wall under different climatic conditions.

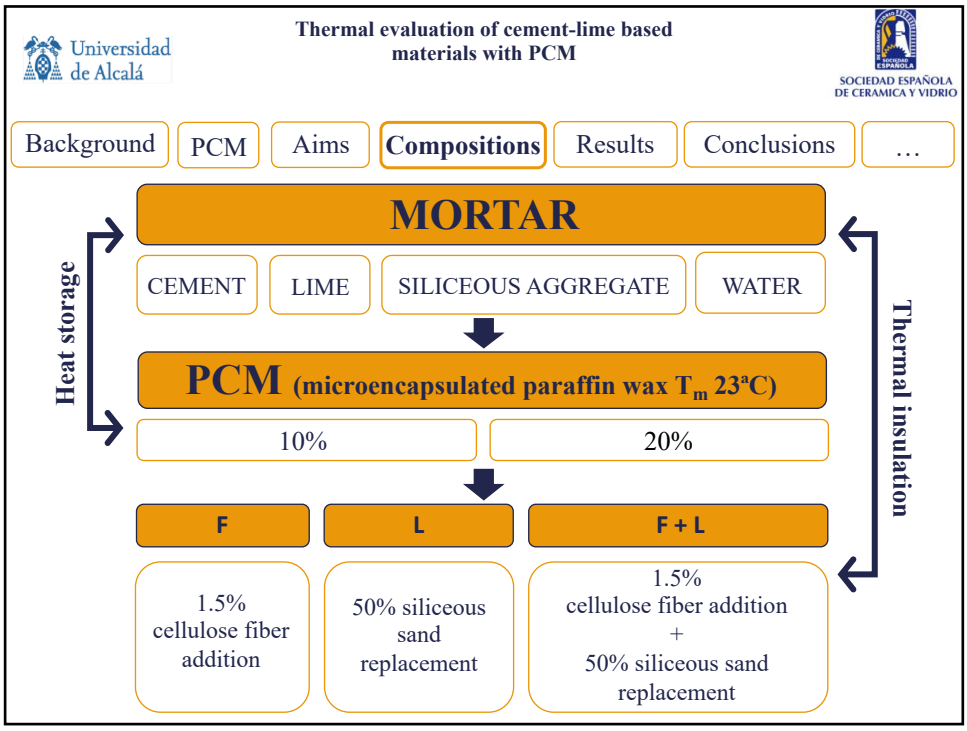

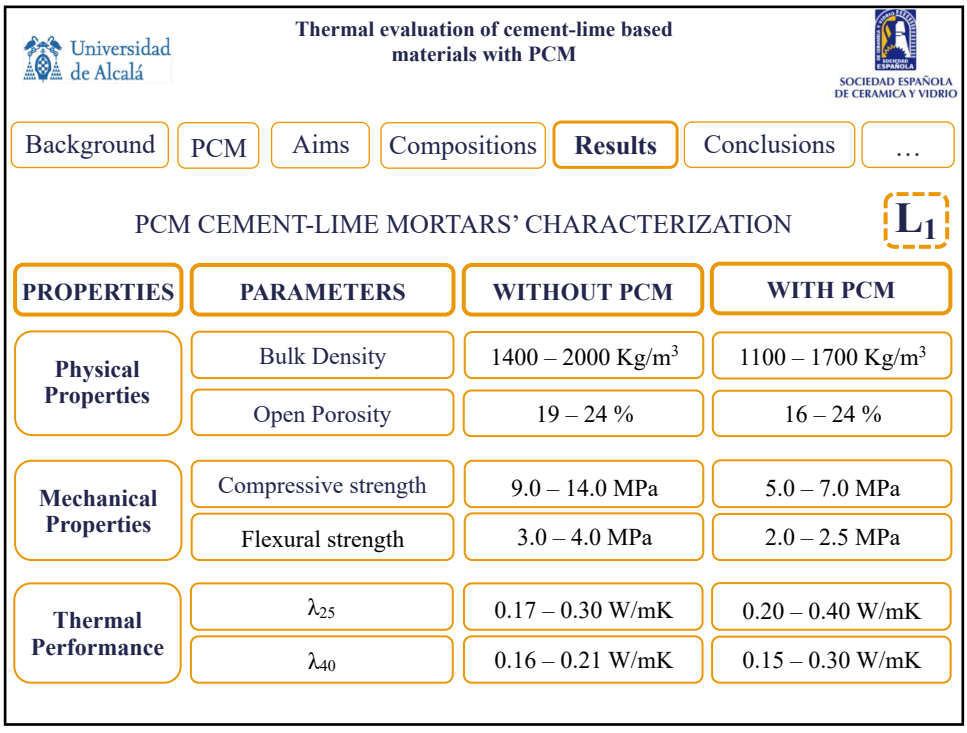

PROPERTIES	PARAMETERS	WITHOUT PCM	WITH PCM
Physical Properties	Bulk Density	1400 – 2000 Kg/m^3	1100 – 1700 Kg/m^3
	Open Porosity	19 – 24 %	16 – 24 %
Mechanical Properties	Compressive strength	9.0 – 14.0 MPa	5.0 – 7.0 MPa
	Flexural strength	3.0 – 4.0 MPa	2.0 – 2.5 MPa
Thermal Performance	λ_{25}	0.17 – 0.30 W/mK	0.20 – 0.40 W/mK
	λ_{40}	0.16 – 0.21 W/mK	0.15 – 0.30 W/mK

Thermal evaluation of cement-lime based materials with PCM

Background | PCM | Aims | Compositions | **Results** | Conclusions | …

DSC (Differential Scanning Calorimetry)

L1

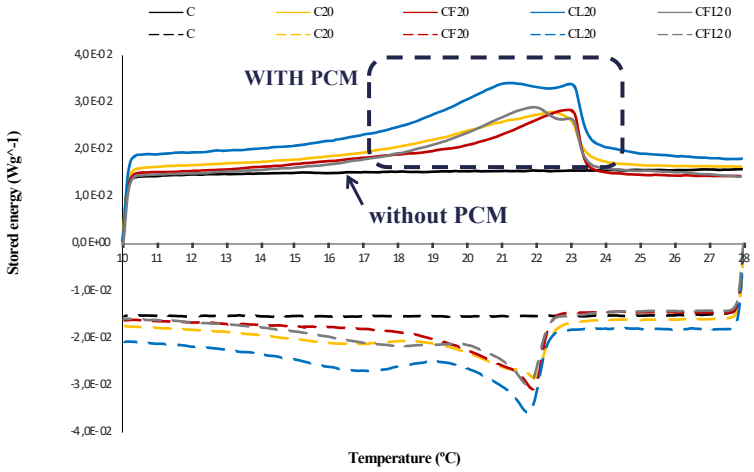

Thermal evaluation of cement-lime based materials with PCM

Background | PCM | Aims | Compositions | **Results** | Conclusions | …

DSC (Differential Scanning Calorimetry)

L1

Phase Change Enthalpy (J/g)

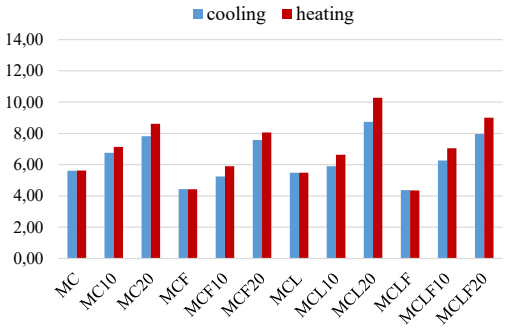

Phase Change Enthalpy (J/g) measurements of the different mixtures during cooling and heating process using DSC.

Universidad de Alcalá

Thermal evaluation of cement-lime based materials with PCM

SOCIEDAD ESPAÑOLA DE CERAMICA Y VIDRIO

Background | PCM | Aims | Compositions | **Results** | Conclusions | …

L_2

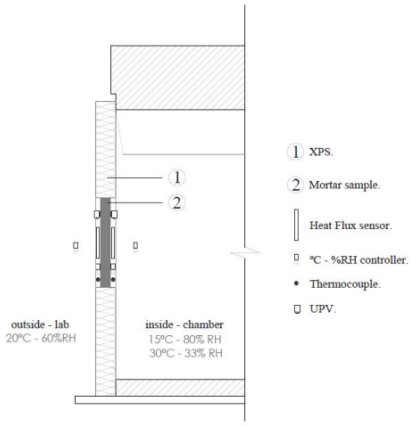

Experimental set up of the samples at different temperature conditions. Heat Flux, Temperature and UPV.

Universidad de Alcalá

Thermal evaluation of cement-lime based materials with PCM

SOCIEDAD ESPAÑOLA DE CERAMICA Y VIDRIO

Background | PCM | Aims | Compositions | **Results** | Conclusions | …

L_2

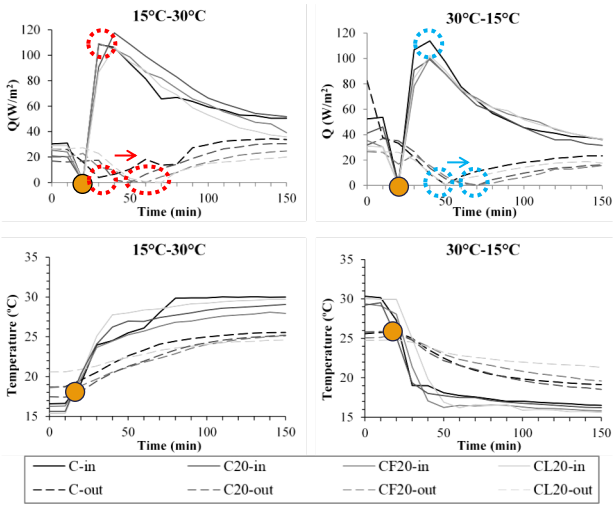

Heat Flux (HF)

- 0 HF inside = 0 Temp. differences int.- out.
- Mixture without PCM: max. HF inside = min. HF out.
- Mixtures with PCM: PCM delayed min. HF outside

Thermal evaluation of cement-lime based materials with PCM

Universidad de Alcalá

SOCIEDAD ESPAÑOLA DE CERAMICA Y VIDRIO

Background | PCM | Aims | Compositions | **Results** | Conclusions | …

NDT (Non Destrcutive Techniques)

L_2

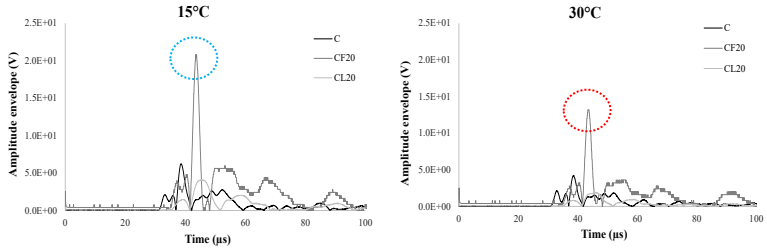

UPV measurements of the samples at different temperature conditions using Hilbert transform algorithm.

- Evaluation of the material structure (solid and pore) through the signal analysis .
- Assesment of the PCM state (solid – liquid) through the signal.
- UPV as a NDT, can be a quality control parameter of the PCM to evaluate on-site applications.

Thermal evaluation of cement-lime based materials with PCM

Universidad de Alcalá

SOCIEDAD ESPAÑOLA DE CERAMICA Y VIDRIO

Background | PCM | Aims | Compositions | Results | **Conclusions** | …

- The use of F, L and PCM modified the properties of the mixtures.
- The cement-lime based mortars developed **heat storage capacity** with the addition of PCM.
- **Higher Phase Change Enthalpy** during the **heating** process.
- The **more PCM** is added (10% - 20%), the **greater the Phase Change Enthalpy** of the mixtures.
- **Higher temperature reduced λ** of the mixtures (PCM in a liquid state).
- The addition of **PCM slowed down** the **Heat Flux** through the mortars.
- **Heat Flux delay** = less use of active systems (cooling and heating systems) = **energy eficiency improvement**.
- **UPV** (Non-Destructive Technique) as a **quality control parameter** to identify the **structure** of the material and the physical **state** of the **PCM** inside the mixture.

Universidad de Alcalá

Thermal evaluation of cement-lime based materials with PCM

SOCIEDAD ESPAÑOLA DE CERAMICA Y VIDRIO

Background | PCM | Aims | Compositions | Results | Conclusions | ...

Ongoing studies

L_3

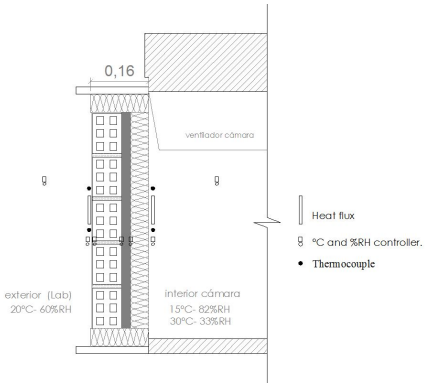

Experimental set up of a constructive solution at different temperature conditions.

Universidad de Alcalá

Thermal evaluation of cement-lime based materials with PCM

SOCIEDAD ESPAÑOLA DE CERAMICA Y VIDRIO

Background | PCM | Aims | Compositions | Results | Conclusions | ...

Conferences and publications

- **Second International RILEM Conference on Bio-based Building Materials. CLERMONT-FERRAND (France).** GUARDIA MARTÍN, Cynthia; BARLUENGA BADIOLA, Gonzalo; PALOMAR HERRERO, Irene. "Phase Change Material cement mortars for thermal retrofitting of façades." (2017) ISBN 978-2-35158-192-6.
- **I Jornadas de Jóvenes científicos en materiales de construcción. Madrid (España).** GUARDIA MARTÍN, Cynthia; BARLUENGA BADIOLA, Gonzalo; PALOMAR HERRERO, Irene. "Morteros funcionales de cemento-cal con PCM para la rehabilitación de fachadas.
- **Aproximaciones Contemporáneas al Paisaje Urbano. II Jornadas Internacionales de Investigación sobre paisaje, patrimonio y ciudad. Alcalá de Henares (España) (2018).** GUARDIA MARTÍN, Cynthia. "Morteros de cemento-cal con materiales de cambio de fase para la rehabilitación de edificaciones existentes dentro del entorno urbano".
- **72 RILEMWEEK 2018 & SLD4 The 4th International Conference on Service Life Design for Infrastructures. DELFT (Países Bajos).** GUARDIA MARTÍN, Cynthia; BARLUENGA BADIOLA, Gonzalo; PALOMAR HERRERO, Irene. "Thermal evaluation of cement-lime base materials with PCM".(2018) ISBN 978-2-35158-213-8.

Acknowledgements

- The authors greatly acknowledge the **Sociedad Española de Cerámica y Vidrio (SECV)** for the invitation and support for the attendance at the conference.
- The support of the companies BASF Construction Chemicals España S. L., Omya Clariana S.L. and Cementos Portland Valderrivas is acknowledge.
- ENEDI Research Group. *Department of Thermal Engineering, Faculty of Engineering of Bilbao, University of the Basque Country UPV/EHU.*

Universidad de Alcalá

V Congreso Hispano-Luso de cerámica y vidrio
LVI Congreso Nacional de la **SECV**
Barcelona 2018

SOCIEDAD ESPAÑOLA DE CERAMICA Y VIDRIO

Thermal evaluation of cement-lime based materials with PCM

C. Guardia[1]*, G. Barluenga[1] & I. Palomar[1]
[1] *Department of Architecture, University of Alcalá, Madrid.*
* *cynthia.guardia@edu.uah.es*

THANK YOU

10.2.4 Thermal evaluation of cement-lime materials with PCM

Guardia, C., *Morteros funcionales de cemento-cal con PCM para la rehabilitación de fachadas. Primer Premio a la mejor ponencia en las I Jornadas de Jóvenes Científicos en Materiales de Construcción.18-19 de junio de 2018.*

Morteros funcionales de cemento-cal con PCM para la rehabilitación de fachadas

C. Guardia[1], G. Barluenga[2], I. Palomar[3]
[1] *Departamento de Arquitectura, Universidad de Alcalá, Madrid, España. Estudiante de doctorado.*
[2] *Departamento de Arquitectura, Universidad de Alcalá, Madrid, España. Doctor. Profesor Titular.*
[3] *Departamento de Arquitectura, Universidad de Alcalá, Madrid, España. Doctor. PDI*
Corresponding author: C. Guardia e-mail: cynthia.guardia@edu.uah.es*!*

Graphical Abstract

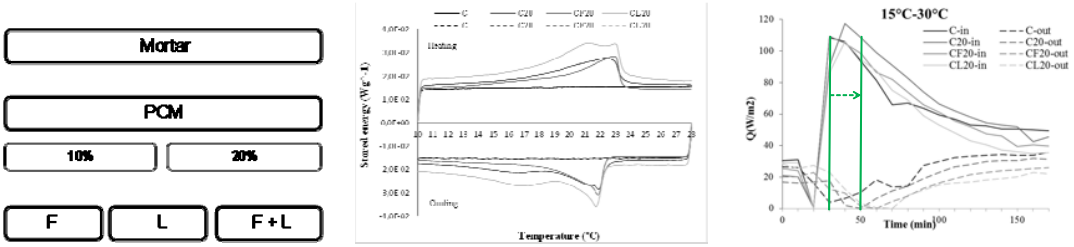

Esquema dosificaciones y primeros resultados: Calorimetría DSC y Evaluación de Flujo térmico.

Abstract

Actualmente existe una constante búsqueda de nuevos materiales para la mejora de la eficiencia energética de los edificios existentes según los estándares establecidos. Algunos autores han desarrollado nuevos morteros funcionales para la mejora del comportamiento térmico de los edificios a través de sus fachadas[1]. Estos materiales, compuestos en base cemento-cal incluyen la adición de materiales como fibras de celulosa y áridos ligeros dotando al material de la capacidad de aislante térmico. Así mismo, existen materiales como los Materiales de Cambio de Fase o PCM cuya principal característica es su capacidad de acumular o liberar energía a través del cambio de fase (sólido–líquido) a una determinada temperatura[2]. Este trabajo plantea una investigación sobre morteros funcionales en base cemento–cal con la adición de fibras de celulosa, áridos ligeros y PCM en diferentes cantidades, para la mejora del comportamiento térmico de fachadas de edificios. Para ello, se han diseñado y evaluado 12 dosificaciones física, mecánica y térmicamente. Se ha estudiado el comportamiento térmico del material a diferentes temperaturas e incorporado en una solución constructiva, utilizando técnicas no destructivas, como flujo de calor, ultrasonidos y sensores de temperatura. Los primeros resultados muestran diferencias físico-mecánicas y térmicas debido no sólo a la adición del PCM, sino que también al efecto del PCM con los otros componentes que forman la mezcla. Igualmente se observan diferencias en el comportamiento térmico según las condiciones de temperatura a la que esté sometido el material debido al calor latente absorbido o cedido por el PCM en los procesos de calentamiento y enfriamiento respectivamente.

[1]Palomar, I.; Barluenga, G.; Puentes, J.; Lime-cement mortars for coating with improved thermal and acoustic performance. Construction and Building Materials, 2015, 75, 306-314, ISSN 0950-0618.
[2] Cabeza, L.F.; Barreneche, C.; Castell, A.; de Garcia, A. et al.; Materials used as PCM in thermal energy storage in building: A review. Renewable and Sustainable Energy Reviews, 2011, 15, 3, 1675-1695, ISSN 1364-0321.

Universidad de Alcalá

I Jornadas de Jóvenes Científicos en Materiales de Construcción, 2018

MORTEROS FUNCIONALES DE CEMENTO-CAL CON PCM PARA LA REHABILITACIÓN DE FACHADAS

C. Guardia[1]*, G. Barluenga[1] & I. Palomar[1]
[1] *Departamento de Arquitectura, Universidad de Alcalá, Madrid.*
* *cynthia.guardia@edu.uah.es*

18-19 de junio de 2018
Madrid

Universidad de Alcalá


Fig.1


Fig.2

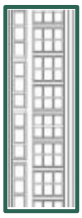
Fig.3

El parque edificatorio (1940-1980) se encuentra en estado de necesaria transformación :

- Pérdida de propiedades estéticas y funcionales.
- Comportamiento térmico deficiente.
- Elevados costes energéticos.

Soluciones actuales:

- Eficiencia energética a través de aislamiento térmico sin considerar inercia térmica.
- Morteros en base cemento-cal con nuevos componentes (I.Palomar 2015):

  Adición de fibras de celulosa. Adición de áridos ligeros.

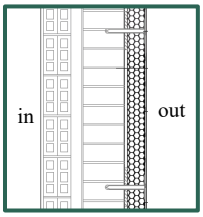

Fig.1, Fig.3 : J. Terés-Zubiaga et al. " Field assessment of thermal behaviour of social housing apartments in Bilbao, Northern Spain." Energy and Buildings. 2013. Vol. 67. p. 118-135. Fig 2: Edificio de viviendas en Bilbao, España.

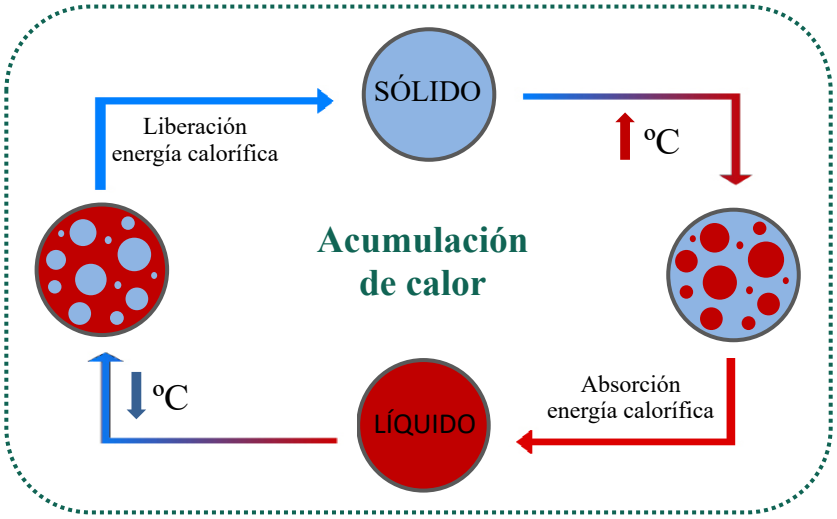

Universidad de Alcalá
MORTEROS FUNCIONALES DE CEMENTO-CAL CON PCM PARA LA REHABILITACIÓN DE FACHADAS
IJJCMC, 2018
Contexto | PCM | Objetivos | Dosificación | Resultados | Conclusiones | Final

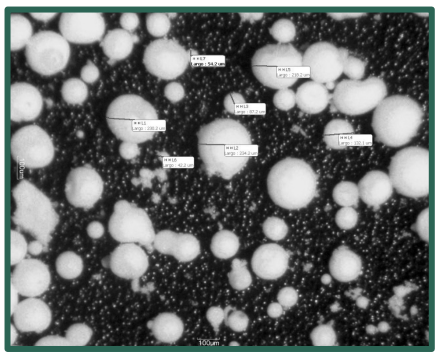

ORGÁNICOS

- Bajo precio.
- Estables térmica y químicamente.
- No requiere aditivos para su uso a largo plazo.
- No son corrosivos.
- Reciclables.

MICROENCAPSULADOS

- Se pueden mezclar fácilmente con otros componentes.
- Desarrollados comercialmente.

PARAFINA MICROENCAPSULADA

Tamaño: ca. 50-300 µm
Temperatura de fusión: ca. 23ºC

- Diseño de morteros funcionales de cemento-cal con PCM para la rehabilitación de fachadas.
- Diseño de un nuevo sistema constructivo incluyendo los morteros de cemento-cal con PCM para mejorar el comportamiento térmico de las fachadas.
- Mejora de la eficiencia energética de los edificios a través de la rehabilitación de fachadas.

Universidad de Alcalá
MORTEROS FUNCIONALES DE CEMENTO-CAL CON PCM PARA LA REHABILITACIÓN DE FACHADAS
IJJCMC, 2018
Contexto | PCM | Objetivos | Dosificación | Resultados | Conclusiones | Final

Evaluación del material (3 niveles):

1. Análisis de las características físicas mecánicas y térmicas del material.
2. Análisis del comportamiento térmico del material bajo diferentes condiciones ambientales.
3. Análisis del comportamiento del material dentro de un sistema constructivo bajo diferentes condiciones ambientales.

Universidad de Alcalá

MORTEROS FUNCIONALES DE CEMENTO-CAL CON PCM PARA LA REHABILITACIÓN DE FACHADAS

IJJCMC, 2018

Contexto | PCM | Objetivos | **Dosificación** | Resultados | Conclusiones | Final

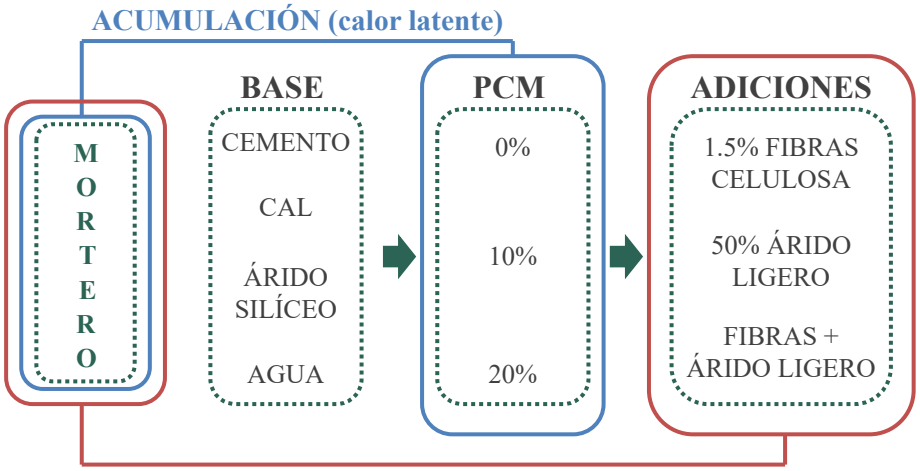

Universidad de Alcalá

MORTEROS FUNCIONALES DE CEMENTO-CAL CON PCM PARA LA REHABILITACIÓN DE FACHADAS

IJJCMC, 2018

Contexto | PCM | Objetivos | Dosificación | **Resultados** | Conclusiones | Final

PROPIEDADES DEL MORTERO DE CEMENTO-CAL CON PCM

		C	C_{10}	C_{20}	CF	CF_{10}	CF_{20}	CL	CL_{10}	CL_{20}	CLF	CLF_{10}	CLF_{20}
Prop. Físicas	Densidad Ap. (Kg/m³)	1900	1690	1600	1960	1720	1660	1430	1180	1270	1430	1110	1160
	Porosidad Abierta (%)	19.56	16.68	17.72	18.93	16.90	16.77	20.95	22.99	23.33	23.94	22.10	23.09
Prop. Mecánicas	Resist. Compresión (MPa)	13.70	7.7	7.3	10.3	6.7	6.0	9.3	5.3	6.0	13.00	5.0	5.3
	Resist. Flexión (MPa)	3.36	2.26	2.40	3.18	2.24	1.79	2.66	1.98	2.20	3.44	1.84	2.16
Prop. Térmicas	λ_{25} (W/mK)	0.23	0.26	0.20	0.29	0.40	0.30	0.17	0.27	0.29	0.22	0.25	0.23
	λ_{40} (W/mK)	0.21	0.32	0.28	0.21	0.26	0.23	0.16	0.19	0.18	0.19	0.21	0.15

Universidad de Alcalá

MORTEROS FUNCIONALES DE CEMENTO-CAL CON PCM PARA LA REHABILITACIÓN DE FACHADAS

IJJCMC, 2018

Contexto | PCM | Objetivos | Dosificación | **Resultados** | Conclusiones | Final

DSC (Differential Scanning Calorimetry)

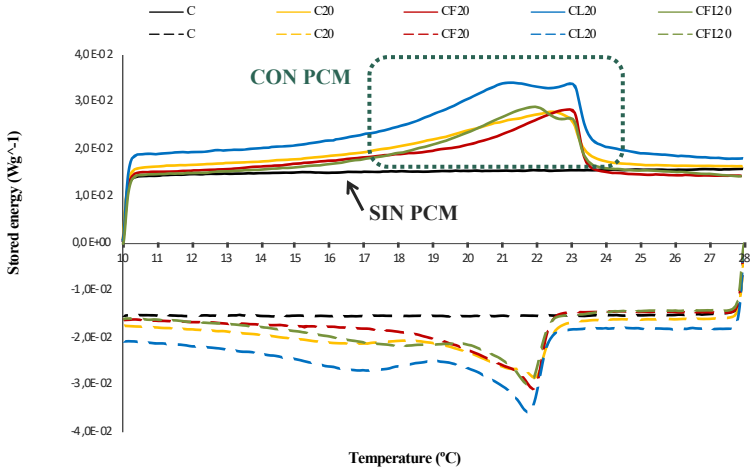

Universidad de Alcalá

MORTEROS FUNCIONALES DE CEMENTO-CAL CON PCM PARA LA REHABILITACIÓN DE FACHADAS

IJJCMC, 2018

Contexto | PCM | Objetivos | Dosificación | **Resultados** | Conclusiones | Final

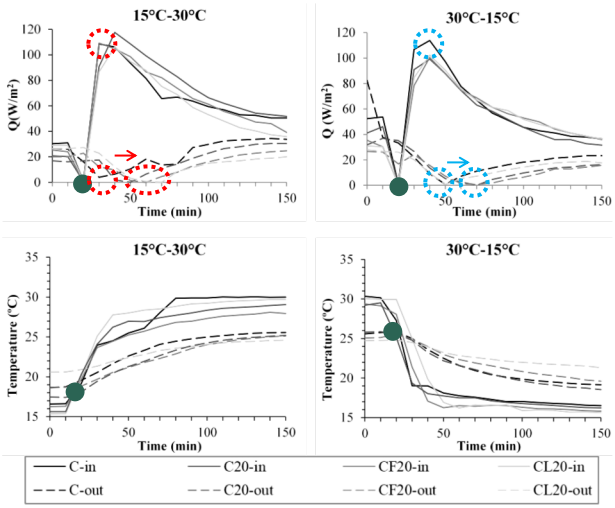

Flujo de Calor (HF)

- 0 FC en interior. 0 diferencia T int.- ext.
- Mezcla sin PCM: momento de máx. HF interior = mín. FC ext.
- Mezclas con PCM: mín. HF exterior retrasado respecto máx. HF interior.

Universidad de Alcalá

MORTEROS FUNCIONALES DE CEMENTO-CAL CON PCM PARA LA REHABILITACIÓN DE FACHADAS

IJJCMC, 2018

Contexto | PCM | Objetivos | Dosificación | **Resultados** | Conclusiones | Final

EVALUACIÓN MORTERO DENTRO DE SISTEMA CONSTRUCTIVO BAJO DIFERENTES CONDICIONES AMBIENTALES

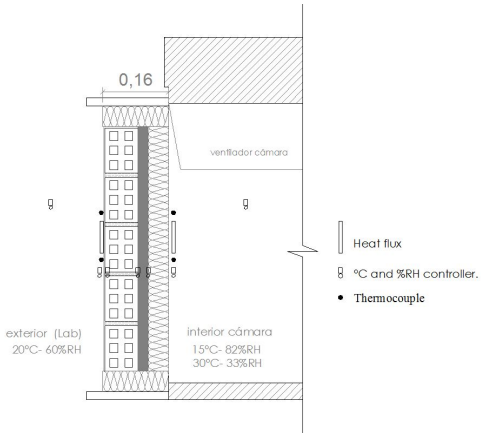

Universidad de Alcalá

MORTEROS FUNCIONALES DE CEMENTO-CAL CON PCM PARA LA REHABILITACIÓN DE FACHADAS

IJJCMC, 2018

Contexto | PCM | Objetivos | Dosificación | **Resultados** | Conclusiones | Final

NDT (Non Destrcutive Techniques)

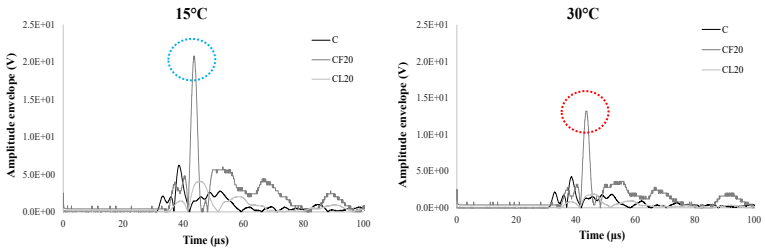

Medidas de ultrasonidos en diferentes condiciones ambientales usando el algoritmo de Hilbert .

- Evaluación estructura material (sólida y porosa) a través del análisis de onda.
- Detectar el estado del PCM (sólido-líquido) a través de la onda.
- Los ultrasonidos como medida de control para evaluación de la durabilidad del PCM y su comportamiento in-situ.

- La adición de PCM al mortero de cemento-cal afecta a las propiedades físicas, mecánicas y térmicas.
- El PCM no se comporta igual térmicamente en estado líquido o sólido.
- A mayor temperatura, la conductividad térmica del mortero con PCM mejora.
- La adición de PCM ralentiza el paso de flujo de calor por el material.
- Retardo en el paso de flujo de calor por el material = disminución de uso de sistemas activos (aire acondicionado, calefacción) = mejora eficiencia energética.

Universidad de Alcalá
MORTEROS FUNCIONALES DE CEMENTO-CAL CON PCM PARA LA REHABILITACIÓN DE FACHADAS
IJJCMC, 2018
Contexto | PCM | Objetivos | Dosificación | Resultados | Conclusiones | **Final**

PRÓXIMO TRABAJO

- Evaluación del **comportamiento del mortero de cemento-cal con PCM** bajo diferentes condiciones ambientales dentro del sistema constructivo.
- Establecer cualitativa- y cuantitativamente la posible **mejora de la eficiencia energética** del sistema constructivo con la aplicación del mortero con diferentes adiciones y cantidades de PCM.

Universidad de Alcalá

I Jornadas de Jóvenes Científicos en Materiales de Construcción, 2018

MORTEROS FUNCIONALES DE CEMENTO-CAL CON PCM PARA LA REHABILITACIÓN DE FACHADAS

MUCHAS GRACIAS

C. Guardia[1]*, G. Barluenga[1] & I. Palomar[1]
[1] *Departamento de Arquitectura, Universidad de Alcalá, Madrid.*
* *cynthia.guardia@edu.uah.es*

10.3. Publicaciones sobre la simulación experimental del cerramiento multicapa mejorado.

10.3.1 PCM Cement-Lime Mortars for Enhanced Energy Efficiency of Multilayered Building Enclosures under Different Climatic Conditions.

Guardia, C.; Barluenga, G.; Palomar, I. (2020) *PCM Cement-Lime Mortars for Enhanced Energy Efficiency of Multilayered Building Enclosures under Different Climatic Conditions*. Materials, 13, 4043. https://doi.org/10.3390/ma13184043.

materials

MDPI

Article

PCM Cement-Lime Mortars for Enhanced Energy Efficiency of Multilayered Building Enclosures under Different Climatic Conditions

Cynthia Guardia *, Gonzalo Barluenga and Irene Palomar

Department of Architecture, University of Alcala, Madrid 28801, Spain; gonzalo.barluenga@uah.es (G.B.); irene.palomar@uah.es (I.P.)

* Correspondence: cynthia.guardia@edu.uah.es; Tel.: +34-918839239; Fax: +34-918839276

Received: 3 August 2020; Accepted: 10 September 2020; Published: 11 September 2020

Abstract: Phase change materials (PCMs) are promising materials for the energy efficiency improvement of building enclosures, due to their energy storage capacity. The thermal behaviour of a multi-layered building enclosure with five different compositions of PCM cement-lime mortars was evaluated under heating and cooling cycles. The behaviour of cement-lime mortars with 20% of microencapsulated PCM mixed with other additions, such as cellulose fibres and perlite, a lightweight aggregate (LWA), were studied under climate conditions of 15 °C—82% RH (cooling) and 30 °C—33% RH (heating) that were applied with a climatic chamber. Temperature and heat flux on both sides of the multi-layered enclosure were experimentally measured in laboratory tests. Temperature was also measured on both sides of the PCM cement-lime mortar layer. It was observed that the addition of the PCM cement-lime mortar layer delayed the heat flux through the enclosure. During a heating cycle, the incorporation of PCM delayed the arrival of the heat wave front by 30 min (8.1% compared to the reference mortar without PCM). The delay of the arrival of the heat wave front during the cooling cycle after adding PCM, compared to the reference mixture, reached 40.6% (130 min of delay). Furthermore, the incorporation of LWA in PCM cement-lime mortars also improved thermal insulation, further increasing energy efficiency of the building enclosure, and can be used not only for new buildings but also for energy rehabilitation of existing building enclosures.

Keywords: phase change materials (PCMs); energy efficiency; cement-lime mortar; experimental characterization; climatic conditions; heat flux

1. Introduction

The design of new building materials for the energy efficiency improvement of existing buildings is a hot research topic [1–3]. The high energy consumption of many dwelling units built in the XX century is a main concern due to their huge carbon footprint [4,5]. Phase change materials (PCMs) are considered as a possible solution for this problem, due to their energy storage capacity [6]. During phase change, which occurs at a selected temperature that can be designed, PCMs absorb or release heat, while the material temperature remains constant (latent heat), acting as energy deposits that can be recovered when necessary [7,8]. Among the different types of PCM [7,8], the most commonly used in construction and building materials are microencapsulated paraffin waxes, which are characterized by their thermal and chemical stability without significant changes to their properties in the temperature range used in this study. They are also commercially available at a competitive price. However, paraffin waxes present low thermal conductivity and low phase change enthalpy [7–10].

Different authors have incorporated this type of microencapsulated PCM in building materials such as cement, gypsum or cement-lime mortars [8–16]. Besides, other additions, such as fibres (cellulose) and lightweight aggregates (LWAs, e.g., perlite), can be also incorporated to improve the thermal insulation capacity of mortars [16–18]. Some authors have studied the combined use of PCMs and these additions in mortars, taking advantage of both the the energy storage capacity of PCMs and the thermal insulation capacity [16]. It was found that PCM efficiency depends not only on the amount of PCM but also on the other components of the mortars [16]. The amount of PCM incorporated modified some thermal, physical and mechanical properties of mortars. Temperature range and variation also influenced the efficiency of PCM-modified mortars [15,19–21].

The experimental characterisation of materials' properties is the first step necessary to evaluate the possibilities of their application for building purposes [1,12–14,16]. However, the actual effect of the newly designed materials for improving building enclosures can only be fully evaluated by considering the multi-layered composition of real enclosures. Accordingly, some authors have studied the behaviour of multi-layered specimens by assessing new mortars with enhanced properties under different climatic conditions [15,17–21]. Climatic chambers can be used to test specific thermal conditions, simulating real environmental conditions [15,17]. It was concluded that the PCM effect on the multilayer enclosure's behaviour depended on the climatic conditions (summer/winter) [9,14,17–25].

In this paper, a study on the behaviour of a multi-layered brick wall enclosure incorporating different cement-lime mortars with the addition of 20% of PCM microencapsulated paraffin wax, LWA (expanded perlite) and cellulose fibres was carried out under different climate conditions. The aim of the study was to evaluate the thermal behaviour of the mortar layer and the overall enclosure under different climatic conditions. For this purpose, a climatic chamber was used, heating (from 15 °C to 30 °C) and cooling (from 30 °C to 15 °C) cycles were programmed and temperature and heat flux through the specimen were evaluated.

2. Materials and Methods

Five PCM-modified cement-lime mortars were analyzed. Figure 1 shows the criteria followed to design mortar compositions, considering the combined effect of energy storage capacity supplied by PCMs with the enhanced thermal insulation provided by LWAs and fibres. The experimental program assessed physical and mechanical properties and thermal conductivity in both liquid and solid states of PCMs. The temperature of the inner enclosure layers and on both external sides of the wall was analyzed. Heat flux inside and outside the enclosure was also measured.

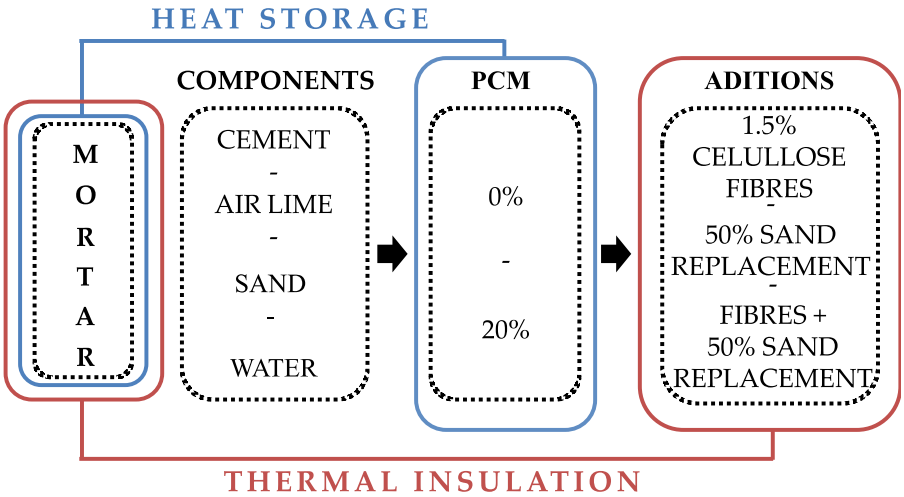

Figure 1. Composition design scheme of PCM cement-lime mortars.

2.1. Material and Mortar Compositions

The components used in the study were:

The cement used was a white type cement named BL II/B-L 32.5 N (UNE-EN 197-1) from Cementos Portland Valderrivas, Madrid, Spain.

(1) CL 90-S was the air lime added to the composition, (UNE-EN 459-1).
(2) The fine aggregate was a siliceous sand with a size between 0–4 mm.
(3) The lightweight aggregate (LWA) used was an expanded perlite (L).
(4) The fibres (F) used in this study were short cellulose fibres with a length of 1 mm—Fibracel® BC-1000 (Ø 20 μm) (Omya Clariana S.L, L'Arboc, Tarragona, Spain).
(5) The phase change material (PCM) chosen for the study was a microencapsulated paraffin wax (Micronal® DS 5040X,) with a melting point of ca. 23 ± 1 °C supplied by BASF Construction Chemicals Company, Madrid, Spain. The bulk density of this PCM is ca. 300–400 kg/m^3 and has a particle size which varies between 50–300 μm.

Table 1 presents the composition of the five mortars under study. Firstly, a reference cement-lime mortar (C) was produced. The cement:lime:aggregate ratio for this mortar was 1:0.5:4.5 by volume. Afterwards, 20% of PCM by volume of fresh mortar was added (C_{20}). In order to improve the thermal insulation capacity of the mortar, 1.5% of dry cellulose fibres considering the total fresh mortar's volume (regarding the reference mortar) was added (CF_{20}). In addition, 50% of the sand was replaced by the lightweight aggregate (CL_{20}). Finally, fibres and perlite were added (CLF_{20}) in order to design a mixture of both additions. Water to binder ratio (w/b) varied in order to get for all the mixtures a similar fresh workability. The minimum compressive strength target value was 3.5 MPa, corresponding to a CS-III grade rendering mortar (medium-high strength according to UNE-EN 998-1). The mixing process in the laboratory began blending all the dry components. Then the liquid water was added. The mixing process took a maximum of 5 min.

Table 1. Compositions of PCM cement-lime mortars, components in kg (adapted from [16]).

Components	C	C_{20}	CF_{20}	CL_{20}	CLF_{20}
BLII/B-L 32.5N	348	348	348	348	348
Air lime	55	55	55	55	55
Fine aggregates	1403	1403	1403	702	702
Fibres	-	-	0.66	-	0.66
LWA	-	-	-	94	94
PCM	-	84.6	84.6	84.6	84.6
Liquid water (*)	220	200	240	250	380
w/b (*)	0.73	0.68	0.78	0.71	0.79
D_{dry} (kg/m^3)	1400	1357	1440	868	-
D_{wet} (kg/m^3)	2264	1937	1885	1562	1561

* Fine aggregate humidity (5.3%) was also considered.

2.2. Experimental Methods

2.2.1. Hardened Properties and Thermal Parameters

The flow table test was used to measure the fresh mortar consistency, according to UNE-EN 1015-3:2000. In order to achieve a plastic consistency, the water to binder ratio was adjusted. Hardened state properties were characterised on 40 mm × 40 mm × 160 mm specimens, according to UNE-EN 1015-11. After 24 h, samples were demoulded and water cured for 28 days (21 ± 3 °C and 95 ± 5% RH). Bulk density (D) and open porosity (OP) (accessible to water) was calculated using a hydrostatic scale (UNE-EN 1015-10). According to UNE-EN 1015-19, the water vapour diffusion resistance factor (VD) was measured. VD was measured by the wet cup method. Cylindrical specimens with a 35 mm diameter and 40 ± 2 mm thickness with a saturated saline dissolution were

used. After 28 days, compressive and flexural strength (CStr, FStr) were tested on standard specimens according to UNE-EN 1015-11:2000.

Thermal conductivity (λ) was measured using a thermally insulated box (hot box method). Plate samples with a size of 210 mm × 210 mm and a thickness of 24 ± 2 mm were used. Laboratory conditions during the test were 20 ± 1 °C and 50 ± 5% RH. A heat source was connected to a thermal regulator and located inside the insulated box. Sensors placed on the inner and outer surface of the sample and inside and outside the box monitored temperature (T) and relative humidity (RH) [26]. Two different temperatures were set inside the box: 25°C and 40 °C. At 25 °C inside the box, the testing specimens remained below the PCM melting point (nominally 23 °C, although experimentally established at 22 °C [16]), while at 40 °C inside the box, all the plates were 30 °C. Thermal conductivities, λ_S (mortar's conductivity when PCM was in a solid state) and λ_L (mortar's conductivity when PCM was in a liquid state) were calculated after a thermal steady state was reached using Fourier's Law [26].

2.2.2. Climatic Chamber Testing Set-Up

A climatic chamber was used to assess the thermal behaviour of brick wall enclosures with PCM cement-lime mortars under different climatic conditions. Figure 2 shows the experimental set-up used. A multi-layered hollow brick enclosure arrangement was selected [4,5], consisting of a hollow brick wall, a gypsum-based internal rendering and an external PCM-modified coating mortar covered by a 5 cm XPS (Extruded polistyrene) insulation layer (external insulation coating system, ETICS). The sample was placed inside the climatic chamber door, and the chamber conditions were modified to produce a thermal transfer through the specimen.

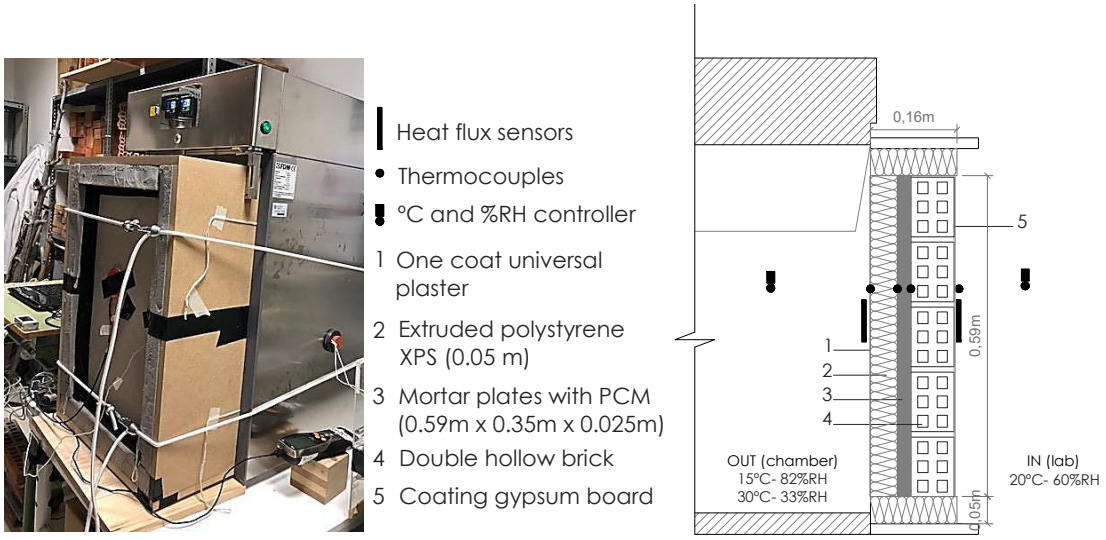

Figure 2. Climatic chamber set-up for monitoring the brick walls in different temperature conditions.

Two climatic conditions were tested in the chamber, simulating outdoor environmental conditions (OUT): a heating cycle and a cooling cycle. The heating cycle consisted of an initial stable condition of 15 °C and 82% relative humidity (RH), changing afterwards to 30 °C and 33% RH. The cooling cycle followed a reversed order, with an initial stable climatic condition of 30 °C and 33% RH, changing to 15 °C and 82% RH. Outside the chamber, the laboratory conditions (IN) remained constant at 20 ± 1 °C and 60% RH. RH inside the chamber was set to limit the water transport through the specimen. Each cycle (both heating and cooling) lasted 1400 min. During both cycles, heating and cooling, temperatures on both sides of the mortar layer, as well as at the external and internal sides of the enclosure, were monitored. Heat flux was also measured using a heat flux plate (Hukseflux HFP01 with an uncertainty degree of ±3%) for each side of the enclosure (Figure 2), registering the W/m² on both sides with a data logger (Hobo UX120, Bourne, MA, USA). As shown

in Figure 2, heat flux sensors were adhered and hermetically sealed to the surface of the material. The temperature and RH inside and outside the climatic chamber were also monitored using thermocouples, coupled temperature and RH sensors (i-button Hygrochrom™ DS1923 (Newbury, Berkshire, UK), with an uncertainty degree of 0.02 °C and a size of Ø 17.35 mm and a thickness of 5.9 mm, and heat flux plates, located as shown in Figure 2.

3. PCM Cement-Lime Mortar Physical and Mechanical Properties

Table 2 presents the experimental results obtained for workability, physical, mechanical and thermal properties of the five mortars under study. Table 2 shows that consistency values varied between 178 mm (C) and 166 mm (C_{20}).

Regarding the hardened mortars' physical properties, the reference mortar (C) presented the highest bulk density (D) value, as expected, with 1900 kg/m^3, while the PCM mortar with LWA and fibres (CLF_{20}) showed the lowest, with 1160 kg/m^3. Open porosity (OP) values varied between 23.33% (CL_{20}) and 16.77% (CF_{20}). Considering the water vapour diffusion resistance factor (VD) of the mixtures under study, C_{20} showed the highest value (4.29) while CLF_{20} showed the lowest one (3.26).

Table 2 also presents the mechanical properties of the mortars. The results for compressive strength (CStr) pointed out that C presented the highest value (14.33 MPa) while CLF_{20} showed the lowest one (5.33 MPa), which agreed with the density values. Although the 20% addition of PCM in the mixtures reduced CStr, all the mortars fulfilled the minimum compressive strength target value of 3.5 MPa, corresponding to a CS-III grade rendering mortar according to UNE-EN 998-1. On the other hand, flexural strength (FStr) values ranged between 3.36 MPa (C) and 1.79 MPa (CL_{20}).

Table 2. Physical, mechasnical and thermal properties of the PCM cement-lime mortars (adapted from [16]).

Properties	C	C_{20}	CF_{20}	CL_{20}	CLF_{20}
Consistency (mm)	178	166	170	170	170
D (kg/m^3)	1900	1600	1660	1270	1160
OP (%)	19.56	17.72	16.77	23.33	23.09
VD	4.13	4.29	3.47	3.62	3.26
CStr (MPa)	14.33	7.17	5.83	6.00	5.33
FStr (MPa)	3.36	2.40	2.20	1.79	2.16
λ_S (W/mK)	0.23	0.20	0.30	0.29	0.23
λ_L (W/mK)	0.21	0.28	0.23	0.18	0.15

Thermal conductivity results of the PCM mortars in both the solid state (λ_S, T < 22°C) and in the liquid state (λ_L, T > 22 °C) are also summarised in Table 2. It can be observed that λ_S varied between 0.30 W/mK (CF_{20}) and 0.20 W/mK (C_{20}). Otherwise, C_{20} presented the highest value for λ_L with 0.28 W/mK and CLF_{20} presented the lowest one with 0.18 W/mK.

As expected, the addition of 20% of PCM modified not only the thermal properties but also other hardened properties. Mechanical properties such as compressive and flexural strength decreased with the addition of PCM. On the other hand, λ_S decreased while λ_L increased when PCM was added, compared to the same mixture without PCM. These results were further analysed and discussed in a previous work [14].

4. Experimental Test Results and Thermal Analysis of Brick Wall Enclosures with PCM Mortars

The brick wall enclosures with PCM mortars were evaluated using the experimental set-up shown in Figure 2 and following the test procedure for a heating and a cooling cycle. For each sample, the thermal performance of the PCM mortar layer and the overall enclosure thermal performance were monitored during the test.

4.1. Thermal Behaviour of the PCM Cement-Lime Mortar Layer Inside the Enclosure Solution under Heating and Cooling Cycles

4.1.1. Heating Cycle

Table 3 shows the experimental results obtained during the heating cycle on both sides of the mortar layer, measured inside the enclosure. The initial and final temperature on both sides of the layer, the outer side in contact with the XPS insulation layer and the inner side in contact with the brick wall, the average values of the mortar layer and the difference in temperature between both sides are summarised.

Initial temperatures on the outer side (XPS) of the mortar layer varied between 20.80 °C (CF_{20}) and 19.00 °C (C_{20} and CL_{20}), while on the inner side (B), temperatures ranged between 21.40 °C for C and 20.60 °C for C_{20} and CL_{20}. Regarding final temperatures (climatic chamber conditions of 30 °C and 33% RH), CF_{20} was the mixture with the highest temperature on the XPS side (25.50 °C) and CL_{20} presented the lowest (23.40 °C). On the brick wall side, the temperature varied between 25.00 °C (CF_{20}) and 21.30 °C (CL_{20}).

Table 3. Temperatures on both sides of the PCM cement-lime mortar layer measured inside the enclosure during the heating cycle (from 15 °C to 30 °C).

Temperatures	**C**	**C_{20}**	**CF_{20}**	**CL_{20}**	**CLF_{20}**
Initial T_i (°C)					
Outer side (XPS)	19.60	19.00	20.80	19.00	20.30
Inner side (B)	21.40	20.60	21.30	20.70	20.60
Final T_f (°C)					
Outer side (XPS)	24.23	23.50	25.50	23.40	25.20
Inner side (B)	22.22	21.60	25.00	21.30	24.80
Layer average T_i	20.50	19.80	21.05	19.85	20.45
Layer average T_f	23.23	22.55	25.25	22.35	25.00
T difference T_i	1.80	1.60	1.30	1.70	0.30
T difference T_f	2.01	1.90	0.50	2.10	0.40

The average temperature of the layer can give an estimation of the solid or liquid state of PCMs. As verified in a previous study, the phase change temperature of the PCM used was 22 °C [16]. Table 3 shows that the initial average temperatures (15 °C inside the chamber) remained under 22 °C in all cases. Therefore, it can be assumed that the PCM was in a solid state. On the other hand, as the average temperature at the end of the heating cycle was above 22 °C (Table 3), it can be said that during each heating cycle, the PCM changed from solid to liquid state in all cases.

With regard to the temperature differences between both sides of the mortar plates (XPS and brick wall), it can be observed that initially the values ranged between 1.80 °C (C) and 0.30 °C (CLF_{20}), while at the end they varied between 2.10 °C (CL_{20}) and 0.40 °C (CLF_{20}).

Figure 3 presents the temperature increases on both sides of the mortar layer. Figure 3a,b compare the samples with and without PCM (C and C_{20}) and Figure 3c,d plot the temperature curves of samples with PCM (C_{20}) and the other components (CF_{20}, CL_{20} and CLF_{20}).

As expected, Figure 3a shows how the temperature on the side of the enclosure in contact with the heating source (XPS) increased continuously until the stabilisation of the system (final temperature). The incorporation of 20% of PCM reduced the slope of the curve, reducing the final temperature on the surface of the mortar layer. The same effect can be observed on the inner side of the plate in contact with the brick wall (B) of the plates. Accordingly, it can be said that PCM reduces the temperature on both sides of the mortar layer. The average temperature of the layer was therefore reduced, although the difference between them was similar (Table 3).

The enclosures with PCM mortars also showed a temperature increase due to the effect of the temperature increase inside the climatic chamber. When compared (Figure 3c,d), two groups of mixtures were identified. C_{20} and CL_{20} showed final temperatures under 23 °C and a slower increase

compared to the mixtures with cellulose fibres (CF_{20} and CLF_{20}), which showed temperatures over 25 °C. Temperature differences between both sides of the C_{20} and CL_{20} plates were 2 °C, while temperature differences between CF_{20} and CLF_{20} were 0.5 and 0.4 °C, respectively. These differences were more significant on the inner side of the enclosure at the end of the test. Consequently, the addition of cellulose fibres increased the overall temperature of the mortar layer.

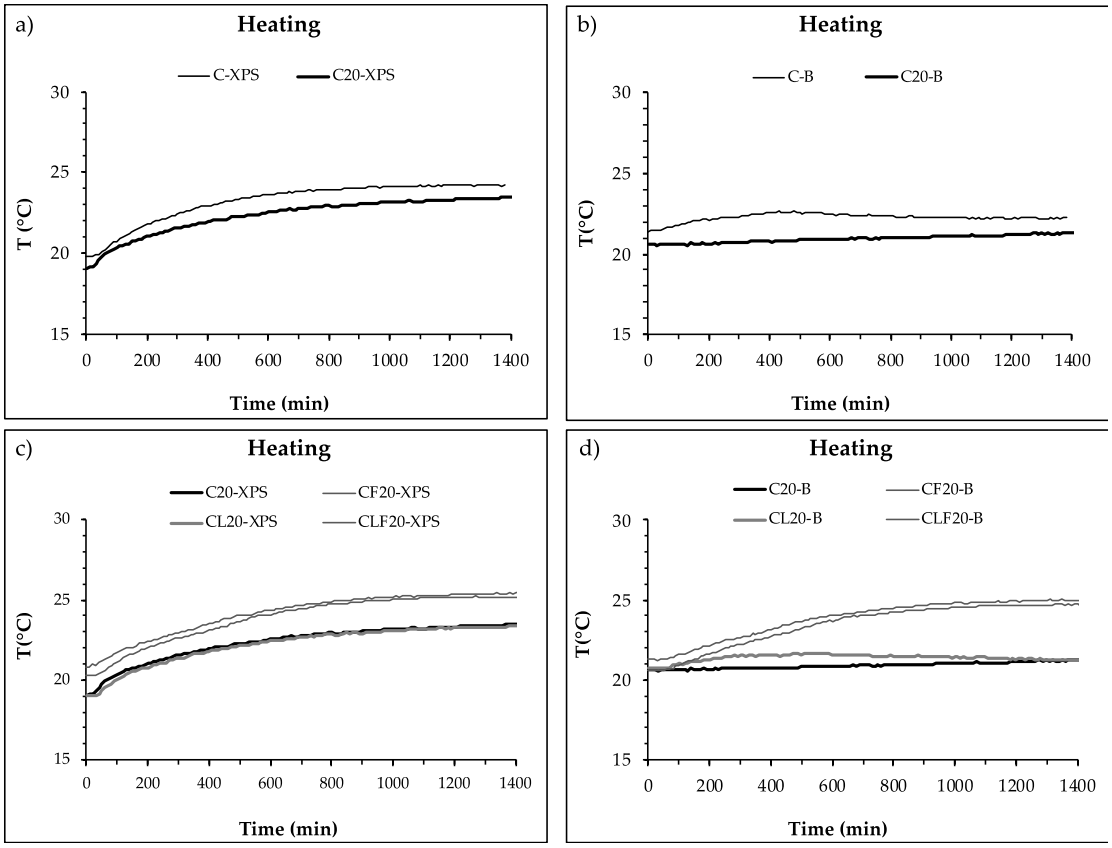

Figure 3. Temperature on both sides of the PCM cement-lime mortar layer during a heating cycle. (**a**) Inner side (XPS) of C and C_{20} plates. (**b**) Outer side (B) of C and C_{20} plates. (**c**) Inner side (XPS) of C_{20}, CF_{20}, CL_{20} and CLF_{20} plates. (**d**) Outer side (B) of C_{20}, CF_{20}, CL_{20} and CLF_{20} plates.

4.1.2. Cooling Cycle

Temperature was monitored on both sides of the mortar layer during the cooling cycle, which was tested after the heating cycle. Table 4 shows the experimental results obtained on both sides of the mortar layer. The initial and final temperature on both sides of the layer, the average values of the layer and the difference in temperature between both sides are summarised.

Initial temperatures on both sides, average temperature of the mortar layer and the difference in temperature were slightly different compared to the end of the previous heating cycles due to the thermal inertia of the enclosure specimen. The initial average temperature was over 22 °C for all mixtures, so PCM was in a liquid state.

Regarding the final temperature, the C mixture presented the highest value (21.50 °C) and CL_{20} the lowest one (19.70 °C) on the XPS side, while on the B side, the temperature ranged between 20.90 °C (C_{20} and CL_{20}) and 21.70 °C (CF_{20}). As the final average temperature was under 22 °C in all cases, PCM was in solid state after the cooling cycle. As occurred during the heating cycle, it can be stated that during the cooling cycle for each mixture, the PCM changed its phase from solid to liquid.

Table 4 shows the values of temperature differences between both sides of the plates at the beginning and end of the cooling cycle. CL_{20} was the mixture that presented the highest value with

2.40 °C, while CF_{20} presented the lowest one with 0.40 °C. The final values ranged between 1.20 °C (CL_{20}) and 0 °C (C).

The temperature evolution on both sides of the mortar layer, inside the enclosure, during a cooling cycle test are plotted in Figure 4: Figure 4a,b show the temperature development during cooling cycles of mortars without PCM (C) and with 20% of PCM (C_{20}) and Figure 4c,d plot the temperature of mixtures with PCM (C_{20}) and with the other components (CF_{20}, CL_{20} and CLF_{20}).

Table 4. Temperatures on both sides of the PCM cement-lime mortar layer measured inside the enclosure during the cooling cycle (from 30 °C to 15 °C).

Temperatures	C	C_{20}	CF_{20}	CL_{20}	CLF_{20}
Initial T_i (°C)					
Inner side (B)	22.30	21.60	25.20	21.50	23.80
Outer side (XPS)	24.10	23.90	25.60	23.90	25.40
Final T_f (°C)					
Inner side (B)	21.50	20.90	21.70	20.90	21.40
Outer side (XPS)	21.50	19.80	21.40	19.70	21.00
Layer average T_i	23.20	22.75	25.40	22.70	24.60
Layer average T_f	21.50	20.35	21.55	20.30	21.20
T difference T_i	1.80	2.30	0.40	2.40	1.60
T difference T_f	0	1.10	0.30	1.20	0.40

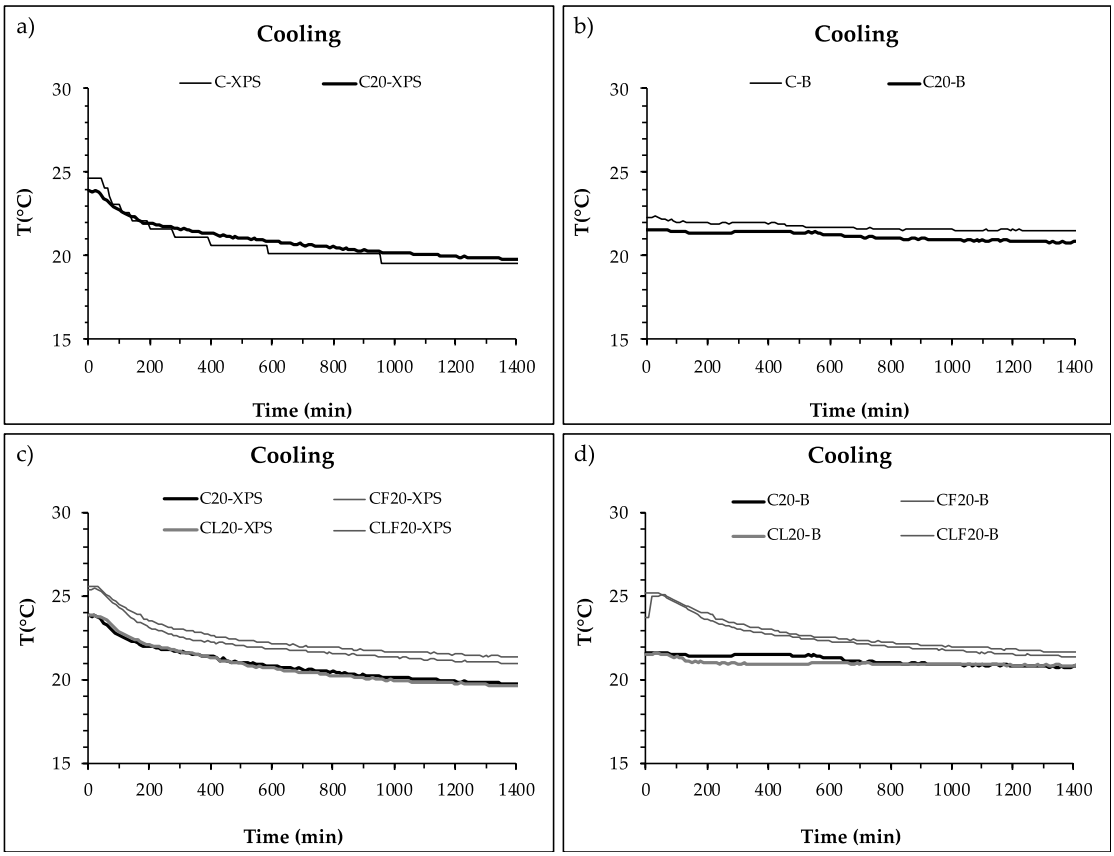

Figure 4. Temperature on both sides of the PCM cement-lime mortar layer during a cooling cycle. (**a**) Inner side (XPS) of C and C_{20} plates. (**b**) Outer side (B) of C and C_{20} plates. (**c**) Inner side (XPS) of C_{20}, CF_{20}, CL_{20} and CLF_{20} samples. (**d**) Outer side (B) of C_{20}, CF_{20}, CL_{20} and CLF_{20} samples.

The results obtained showed that there was no significant difference when PCM was incorporated into the mortar (Figure 4a,b). However, when cellulose fibres or LWA were added,

some differences arose. Mortar with LWA only did not show significant differences in C_{20}, although the use of cellulose fibres (both with or without LWA) increased the slope of the temperature curve, especially on the inner side of the enclosure (Figure 4d).

Summarising the results measured for a cooling cycle, the addition of PCM increased the temperature difference between the outer and the inner side of the mortar layer, LWA did not produce significant changes in temperature and cellulose fibres reduced the difference. C_{20} and CL_{20} showed a final temperature difference of over 1 °C, while for CF_{20} and CLF_{20} the difference was under 0.5 °C.

For both heating and cooling cycles, mortars with LWA and 20% of PCM recorded the highest temperature differences between the outer and inner sides of the mortar layer inside the enclosure. Considering the differences between the initial and final temperatures on both sides of the mortar layer, PCM showed greater influence during the cooling cycle than during the heating cycle. On the other hand, the addition of fibres reduced the effect of PCM and PCM plus LWA on the temperature changes produced by the heating and cooling cycles.

4.2. Effect of the PCM Cement-Lime Mortar Layer on the Overall Thermal Performance of the Brick Wall Enclosure under Heating and Cooling Cycles

Temperature and heat flux (HF) were measured for enclosure specimens with an intermediate mortar layer with PCM, LWA and cellulose fibres. Heating and cooling cycles were applied with a climatic chamber and the results were compared.

4.2.1. Heating Cycle

The experimental results of temperature and heat flux on both sides of the enclosure during a heating cycle are plotted in Figure 5 and the main data are summarised in Table 5. Figure 5a,c relate the temperature evolution of mortars with and without PCM while Figure 5b,d compare the heat flux (HF) evolution during a heating cycle (from 15 °C to 30 °C). Figure 5a compares the temperature curve of enclosures with mortar layers without and with PCM, C and C_{20}, respectively. During the test, the temperature on the external side of the enclosure increased until 30 °C was reached at 200 min, remaining constant until the end of the test. Temperatures on the inner side of the wall (in laboratory conditions) were almost constant until 200 min, increasing slightly afterwards due to the arrival of the thermal wave front. It can be observed that the addition of PCM to the cement-lime mortar layer reduced the inner temperature by 1 °C compared to the same mortar without the addition of PCM.

Figure 5c compares the temperature of enclosures with PCM mortars with different compositions (C_{20}, CF_{20}, CL_{20} and CLF_{20}). As expected, no difference in the outer temperature was observed. However, two groups of inner temperature curves were identified, related to whether they had cellulose fibres (CF_{20} and CLF_{20}) or not (C_{20} and CL_{20}). Enclosures with a PCM mortar layer with fibres reached 3 °C above the inner temperature of enclosures without fibres, which barely reached 21 °C.

The heat flux measured on both sides of the enclosures during a heating cycle is plotted in Figure 5b (mortar with and without PCM) and in Figure 5d (PCM mortars with different compositions). A general trend can be observed in the outer HF, with a sharp initial increase until a peak value, followed by a fast decrease and then a slow decrease until a final stabilisation at a steady-state heat flux.

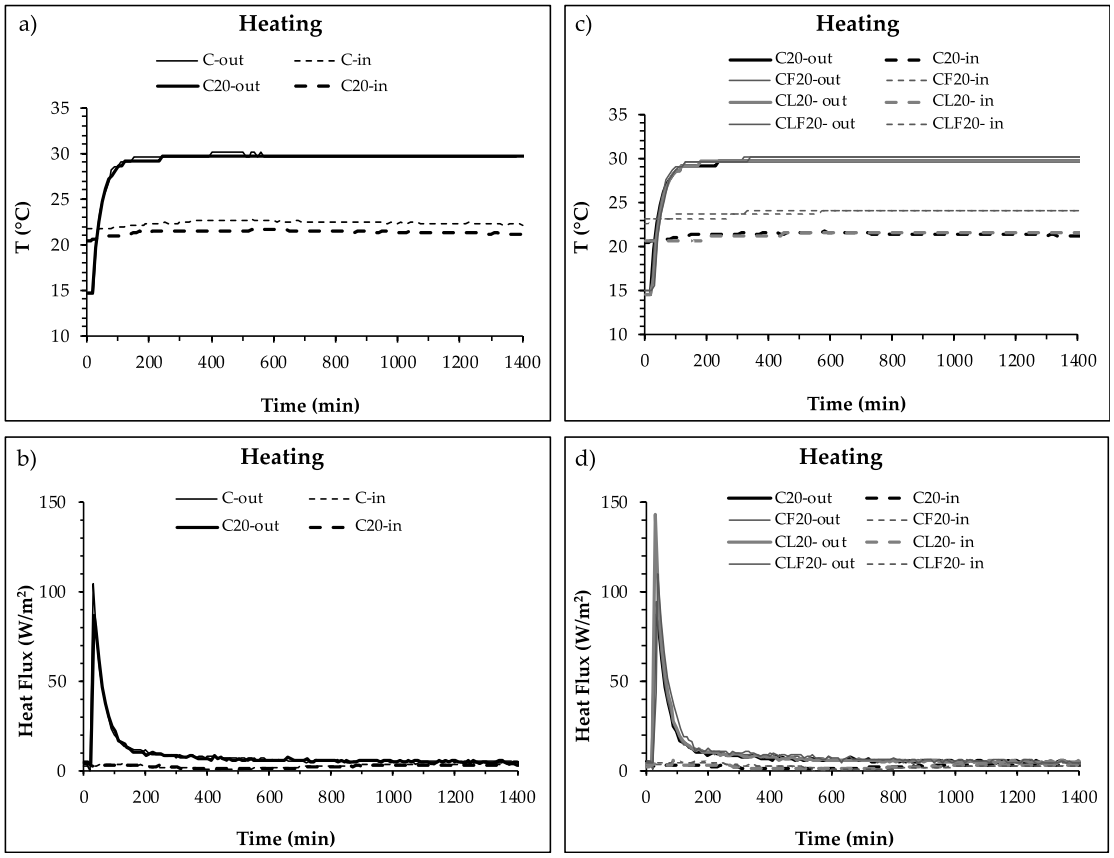

Figure 5. Temperature and heat flux monitored on the inner and outer sides of enclosures with a PCM cement-lime mortar layer during a heating cycle (from 15°C to 30°C). (**a**) Temperature of enclosures with and without PCM mortar layer (C and C_{20}). (**b**) Heat flux of enclosures with and without PCM mortar layer (C and C_{20}). (**c**) Temperature of enclosures with different types of PCM mortar (C_{20}, CF_{20}, CL_{20} and CLF_{20}). (**d**) Heat flux of enclosures with different types of PCM mortar (C_{20}, CF_{20}, CL_{20} and CLF_{20}).

Figure 5b,d also record the heat fluxes on the inner side of the enclosure. The curves followed a general trend, where the heat flux showed a slight decrease until the arrival of the thermal wave front and a moderate increase afterwards until reaching the steady-state stabilisation value.

Table 5. Summary of temperature and heat flux main results on both sides of the brick wall enclosure with a PCM cement-lime mortar layer during a heating cycle.

Thermal Parameters	C	C_{20}	CF_{20}	CL_{20}	CLF_{20}
Initial inner T_i (°C)	21.13	20.50	23.11	20.63	22.61
Final inner T_f (°C)	22.63	21.20	24.11	21.63	24.11
T_{inner} difference (°C)	1.5	0.7	1	1	1.5
Max. outer HF (W/m²)	105	90	95	140	110
Inner infl. point (min)	370	400	580	440	540
Final outer HF (W/m²)	3.24	4.60	3.92	3.15	4.47
Final inner HF (W/m²)	1.82	3.15	3.15	2.55	2.55

Table 5 summarises temperature values on the inner side of the enclosure. The initial temperature varied between 23.11 and 20.50 °C, while the final temperature ranged between 21.20 and 24.11 °C (CF_{20} and C_{20}, respectively). Enclosures with PCM mortar with cellulose fibres (CF_{20} and CLF_{20}) recorded the highest values of final temperature, which can be considered the worst scenario, while C_{20} and CL_{20} showed the most advantageous behaviour.

The peak HF values measured on the outer side of the wall (in direct contact with the climatic chamber conditions) are also presented in Table 5. The maximum peak HF value (140 W/m²) was measured for PCM mortar with lightweight aggregate (CL_{20}) due to the lower conductivity provided by the LWA (Table 2). Accordingly, the combination of PCM and LWA showed the most advantageous behaviour, delaying the advance of the heat wave front through the enclosure.

Table 5 also presents the time of arrival of the heat wave front to the inner side of the enclosure (inner HF inflexion point). It can be observed that the enclosures with lower thermal conductivity (λ_L in Table 2) delayed the arrival of the heat wave to the inner side, increasing the effective thermal inertia of the enclosure.

The final HF measured after thermal and HF stabilisation showed small differences among the enclosures tested, ranging between 3.15 and 4.60 W/m² on the outer side and between 1.82 and 3.15 W/m² on the inner side. The small difference between the outer and the inner sides can be attributed to mass transfer related to water movement through the enclosure.

Based upon the temperature and heat flux results during the heating cycle, some analyses can be done. It can be seen that C presented an initial temperature 0.66 °C higher than C_{20}, although both constructive systems were stabilised under the same climatic conditions both inside and outside. Likewise, C and C_{20} presented great differences in the temperature increase during the test, as C increased its temperature 1 °C more than C_{20}, which could be related to the addition of 20% of PCM to the mortar. Regarding the heat flux measured on the inner side, the incorporation of PCM delayed by 30 min the arrival of the heat wave front, delaying the inflexion point from 370 to 400 min, which could be related to the heat storage capacity of PCM.

Considering mortars with 20% of PCM, two groups were identified related to the presence of cellulose fibres. Mixtures with fibres (CF_{20} and CLF_{20}) showed an initial temperature 2–3 °C higher than mortars without fibres (C_{20} and CL_{20}). This difference remained almost constant during the test. Regarding the HF peak, the compositions with lightweight aggregate showed the largest values (140 W/m² and 110 W/m²) and, therefore, the larger delay in the heat wave front. It can be seen that the reference mixture (C) also showed similar values due to its higher density (Table 2) and, consequently, its higher thermal inertia.

Finally, the incorporation of lightweight aggregates and cellulose fibres also produced an extra delay in the arrival of the heat wave front to the inner side of the enclosure (Table 5 and Figure 5d). Accordingly, the delay above 400 min can be attributed to the other components beyond the effect produced by PCM alone. The delay was longer for mixtures with fibres than mixtures with LWA.

4.2.2. Cooling Cycle

The experimental results of temperature and heat flux on both sides of the enclosure during a cooling cycle (from 30 °C to 15 °C) are plotted in Figure 6 and the main data are summarised in Table 6. Figure 6a,c relate the temperature evolution of mortars with and without PCM, while Figure 6b,d compare the heat flux (HF) evolution during a heating cycle.

Figure 6a compares the temperature curve of enclosures with mortar layers without and with PCM, C and C_{20}, respectively. During the test, the temperature on the external side of the enclosure decreased until 15 °C was reached at 200 min, remaining constant until the end of the test. Temperatures on the inner side of the wall (in laboratory conditions) were almost constant until 200 min, slowly decreasing slightly afterwards due to the arrival of the thermal wave front. The addition of PCM to the cement-lime mortar layer reduced the inner temperature by 1 °C compared to the same mortar without the addition of PCM.

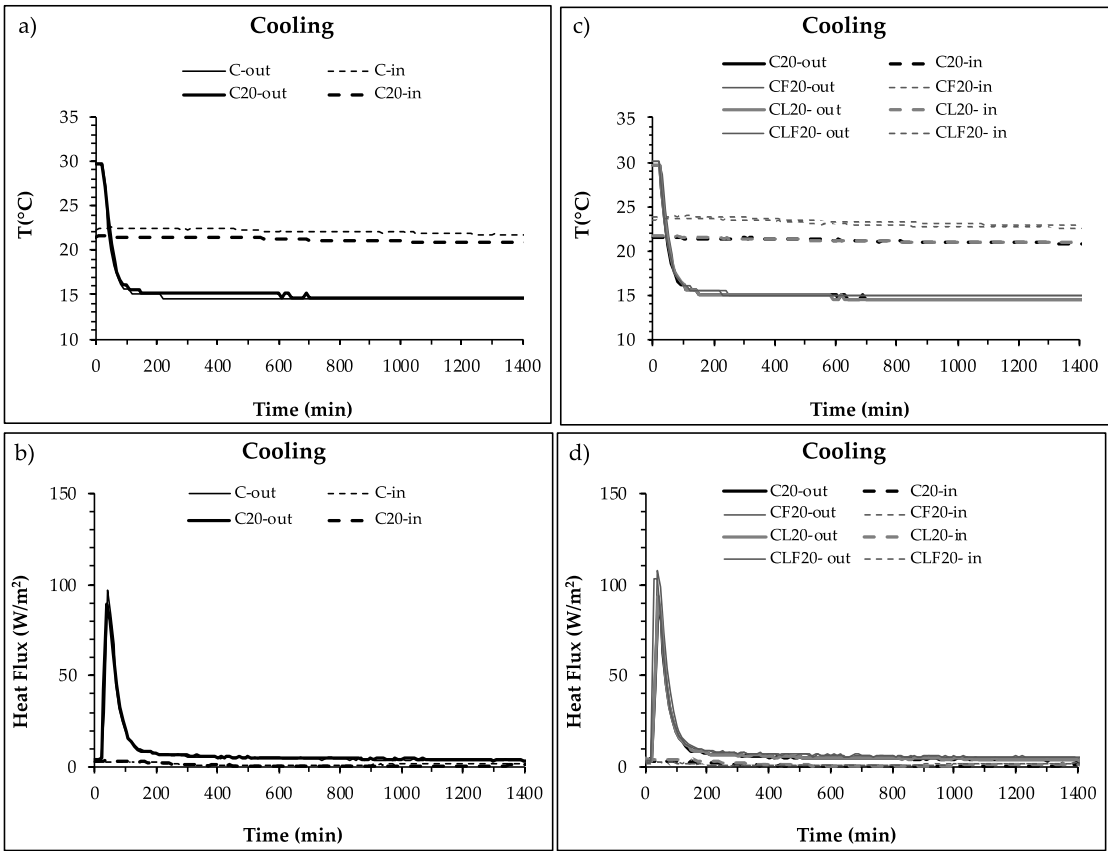

Figure 6. Temperature and heat flux monitored on the inner and outer sides of enclosures with a PCM cement-lime mortar layer during a cooling cycle (from 30 °C to 15 °C). (**a**) Temperature of enclosures with and without PCM mortar layers (C and C_{20}). (**b**) Heat flux of enclosures with and without PCM mortar layers (C and C_{20}). (**c**) Temperature of enclosures with different types of PCM mortar (C_{20}, CF_{20}, CL_{20} and CLF_{20}). (**d**) Heat flux of enclosures with different types of PCM mortar (C_{20}, CF_{20}, CL_{20} and CLF_{20}).

Figure 6c compares the temperatures of enclosures with PCM mortars with different compositions (C_{20}, CF_{20}, CL_{20} and CLF_{20}). The temperatures measured on the outer side followed the same curve in all cases, as expected. On the inner side, as happened for the heating cycle, two groups of temperature curves can be seen, corresponding to the incorporation of cellulose fibres (CF_{20} and CLF_{20}), which remained roughly 2 °C above the other mixtures.

The heat flux measured on both sides of the enclosures during the heating cycle is plotted in Figure 6b (mortar with and without PCM) and in Figure 6d (PCM mortars with different compositions). The HF curves showed a general pattern similar to that observed for the heating cycle, although the heat moved to the opposite direction in this case. The curves of the outer HF began with a sharp initial increase until a peak value, followed by a fast decrease and a final slow decrease afterwards until a stabilisation at a steady-state heat flux.

Figure 5b,d also record the heat fluxes on the inner side of the enclosure. The curves followed a general trend, where the heat flux showed a slight decrease until the arrival of the thermal wave front and a moderate increase afterwards until reaching the stabilisation steady-state value. In the case of the cooling cycle, the addition of PCM did not cause significant changes in the thermal capacity of the mortar when it changed from liquid to solid phase. On the other hand, it can be observed that mixtures with fibres presented a higher initial temperature in comparison with the mixtures without them. This trend continued over time (Figure 6d).

Table 6. Summary of temperature and heat flux main results on both sides of the brick wall enclosure with PCM cement-lime mortar layer during a cooling cycle.

Thermal Parameters	C	C_{20}	CF_{20}	CL_{20}	CLF_{20}
Initial inner T_i (°C)	22.63	22.13	24.11	21.63	24.11
Final inner T_f (°C)	21.63	21.13	23.61	20.63	23.11
T_{inner} difference (°C)	1	1	0.5	1	1
Max. outer HF (W/m²)	100	90	110	95	105
Inner infl. point (min)	320	450	270	540	270
Final outer HF (W/m²)	3.24	3.24	3.92	4.47	5.13
Final inner HF (W/m²)	1.82	1.32	1.82	1.87	1.87

Table 6 summarises temperature values on the inner side of the enclosure. The initial temperature varied between 24.11 °C (CF_{20} and CLF_{20}) and 21.63 °C (CL_{20}), while the final temperature ranged between 20.63 and 23.63 °C (CL_{20} and CF_{20}, respectively). Enclosures with PCM mortar with cellulose fibres (CF_{20} and CLF_{20}) recorded the highest values of final temperature.

The peak HF values measured on the outer side of the wall (in direct contact with the climatic chamber conditions) are also presented in Table 6. The maximum peak HF value (110 W/m²) was measured for PCM mortar with cellulose fibres (CF_{20}) because it also showed the highest initial temperature. However, when the time to reach the inflection point on the inner side of the enclosure, corresponding to the time of arrival of the heat wave front, was considered, CF_{20} did not show the longest delay. As happened for the heating cycle, C_{20} and CL_{20} showed the longest delays. It can be observed that the enclosures with lower thermal conductivity (λ_L in Table 2) delayed the arrival of the heat wave to the inner side, increasing the effective thermal inertia of the enclosure. In this case, PCM showed a greater effect (130 min) than LWA (90 min).

The final HF measured after thermal and HF stabilisation showed small differences among the enclosures tested, ranging between 3.24 and 5.13 W/m² on the outer side and between 1.32 and 1.87 W/m² on the inner side. The small difference between the outer and the inner sides can be attributed to mass transfer related to water movement through the enclosure.

Based upon the temperature and heat flux results during the cooling cycle, it can be seen that the inner temperature depended more on the initial inner temperature rather than on the mortar composition. Regarding the heat flux measured on the inner side, the incorporation of PCM delayed by 130 min the arrival of the heat wave front, due to the heat storage capacity of the PCM, while LWA supplied 90 extra minutes of delay. On the contrary, cellulose fibres did not increase the positive effect of the PCM.

5. Conclusions

An experimental study to evaluate the behaviour under different climatic conditions of a new enclosure solution containing microencapsulated phase change material cement-lime mortars with LWA and fibres inside was carried out. The experimental program assessed the thermal behaviour of the mortar layer and the overall enclosure by measuring the temperature and heat flux during heating and cooling cycles. The main conclusions of this study were:

(1) The addition of PCM to a conventional cement-lime mortar modified the physical, mechanical and thermal properties of the mortar, reducing density and strength, while increasing heat storage capacity.
(2) The addition of lightweight aggregates and fibres also modified mortar heat transfer capacity, increasing some properties already improved by PCM.
(3) The thermal behaviour of the PCM cement-lime mortars depended not only on the composition but also on the climatic conditions to which they were subjected.
(4) The addition of cellulose fibres facilitated the heat/cold transfer through the mortar layer, increasing or decreasing the average temperature of the mortars, which can be less favourable, especially in heating conditions.

(5) The addition of PCM delayed by 30 min the arrival of the heat wave front (8.1%) during the heating cycle. During the cooling cycle, the addition of PCM delayed by 130 min (40.6%) the arrival of the heat wave front compared to the reference mixture without PCM.
(6) LWA reduced thermal conductivity, increasing thermal insulation capacity and, therefore, producing an advantageous coupled effect with PCM energy storage capacity. Consequently, the combined use of PCM and LWA produced a remarkable delay of the heat wave front on the inner side of the enclosure in both heating (19%) and cooling conditions (68.7%), compared to the reference mixture.
(7) The combination of cellulose fibres and PCM showed a reduced synergic effect, but only in heating conditions.

Author Contributions: Conceptualisation, C.G., G.B., I.P.; methodology, C.G., G.B., I.P.; formal analysis, C.G., G.B.; data curation, C.G.; investigation, C.G., G.B., I.P.; writing—original draft preparation, C.G., G.B.; writing—review and editing, C.G., G.B., I.P.; supervision, G.B.; project administration, G.B., I.P.; funding acquisition, I.P. All authors have read and agreed to the published version of the manuscript.

Acknowledgments: Some of the components were supplied by BASF Construction Chemicals España S.L., Omya Clariana S.L. and Cementos Portland Valderrivas.

Funding: Financial support for this research was provided by the Reasearch Program for the Promotion of Young Researchers, co-funded by Comunidad de Madrid and the University of Alcala (Spain), as part of the project IndoorComfort (CM/JIN/2019-46).

Conflicts of Interest: The authors declare no conflict of interest.

Nomenclature

PCM	Phase change material	RH	Relative humidity
F	Cellulose fibre	T_i	Initial temperature
LWA	Lightweight aggregate	T_f	Final temperature
D	Bulk density	XPS	Insulation layer
OP	Open porosity	B	Brick layer
VD	Water vapour resistance factor	HF	Heat flux

References

1. Palomar, I.; Barluenga, G.; Puentes, J. Lime–cement mortars for coating with improved thermal and acoustic performance. *Constr. Build. Mater.* **2015**, *75*, 306–314, doi:10.1016/j.conbuildmat.2014.11.012.
2. Sala, E.; Zanotti, C.; Passoni, C.; Marini, A. Lightweight natural lime composites for rehabilitation of Historical Heritage. *Constr. Build. Mater.* **2016**, *125*, 81–93, doi:10.1016/j.conbuildmat.2016.08.033.
3. Bentchikou, M.; Guidoum, A.; Scrivener, K.; Silhadi, K.; Hanini, S. Effect of recycled cellulose fibres on the properties of lightweight cement composite matrix. *Constr. Build. Mater.* **2012**, *34*, 451–456, doi:10.1016/j.conbuildmat.2012.02.097.
4. Terés-Zubiaga, J.; Martín, K.; Erkoreka, A.; Sala, J.; Escudero, K.M. Field assessment of thermal behaviour of social housing apartments in Bilbao, Northern Spain. *Energy Build.* **2013**, *67*, 118–135, doi:10.1016/j.enbuild.2013.07.061.
5. Terés-Zubiaga, J.; Campos-Celador, A.; González-Pino, I.; Escudero-Revilla, C. Energy and economic assessment of the envelope retrofitting in residential buildings in Northern Spain. *Energy Build.* **2015**, *86*, 194–202, doi:10.1016/j.enbuild.2014.10.018.
6. Ryms, M.; Januszewicz, K.; Kazimierski, P.; Zaleska-Medynska, A.; Klugmann-Radziemska, E.; Lewandowski, W.M. Post-Pyrolytic Carbon as a Phase Change Materials (PCMs) Carrier for Application in Building Materials. *Materials* **2020**, *13*, 1268, doi:10.3390/ma13061268.
7. Sharma, A.; Tyagi, V.; Chen, C.; Buddhi, D. Review on thermal energy storage with phase change materials and applications. *Renew. Sustain. Energy Rev.* **2009**, *13*, 318–345, doi:10.1016/j.rser.2007.10.005.
8. Cabeza, L.F.; Castell, A.; Cabeza, L.F.; De Gracia, A.; Fernandez, A.I. Materials used as PCM in thermal energy storage in buildings: A review. *Renew. Sustain. Energy Rev.* **2011**, *15*, 1675–1695, doi:10.1016/j.rser.2010.11.018.

9. Ryms, M.; Klugmann-Radziemska, E. Possibilities and benefits of a new method of modifying conventional building materials with phase-change materials (PCMs). *Constr. Build. Mater.* **2019**, *211*, 1013–1024, doi:10.1016/j.conbuildmat.2019.03.277.
10. Rao, V.V.; Parameshwaran, R.; Ram, V.V. PCM-mortar based construction materials for energy efficient buildings: A review on research trends. *Energy Build.* **2018**, *158*, 95–122, doi:10.1016/j.enbuild.2017.09.098.
11. Jayalath, A.; Nicolas, R.S.; Sofi, M.; Shanks, R.; Ngo, T.; Aye, L.; Mendis, P. Properties of cementitious mortar and concrete containing micro-encapsulated phase change materials. *Constr. Build. Mater.* **2016**, *120*, 408–417, doi:10.1016/j.conbuildmat.2016.05.116.
12. Pavlík, Z.; Fořt, J.; Pavlíková, M.; Pokorný, J.; Trník, A.; Černý, R. Modified lime-cement plasters with enhanced thermal and hygric storage capacity for moderation of interior climate. *Energy Build.* **2016**, *126*, 113–127, doi:10.1016/j.enbuild.2016.05.004.
13. Lucas, S.S.; Ferreira, V.; Aguiar, B. Latent heat storage in PCM containing mortars—Study of microstructural modifications. *Energy Build.* **2013**, *66*, 724–731, doi:10.1016/j.enbuild.2013.07.060.
14. Cunha, S.; Lima, M.; Aguiar, B. Influence of adding phase change materials on the physical and mechanical properties of cement mortars. *Constr. Build. Mater.* **2016**, *127*, 1–10, doi:10.1016/j.conbuildmat.2016.09.119.
15. Mankel, C.; Caggiano, A.; Ukrainczyk, N.; Koenders, E. Thermal energy storage characterization of cement-based systems containing microencapsulated-PCMs. *Constr. Build. Mater.* **2019**, *199*, 307–320, doi:10.1016/j.conbuildmat.2018.11.195.
16. Guardia, C.; Barluenga, G.; Palomar, I.; Diarce, G. Thermal enhanced cement-lime mortars with phase change materials (PCM), lightweight aggregate and cellulose fibers. *Constr. Build. Mater.* **2019**, *221*, 586–594, doi:10.1016/j.conbuildmat.2019.06.098.
17. Palomar, I.; Barluenga, G.; Ball, R.J.; Lawrence, M. Laboratory characterization of brick walls rendered with a pervious lime-cement mortar. *J. Build. Eng.* **2019**, *23*, 241–249, doi:10.1016/j.jobe.2019.02.001.
18. Wi, S.; Yang, S.; Park, J.H.; Chang, S.J.; Kim, S. Climatic cycling assessment of red clay/perlite and vermiculite composite PCM for improving thermal inertia in buildings. *Build. Environ.* **2020**, *167*, 106464, doi:10.1016/j.buildenv.2019.106464.
19. Alonso, C.; Oteiza, I.; García-Navarro, J.; Martín-Consuegra, F. Energy consumption to cool and heat experimental modules for the energy refurbishment of façades. Three case studies in Madrid. *Energy Build.* **2016**, *126*, 252–262, doi:10.1016/j.enbuild.2016.04.034.
20. Arıcı, M.; Bilgin, F.; Nižetić, S.; Karabay, H. PCM integrated to external building walls: An optimization study on maximum activation of latent heat. *Appl. Therm. Eng.* **2020**, *165*, 114560, doi:10.1016/j.applthermaleng.2019.114560.
21. Rathore, P.K.S.; Shukla, S.K. An experimental evaluation of thermal behavior of the building envelope using macroencapsulated PCM for energy savings. *Renew. Energy* **2020**, *149*, 1300–1313, doi:10.1016/j.renene.2019.10.130.
22. Fachinotti, V.; Bre, F.; Mankel, C.; Koenders, E.A.B.; Caggiano, A. Optimization of Multilayered Walls for Building Envelopes Including PCM-Based Composites. *Mater.* **2020**, *13*, 2787, doi:10.3390/ma13122787.
23. Kishore, R.A.; Bianchi, M.V.; Booten, C.; Vidal, J.; Jackson, R. Optimizing PCM-Integrated Walls for Potential Energy Savings in U.S. Buildings. *Energy Build.* **2020**, *226*, 110355, doi:10.1016/j.enbuild.2020.110355.
24. Qiao, Y.; Yang, L.; Bao, J.; Yang, L.; Liu, J. Reduced-scale experiments on the thermal performance of phase change material wallboard in different climate conditions. *Build. Environ.* **2019**, *160*, 106191, doi:10.1016/j.buildenv.2019.106191.
25. Khan, R.J.; Bhuiyan, Z.H.; Ahmed, D.H. Investigation of heat transfer of a building wall in the presence of phase change material (PCM). *Energy Built Environ.* **2020**, *1*, 199–206, doi:10.1016/j.enbenv.2020.01.002.
26. Herrero, S.; Mayor, P.; Olivares, F.H. Influence of proportion and particle size gradation of rubber from end-of-life tires on mechanical, thermal and acoustic properties of plaster–rubber mortars. *Mater. Des.* **2013**, *47*, 633–642, doi:10.1016/j.matdes.2012.12.063.